DETAILED STUDY ON MEMBRANE DISTILLATION:

SCALING AND FOULING CONTROL

by

GAYATHRI DANASAMY NAIDU

A Thesis submitted in fulfilment for the degree of

Doctoral of Philosophy

School of Civil and Environmental Engineering
Faculty of Engineering and Information Technology
University of Technology, Sydney (UTS)
New South Wales, Australia

October 2014

CERTIFICATE OF AUTHORSHIP/ORIGINALITY

I certify that this thesis has not previously been submitted for a degree nor has it been submitted as part of requirements for a degree except as fully acknowledge within the text.

I also certify that the thesis has been written by me. Any help that I have received in my research work and the preparation of the thesis itself has been acknowledged. In addition, I certify that all information sources and literature used are indicated in the thesis.

Signature of Candidate

Gayathri Danasamy Naidu

ACKNOWLEDGEMENTS

"Your legs will get heavy and tired. Then comes a moment of feeling

the wings you've grown, lifting ~ Rumi"

This work would not have been possible without the help of many people that I acknowledge below.

Journal Articles Published

1. ***<u>Naidu, G.</u>,** Choi, Y., Jeong, S., Hwang, T. M., & Vigneswaran, S. (2014). Experiments and modeling of a vacuum membrane distillation for high saline water. Journal of Industrial and Engineering Chemistry, 20(4), 2174-2183.

2. ***<u>Naidu, G</u>**., Jeong, S., & Vigneswaran, S. (2014). Influence of feed/permeate velocity on scaling development in a direct contact membrane distillation. Separation and Purification Technology, 125, 291-300.

3. ***<u>Naidu, G</u>**., Jeong, S., Kim, S., Kim, I. S., & Vigneswaran, S. (2014). Organic fouling behaviour in direct contact membrane distillation. Desalination, 347(0), 230-239.

4. ***<u>Naidu, G</u>**., Jeong, S., Vigneswaran, S., & Rice, S. A. (2013). Microbial activity in biofilter used as a pretreatment for seawater desalination. Desalination, 309, 254-260

5. *Jeong, S., **<u>Naidu, G</u>**., & Vigneswaran, S. (2013). Submerged membrane adsorption bioreactor as a pretreatment in seawater desalination for biofouling control. Bioresource technology, 141, 57-64.

6. ****** Jeong, S., **<u>Naidu, G</u>**., Vigneswaran, S., Ma, C. H., & Rice, S. A. (2013). A rapid bioluminescence-based test of assimilable organic carbon for seawater. Desalination, 317, 160-165.

7. ***<u>Naidu, G</u>**.,Jeong, S., Choi, Y., Jang, E., Hwang, T. M., & Vigneswaran, S. (2014). Application of vacuum membrane distillation for small scale drinking water production**.** Desalination, 354, 53-61.

8. ***<u>Naidu, G</u>**., Jeong, S., Vigneswaran, S. Interaction of humic on organic and biofouling in membrane distillation for seawater desalination (*manuscript submitted to Chemical Engineering Journal*).

*Articles related to the thesis.

**Publications made during the PhD candidature including articles not entirely related to the thesis.

Conference papers and presentations

1. *__Naidu, G__., Jeong, S., & Vigneswaran, S. Vacuum Membrane Distillation for high saline water treatment. Singapore International Water Week. 1 - 5 June 2014, Singapore.

2. *__Naidu, G__., Jeong, S., & Vigneswaran, S. Sustainable operation of membrane distillation in desalination plants. International Conference on Innovative Technologies and Management for Water Security. 12-14 February 2014, India.

3. *__Naidu, G__., Jeong, S., & Vigneswaran, S. Influence of Operating Parameters and Configurations on Scaling in Membrane Distillation System. The 7th IWA Specialised Membrane Technology Conference and Exhibition for Water and Wastewater Treatment and Reuse. August 25 - 29, 2013, Toronto, Canada.

4. *__Naidu, G__., Jeong, S., & Vigneswaran, S. Vacuum Membrane Distillation for high NaCl treatment and scaling development. UTS Faculty of Engineering and Information Technology Research Showcase. 5 June 2013, Sydney, Australia.

5. **Jeong, S., __Naidu, G__., Vigneswaran, S., Ma, C. H., & Rice, S. A. A novel and rapid bioluminescence-based tests of assimilable organic carbon for seawater. The 5th International Seawater Desalination Workshop. 28-31 October 2012, Jeju, Republic of Korea.

6. *Jeong, S., __Naidu, G__., Vigneswaran, S. Submerged membrane adsorption bioreactor as a pretreatment in seawater desalination for biofouling control. The 5th CESE Conference. 9 - 13 September 2012, Melbourne, Australia.

7. *__Naidu, G__., Jeong, S., Nguyen, T.V., & Vigneswaran, S. Biofouling challenges in seawater reverse osmosis (SWRO): Understanding the role of microbial activity in biofilter performance. Singapore International Water Week. 1 - 5 July 2012, Singapore.

8. *__Naidu, G__., Jeong, S., & Vigneswaran,.S. Microbial activity in biofilter as a pretreatment for seawater desalination. UTS Faculty of Engineering and Information Technology Research Showcase. 13 June 2012, Sydney, Australia (Best poster presentation)

*Articles related to the Thesis.

**Publications made during the PhD candidature including articles not entirely related to the Thesis

LIST OF ABBREVIATIONS

AA	: Alginic acid
AGMD	: Air gap membrane distillation
AOC	: Assimilable organic carbon
ATP	: Adenosine tri-phosphate
BB	: Building blocks
BSA	: Bovine serum albumin
CF	: Concentration factor
CFU	: Colony forming unit
CP	: Concentration polarisation
CSD	: Crystal size distribution
DCMD	: Direct contact membrane distillation
DI	: Deionized
DOC	: Dissolved organic carbon
EBCT	: Empty bed contact time
EDS	: Energy dispersion spectrometry
FE-SEM	: Field emission scanning electron microscope
GAC	: Granular activated carbon
GE	: General Electrics
GOR	: Gain output ratio
HA	: Humic acid
HMW	: High molecular weight
HRT	: Hydraulic retention time
HS	: Humic substances
IC	: Ion chromatography
ICP	: Inductively coupled plasma
LC-OCD	: Liquid chromatography-organic carbon detection
LMW	: Low molecular weight
MD	: Membrane distillation
MF	: Microfiltration
MO	: Mixed organic
MP-AES	: Microwave plasma atomic emission spectrometer
MW	: Molecular weight

NF   : Nanofiltration

NOM   : Natural organic matter

PAC   : Powder activated carbon

PP   : Permeate production

PTFE   : Polytetrafluoroethylene

RO   : Reverse osmosis

RR   : Recovery ratio

SGMD   : Sweeping gas membrane distillation

SMABR   : Submerged membrane adsorption bioreactor

SR   : Saturation ratio

SW   : Seawater

SWRO   : Seawater reverse osmosis

TDC   : Total direct cell count

TDS   : Total dissolved solids

TP   : Temperature polarisation

TSS   : Total suspended solids

UF   : Ultrafiltration

UF-MFI   : Ultrafiltration-modified fouling index

UV   : Ultraviolet

VCF   : Volume concentration factor

VMD   : Vacuum membrane distillation

V-MEMD   : Vacuum multi effect membrane distillation

VR   : Vapour transport resistance

LIST OF SYMBOLS

b	: bulk
f	: feed
m	: membrane surface
v	: vacuum
ΔH_v	: Latent heat of vaporization (J/ kg)
A	: Membrane area (m^2)
B	: Membrane coefficient (kg /m^2 .s. Pa)
C	: Solute concentration (mol /L)
d	: Molecular diffusion coefficient (m^2/ s)
D[4, 3]	: Volume weighted mean size (µm)
d_h	: Hydraulic diameter (m)
D^{kn}	: Knudsen diffusion coefficient of solute
E_{pump}	: Pumping energy (W)
H	: Global heat transfer coefficient
T_h	: Heating temperature (ºC)
h_w	: Heat transfer coefficient (W/m^2/K)
J_w	: Water flux (L m^{-2} h^{-1} = LMH)
K	: Mass transfer coefficient (m/s)
K_m	: Thermal conductivity (W /m/ K)
L	: Length of the channel (m)
m	: Molar concentration (mol/m$^{3)}$)
M	: Molecular mass of water (kg/mol)
N	: Heat flux (L m^{-2} h^{-1}/ LMH)
Nu	: Nusselt number
P	: Pressure (Pa)
P'	: Applied pressure (Pa)
P_m	: Vapour pressure on membrane surface (Pa)
P_p	: Permeate pressure (kPa)
Pr	: Prandtl numbers
Q	: Flow rate (L/h)
R	: Gas constant (J /mol/ K)
r	: Pore size (m)

Re	: Reynolds number
S	: Water-specific heat capacity (kJ/kg)
Sc	: Schmidt number
Sh	: Sherwood number
T	: Temperature (ºC)
t	: Time (min)
t_{ind}	: Induction period (min)
v	: Velocity (m/s)
δ	: Membrane thickness (m)
ε	: Porosity
$\zeta.$	: Zeta potential (mV)
λ	: Mean free path of water molecules (m)
μ	: Viscosity (Pa s)
ρ	: Density (kg/m^3)
τ	: Tortuosity

TABLE OF CONTENTS

LIST OF FIGURES

LIST OF TABLES

ABSTRACT

Around 40% of the world's population lives in arid and semi-arid regions where rainfall is low. These regions are facing challenges of declining water tables and increasing ground water salinity. Providing good quality drinking water for small communities in these areas is highly challenging. Although existing membrane technologies are able to produce potable quality water, issues such as high energy consumption, osmotic pressure constraint, brine management and large centralized designs make them unsuitable for application in these areas. Membrane distillation (MD), a thermal integrated membrane process, is a burgeoning technology with the potential to address and overcome these issues. As a vapour pressure operated system, MD is not restricted by saline feed solutions and therefore can achieve good quality distillate with minimal brine discharge. Furthermore, an MD system can be built as a standalone compact system suitable for small community application. The modest temperature requirement for MD operation (generally between 60ºC to 80ºC) enables the system to use alternative energy sources such as solar power. Despite such advantages, MD has not as yet been used widely in commercial applications. Several essential problems concerning MD process performance, namely, lower production rate, fouling propensity, energy efficiency and long term performance must be addressed.

In this study, the performance of a scaled-up modified design vacuum membrane distillation system termed 'vacuum multi effect membrane distillation (V-MEMD)' was evaluated. A bench scale direct contact membrane distillation (DCMD) was employed for detailed fouling analysis. The four main sections of this work incorporate: (i) V-MEMD operation; (ii) scaling development in MD; (iii) organic fouling development in MD; and (iv) pretreatment and membrane cleaning in MD. These sections present and explain critical aspects of MD performance in the context of drinking water production.

V-MEMD operation Firstly, in this study the beneficial features of a modified V-MEMD system were highlighted. These include the internal heating and internal condensing which reduces heat loss and makes operation possible at modest feed temperatures from 45°C to 55°C. A semi-empirical mathematical modeling in this study showed that operating at these feed temperature ranges minimized the effect of temperature polarization (TP) to a low range of between 0.96 and 0.99. The findings of the V-MEMD performance analysis indicated that feed temperature and permeate pressure were the most influential operating parameters. Lowering the permeate pressure from P_p =15.0 kPa to 10.0 kPa increased the permeate flux by almost 200%, whereby the highest permeate flux of 13.5 L m^{-2} h^{-1} (LMH) was achieved when the permeate pressure was reduced to P_p =5.0 kPa. In the V-MEMD concept, vacuum application is essential in order to create a sustainable driving force, especially for a scaled up modular unit with several membrane stages. At the same time, increased feed temperature exponentially increased the permeate flux. A small variation of feed temperature from 45.0°C to 65.0°C significantly improved the permeate flux from 3.6 LMH to 11.8 LMH.

The V-MEMD system proved to be suitable for producing 9.4 LMH of good quality permeate (more than 99.5% rejection rate) with highly saline feed water (1 M of NaCl feed solution concentrated up to 3 M of NaCl). Only a 10-15% reduction in permeate flux was observed at high feed concentration. The modeling data revealed that high turbulent feed flow velocity of 2.2 m/s (Re = 17, 300) in the V-MEMD system effectively minimized concentration polarization (CP), but the recovery ratio reduced with increased feed flow velocity. An intermediate feed flow velocity of 1.1 m/s (Re = 6,100) was more appropriate for balancing the effect of CP and maintaining a reasonable recovery ratio.

Scaling development in MD In achieving near zero liquid discharge under thermal conditions, inevitably, the MD membrane would be exposed to highly concentrated sparingly soluble salts such as calcium sulphate ($CaSO_4$). In this study, an evaluation of $CaSO_4$ scaling development in MD operation was carried out, focusing on the role of hydrodynamic (flow velocity) conditions. This study found that permeate condition influenced $CaSO_4$ scaling development. For instance, in the V-MEMD system, the $CaSO_4$ crystal size in the membrane module increased from 62.68 μm to 522.28 μm, with increased permeate pressure from 10.0 kPa to 15.0 kPa. Similarly, in a DCMD configuration, a small change in the permeate velocity from 0.8 m/s to 1.1 m/s was effective in changing the scaling pattern from surface crystallization to a more dominant bulk crystallization, without the need to change the feed velocity while improving the system's performance (i.e. increase recovery ratio, reduce pumping energy, increase permeate flux). Importantly, the findings of this study also revealed that the crystals were only loosely deposited on the membrane.

In the V-MEMD system, the loose deposition was attributed to the lack of hydraulic pressure, low feed temperature (T_f = 47.6 °C), high turbulence (Re = 5665.6, 0.9 m/s) and short membrane retention time (21.6 s). Increasing the feed flow velocity from 0.3 m/s to 0.9 m/s in the V-MEMD reduced the gypsum crystal size in the membrane module from 339.03 μm to 62.68 μm. Likewise, in the DCMD configuration the high feed velocity (turbulence) played an important role in controlling the membrane surface crystallization. The Field Emission Scanning Electron Microscope (FE-SEM) analysis with EDS showed significantly higher calcium and sulphate element deposition on the membrane at low feed velocity (0.5 m/s) compared to the high flow velocity (2.2 m/s).

Organic fouling development in MD Organic fouling is a ubiquitous problem in membrane processes. Compared to pressure driven membrane processes, the fouling

phenomenon in MD operation is unique due to the presence of thermal conditions on a hydrophobic membrane at supersaturated feed concentration levels. In depth understanding of the MD fouling phenomenon is crucial if MD is to be successfully implemented in a proto-scale. This research carried out a detailed fouling development analysis using Liquid Chromatography-Organic Carbon Detection (LC-OCD) to characterize the behavior of organic compounds under thermal MD operation. The findings of this research established that organic fouling in MD was influenced by the type of organic compound present in the feed solution, the thermal state as well as the physico-chemical condition of the feed solution. Based on the LC-OCD analysis of the feed and permeate solution and membrane foulant as well as membrane analysis (contact angle and SEM-EDS analysis), both the humic acid (HA) and bovine serum albumin (BSA) compounds showed dominant fouling tendencies while the alginic acid (AA) compound exhibited minimal fouling tendencies. The latter was due to its hydrophilic nature and negative electrostatic repulsion.

The membrane SEM-EDS analysis showed that mainly the BSA compound was deposited on the membrane surface (800.6 mg/m^2 organic mass per membrane area) compared to the HA compound (423.2 mg/m^2). This was due to the hydrophobic nature of the BSA compound which allowed it to bond with the hydrophobic MD membrane. Meanwhile, the humic substances (HS) showed changes under MD thermal conditions. The LC-OCD analysis of the HA feed solution revealed the thermal disaggregation of the HS, forming low molecular weight–HS (LMW-HS) organics. Further, the cross-section membrane SEM-EDS line analysis showed the penetration of the LMW-HS organics through the membrane pores, resulting in partial wetting. The findings for the influence of physico-chemical state of the feed solution revealed that the addition of salinity (NaCl) contributed to higher HS disaggregation to LMW-HS organics. This

resulted in severe penetration of the LMW-HS organics to the permeate side. Meanwhile, in the presence of inorganics Ca^{2+} ion that acts as a binding agent, a cake layer was formed on the membrane.

Pretreatment and membrane cleaning in MD Finally, a practical application of MD was presented in this study by analysing the pretreatment and membrane cleaning in MD. In the first part of this section, the performance of two chemical-free pretreatments (namely, deep-bed biofilter and a submerged membrane adsorption bioreactor system (SMABR) was evaluated in terms of organic fouling reduction. Both these pretreatment systems helped to reduce HS and LMW organics as well as assimilable organic carbon (AOC) concentrations through adsorption and biodegradation mechanisms. In the second part of this section, MD performance with natural seawater was compared to SMABR pre-treated seawater. The natural seawater, which predominantly contains HS, resulted in the formation of LMW-HS organics under MD thermal conditions and pore penetration was observed to occur through the membrane.

The biofouling potential of MD operation with SW was highlighted based on the AOC concentration of the membrane foulant and feed solution. In the meantime the SMABR pre-treated seawater feed solution containing low concentrations of HS and LMW organics, resulted in more stable permeate flux and minimal LMW-HS organics pore penetration. The findings established the suitability of chemical-free pretreatments to reduce organic fouling in MD. Additionally, the membrane cleaning by water was carried out to flush away the loose deposition of crystals in the V-MEMD system. Based on the feed solution ion mass balance, with only 2 L of DI water, most ions in the feed solution, specifically the Mg, Na and Cl ions, were removed. This finding established the effectiveness of frequent DI water flushing for the V-MEMD system

CHAPTER 1

INTRODUCTION

University of Technology Sydney

Faculty of Engineering & Information Technology

1.1   BACKGROUND OF RESEARCH

1.1.1   Global demand for drinking water

The world's increasing population, economic development and climate change are driving the demand for more drinking water (UN-Water, 2012). The current water consumption rate is more than double that of the population rate of increase (UN-Water, 2012). In view of the limited volume of available and accessible drinking water, it is a challenge for the water industries to meet global water requirement needs. Water industries are consequently shifting technology trends towards seawater desalination process that offers the capacity to produce drinking water from the world's major alternative water source - seawater (Macedonio et al., 2007).

Presently, seawater reverse osmosis (SWRO) technology is the most widely used membrane technology in desalination plants (Macedonio et al., 2007; Greenlee et al., 2009). SWRO technology is successful due to its low energy requirements compared to thermal technologies; it is also easy to control and retains a good degree of stability in achieving a high rejection rate of dissolved salts in seawater (Greenlee et al., 2009).

1.1.2   Fresh water for remote areas in Australia

Apart from large seawater desalination systems, the requirements for small-scale stand-alone desalination units are essential for dry, inland areas. Most of these areas have highly saline groundwater as their main natural water source and are occupied by a low-density population. However, these small communities still lack proper drinking water supplies (Koschikowski et al., 2009).

Specifically, three-quarters of Australia's total area comprises of inland arid and semi-arid areas with low rainfall (Morton et al., 1995) (**Figure 1.1**). Approximately 3.0% of Australia's population lives in these remote areas, the majority consisting of indigenous

people (Bailie and Wayte, 2006). The indigenous communities here rely mainly on brackish groundwater, which can be found in significant volumes throughout the remote areas. Generally, the brackish groundwater bores in Australia are highly saline, with a total dissolved solids (TDS) ranging from 15,000- 30,000 mg/L (Herczeg et al., 2001; Richards and Schäfer, 2003). Some of this brackish ground water contains high ion concentrations.
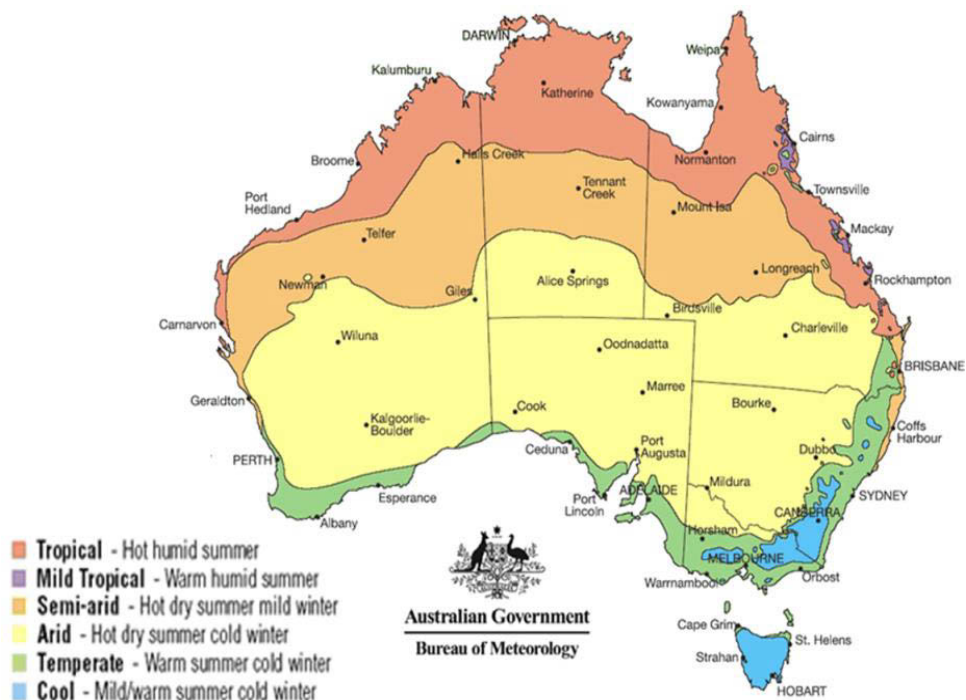
Figure 1.1 Arid and semi-arid areas in Australia (adopted from Australian Bureau of Meteorology, 2014).

The application of reverse osmosis (RO) technology is not suitable for these areas since generally, RO operations are built as large centralized desalination plants. Consequently they are more economical and suitable for areas of high population density (Malaeb and Ayoub, 2011). Further, the energy requirements for RO treatment of brackish, high saline water remain an economic challenge (Greenlee et al., 2009). At the same time, the generation of large quantities of brine with saline water will require extra brine

disposal management in inland areas (Martinetti et al., 2009; Pérez-González et al., 2012). In coastal areas, brine stream is discharged to the sea with dilution of brine concentrate. Recently, membrane distillation (MD) has been identified as a promising alternative technology for standalone high saline water treatment (Martinetti et al., 2009; Koschikowski et al., 2009).

1.1.3 Membrane Distillation

MD is a technology that integrates both thermal distillation and membrane process. MD possesses a number of unique features that differ from other membrane and thermal technologies. One of the distinct features of MD is that the driving force is the difference in vapour pressure of water across the membrane, rather than hydraulic pressure. In this type of operation, partial water vapour pressure will only be minimally reduced by salt concentration (Martinetti et al., 2009). Therefore this technique is particularly useful for high saline water treatment. In MD, the feed solution can be concentrated so that a water recovery rate of 80 to 90% is achieved while producing high quality distillate (Ji et al., 2010). This eliminates the need for sophisticated brine management technology in remote inland areas. Meanwhile, the thermal process in MD requires only low operating temperature and therefore it is possible to utilize alternative energy sources such as waste heat or solar energy (Khayet, 2011). Additionally, the MD system can be constructed as a small-scale and compact unit that is suitable for small communities. With these advantages MD can operate as a standalone saline water treatment process in remote areas where RO and thermal distillation technology applications are challenged (Alkhudhiri et al., 2012).

The concept of MD technology was first patented in 1967, when it reported a low flux performance of 1 kg/m^2/h (Findley, 1967). A major impetus for the application of MD technology in drinking water was the development of Gore's MD membrane for

desalting NaCl solutions (Gore, 1982). Since then, research in MD has rapidly increased as shown in **Figure 1.2**. In recent times, enhancements have included higher operating cross-flow velocity, the use of acrylic plastic as membrane cell construction material and the utilization of composite membranes with very thin active layers increased MD permeate flux to as high as 50-80 kg/m^2/h (Cath et al., 2004). The MD system consists of various configurations, namely direct contact MD (DCMD), vacuum MD (VMD), air gap MD (AGMD) and sweeping gas MD (SGMD). More than 60% of MD studies are focused on the DCMD system.
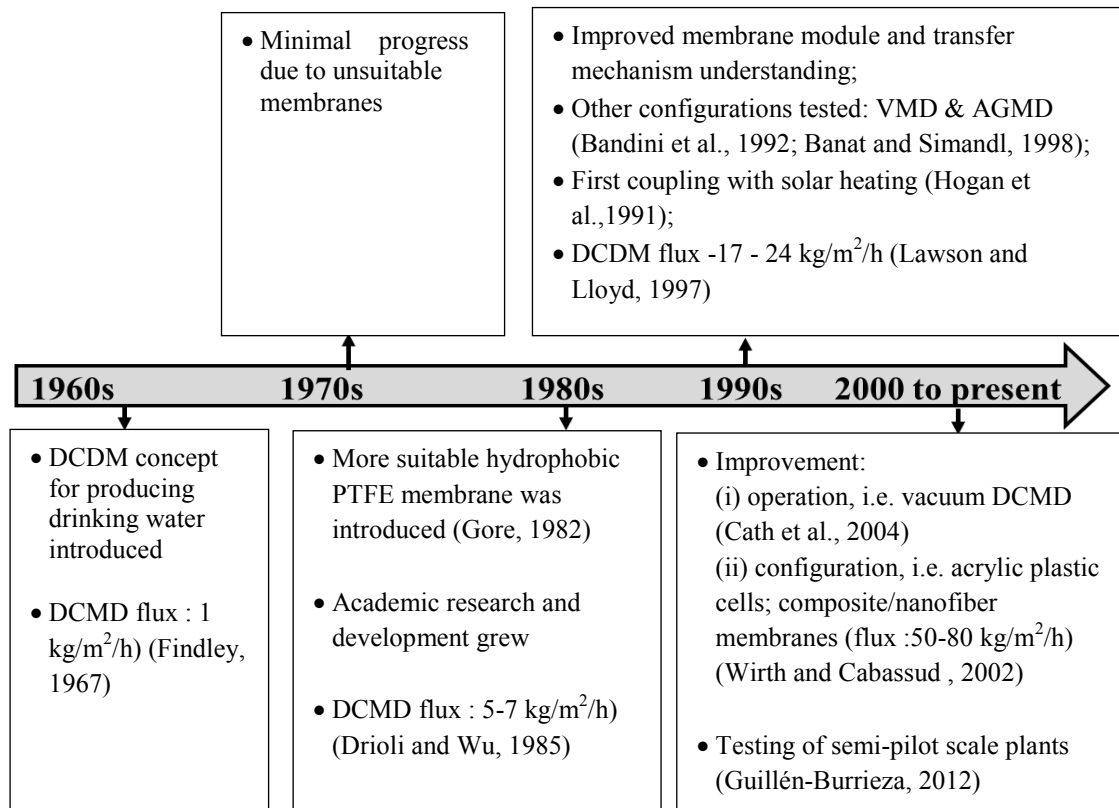
Figure 1.2 Timeline of MD application to the production of drinking water.

1.1.4 Industrial application of MD for drinking water

Widely available research studies in MD have focused on aspects of transport mechanism and membrane fabrication as shown in **Figure 1.2**. These mathematical model concepts provide useful information concerning the heat and mass transfer

mechanism of MD configurations as well as the effect of operating parameters (Banat and Simandl, 1998; Khayet, 2011).

Meanwhile, limited MD studies have explored the feasibility of practical application such as membrane fouling, wetting index and long-term operational outcomes. Specifically, it is essential to evaluate the membrane fouling development in MD in the context of drinking water production. This is because, as a thermal operated system, MD is more susceptible to membrane fouling. Also, MD membrane is in contact with a highly concentrated feed solution to fulfil the expectation of near zero liquid discharge (ZLD).

It is also important to highlight that most MD studies have been carried out using bench scale systems. A bench scale system may not reflect the performance in an industrial level. In fact a semi-pilot scale AGMD system highlighted that the results obtained from theoretical calculations and lab scale experiments were not reflective of the semi-pilot scale results (Guillén-Burrieza et al., 2012). This study recommended more research to focus on scaled-up MD systems as an important factor in successful MD industrial implementation. In another study, a pilot plant operation's DCMD performance was conducted for 3 months with satisfactory results of 15 to 33 $kg/m^2/h$ permeate flux. However, this study reported reduction of the membrane's hydrophobicity upon exposure to salt solutions at high temperature and recommended further studies with scaled-up units (Song et al., 2008).

Due to these factors, although the potential of MD in water treatment has been recognized worldwide, it has yet to be widely implemented in the water industry.

1.1.5   Membrane scaling and fouling phenomena in MD

Fouling is a problem common to all types of membrane processes. In the fouling phenomenon, constituents in feed water that are retained on the membrane surface or in the membrane pores are called foulants, i.e. precipitations of organic and inorganic matter or biofilm (Shirazi et al., 2010). Due to fouling, the productivity of the membrane process will decline, product quality decreases and ultimately membrane life span is shortened, incurring additional operational costs. Hence, a more detailed understanding and control of membrane fouling is essential.

In MD studies, membrane fouling is considered less significant mainly due to the vapour pressure application in comparison to hydraulic pressure application of the RO membrane system. However, fouling is a complex phenomenon and is influenced by several factors, such as feedwater and membrane characteristics and operating conditions (Goosen et al., 2005). The study by Gryta (2000) was one of the initial MD drinking water application studies that acknowledged the presence of membrane fouling. In MD processes aimed at treating highly saline and concentrated feed solutions to almost ZLD, the sparing salts and foulants deposited on the membrane could be severe as suggested by some MD studies (Tun et al., 2005). For instance, Karakulski and Gryta (2005) observed the precipitation of $CaCO_3$ onto the MD membrane surface with concentrated tap water. Additionally, the thermal application in MD has been demonstrated to increase the scaling intensity due to inverse solubility of certain salts (Song et al., 2008). Hsu et al. (2002) reported permeate flux decline with seawater, linking the thermal application to membrane fouling in MD. Similarly, studies have also observed more intense membrane deposition of protein-based natural organic compound under MD thermal conditions (Gryta et al., 2001).

The relationship between membrane hydrophobicity and fouling development in MD has been investigated. For instance, one study pointed out that membranes with higher hydrophobicity exhibited a more severe fouling pattern (Khayet et al., 2004). As a consequence, a membrane may lose its separation properties and wetting will occur. Wetting in MD happens when the liquid-vapour equilibrium pressure at the entrance of the membrane is exceeded. In MD the pressure at which the liquid penetrates into the membrane is defined as the liquid entry pressure (García-Payo et al., 2000; Franken et al., 1987). Nevertheless, detailed studies on MD fouling phenomena associated with membrane hydrophobicity and wetting still lack depth (Srisurichan et al., 2005).

In terms of biofouling development, a recent hollow fibre DCMD study observed substantial biofilm formation with seawater, which was attributed to the presence of mixed organics and bacteria. However, biofilm reduction was observed when the feed temperature increased (Krivorot et al., 2011). Nevertheless the development of biofouling in MD must be given due consideration because thermophile bacteria may be present in saline water condition.

Despite the indication of fouling in MD, in-depth analyses of fouling development are still lacking in many MD studies. The lack of understanding on fouling and wetting phenomena in MD and its related mitigation has been cited as one of the main constraints on commercial MD implementation. For this very reason more studies are now focused on this subject. In line with this, the number of published MD papers on the topic of membrane fouling has gradually increased over the past two decades, especially for MD scaling development as shown in **Figure 1.3.**
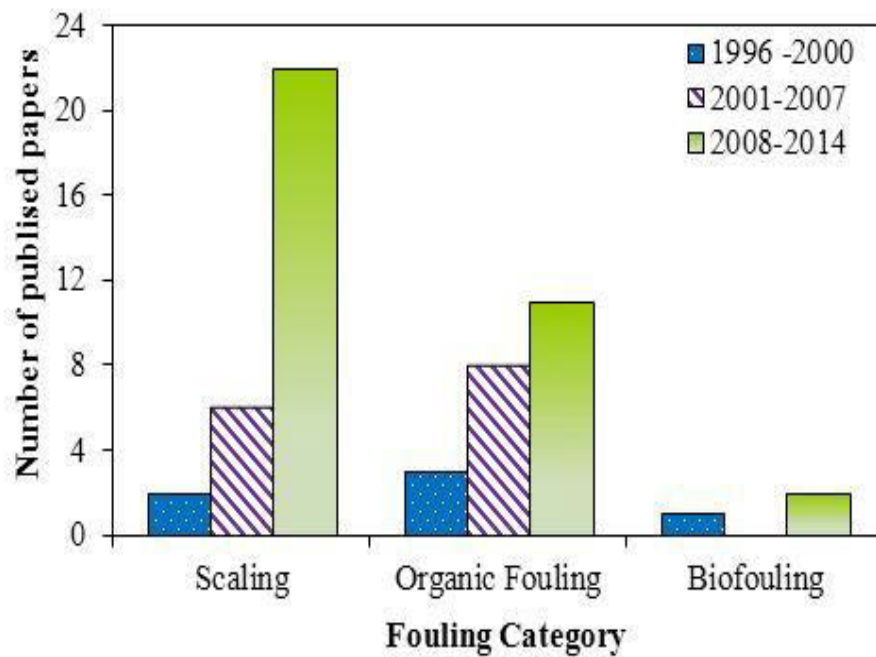
Figure 1.3 Published papers on fouling analysis in MD from 1996 to 2014 (as searched through Scopus).

1.2   RATIONALE OF RESEARCH

1.2.1   Novel modified design VMD system

One of the difficulties constraining MD systems implementation in the production of drinking water is the lack of pilot scale data. Although extensive research is available on the performance of MD systems, they have mostly been carried out on bench-scale equipment with small membrane areas. Research using small-scale equipment may not be able to represent what happens in real conditions, especially the representation of the polarization effect and the influence of operating parameters on these effects. These are important factors for estimating the water production rate of a pilot scale application. Such aspects can be achieved effectively on scaled-up equipment.

Most studies on MD have concentrated on DCMD configuration due to its simple configuration with condensation taking place within the system. Nevertheless, the direct contact element results in more heat loss by conduction in the membrane. The MD

energy efficiency data projected from DCMD bench scale systems constitutes a barrier for the lack of MD industrial implementation. The VMD configuration incorporated with vacuum pressure on the permeate side (higher driving force) promises more potential in achieving greater flux with reduced conduction heat loss. One of the limitations of general VMD system design is the requirement for external condensation, resulting in heat loss as vapour produced is condensed outside the module. This limitation can be mitigated by incorporating internal condensation as well as internal heating, thus enabling heat recovery. Furthermore, a multi-stage effect design is possible in a VMD configuration because of the higher vapour pressure difference from the permeate vacuum pressure. This enables a reasonable distribution of vapour pressure in each stage. The multi-stage design will increase the production rate and requires only a reasonable amount of heating and cooling energy (Zhao et al., 2013).

Ultimately, the feasibility of a new technology depends on whether it can demonstrate its advantages in a specific area compared to existing technologies.

1.2.2 Analysis of Membrane Fouling Phenomena in MD

Despite the available information in MD literature, fouling in MD has garnered the least amount of research attention in MD studies. The presence of membrane fouling in MD has been acknowledged, specifically in processes aimed at treating highly saline and concentrated feed solutions. Both inorganic salt and natural organic matter (NOM) have been identified as major foulants in MD (Gryta, 2008b). Nevertheless, we still lack detailed understanding of specific correlations such as the influence of operating parameters on the fouling pattern in MD. This is especially relevant for MD that employs a combination of both hydrodynamic flow rate and thermal heating as operating parameters.

NOM represents a combination of various components, mainly proteins (biopolymer), polysaccharides, humic substances and low molecular weight (LMW) organics (Huber et al., 2011). During the treatment process these substances interact with the membrane in a variety of ways. Due to the complexity of fouling phenomenon, detailed studies on individual NOM fouling patterns on the MD hydrophobic membrane have been investigated. Additionally, the influence of the thermal operation in MD on the foulant characteristics has not been analysed in detail.

Fundamental information on the characteristics of major organic compounds and a quantitative assessment of their content is required in order for their removal mechanisms to be properly assessed. Then the appropriate fouling control strategies can be recommended. Fouled membranes can be cleaned if the fouling is reversible. However, irreversible fouling can also occur. The effect of hydrophobicity and membrane wetting must be given due consideration in any MD operation. Permanently fouled or chemically degraded membranes must be replaced. Membranes form a significant operational expense in that they have to be replaced from time to time.

1.2.3   Practical approaches for fouling mitigation in MD

Apart from a detailed understanding of membrane fouling in MD operations, practical approaches to mitigating and controlling membrane fouling in MD must be given due consideration. Control approaches such as pretreatment may incur additional costs and chemical usage (Karakulski et al., 2002; Karakulski and Gryta, 2005). Hence employing an appropriate sustainable pretreatment strategy is critical to enhancing the performance of MD operations.

1.3   OUTLINE (STRUCTURE) OF THIS STUDY

In this thesis, a novel modified scaled-up VMD design was studied. Memsys developed this commercial MD system that combines the advantages of multi-effects and vacuum to achieve a highly efficient system. For easy reference, the term 'one-stage vacuum multi-effect membrane distillation (V-MEMD)' was employed to represent this VMD system described in the following sections. This study used the V-MEMD system where the objective was to evaluate the scaled-up performance of MD. This system is also incorporated with internal heating and cooling**]**, making it possible to achieve a more energy efficient MD system. The performance of the V-MEMD was assessed under different operating conditions with high saline water, experimentally and through modeling data.

This study also aims to fill in the knowledge gap on the aspects of membrane fouling in MD. For this purpose, a detail membrane fouling analysis was carried out. Apart from the V-MEMD system, a bench scale DCMD system was employed to achieve the objectives of this study. The V-MEMD system was primarily used to reflect the performance of an MD system with enhanced features. Meanwhile, the scaling and fouling analysis was mainly conduced with the bench scale DCMD system using the same flat sheet membrane as the V-MEMD system. This enabled detail membrane autopsy analysis to be carried out using a quantitative methodology that represents the fouling intensity of the various foulants in the feed solution. **Figure 1.4** shows how the chapters in this thesis are organized.

Chapter 2 (literature review) presents a detailed review of MD application in drinking water production for small communities. This chapter contains: (i) the background and historical development of MD and related transport mechanisms; (ii) advantages and

challenges of MD application in drinking water production; (iii) MD organic fouling and scaling observations; and (iv) MD fouling reduction approaches. More specific details are presented in the following chapters (**Chapters 4 to 7**).
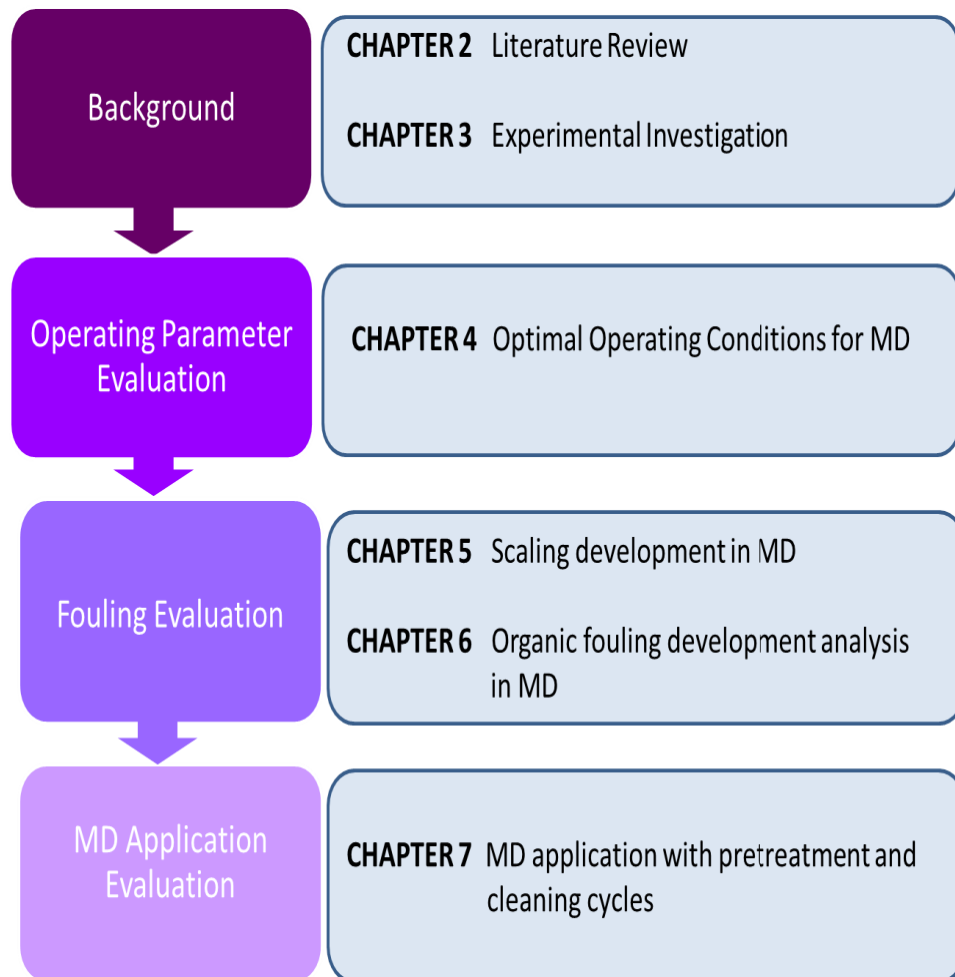
Figure 1.4 Outline (structure) of this thesis.

Chapter 3 encompasses the general experimental investigation used in this study. This includes basic materials, methods and experimental analyses. The descriptions of specific experimental and analytical methods are located in the respective chapters (**Chapters 4 and 7**).

Chapter 4 evaluates the influence of operating parameters on the performance of the V-MEMD and DCMD system, presented in three sections. In the first two sections, the V-

MEMD performance in terms of permeate flux and the effect of polarization was studied through the experimental and modelling approach These two sections contain: (i) baseline study to represent the relationship of different operating parameters on the performance of the V-MEMD system; and (ii) performance of V-MEMD with high saline water. The third section describes how well the DCMD systems functioned in terms of suitable feed and permeate velocity combinations.

Chapter 5 evaluates the scaling pattern in MD, primarily gypsum scaling development in the V-MEMD and DCMD systems. A detailed analysis of the influence of operating conditions on the scaling development was carried out. Membrane autopsy was also conducted to understand the factors influencing the scaling pattern in MD.

Chapter 6 evaluates the organic fouling pattern in MD. The contribution of different types of organic compounds in the feed water (humic substances, polysaccharide and protein) as well as physico-chemical condition of the feed solution on MD fouling development was evaluated. The organic fouling pattern was analysed in terms of permeate flux, organic characterization, membrane hydrophobicity and membrane autopsy.

Chapter 7 presents the performance analysis of two chemical-free pretreatment systems for organic removal efficiency. The performance of MD with pretreatment was analysed. Also, the suitable membrane cleaning cycles for practical MD performance application on site was discussed.

Chapter 8 presents the conclusions and recommendations based on this study. Additionally, **Chapter 4** to **7** contains short summaries of specific findings at the end of the chapters

CHAPTER 2

LITERATURE REVIEW

University of Technology Sydney

Faculty of Engineering & Information Technology

2.1 INTRODUCTION

This chapter presents a general review associated with the application of MD for the production of drinking water. Using a broad perspective, this review describes the context of MD applied to drinking water production, its advantages and its limitations. Specifically, this review focuses on the scaling and organic fouling development in MD. The influence of feed solution characteristics and operational parameters on MD fouling and related areas requiring future investigations are discussed. Furthermore, the study highlights a number of approaches on fouling reduction in MD. A detailed review on specific aspects of MD is presented in Chapters 4 to 7.

2.1.1 Background of MD in drinking water production

Presently reverse osmosis (RO) is the fastest growing desalination technology for producing drinking water (Greenlee et al., 2009). Large RO desalination plants in countries such as Israel, Algeria, Australia, Saudi Arabia and Singapore have the capacity to produce drinking water from 300,000 m^3/d up to 500,000 m^3/d (Lee et al., 2011).

Fundamentally, RO operations are built as large centralized desalination plants due to energy recovery capacity in large plants (Elimelech and Phillip, 2011). As such, RO units are suitable for high population density areas. However, numerous low-density population areas located in inland, rural areas lack fresh water, requiring small-scale, stand-alone desalination units. Further, the high brine production due to the osmotic limitation of the RO application in treating brackish, high saline water remains an economic challenge (Greenlee et al., 2009).

Membrane distillation (MD) has emerged as a promising alternative technology option for drinking water production. MD is a thermal integrated membrane process. MD

differs from other membrane technologies as its driving force is vapour pressure of water across the membrane. As a process not restricted by feed solution salinity and operating at low thermal requirements, MD can operate where RO and thermal distillation technology applications are challenged (Alkhudhiri et al., 2012). The potential of MD technology has been acknowledged by several review papers on state-of-the-art treatment technologies associated with renewable energies for seawater and brackish water desalination (Charcosset, 2009; Pe´rez-Gonza´lez, 2012; Al-Obaidani et al., 2008; Alkhudhiri et al., 2012). It is therefore essential to evaluate the function of MD as a standalone treatment process in remote areas. MD should not be viewed as a substitute for conventional pressure operated membrane treatment technologies. Instead, it plays an important role in filling the gap in existing treatment technologies.

2.1.2 A brief history of MD application for drinking water production

The, history of applying MD to the production of drinking water is shown in **Figure 1.2** (see Chapter 1). The pioneer MD study for the purpose of drinking water production from seawater was conducted as early as 1964. This study reported a low production rate of 1 kg/m^2/h (Findley, 1967). Following this, a few early investigations acknowledged the potential application of MD for the production of high purity water through the process of desalination (Drioli et al., 1987; Andersson et al., 1985; Schofield et al., 1987). Interest in this area advanced further due to the development of Gore's MD membrane for desalting NaCl solutions (Gore, 1982). In addition, more work was undertaken on the experimental and theoretical concept of transport mechanism in MD for seawater desalination (Schofield et al., 1987; Kimura et al., 1987).

The first study on conventional direct contact MD (DCMD) set-up reported a permeate flux in the range of 5 to 7 kg/m^2/h with seawater as feed solution (Drioli and Wu, 1985).

By late 1990s, MD studies indicated the feasibility of working at high permeate flux, ranging from 17 to 24 kg/m^2/h (Lawson and Lloyd, 1996; Martinez-Diez et al., 1999). The increased permeate flux was attributed to improved membrane module and understanding on heat and mass transfer mechanisms coupled with operating at suitable conditions. It is also worth highlighting that during this period, the first study on the coupling of solar energy with MD was tested by Hogan et al. (1991) using a hollow fibre membrane at a production rate of 17 L/day/m^2. Further, detailed literature reviews of MD configurations became available (Lawson and Lloyd, 1997).

In recent times, further enhancement such as higher operating cross-flow velocity, the use of acrylic plastic as membrane cell construction material and the utilization of composite membranes with very thin active layers led to permeate flux as high as 50-80 kg/m^2/h (Cath et al., 2004). Apart from DCMD the performances of other MD configurations (air gap membrane distillation (AGMD), sweeping gas membrane distillation (SGMD) and vacuum membrane distillation (VMD) have been explored for their suitability in producing drinking water. For instance, the VMD configuration was analysed by a number of researchers who reported promising results for seawater desalination (Lawson and Lloyd, 1996; Bandini et al., 1992; Li and Sirkar, 2005). The incorporation of vacuum in the VMD configuration led to achieving a high flux in the range of 12-16 kg/m^2/h through the usage of vacuum while maintaining lower polarization due to the negligible presence of a boundary layer on the permeate side (Safavi and Mohammadi, 2009; Khayet, 2011). Meanwhile, the AGMD configuration has also been evaluated in seawater desalination research. The AGMD configuration has an additional air gap interposed between the membrane and the condensation surface. Although heat loss by conduction is reduced by higher heat and mass transfer resistances, the penalty is flux reduction. For example, Hsu et al. (2002) found that the

permeate flux produced by DCMD was higher than that produced by AGMD (5 to 6 kg/m^2/h).

Presently, a number of semi-pilot scale plants and pilot scale plants have been examined for the production of drinking water. For instance, Guillén-Burrieza (2012) reported a positive outcome from a two-year testing of pre-commercial Keppel Seghers AGMD desalination modules. Meanwhile Gabsi and Chehbouni (2013) investigated the feasibility of a solar integrated VMD configuration for seawater desalination in Mahares, Tunisia. Similarly, Banat and Jwaied (2010) observed the performance of an autonomous solar-powered membrane distillation with seawater desalination for one year (average of 800 L/d) and highlighted the plant's potential in providing remote coastal areas with clean drinking water. In this regard, Zhao et al. (2013) reported on the development of a modified design pilot scale VMD system by MemSYS. MemSYS designed its commercial novel unit to incorporate internal heating, enabling it to operate at a low range of feed temperatures between 45ºC to 60ºC. The solar driven MemSYS VMD system was evaluated for seawater desalination; it performed well with an average permeate flux at approximately 7 LMH on a sunny day. Testing the pilot scale plants reflects the emergence of MD as a new and key technology.

2.1.3 Advantages of MD technology for drinking water production

MD has a number of attractive features that make it a versatile alternative technology for producing drinking water for inland communities. The feasibility of a new technology will ultimately depend on whether it provides significant advantages over existing technologies. The advantages of MD technology are presented in **Table 2.1**.

Table 2.1 Advantages of MD technology

Advantages	Description	Related studies
Salinity treatment	Ability to treat highly concentrated salt solutions (i.e. seawater and saline brackish groundwater) as the driving force (vapour pressure) is minimally affected by high salinity.	(i) Martinez-Diez,and Florido-Diaz (2001); Cath et al. (2004) DCMD operated at 100 to 300 g/L of NaCl showed only a 13 to 20% flux reduction (ii) Mericq et al. (2010) VMD with RO brine concentrated from 64 g/L to 300 g/L showed minimal effect of CP with 17 LMH flux. (iii) Safavi and Mohammadi (2009) VMD achieved 14.4 LMH flux at 100 g/L NaCl with minimal flux decline
High quality distillate	Phase separation enables high quality distillate; reliable for drinking water production in small communities. Drawback of existing *in situ* desalination (ISD-combination of RO membrane and bore pump) is inconsistent water quality	(i) Mericq et al. (2009) VMD using RO brine feed with high TDS (40 to 50 mS/cm)was able to maintain high salt rejection (99 to 100%,) with high quality permeate (10 to 40 µS/cm) (ii) Hsu et al. (2002); Banat and Jwaied (2010) Reported good quality distillate production with TDS less than 40 µS/cm using saline brackish groundwater and seawater
Small footprint with compact standalone design	Designed as stand-alone compact units	(i) Alklaibi and Lior (2005) Significantly smaller MD operation (0.01 m membrane cell height) with 40% higher production rate compared to traditional thermal distillation (4 to 6 m stage height). (ii) Guillén-Burrieza et al. (2012) Small footprint with multi-stage concept in MD that also makes heat recovery possible.
Simple operational maintenance	Minimal maintenance requirement compared to traditional methods such as multimedia filters used in inland areas	(i) Pe´rez-Gonza´lez et al. (2012) Costly brine treatment not required with supersaturated feed concentrate MD. (ii) Curcio et al. (2001); Tun et al. (2005); Ji et al. (2010) MD incorporated with crystallization achieves zero liquid discharge (ZLD)
Integration with renewable	Less thermal requirement compared to traditional distillation system, giving MD	(i) Cabassud and Wirth (2003) Hollow fibre VMD coupled with solar energy can compete with RO for high saline water treatment.

energy	the advantage of being coupled with low grade waste or solar system.	(ii) Koschikowski et al. (2003) Acknowledged MD potential as low maintenance solar desalination systems for remote areas.
		(iii) Banat and Jwaied (2010); Gabsi and Chehbouni (2013) Positive results of solar MD application in semi-pilot scale and pilot scale studies
		(iv) Qtaishat and Banat (2013) Small scale solar MD for drinking water production in remote areas lacking water and electricity facilities.
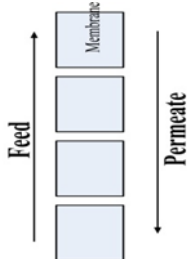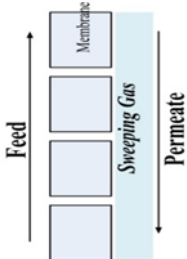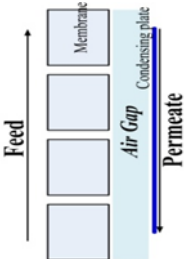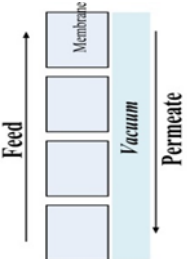
2.2   FUNDAMENTALS OF MD

2.2.1   MD configurations

In all four MD configurations (DCDM, AGMD, SGMD and VMD), the feed solution will be in direct contact with the feed side membrane. The hydrophobic nature of the membrane creates a surface tension force that prevents liquid solutions from entering the membrane pores. Hence, a liquid/vapour interface is formed at the entrance of the membrane pores. The membrane pores should remain dry throughout the MD operation. The MD configuration differs based on the nature of the cold side processing of the permeate as described in **Table 2.2**.

Table 2.2 MD configuration description

Configuration	DCMD	SGMD	AGMD	VMD
Permeate side setting	Cooling water (internal condensation)	Cold sweeping gas (external condensation)	Air gap with condensing plate (internal condensation)	Vacuum (external condensation)
Primary Transport Mechanism	Molecular and Knudsen diffusion	Molecular diffusion	Molecular diffusion	Knudsen diffusion
Main advantage	Simple structure	Lower heat loss than DCMD	Recoverable latent heat	High flux
Main Disadvantage	High heat loss	Additional equipment	Lowest flux due to resistance	Risk of membrane wetting, additional equipment

2.2.2 Transfer mechanism

The MD process involves both heat and mass transfer mechanisms as shown in **Figure 2.1**. Since the 1980s many studies have been dedicated to analysing the fundamentals of MD transfer mechanism (Schofield et al., 1987; Kimura et al., 1987; Schofield et al., 1990; Banat and Simandl, 1994; Martínez-Díez and Vázquez-Gonzàlez, 1996; Lawson and Lloyd, 1997; Imdakm and Matsuura, 2004; Khayet, 2011). These theories and model simulations made important contributions to our understanding of the MD process.
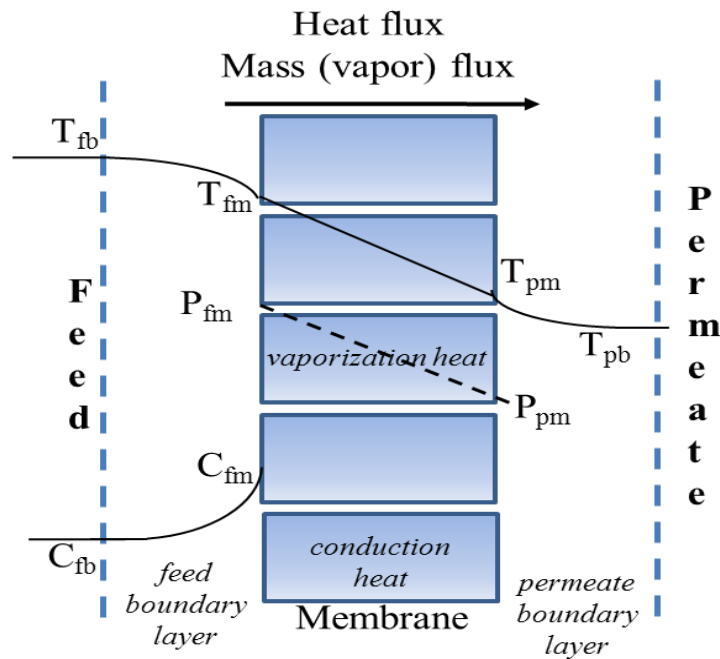
Figure 2.1 Schematic diagram of heat and mass transfer in MD

2.2.2.1 Mass transfer

2.2.2.1.1 Mass transfer across the membrane

In MD membranes the mass transport across the membrane pores are governed by the Knudsen flow model, Poiseuille flow model (viscous), molecular diffusion model or the combination of them, known as the transition model.

The dusty gas model is generally adopted for representing the MD mass transfer operation regardless of the mass transport mechanism. This model was first applied to describe the MD transfer by Lawson and Lloyd (1997). The model is based on the membrane surface vapour pressure difference in the feed and permeate side (ΔP) as the driving force. Hence, when water is transported through the membrane, the water vapour flux, J_w is expressed as follows (Schofield et al., 1987; Khayet, 2011):

$$J_w = B\Delta P = P_{fm}\left(T_{fm,} C_{fm}\right) - P_{pm}\left(T_{pm}\right) \tag{2.1}$$

where, B is the MD coefficient of the membrane, P_{fm} and P_{pm} is the water vapour pressure on the membrane surface in the feed and permeate side, T_{fm} and T_{pm} are the membrane surface feed and permeate temperature, and C_{fm} is the solute concentration on the membrane surface in the feed side. The water vapour pressure on the membrane surface, P_m can be related to the feed and permeate temperature (in K) and feed solution concentration (in g/kg). The vapour pressure can be determined using Antoine's equation (Banat and Simandl, 1994; Khayet, 2011).

The MD membrane coefficient, B to suit the respective MD configuration, is determined using the Knudsen number (Kn) which is the ratio of the mean free path, λ, of the transported molecules to the pore size, r (Lawson and Lloyd, 1997; Khayet 2011).

2.2.2.1.2 Mass transfer through the feed side boundary

Generally, the film theory model is used to express the mass transfer through the feed side boundary (liquid phase). The relationship between flux, flux, J_w, the mass transfer coefficient, k_w, and the solution concentrations, C, at various locations is as follows (Lawson and Lloyd, 1997):

$$\frac{J_w}{mk_w} = ln\left[\frac{C_{fm} - C_p}{C_{fb} - C_p}\right] \hspace{4cm} (2.2)$$

where m is the molar concentration in the liquid phase, mol/m^3, k_w is the mass transfer coefficient.

The mass transfer coefficient, k_w is usually determined by the mass transfer empirical correlations. This is related to the Sherwood number (Sh) and Schmidt number (Sc). The empirical correlations are applied based on the turbulent, transition and laminar flow ranges based on the Re value (Lawson and Lloyd, 1997; Bandini and Sarti, 1999; Banat and Simandl, 1994; Schofield et al., 1987; Mengual et al., 2004).

2.2.2.2 Heat transfer

In an MD system, heat transfer occurs through latent heat transfer and conduction heat transfer as shown in **Figure 2.1** (Khayet, 2011).

The presence of a boundary layer at the membrane surface results in a lower temperature at the membrane surface, T_m, compared to the corresponding value at the feed temperature, T_f. For different configurations, the heat transfer differs based on the resistance to the heat transfer on the permeate side. For instance, referring to the VMD configuration, the conductive heat across the membrane is negligible due to the low pressure on the permeate side of the membrane (Bandini and Sarti, 1999). Khayet (2011) represented the heat transfer through the feed boundary layer-membrane-permeate boundary layer by a global heat transfer coefficient as shown in Eq (2.3) below:

$$h_{w,f}\left(T_{fb} - T_{fm}\right) = \frac{k_m}{\delta}\left(T_{fb} - T_{fm}\right) + \sum_i J_i\, \Delta H_{v,i} = h_{w,p}\left(T_{pm} - T_{pb}\right) \qquad (2.3)$$

$$= H\left(T_{fb} - T_{pb}\right)$$

where, ΔH_v is the latent heat of vaporization, H is the global heat transfer coefficient of the MD process, T_{fm}, T_{pm}, T_{fb} and T_{pb} are membrane surface temperatures and fluid bulk temperatures at the feed and permeate side, k_m is the thermal conductivity of the membrane, $h_{w,f}$ and $h_{w,p}$ are the heat transfer coefficient in the feed and permeate boundary layers, respectively. Similar to the mass transfer coefficient, the MD heat transfer coefficient is usually estimated from the heat transfer empirical correlation of the Nusselt number (Nu) and the Prandtl number (Pr).

2.2.2.3 Polarization Effect in MD

In an MD system, when mass transfer of non-volatile salt occurs, a separation process takes place. Over time the concentration of salt at the membrane surface becomes higher than that at the bulk feed, creating a concentration gradient (El-Bourawi et al., 2006). This is the effect of concentration polarization (CP). Based on the film theory, the CP can be represented as Eq (2.4) below for feed aqueous solution containing non-volatile solutes (Khayet, 2011):

$$\frac{C_m}{C_f} = exp\left(\frac{J_w}{k_w}\right) \qquad (2.4)$$

where, C_f is the concentration in the bulk feed solution and k_w is the mass transfer coefficient. As explained in **Section 2.2.2.1.2**, k_w, can be calculated by the relationship of the dimensionless numbers.

Meanwhile, the mass transfer in MD is based on phase change, whereby the latent heat of vaporization must be converted from the feed temperature. Consequently a lower

temperature is formed at the boundary layer of the feed side membrane, creating a temperature difference. This is the effect of temperature polarization (TP) (Martínez-Díez et al., 1999). TP is generally defined as the difference of the transmembrane feed temperature to the bulk feed temperature represented as Eq (2.5) below (Martínez-Díez et al., 1999; Khayet, 2011, Lawson and Lloyd, 1997).

$$\tau = \frac{T_{fm} - T_{pm}}{T_{fb} - T_{pb}} \qquad (2.5)$$

It is important to highlight that for certain configurations, the polarization representation may differ slightly. For instance, for the VMD configuration, the permeate side effect would not be applicable due to the application of vacuum in the permeate side.

2.2.2.3.1   Implication of polarization effect in MD

Polarization effect has been acknowledged since MD investigations began as a major phenomenon that reduces the efficiency of MD operation, (Schofield et al., 1987; Lawson and Lloyd, 1997). The critical implication of the polarization effect in MD is the loss of driving force due to concentration and thermal gradients in the membrane boundary layer. In MD, the CP effect is considered to be less significant compared to the TP effect because MD is a thermally driven membrane process (Khayet et al., 2004; Martínez-Díez and Vázquez-González, 1998; Martínez-Díez et al., 1999; Schofield et al., 1990). A number of studies have established that the polarization effect in MD can be reduced by firstly, the appropriate operation parameter conditions and secondly, MD configurations as shown in **Table 2.3.** On the other hand, the implication of these choices must be given due consideration. Hence, a balanced compromise must be made between maintaining a reasonable flux, while minimizing TP and CP effect and membrane wetting.

Table 2.3 Polarization reduction strategy with different operational settings

Operating settings	Polarization reduction strategy	Implication for operating performance	Reference
Feed temperature	Reduce feed temperature - lower thermal loss at membrane surface	Reduced permeate flux	Phattaranawik et al., 2003; Laganà et al., 2000; Martínez-Díez et al., 1999.
Flow velocity	Increase flow velocity - higher heat and mass transfer reduces boundary layer thickness	Higher risk of wetting	Schofield et al., 1990; Ortiz-Zárate et al., 1991; Martínez-Díez, and Vázquez-González, 1996; Gryta, 2000; Cath et al., 2004.
MD configurations	Substitute DCMD to VMD (vacuum) or SGMD (gas)- less conduction heat loss	Additional equipment required	Lawson and Lloyd, 1997; El-Bourawi et al., 2006.

2.3   CHALLENGES OF MD TECHNOLOGY FOR DRINKING WATER PRODUCTION

2.3.1   Lack of commercial application

Although MD was introduced in the 1960s its commercial application is still limited because other technologies have been more successful (Alkhudhiri et al., 2012). In recent times a few companies have produced commercial units. These include modified design AGMD modules developed by Fraunhofer Institute for Solar Energy System (ISE) in Germany, TNO (Netherlands Organisation for Applied Scientific Research) and Keppel Seghers in Belgium as well as Scarab AB (MEDOSOL project). Meanwhile, MemSYS Germany developed a modified VMD system. The performance of these pilot units are still being explored on a trial testing basis.

2.3.2   Cost and energy efficiency

MD as a thermal process is energy intensive. Therefore, the energy consumption and its related cost is still a challenge compared to membrane processes such as RO (Al-Obaidani et al., 2008). For instance, an estimate of the water production cost of MD system was done by Walton et al. (2004), in which it was assumed the capital cost was the same as the seawater RO system. The estimated total water production cost of MD was $0.815/m^3 which was much higher compared to RO at $0.375/m^3. Similarly, Li and Sirkar (2004) estimated the total production cost of water using the DCMD process to be $0.78/m^3. Some studies have highlighted that MD process can be more competitive than RO process with the usage of alternative energy such as solar system or if the water source is a challenge to be treated with RO system (Alklaibi and Lior, 2005). Nevertheless, the additional capital cost of solar modules and solar collectors must be given due consideration (Qtaishat and Banat, 2013).

2.3.3   Fouling development in MD related to drinking water production

Despite the promising potential of MD in the production of drinking water, the evidence of membrane fouling development in MD is a major concern. The work of Hsu et al. (2002) was one of the initial DCMD studies on drinking water production with seawater that reported permeate flux decline was attributable to fouling. The study highlighted the susceptibility of MD operations to membrane fouling due to thermal application. In two other studies, MD's performance in producing high purity water was evaluated with tap water and these studies observed precipitation of $CaCO_3$ onto the membrane surface (Karakulski et al., 2002; Karakulski and Gryta, 2005). A long-term DCMD study (for 100 days) with actual seawater reported a permeate flux decline from 23.8 LMH to 14.4 LMH after 30 days of operation and observed membrane fouling due to inorganic scalants (He et al., 2011). More recently, Shirazi et al. (2012) carried out a long-term

study to evaluate the feasibility of DCMD as a stand-alone seawater desalination process. After 240 h, the study observed a sharp decrease in permeate flux from around 47 LMH to 37 LMH and the study attributed this to scale formation on the membrane surface. Although the challenges associated with fouling are evident from these MD studies, detailed investigation is still lacking in this area. The lack of understanding the development of membrane fouling is one of the key constraints to the prospective commercial application of MD. The following sections will focus on phenomena associated with fouling in MD.

2.4 FOULING PHENOMENA

This section is directed towards understanding the fouling phenomenon in MD by reviewing existing studies. Specifically, this section focuses on the factors influencing organic fouling and scaling development in MD, to draw a relationship between operating parameters and fouling development in MD. An understanding on the influencing factors will make possible the best recommendations for implementing an appropriate mitigation strategy.

2.4.1 Background of fouling

The term 'fouling' is a phenomenon common to all types of membrane processes resulting in the loss of membrane performance. It is a challenge to precisely define membrane fouling as it is an extremely complex phenomenon. In general, during membrane filtration operation, feed solution being transported across the membrane results in the accumulation of foulants (particles and dissolved components) on or inside the membrane. As a consequence, the permeate flux declines with constant operating parameters implying the occurrence of membrane fouling.

According to Vrouwenvelder, and Van der Kooij (2001), it is essential to diagnose the type of fouling to understand the fouling phenomena. In a number of water and wastewater treatment studies, the main fouling categories are classified as organic, inorganic, biological and particular/colloidal fouling, based on the foulant type (Baker and Dudley, 1998; Amy, 2008; Li et al., 2011; Shirazi et al., 2010). The main fouling categories are summarized in **Table 2.4**.

Table 2.4 Description of fouling categories.

Category of fouling			
Particle fouling	**Scaling**	**Organic**	**Biofouling**
Type of foulant	Type of foulant	Type of foulant	Type of foulant
Suspended solids/larger particles as well as smaller particles and metal hydroxide in source water	High concentrations of inorganic salts in the source water	Natural organic matter (NOM) in the source waters.	Aquatic organisms, such as fungi, microorganisms, and algae in the source water
General Description	General Description	General Description	General Description
Fouling occurs due to the accumulation of particles on the membrane surface and inside the membrane pores, forming a cake layer	Fouling occurs because precipitation deposits cause membrane crystallization and bulk crystallization	Fouling occurs through adsorption of NOM compounds on the membrane, causing gel formation of macromolecular substances.	Fouling occurs when biofilm forms on the membrane

2.4.2 Fouling development in MD

In pressure driven membrane processes, scaling and organic fouling layer on the membrane surface is largely attributable to compaction due to hydraulic pressure (Goosen et al., 2005; Lee et al., 2010). On the other hand, due to the application of vapour operation and the absence of hydraulic pressure, membrane fouling in MD is expected to be less severe compared to pressure driven membrane processes. As such,

membrane fouling in MD has not been studied widely in comparison to pressure driven membrane processes such as ultra-filtration (UF), nano-filtration (NF) and RO (Gao et al., 2011; Shirazi et al., 2010; Goosen et al., 2005). In fact, initial MD studies dismissed fouling in MD and linked the permeate flux decline caused by organic juice concentration and bovine serum albumin to the polarization effect only (Calabro et al., 1994; Ortiz de Zárate, 1998). Further, the larger membrane pore size in MD was also associated with minimal fouling/clogging (Lawson and Lloyd, 1997).

In contrast the concentrated feed usage in MD to meet near ZLD discharge, coupled with the thermal application on a hydrophobic membrane makes MD operation susceptible to membrane fouling. On this theme, most MD studies on membrane fouling development focused on scaling and organic fouling. Biofouling in MD has been examined to date by only two studies (Gryta, 2002; Krivorot et al., 2011). Microbial growth was deemed to have minimal influence in MD operation. This is due to the high saline concentrate and thermal condition used in MD.

In terms of the severity of the scaling and organic fouling in MD, some studies have reported only loose deposits on the membrane surface which was reversible through simple flushing (Gryta, 2008b; He et al., 2008; Srisurichan et al., 2006). However, one of the main concerns of fouling in MD is the loss of membrane hydrophobicity. Studies have shown that the deposit layer on the membrane may cause the hydrophobicity loss, which would be further intensified by membrane wetting and membrane pore penetration of the foulants (Alklaibi and Lior, 2005; Gryta, 2002; Gryta, 2007; Tun et al., 2005).

Studies on fouling caused by other membrane processes such as RO, UF and NF have well established the key factors that influence scaling and organic fouling development,

namely operating conditions, physico-chemical properties of the feed solution, as well as membrane and module configuration (Shirazi et al., 2010; Al-Amoudi and Lovitt, 2007). Although there are a few available reviews related to MD fouling, the key factors influencing fouling and scaling development have not been examined explicitly (El-Bourawi et al., 2006; Alkhudhiri et al., 2012; Alklaibi and Lior, 2005).

To improve our understanding of MD fouling regarding drinking water production, this review analyzed the factors influencing organic fouling and scaling in MD based on feed physico-chemical condition and operating conditions.

2.4.3   Factors influencing organic fouling and scaling in MD

2.4.3.1 Physico-chemical condition of the feed solution

The physico-chemical condition of the feed solution is an important aspect that can determine the fouling intensity in a membrane separation process (Goosen et al., 2005). In an MD operation, the consequence of a unique operation combination, namely the presence of a heating condition but the lack of hydraulic pressure compression, will result in selective foulant types exhibiting more pronounced fouling and scaling tendencies. The following sections focus on the influence of the main foulant types in feed solution with reference to drinking water production.

2.4.3.1.1   Influence of foulant type

2.4.3.1.1.1 Scaling

Scaling studies in MD related to drinking water production have predominantly focused on calcium sulphate, $CaSO_4$ (He et al., 2008; Nghiem et al., 2011; Gryta, 2009a) and calcium carbonate $CaCO_3$ (He et al., 2009; Curcio, 2010, Karakulski and Gryta, 2005), while a few studies examined silica (Gilron et al., 2013; Karakulski & Gryta, 2005). $CaSO_4$ and $CaCO_3$ are the main mineral salts in natural water sources. Furthermore

these salts are also inversely soluble at increased temperatures, thus enhancing the rate of precipitation (He et al., 2009).

Comparatively, a number of studies have established $CaSO_4$ as the more dominant scalant in MD (Nghiem and Cath, 2011; He et al., 2008). For instance, Gryta (2009a) conducted a systematic study of the behavior of $CaSO_4$ and $CaCO_3$ scaling in MD. The study reported a severe case of pore flooding and deterioration of the distillate quality due to membrane scaling when saline wastewater containing $CaSO_4$ was used as the feed solution compared to $CaCO_3$. Similarly, in another study, the SEM analysis of a DCMD fouled membrane using tap water showed predominant $CaCO_3$ deposit ion on the membrane surface. Meanwhile, compounds of calcium, sulphur, magnesium and silica had accumulated inside the membrane wall, indicating that these elements contribute to more severe scaling (Gryta, 2008a). A recent study compared the scaling performance with different mineral salts and highlighted that scaling caused by $CaSO_4$ on MD membrane was much more severe than scaling caused by $CaCO_3$ or silica (Nghiem and Cath, 2011).

By contrast, He et al. (2009) observed that in a scaling experiment, $CaSO_4$ crystals were found to be only loosely attached to the inner wall of the glass beaker, with free floating crystals. Meanwhile $CaCO_3$ crystals on the beaker wall were powdery and tightly stuck to the glass beaker surface. This study concluded that $CaCO_3$ crystals under thermal conditions were more adherent and tenacious in nature compared to $CaSO_4$ crystals in MD operation.

2.4.3.1.1.2 Organics

Organic fouling is largely attributed to natural organic matter (NOM) in the feed solution as shown in **Table 2.4**. NOM is ubiquitous in natural waters, classified by a

group of low molecular weight (LMW) to high molecular weight (HMW) organic compounds, and quantified as dissolved organic carbon (DOC). In surface water, ground water and seawater, humic substances are the major constituents of NOM, followed by carbohydrates (including polysaccharides), protein and a variety of acidic and LMW species (Jermann et al., 2007; Yuan and, Zydney, 1999; Huber et al., 2011).

The correlation of membrane fouling intensity based on the composition of NOM in a feed solution, has been studied widely in pressure driven membrane processes. In these studies, polysaccharides are generally represented by alginic acid compound (AA), humic substances are represented by humic acid compound (HA) and protein substances are represented by bovine serum albumin compound (BSA) (Jeong et al., 2013a). It is important to highlight that in these studies, more detailed methods have been employed to represent organic foulants characteristics, specifically the Liquid Chromatography-Organic Carbon Detection (LC-OCD) (Jeong et al., 2013a; Huber et al., 2011).

In MD studies, organic fouling analysis is still limited and primarily based on permeate flux. It is especially essential to understand the detailed characteristics and role of organics (NOM) in membrane fouling under MD operating conditions. This is because organic foulants, which are generally small in size are assumed to cause more significant membrane wetting problems in micro-sized hydrophobic MD pores (Burgoyne and Vahdati, 2000). In terms of size, biopolymers compounds generally range from 10 kDa to 50 kDa; humic substances (HS) are generally in the 0.8 to 1.5 kDa range, while building blocks (BB) are in the 0.5 to 0.8 kDa range, and LMW organics are less than 0.3 kDa (Huber et al., 2011; Jeong et al., 2013a). Based on the available MD studies that have investigated organic fouling, the implications of different organic compounds (AA, HA and BSA) in MD membrane fouling are discussed below.

AA compound: In MD studies, thus far, no clear trend has been drawn concerning the intensity of AA compound on MD organic fouling. In a MD bioreactor study by Phattaranawik et al. (2008), the polysaccharide in the submerged MD bioreactor was observed to result in cake/fouling attachment on the membrane surfaces. Nevertheless, due consideration must be given to the repulsion between the hydrophilic nature of the AA compound and the negatively charged hydrophobic membrane, resulting in less adhesion on the membrane surface as mentioned by a UF study (Jerman et al., 2007).

HA compound : The contribution of HA compound onto organic fouling intensity in MD has been investigated by a few studies (Khayet et al., 2004; Srisurichan et al., 2005; Srisurichan et al., 2006; Curcio et al., 2010). Previous membrane studies such as UF membrane have highlighted that HA compound absorbs more favourably onto hydrophobic membrane (Jucker and Clark, 1994). In fact, a DCMD study analysed HA fouling using two commercial MD membranes observed higher fouling effect on the more hydrophobic membrane (Khayet et al., 2004). This same study demonstrated that membrane cleaning with water flushing after HA fouling experiment in DCMD was not sufficient to recover the initial permeate flux. This suggests that HA fouling could be irreversible in the MD process. Nevertheless, this can only be established when more detailed studies have been done.

BSA compound: The relationship of between BSA foulant and MD membrane fouling intensity was examined by a number of researchers. MD studies acknowledged that feed water containing NOM compounds of proteins showed a strong tendency to deposit on the hydrophobic membrane (Gryta et al., 2001; Gryta, 2008b). These studies indicated that BSA/ protein fouling caused almost 60 to 70% permeate flux decline in MD. The application of high feed temperature (60°C and above) in MD operation was related to

the intensive protein-based NOM fouling (Ortiz de Zárate et al., 1998; Gryta et al., 2001).

It is worth highlighting that most MD studies have represented fouling intensity in terms of the permeate flux declining pattern. A number of other factors such as organic characteristics changes with LC-OCD, membrane autopsy and hydrophobicity, as well as flux reversibility must also be accounted for in determining the severity of the specific organic compound to MD fouling development.

2.4.3.1.2   Influence of pH and ionic strength

The influence of feed solution pH on fouling development in MD has been investigated by only a few studies. In one study, Karakulski and Gryta (2005) highlighted that $CaCO_3$ precipitation on the membrane surface was significantly limited by the acidification of the feed water to pH 4. In another study, Srisurichan et al. (2005) investigated HA fouling pattern at pH solutions of 3 and 7 in a DCMD unit. Their study reported no significant difference in permeate flux. The study, however, did mention that the complexion of HA with Ca^{2+} was affected by solution pH, whereby at pH of 7, a 68.3% precipitation was reduced to 30.1% at pH of 3. Other membrane studies such as RO and UF have indicated the importance of feed solution pH in changing the structure/ and shape of foulant compounds (Jucker and Clark; 1994; Potts et al., 1981; Childress and Elimelech, 1996). To establish the influence of feed solution pH on fouling development under hydrophobic MD operating conditions, more detailed studies must be carried out.

In terms of ionic strength, a few studies observed a slightly higher permeate flux reduction as well as more intense foulant adhesion on the hydrophobic MD membrane in the presence of salt (Khayet and Mengual., 2004; Gryta et al., 2001). For instance,

Khayet and Mengual (2004), observed 4.2% higher permeate flux decline when 0.1 M NaCl was added to the HA compound. More detailed HA characterization analysis will contribute to a better understating of this phenomenon in MD.

2.4.3.2 Operating parameters

The performance efficiency of MD attributed to different operation parameters has been widely investigated experimentally and through a modeling approach (Khayet, 2011). Previous studies have established that the key operating parameters in MD are feed temperature, feed flow rate and permeate side condition such as the presence of vacuum (Criscuoli et al., 2008; El-Bourawi et al., 2006). The effect of MD fouling development on the main operating parameters of feed temperature and feed flow rate is discussed in this section.

2.4.3.2.1 Influence of feed temperature

2.4.3.2.1.1 Scaling

A number of MD fouling studies have acknowledged the increase of scaling intensity due to thermal heating (El-Bourawi et al., 2006; He et al., 2008; Gryta, 2008b; Nghiem and Cath, 2011). Specifically, classical nucleation phenomena, the inversely soluble behaviours of $CaSO_4$ and $CaCO_3$ at increased temperature, have been investigated in MD studies (Partridge and White, 1929; He et al., 2008).

He et al. (2008) used thermodynamic model and experimental results to establish the shorter induction period (217 min to 0 min) for $CaSO_4$ (gypsum) when the temperature was increased from 60ºC to 90ºC. In scaling studies the induction time is defined as the time taken to form detectable crystals (between the creation of supersaturation and the appearance of a new solid phase) (Oh et al., 2009). Similarly, the scaling of $CaCO_3$ increases with feed temperature, whereby under thermal heating, the HCO_3^- ions present

in the feed water decompose, resulting in $CaCO_3$ precipitation on the membrane surface (Gryta, 2008a; Gryta et al., 2006; Drioli et al., 2004; He et al., 2009). **Table 2.5** details the influence of feed temperature on scaling as reported by MD scaling studies.

Table 2.5 Influence of feed temperature on scaling development in MD

Reference	Configuration	Scalant type	Feed temperature, F_t (ºC)	Fouling Impact
Nghiem and Cath (2011)	DCMD	$CaSO_4$	F_t = 40; 50; 60	SEM crystal formation/ induction time 40ºC – thin needles/ long induction time 50ºC – large needles 60ºC – very large needles/ short induction time
He et al. (2008)	DCMD	$CaSO_4$	$F_t = 60; 90$	As F_t increases from 60 to 90ºC, induction period declines from 217 to 0 min.
Gryta (2008a)	DCMD	$CaCO_3$ from tap water	$F_t = 80; 90$	80ºC Induction time = 100 h 90ºC Induction time = 80h
Gryta (2009b)	DCMD	Tap water (alkalinity 2.1 mmol HCO_3/dm^3	$F_t = 80$	SEM image of $CaCO_3$ scale when : (i) membrane surface temperature similar to bulk F_t, : the formation of both aragonite and calcite is observed; (ii) membrane surface temperature less than the bulk F_t :formation of only crystallization of calcite is observed

2.4.3.2.1.2 Organic fouling

In terms of organic fouling, the influence of feed temperature has been linked only to BSA compound (Gryta et al., 2001; Gryta et al., 2006). For instance, wastewater albumin protein as feed solution operated with DCMD at a high feed temperature of 85˚C indicated a significant gel-like formation on the membrane surface and significant flux decline (from 558 to 156 $dm^3/m^2/d$).

HS is one of the major organic compounds in natural water sources used for drinking water production (Jermann et al., 2007). However, the thermal relationship of HS has not been explored in detail in MD studies. This is an important aspect because studies on HS characteristics (using HA compound), have highlighted its tendencies to disaggregate at high temperature (Drastik et al., 2013). In this regard, one MF fouling study indicated that the rate of HA aggregation increased with temperature, resulting in increased fouling development, as observed on the fouled SEM image (Yuan and Zydney, 1999). Thus far, only one MD study on HA fouling indicated that the feed temperature affected the flux decline (Srisurichan et al., 2006). This particular study investigated the fouling phenomenon in MD using HA solution (100 mg/L) containing 3.775 mM $CaCl_2$. The permeation flux was much higher at 70 ˚C than that of 50 ˚C. As a consequence, at 70 ˚C, more amount of HA coagulates were retained at the membrane surface, significantly reducing the induction time.

2.4.3.2.2 Influence of feed flow rate

2.4.3.2.2.1 Scaling

Previous MD studies have indicated the correlation between scaling development and feed flow rate. Gryta (2008b) highlighted the fact that hydrodynamic conditions significantly influenced the size, structure and morphology of scale formation. The study indicated that a porous thin deposit was formed at high feed flow velocity (e.g. 1.2 m/s), reduced heat transfer resistance on the membrane, while a non-porous and thick deposit was formed at low feed flow velocity (e.g. 0.35 m/s). Similarly, He et al. (2008) recommended a high flow velocity for reducing the flux decline in the presence of a significant amount of precipitate in their MD study using hollow fibre membrane. Nghiem and Cath (2011) used high feed flow velocity as a mitigation strategy of membrane surface crystallization of $CaSO_4$.

In pressure driven membrane separation processes, optimizing hydrodynamic conditions is a general approach to control fouling (Goosen et al., 2005). Similarly, in MD studies, high flow velocity will reduce the loose crystal deposit that has accumulated on the membrane surface. However, it is important to point out that in MD, the pressure of high flow velocity will increase the risk to membrane wetting as shown by other studies (Zhang et al., 2010).

Hence, more detailed investigations must be carried out on a suitable operating feed flow velocity combination that will achieve sustainable performance while reducing membrane surface deposits and membrane wetting.

2.4.3.2.2.2 Organic fouling

Regarding organic fouling, one DCMD study investigated this phenomenon using HA solution at a concentration of 100 mg/L containing NaCl and $CaCl_2$ as feed (Srisurchan et al., 2005). The study acknowledged the advantage of using high cross-flow velocity to reduce polarization in MD system that directly influences the fouling pattern. However, the study also noted the risk of membrane wetting at high cross-flow velocity. The influence of hydrodynamic effect on organic fouling reduction in MD system has not been explored in detail.

2.5 APPROACHES TO REDUCE FOULING IN MD

2.5.1 Pretreatment

Generally, in any pressure driven membrane processes, a pretreatment of raw feed water is adopted as a fouling reduction strategy (Sutzkover-Gutman and Hasson, 2010). Pretreatment enables to remove undesirable compounds from the raw feed solution, which otherwise could adversely affect the membrane operation and lead to membrane fouling.

Pretreatment is broadly categorized into two types - conventional pretreatment and membrane-based preteatment (Vedavyasan, 2007). Conventional pretreatment technologies includes coagulation, multimedia filter, deep-bed filtration, dissolved air flotation while membrane-based pretreatment methods include nanofiltration (NF), ultrafiltration (UF) and microfiltration (MF). The appropriate pretreatments are selected based on the raw feedwater characteristics (suspended solids, turbidity, organic matters, etc.) and the cost incurred (Prihasto et al., 2009).

The main advantage of conventional pretreatment such as deep-bed filtration is the strategic ability to control organic fouling and biofouling (Halle et al., 2009). Physico-chemical adsorption by the media in the filters coupled with the presence of biological activity can remove dissolved organic matter, thereby reducing membrane fouling. These pretreatments are especially sustainable and cost effective enough to support the production of drinking water in small communities. The main disadvantages of the conventional pretreatment, for instance flocculation are the intensive consumption of chemicals and inconsistency in operation (Teng et al., 2003). At the same time, the requirement of regular backwashing and inconsistent water quality are associated with filter systems (Chua et al., 2003).

Meanwhile, the main advantage of membrane-based pretreatments such MF and UF is performance stability compared to conventional pretreatments (Vedavyasan, 2007). However, the performance of membrane-based pretreatments is compromised when treating feed solution with highly concentrated organic and inorganic compounds. It results in severe membrane fouling and plugging of fibres as observed in a number of studies (Wilf and Schierach, 2001; Brehant et al., 2002).

2.5.1.1 Pretreatment in MD

Studies have evaluated the performance of MD with pretreatment in the fruit juice processing industry (Jiao et al., 2004). Nevertheless, the use of pretreatment in the MD system for the production of drinking water has not been explored in great detail. A few analyses have indicated improved MD permeate flux when using NF, UF and MF membrane pretreatment (Hsu et al., 2002; Karakulski et al., 2002; Karakulski and Gryta, 2005). These studies highlighted that the membrane pretreatment made it possible to produce a continuously good quality of feed water (consistently reduced turbidity and particles). For instance, Hsu et al. (2002) reported permeate flux improved by about 25% when MF pretreated seawater was utilized. Nevertheless their study highlighted that membrane pretreatment did not particularly address the issue of organic removal in the seawater, which in the long-term causes permeate flux decline. Hence, due consideration must be given to the specific purpose of the pretreatment as well as the additional costs incurred.

2.5.2 Advances in technology

Presently, extensive advances in research are leading to MD membranes serving as alternatives to polymeric materials. For instance the performance of MD with ceramic membrane, carbon nanotubes and nanoparticles incorporated membrane have been evaluated (Hendren et al., 2009; Gethard et al., 2012; Cao et al., 2006). These studies

have reported on the beneficial characteristics exhibited by these membranes, such as higher thermal resistance, chemical stability and oxidant tolerance as well as better fouling control. However, fouling evaluations have not been carried out with these membranes. Similarly, nanoparticles in the manufacturing of MD membranes would be able to control membrane wetting and fouling.

Additionally, new modified MD design configurations have been developed by companies such as Keppel, Memstill and MemSYS. These new MD design configurations have incorporated beneficial features that can contribute to less membrane fouling. For instance, MemSYS modified its VMD system, incorporating features such as internal heating and internal cooling that enabled it to operate at lower feed temperatures (Zhao et al., 2013). This helps to reduce membrane fouling that is very much associated with high thermal operation in MD.

2.6   SUMMARY

In summary, MD appears suitable for commercial implementation with its advantages features. In this regards, identification of opportunities that maximise the advantages of MD over competing technologies would be highly pertinent. Research studies should endure to explore in detail a number of areas that would enable to better represent the performance of MD. The summary of MD research gaps is presented in **Table 2.6**.

Based on the MD studies that have been reviewed here and the summarized research gap, this thesis presents a detailed investigation on organic fouling and scaling development in MD. Exploring this research gap would enable to firstly, evaluate the feasibility of MD operation with high concentrated feed solution; and secondly, make recommendations on the best or appropriate mitigation strategy.

Table 2.6 Summary on the research gaps in MD studies

Research Gaps	Description
(i) Scaling and fouling phenomena	Extensive development in the area of MD membrane technology has been explored in recent times. This has led to the contribution of new membranes such as carbon nanotubes, electrospun membranes and others (Gethard et al., 2012; Liao et al., 2014). Nevertheless, the aspects of fouling and scaling intensity are still prematurely represented in MD research studies. More detail fouling phenomena description would enable to provide a more representative performance of present and new MD membranes.
(ii) Membrane maintenance and lifetime	The maintenance and lifetime span of the membrane is an important contributor to the overall production cost in MD operations. MD studies have been carried out on membrane rinsing and chemical cleaning as well as the usage of antiscalant (Gryta & Barancewicz, 2010; He et al., 2009). Nevertheless, the aspect of long term maintenance of membrane hydrophobicity and membrane wetting must be studied in more detail to predict the lifetime span of MD membranes more accurately.
(iii) Alternative energy integration	High thermal consumption is one of the main implementation limitations of MD operation. Utilizing alternative energy is an essential factor to achieve a more sustainable MD operation. In this regard, studies have successfully evaluated MD operation with solar integrations (Gabsi & Chehbouni, 2013; Qtaishat & Banat, 2013). Nevertheless, only few studies have been carried out on the usage alternative energy option such as waste heat (Tay et al., 1996; Xu et al., 2006). This option may be a less costly than solar application in MD.
(iv) MD integration with crystallizers	One of the attractive features of MD operation is the possibility of achieving almost zero liquid discharge. Studies have explored MD-crystallizer performance (Guan et al., 2012; Chen et al., 2014; Tun et al., 2005). More extensive research in this area would enable to contribute towards better designing of MD systems and determining the optimum MD operating conditions. Zero liquid discharge is especially important for inland MD desalination application to minimize brine management. Further, exploring the aspect of mineral recovery with MD-crystallizer integration would be an added value for MD economic benefit.
(v) Pilot scale performance	The performances of MD pilot units are still being explored on a trial testing basis (Zhao et al., 2013; Guillén-Burrieza et al., 2012). More extensive research in this area and long term operation research data would contribute towards more extensive commercialization of MD application.

CHAPTER 3

EXPERIMENTAL

INVESTIGATIONS

University of Technology Sydney

Faculty of Engineering& Information Technology

This chapter presents the details on the experimental materials, experimental methods and experimental analysis adopted for the main investigations of this research. Detailed and specific experimental details used are discussed in **Chapters 4** to **7**.

3.1 EXPERIMENTAL MATERIALS

The main experimental materials used in this study are categorized based on membrane and solution type as shown in **Figure 3.1** below.
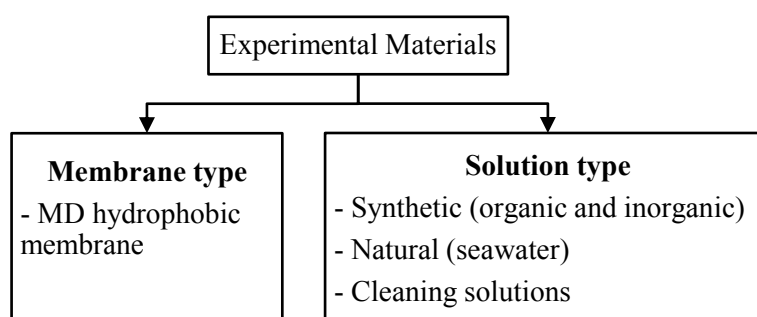
Figure 3.1 Experimental material categories in this study.

3.1.1 Membrane

The MD membrane used in this study was a flat sheet hydrophobic membrane. Details of the membrane characteristics are presented in **Table 3.1**. They were obtained from the manufacturer.

Table 3.1 Characteristics of membrane used in this study.

Material	Polytetrafluoroethylene (PTFE)
Manufacturer	General Electrics, US (GE)
Thickness (δ), ụm	179
Porosity (ε), %	70-75
Mean pore size (r), ụm	0.2

3.1.2   Solutions

3.1.2.1   Synthetic solutions

The synthetic chemical solutions used in this study were categorized into inorganic chemicals and organic chemicals as shown in **Figure 3.1**.

3.1.2.1.1   Inorganic chemicals

The inorganic chemicals were used to represent the major scalants in natural water sources as shown in **Table 3.2**.

Table 3.2 Inorganic chemical solutions used in this study.

Generic Name	Chemical Name	Chemcial Formula	Purity (%)	Supplier
Salt	Sodium Chloride	NaCl	99	Sigma Aldrich
Gypsum	Calcium Sulphate Dihydrate	$CaSO_4.2H_2O$	98-103	SHOWA Chemical Co Ltd
-	Calcium Chloride Dihydrate	$CaCl.2H_2O$	99	Chem Supply Pty Ltd
-	Sodium Sulphate	Na_2SO_4	99	Chem Supply Pty Ltd

3.1.2.1.2   Organic chemicals

The organic chemicals used in this study were alginic acid (AA), humic acid (HA), and bovine serum albumin (BSA) as shown in **Table 3.3**. According to the manufacturer, the molecular weight (MW) of BSA was approximately 66 kDa. The sodium alginate extracted from brown seaweed has a MW ranging from 12 to 80 kDa (Lee and Elimelech, 2006). Meanwhile the HA has a MW ranging from 4-20 kDa (Tang et al., 2007).

Table 3.3 Organic chemical solutions used in this study.

Generic Name	Chemical Formula	MW (kDa)	CAS No.	Supplier
Humc Acid	$C_{187}H_{186}O_{89}N_9S$	4 to 50	1415-93-6	Sigma Aldrich
Alginic Acid	$(C_6H_8O_6)_n$	12 to 80	9005-32-7	Sigma Aldrich
Bovine Serum Albumin	607 amino acids in length	66	9048-46-8	Sigma Aldrich

3.1.2.2 Natural solutions

Seawater was used as the natural water source for all experiments. The seawater was drawn from Chowder Bay, Sydney, Australia, pumped from 1 m below the sea surface level and filtered using a centrifuge filtration system to remove any large particles. The characteristics of the seawater are presented in **Table 3.4**.

Table 3.4 Characteristics of seawater in Chowder Bay in Sydney, Australia.

Analysis category	Measurement value
pH	8.2
Conductivity (mS/cm)	51.8–55.5
TSS (mg/L)	3.6
Salinity (g/L)	35.5
UF-MFI (s/L^2)	15,848
Turbidity (NTU)	0.41
UV_{254} (/cm)	0.026
DOC (mg/L)	1.29

3.1.2.3 Cleaning Solutions

The two cleaning solutions used in this study were citric acid anhydrite (Chem Supply Pty Ltd) and sodium hydroxide, NaOH (Chem Suppy Pty Ltd) at a concentration of 0.1 M. The cleaning solutions were predominantly used for chemical cleaning of the membrane foulant as well as to remove deposits and neutralize the membrane module and experimental set-up before each experiment.

3.2 EXPERMENTAL METHODS

The two main experimental set-up used for the MD study was the lab scale vacuum multi effect membrane distillation (V-MEMD) system as well as the bench scale DCMD system as discussed below.

3.2.1 Lab scale vacuum multi effect membrane distillation (V-MEMD)

The V-MEMD system designed by Memsys is a novel model composed of a steam raiser, a membrane module (vapour-liquid stage) and a condenser as shown in **Figure 3.2**. It is an integration of the basic concept of VMD with a multi-effect distillation process system (Zhao et al., 2013). Hence, all the three effects - heating effect (steam-raiser), evaporation-condensation effect and cooling effect (condensation) occur in one system. The term one-stage 'vacuum multi - effect membrane distillation (V-MEMD)' was employed to represent this system.

In a general VMD system design, vapour produced is condensed outside the module without heat recovery. However, the V-MEMD system design has the advantage of less heat loss due to internal condensing (Zhao et al., 2013). Similarly, in a general VMD system, the feed solution is heated externally and then directed to the feed water channel for thermal evaporation while the V-MEMD system design is incorporated with internal

heating. The modular design of the V-MEMD system enables less specific heat transfer and heat consumption (Zhao et al., 2013).
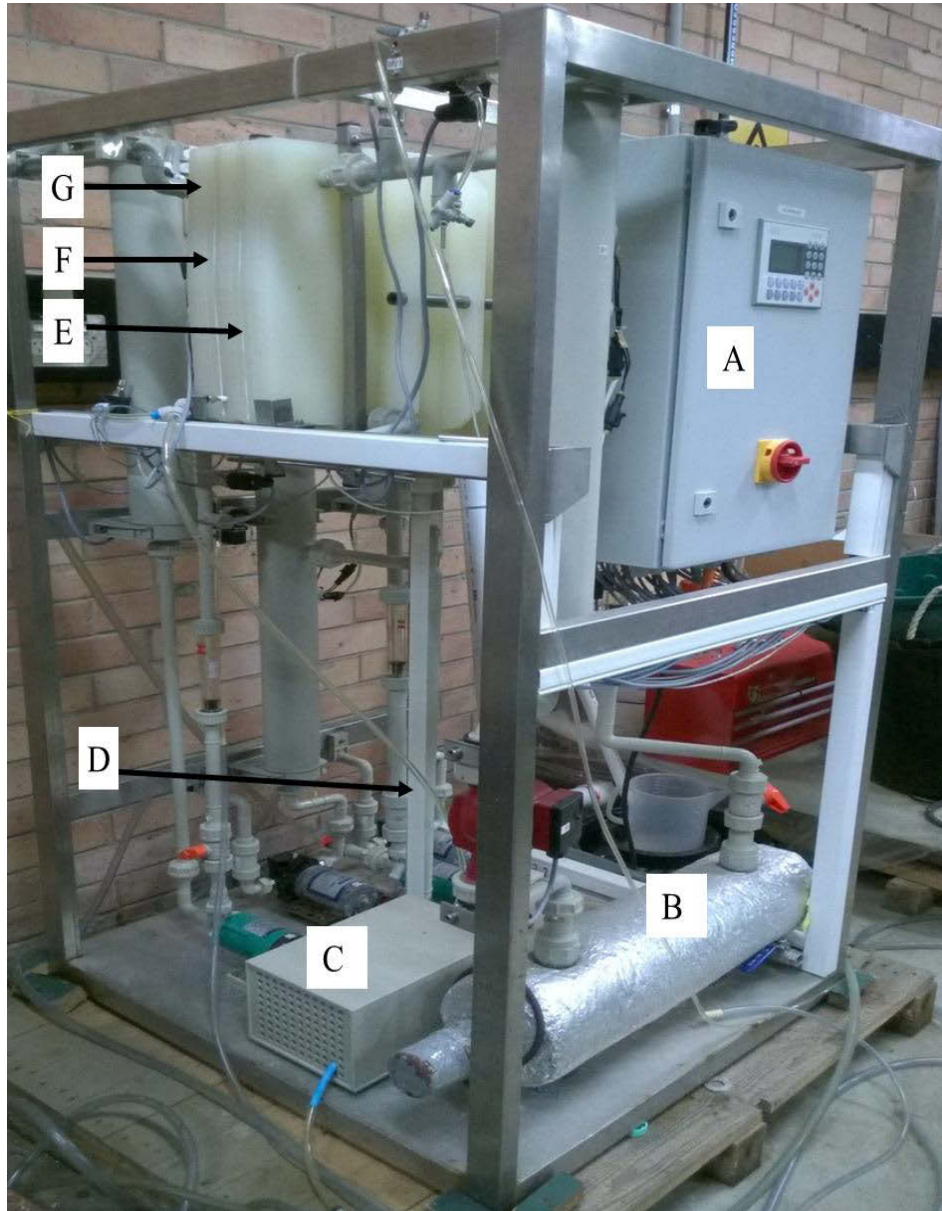
Figure 3.2 Image of the Memsys one stage V-MEMD system used in this study (A : control panel; B: heating unit; C: vacuum pump; D: distillate storage unit; E : stream raiser; F : membrane module; G : condensing system.

The schematic diagram of the V-MEMD system presenting the detail water flow and temperature distribution is shown in **Figure 3.3.** In the one-stage V-MEMD system, water in the steam raiser unit (set at lower pressure than the ambient pressure) is heated

by an internal heat source and turned into steam. Hot steam flows and condenses at the condensation foil, releasing heat to the feed water. The space between the foil and membrane is the feed water channel. The feed water is heated by the heat energy released from the steam raiser unit and evaporates under corresponding negative pressure. Vacuum is applied to the permeate side of the membrane. The vapour produced is condensed in the condensing stage, and then incorporates at the permeate side of the system.

Membrane and Condensing Foil: The membrane size was 0.33 m × 0.48 m with an effective membrane area of 0.16 m^2. The membrane characteristics are listed in **Table 3.1**. The condensation foil is made of polypropylene with a thickness of 23 μm.

Vacuum pump: In this system, the vacuum pump was used to suck non-condensable gases. If non-condensable gases are not removed, it accumulates in the system and reduces the heat and mass transport. Hence, the vacuum pump was able to reduce the heat losses to obtain higher vapour flow rate in the system. The permeate vacuum pressure was adjusted by tuning the throttle valve on the vacuum tube line connected to the vacuum pump.

Temperature: The detailed schematic diagram of the temperature distribution (change) in the one-stage V-MEMD is shown in **Figure 3.3**. The temperature sensors (±0.1 $^\circ$C) automatically recorded the temperature values throughout the experiment. Each experiment was carried out with 2 L of distilled water (fed from the permeate tank) for the heating system. This water was heated (to the corresponding control panel temperature, T_1) and turned into steam in the steam raiser. T_1 is the steam raiser inlet temperature, represented as the heating temperature, T_h. In this system design, the heating temperature is the only temperature that can be set in the main control panel.

The subsequent temperatures were based on the corresponding heating temperature value and these values were displayed on the control panel by the respective temperature sensors. The exchange (liquid to steam) required latent heat and as such T_1 value was reduced to T_2 (steam raiser outlet temperature). The temperature of the inlet feed water increased to T_3 with the steam heat. T_3 represents the bulk feed temperature, T_{fb}. The temperature of the outlet feed water of the feed channel (brine) was reduced to T_4. The feed outlet water was recirculated to the feed tank for continuous operation. Meanwhile the feed temperature inside the module is the feed temperature, T_f, while the feed temperature on the membrane surface is T_m. Outlet and inlet cooling temperature values were retrieved from the temperature sensor. Tap water was used as cooling water source for the condenser.
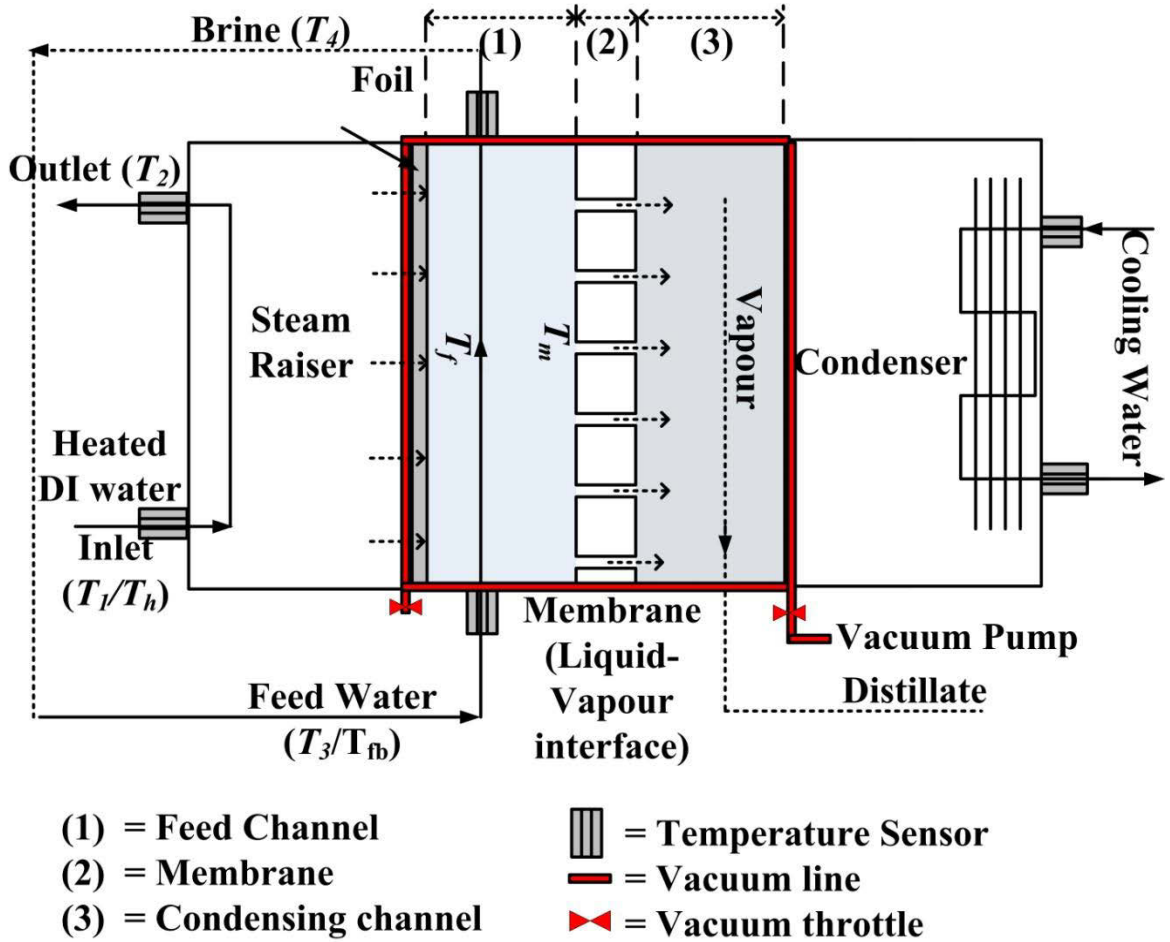
Figure 3.3 Schematic diagram of the water flow and temperature distribution (change) ($T_1 > T_2 > T_3 > T_4$) through the one stage V-MEMD system (External temperatures from temperature sensors -T_1= steam raiser (inlet) temperature/ heating temperature, T_h; T_2=steam raiser (outlet) temperature; T_3= feed temperature (inlet)/ bulk feed temperature, T_{fb}; T_4 = feed temperature (outlet) /brine & Internal temperatures - T_f =feed temperature in membrane module; T_m = temperature on the membrane surface.

3.2.2   Bench scale direct contact membrane distillation (DCMD)

A bench scale DCMD system as shown in **Figure 3.4** was used for the scaling and organic fouling study. The schematic diagram of the DCMD system is shown in **Figure 3.5**. The membrane was placed between the feed and permeate side in the membrane module. Feed solution was heated at the set temperature in a sealed feed tank encased with an electric heating blanket. The temperature of the permeate side was regulated by a cooling unit (2 L of distilled water was used as the condensing fluid in the permeate tank). Initially, feed solution and cooling water were circulated into the membrane module by a peristaltic pump until a stable temperatures is achieved. The temperature of the feed solution and cooling water were measured at the inlet and outlet of the membrane module with temperature sensors. The hydraulic pressure on the feed inlet and permeate side outlet were measured with pressure gauges. The hydraulic pressure inlet and outlet remained the same throughout the experiments. The feed and permeate tanks were placed on electronic balances to monitor the permeate production and feed reduction over time. The volumetric flow of both the feed and permeate were measured by flow meters. The system was operated on a counter-current flow mode.
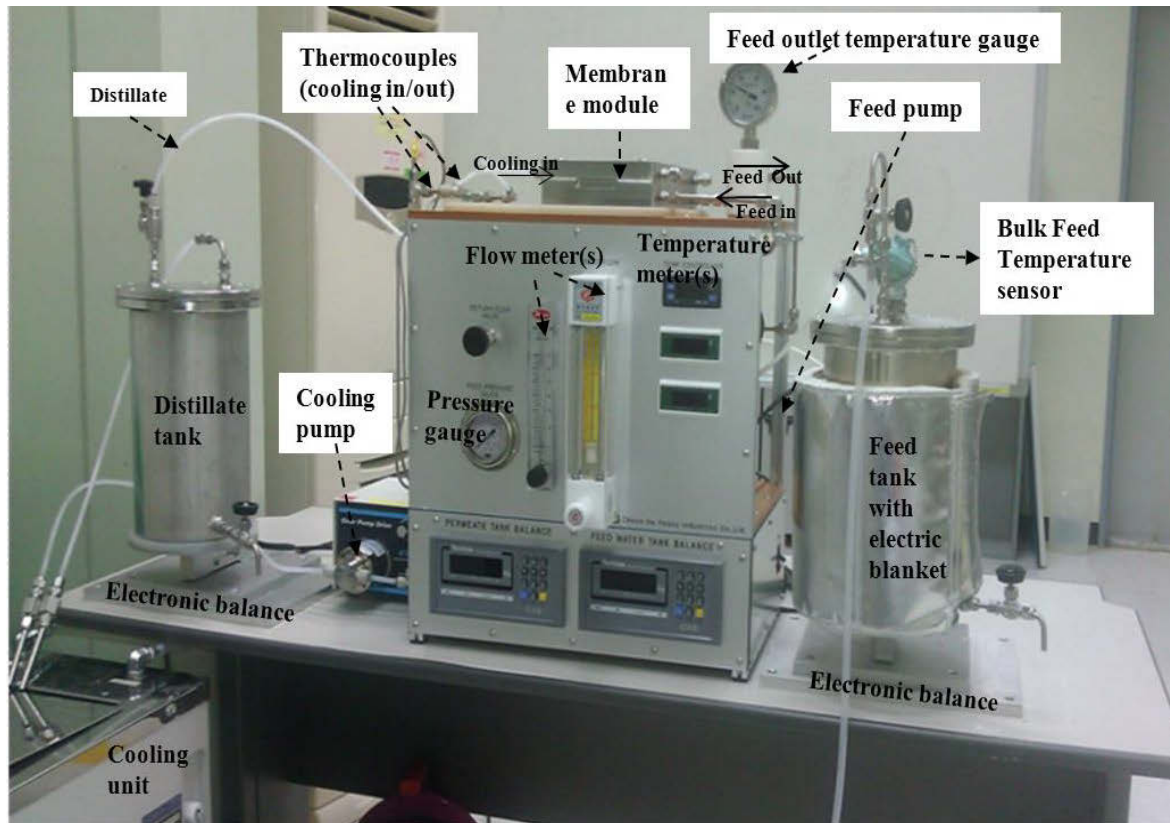
Figure 3.4 Image of the DCMD experimental set-up.
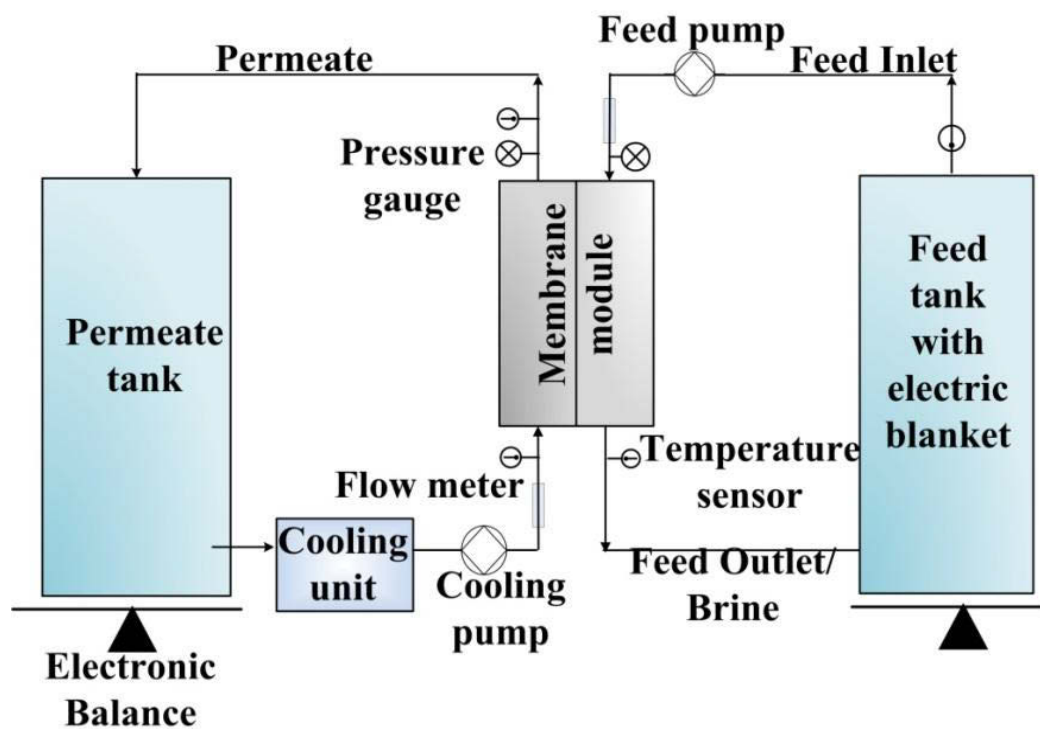
Figure 3.5 Schematic diagram of the DCMD experimental setup

3.3 EXPERIMENTAL ANALYSES

In this study, due to varied types of experimental samples, analysis was categorized by solution (feed and permeate) and membrane foulant characterization as well as membrane characterization. The characteristics were further classified into inorganic, organic as well as biological. Analyses were carried out to analyse the solutions and membrane foulant. Summary of experimental analyses is presented in **Table 3.5.**

For membrane foulant analysis, the foulant residues were extracted by cutting the MD membrane into small parts and placing them in a beaker with predetermined volume of MQ water. The beaker was sonicated to extract the foulant residues out. The sonication was carried out with an ultrasonic bath (Powersonic 420, Thermoline Scientific, 300 W) for a short time (10 mins) to prevent organic matter from denaturing and any modification.

3.3.1 Solution and Foulant Characteristics

3.3.1.1 Primary analysis

The primary analyses of sample solutions - pH, TDS (mg/L) and conductivity (mS/cm) were made with auxiliary laboratory instruments. A multipurpose probe (HQ40d, HACH) was used for the measurement of pH, TDS and conductivity. Meanwhile the turbidity was measured using a turbidity meter (HACH 2100P).

3.3.1.2 Inorganic analysis

The ion concentration of the solutions and membrane foulant samples, specifically the calcium ion concentration $[Ca]^{2+}$ was measured using microwave plasma atomic emission spectrometer (MP-AES, Agilent 4100). The MP-AES instrument is an atomic emission spectrometer integrated with a microwave plasma as the emission source. The emission source is sustained with nitrogen gas (100 to 240 kPa gas pressure).

Importantly, the scanning spectrometer of the Agilent 4100 MP-AES is incorporated with a CCD detector This enabled the MP-AES to measure low ppb detection limits of ion concentration. Hence this measurement analysis instrument was suitable for this study.

The samples were filtered with 0.45 μm filter prior to analysis. Firstly, the reagent blank (MQ water) and four $[Ca]^{2+}$ calibration standards (0, 0.25, 5.0, 10.0 mg/L) were introduced to the MP-AES. Instrument detection limits were calculated as 3 times the standard deviation of the blank concentration. A peristaltic pump was used for channelling the sample solution to the nebulizer transducer from the host MP-AES at an uptake time of 40s. The sample values were detected at a correlation coefficient range of 0.97 to 0.99. A stabilization time of 80s and read time of 5s was used for each sample measurement. Between each sample, the instrument was rinsed with nitric acid for 80s. The measurement was repeated the reading 7 times and the mean value was reported in this thesis

3.3.1.3 Organic analysis

3.3.1.3.1 Modified Fouling Index (MFI)

The MFI was established by Schippers and Verdouw (1980) to evaluate the membrane fouling. The schematic diagram and figure of MFI experimental set-up are shown in **Figure 3.6**. MFI is determined at standard reference values of 207 ± 3 kPa, a feed water temperature of 20°C and UF with a 47 mm diameter and molecular cut-off of 17.5 kDa. The ultrafilter - modified fouling index (UF-MFI) can indicate whether a pretreated feed solution was effective in reducing the membrane's fouling potential.
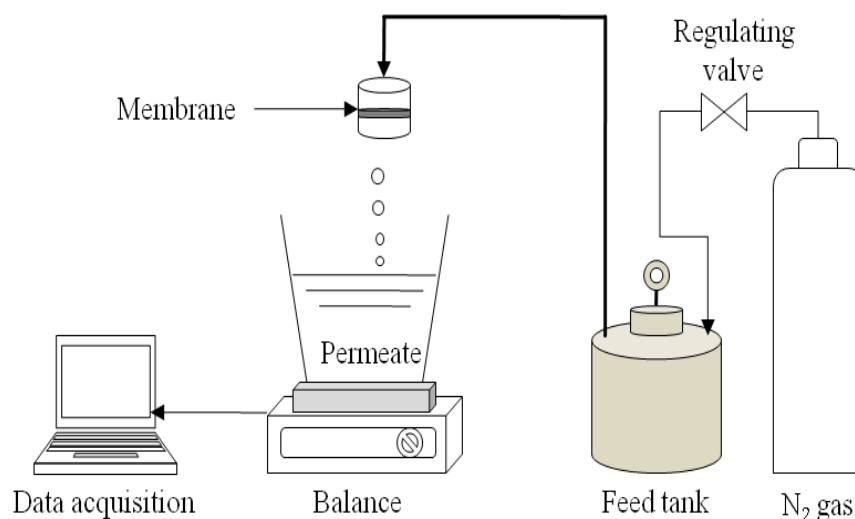
Figure 3.6 UF-MFI experimental set-up.

3.3.1.3.2 Dissolved organic carbon (DOC)

Dissolved organic carbon (DOC) and detailed organic fractions of the solutions and membrane foulant samples were measured using DOC-LABOR Liquid Chromatography - Organic Carbon Detector (LC-OCD) (**Figure 3.7**). The LC-OCD system consists of a size exclusion chromatography column, which separates hydrophilic organic molecules according to their molecular size. The separated compounds were then detected using two different detectors: a UV detector (absorption at 254 nm) and a DOC detector (after inorganic carbon purging). Depending on the size of the molecules, the different fractions of the organic matter can be identified and quantified. This method was adopted based on Huber and Frimmel (1994).

LC-OCD measurement was made at least in duplicate and their deviation was less than 5%. Thus mean value is reported in the thesis. In this LC-OCD analysis, a Toyopearl TSK HW50S column (TOSOH Bioscience GmbH, Stuttgart, Germany) was utilized with phosphate buffer mobile phase of pH 6.4 (2.6 g/L KH_2PO_4 and 1.5 mol/L Na_2HPO_4) at a flow rate of 1.1 mL/min. Injection volumes and retention time were 1,000 μL and 120 min, respectively. The chromatographic column was a weak cation exchange column based on polymethacrylate.

3.3.1.3.2.1 Detailed organic fractions

Organic matter was divided into two parts by LC-OCD. In LC-OCD system, hydrophobic organic carbon was calculated from the difference of DOC and chromatographic DOC. All organic matter retained in the column was defined as hydrophobic. This could be either dissolved hydrocarbons or micro particulate including humic substances (HS). Chromatographic DOC is calculated from the area enclosed by the total chromatogram.

Figure 3.7 DOC-LABOR Liquid Chromatography-Organic Carbon Detector.

Natural organic matter (NOM) in seawater mainly contains biopolymers, HS, building blocks (BB) and low molecular weight (LMW) acid and neutrals (Huber et al., 2011).

Biopolymer has a very high molecular weight (20,000-100,000 g/mol) representing compounds such as polysaccharides amino sugars, polypeptides, proteins, "extracellular polymeric substances", hydrophilic fraction and not UV-absorbing. In surface water, BP exists as colloidal transparent exopolymeric particles and polysaccharide. HS represent compounds with molecular weights approximately 1000 g/mol. BB is defined as humic-hydrolysates, sub-units of HS with MW between 300-450 g/mol. There are mainly weathering and oxidation products of HS. LMW neutrals are weakly charged hydrophilic or slightly hydrophobic "amphiphilic" compounds such as alcohols, aldehydes, ketones and amino acids.

3.3.1.4   Biological analysis

3.3.1.4.1 Assimilable Organic Carbon (AOC)

In this study, a marine assimilable organic carbon (AOC) assay was used to measure the biofouling potential in the feed water, brine, on the membrane foulant as well as the permeate solution..

AOC refers to a fraction of "labile" or "bio-available" dissolved organic carbon (DOC) that is readily assimilated and utilized by microorganisms resulting in an increase of biomass. Thus, the concentration of AOC can influence biological fouling (biofouling) in water treatment systems and distribution processes by promoting growth of fouling organisms. A high level of AOC is directly linked with rapid biofilm formation and loss of performance in membrane processes (Hambsch and Werner, 1996). Therefore, assays that quantify AOC can be used as an indicator of the relative fouling potential of specific samples, such as seawater entering an RO plant.

The AOC test was carried out with a 24-well multiwell, tissue culture treated plate (353047 - BDFalcon™) that was covered with parafilm to minimize the evaporation. Artificial Seawater was inoculated with 3.0×10^4 CFU/mL of V. fischeri from a concentrated (3.0×10^6 CFU/mL) stock solution (initial luminescence was set at approximately 1.0×10^6 counts per second (CPS). The stocks that were kept frozen at $-80\ °C$ in marine broth and 10% glycerol by streaking onto marine agar containing (per liter) 37.4 g marine broth and 15.0 g bacto agar (Difco™ and BBL™), and incubated (room temperature 25 °C) overnight. Upon checking the luminescence, the strain was transferred to a 2 mL tube for washing with culture media three-times. Luminescence was measured using a Wallac 1420 VICTOR2™ plate reader (PerkinElmer Inc., US).

The AOC stock was prepared by re-suspending the bacteria colonies from the marine agar plate into artificial seawater (SW) and concentrated for inoculation. The artificial SW ingredients details are reported in the published paper by Jeong et al. (2013b).

The SW and membrane foulant samples for AOC assay were prepared by filtering large particles (0.45 μm PES filter). Bacteria were inactivated at 70 °C for 30 min, and the seawater samples were then filtered again (0.22 μm PES filter). Predetermined cell numbers of each bacterium were spiked to the sample (2 mL). For the standard curve, glucose was added to the artificial SW as a sole carbon source at a range of concentrations (0, 10, 25, 50 and 100 μg-C/L; stock solution-100 mg-C/L). In this study, all the measurement was triplicated.

3.3.1.4.2   Other biological measurement

A number of other biological measurements were used, specifically with regards to the biofilter pretreatment (**Chapter 7**). The microbial activity (active biomass) was determined by measuring the adenosine triphosphate (ATP) concentration. At the same time, total direct cell counts (TDC values) were performed to quantify the number of bacterial cells in the water samples.

3.3.2   Membrane Characterization

3.3.2.1   Field emission scanning electron microscope (FE-SEM)

Field Emission Scanning Electron Microscope (Zeiss Supra 55VP) was used to investigate the clean (virgin) and fouled membrane morphology and to observe the composition of the deposit formed on the membrane.

For the SEM analysis, the fouled membrane coupons were dried in a desiccator and analyzed without any further treatment. Both the top surface and the cross-section of the

fouled membrane coupons were analysed. They were mounted on a holder using double-sided carbon tape.

The FE-SEM operated at 15 kV in conjunction with Bruker XFlash SDD EDS detector was used to obtain chemical information. EDS spot analysis was carried out using a spot diameter of about 5 nm at selected areas on the samples.

3.3.2.2   Contact angle measurement

The contact angle of membrane surface was measured to determine the hydrophobicity range of the membrane surface. This measurement was carried out, by sessile drop method using a goniometer (Theta Lite). The images were captured and interpreted by OneAttention Image Advanced software. The shape of a liquid droplet is determined by the surface tension of the liquid. To form a water drop (1.8 to 2.0 mL of milli-Q water) on the dried membrane surface, a milliliter syringe was used. Measurements were repeated 5 times and the average reading was reported in this study.

Table 3.5 Summary of experimental analyses used in this study.

Clarification		Objective	Method	Notes
Characteristics of solutions and foulant	Inorganic	Ion concentration	MP-AES	Quantification of $[Ca]^{2+}$ ion concentration in the feed solution, concentrated brine and permeate solution
	Organics	DOC and detail organic faction	LC-OCD	Quantification of organic concentration in the solution and foulants and detail fractionation of the organic contents
		Modified fouling index (MFI)	MFI filtration test	Colloidal and organic fouling potential using UF membrane
	Biological	Bacterial regrowth or biofouling potential	AOC	Bioluminescence method using *Vibrio fischeri*
		Total cell number	TDC	Plate count
		Active biomass	ATP	ATP assay kit and Luminescence spectrophotometer
Membrane Autopsy		Membrane structure and chemical composition	FE-SEM with EDS	
		Hydrophobicity	Contact angle	

CHAPTER 4

OPTIMAL OPERATING

CONDITIONS FOR MD
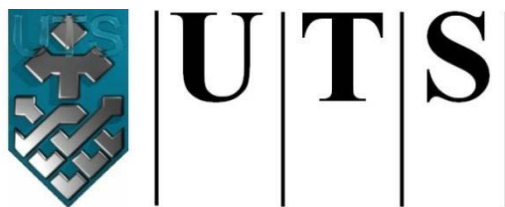
University of Technology Sydney
Faculty of Engineering & Information Technology

This chapter discusses the operating parameters that influence the performance of the MemSYS V-MEMD system. These parameters are presented in detail in **Section 4.1** and **Section 4.2**, while **Section 4.3** evaluates the performance of the DCMD system.

Section 4.1 introduces the main operating parameters that influences the performance of the MD system. This is followed by a baseline study on how different operating parameters are related to the performance of the V-MEMD system. The range of optimum operating conditions for the V-MEMD system is highlighted.

The second section, **Section 4.2**, analyses the performance of V-MEMD for different operating parameters under high saline water. In this section a mathematical model and experimental data was used to predict the V-MEMD performance and the effect of polarization. This was done in order to identify the optimum operating parameter combination for the V-MEMD system working in high saline conditions.

The third section, **Section 4.3**, highlights the baseline study on the performance of a DCMD system using different feed and permeate velocity combinations. The range in which the optimum feed and permeate velocity combinations for the DCMD system work is highlighted.

\<Publications related to this chapter\>

Naidu, G., Choi, Y., Jeong, S., Hwang, T. M., & Vigneswaran, S. (2014). Experiments and modeling of a vacuum membrane distillation for high saline water. Journal of Industrial and Engineering Chemistry,20(4), 2174-2183.

Naidu, G., Jeong, S., & Vigneswaran, S. (2014). Influence of feed/permeate velocity on scaling development in a direct contact membrane distillation. Separation and Purification Technology, 125, 291-300.

4.1 OPERATING PARAMETERS INFLUENCING THE PERFORMANCE OF V-MEMD SYSTEM

4.1.1 INTRODUCTION

The performance of MD in terms of permeate flux is governed by a number of operating parameters, mainly feed temperature, feed flow rate and feed concentration (El-Bourawi, 2006; Lawson and Lloyd, 1997). The impact of feed temperature on MD performance has been widely analyzed. It has been acknowledged that a high feed temperature strongly enhances MD permeate flux (El-Bourawi, 2006). This is associated with the exponential increase of the vapour pressure when feed temperature is introduced (Lawson and Lloyd, 1997). Generally, therefore, MD systems are operated at feed temperature ranges between 60°C and 80°C (Alkhudhiri et al., 2012).

The importance of feed velocity turbulence in mitigating the effect of polarization in MD has been investigated in a number of studies (Safavi and Mohammadi, 2000; Mericq et al., 2009). The feed velocity turbulence increases the heat and mass transfer in the feed channel, and reduces the temperature and concentration polarization effect. As a result, higher permeate flux is achieved and for this reason many MD studies have recommended operating under turbulence regime/higher circulation velocity to obtain more productivity (Martínez-Díez et al., 1999; El-Bourawi, 2006).

In a VMD configuration, the presence of a vacuum is an additional positive influence on the permeate flux. The presence of this vacuum reduces the pressure on the permeate side, creating a higher driving force in the system. As a result, the heat and mass transfer is increased, enhancing permeate flux (Banat et al., 2003). Recent studies have highlighted that lower permeate pressure is one of the major operating parameters that enables a VMD system to achieve high permeate flux (Mericq et al., 2009; Safavi and

Mohammadi, 2009; Zhao et al., 2013). In one study, Safavi and Mohammadi (2009) applied statistical methods and established vacuum pressure as the most dominant operating factor enhancing the permeate flux in VMD. Similarly, Mericq et al. (2009) showed that vacuum pressure was beneficial. Reducing permeate pressure from 1.5 kPa to 0.1 kPa, resulted in a 10-fold permeate flux increment without requiring major energy (less than 2%) (Mericq et al., 2009). Khayet (2011) reported on the ability of VMD to obtain high permeate flux between 36 and 40 LMH due to the presence of vacuum pressure.

It is worth noting that although many parametric MD studies have been published, most of these studies analyzed the influence of operating parameters on the performance of MD, specifically in terms of permeate flux enhancement. For instance, Mericq et al. (2010) recommended a combination of low permeate pressure, high feed temperature, and turbulent fluid regime for high permeate flux. In another study, Safavi and Mohammadi (2009) emphasized that VMD performance, measured in terms of permeate flux, was enhanced by increasing feed temperature and flow rate and decreasing vacuum pressure.

Besides permeate flux, other combination performance factors of the system such as recovery ratio (RR), gain output ratio (GOR) as well as pumping energy must also be given due consideration when analyzing the influence of each operating parameter. Recent studies have used this approach (Zuo et al., 2011; Zhao et al., 2013). For instance, Zuo et al. (2011) used DCMD experiments to highlight the importance of identifying the appropriate operating parameters based on the relationship of permeate flux as well as the gain output ratio (GOR) to reflect the system's energy efficiency. In another study, Saffarini et al. (2012) stated that the RR value can well reflect the performance of the system since the RR value is based on the obtained permeate flow

rate from a given feed flow rate. A higher permeate flux may indicate a low RR which translates into increased energy consumption.

Hence, in this chapter, a baseline deionized (DI) water study was conducted to measure the performance of the V-MEMD and DCMD system using a range of operating parameters: feed velocity, permeate pressure, permeate velocity and feed temperature. The system's performance was evaluated in terms of permeate flux, RR, GOR and pumping energy. The range of suitable operating conditions for the V-MEMD system was identified based on these indicators. Further, the performance of the V-MEMD system was also analysed under high saline condition through experimental and modelling data.

4.1.2   MATERIALS AND METHODS

4.1.2.1   Experimental Set up

Experiments were carried out with the MemSYS V-MEMD system and these are discussed in **Sections 4.1** and **4.2**. The bench scale DCMD unit was used for **Section 4.3**. The detailed set up and membrane characteristics were described in **Chapter 3**.

4.1.2.2   Experimental Operating Conditions

4.1.2.2.1   Heating Temperature (T_h)

In the V-MEMD system, direct control of the feed temperature was not possible as explained in **Section 3.2.1**. Consequently the experiments were carried out by adjusting the steam raiser temperature or heating temperature (T_l/T_h) from 45.0°C to 65.0°C, which was the maximum achievable temperature when using this system.

4.1.2.2.2   Feed velocity (v_f)

Feed water (DI water) was circulated through the feed flow channel at a feed flow rate, Q_f of 15 L/h and 100 L/h which corresponds to a feed velocity and Reynolds number of

v_f = 0.3 m/s (Re = 2,077) and v_f = 2.2 m/s (Re = 17, 300), respectively. This feed velocity was calculated based on the hydraulic area of the feed flow channel (a thickness of 1.50 mm).

4.1.2.2.3 Permeate vacuum pressure (P_p)

The permeate vacuum pressure was set in the range of 5.0 to 15.0 kPa. The permeate vacuum pressure was adjusted by tuning the throttle valve on the vacuum tube line connected to the vacuum pump.

4.1.2.2.4 Cooling Temperature

Tap water was used as the cooling water source for the condenser. The cooling water was not re-circulated in order to maintain a constant cooling temperature range. Outlet and inlet cooling temperature values were retrieved from the temperature sensor. The inlet temperature was 23.2±0.1°C and the outlet temperature was 25.3±1.5°C during the experiment.

4.1.2.3 Performance measurement methods

4.1.2.3.1 Permeate flux

The produced permeate was collected in a tank placed onto an electronic balance. At the same time the decreasing feed tank water volume was recorded throughout the experiment. The corresponding value (volume of decreased feed and produced permeate) with the operation time was used to calculate the permeate flux in kg/m^2/s. The decreased feed volume was consistent with the collected permeate volume and evaporation or leakage was minimal or zero.

4.1.2.3.2 Recovery Ratio (RR)

The *RR* is defined as the percentage of permeate production, *PP* over the feed flow rate, Q_f. A higher percentage of recovery ratio reflects that less feed solute is released as

brine and more permeate water is made (Saffarini et al., 2012). The formula adopted in this study is as follows (Guillén-Burrieza et al., 2012):

$$\% \ RR = PP/Q_f \quad \text{x } 100\% \tag{4.1}$$

where PP is permeate flow rate of the membrane area, $PP = J. \ A$ (where J is the permeate flux and A is the membrane area).

4.1.2.3.3 GOR measurement

The GOR which represents the ratio of heat associated with mass transfer to the energy input, was used to assess the performance of the system under different feed temperatures. The GOR equation was expressed as follows (Zhao et al., 2013):

$$GOR = (60 \cdot Q_{permeate} \cdot \Delta H_v) \ / \ (S \cdot Q_{heating} \ [(T_{h\_inlet}) - (T_{h\_outlet})]) \tag{4.2}$$

where, ΔH_v is the latent heat of vaporization, S is the water-specific heat capacity (4.19 kJ/kg), $Q_{heating}$ is the heating flow rate, $Q_{permeate}$ is the permeate flow rate, T_{h_inlet} is the inlet heating temperature and T_{h_outlet} is the outlet heating temperature.

4.1.2.3.4 Pumping Energy

Pumping energy, E_{pump} was calculated based on the equation reported by an energy analysis MD study as follows (Bui et al., 2010):

$$E_{pump} = Q_f p'_f + Q_p p'_p \tag{4.3}$$

where, Q_f is the feed flow rate and Q_p is the permeate flow rate, p'_f and p'_p are the applied pressure of the feed and permeate side, respectively. The applied pressure values were obtained from the feed inlet and permeate outlet pressure gauge.

4.1.3 RESULTS AND DISCUSSION ON OPERATING PARAMETERS INFLUENCING THE PERFORMANCE OF THE V-MEMD SYSTEM

4.1.3.1 Influence of feed velocity

In this study the influence of v_f on the performance of the V-MEMD system was analyzed by varying v_f from the lowest range of the system's limit, 0.3 m/s up to the highest range limit, 2.2 m/s at $T_h = 65.0°C$ and $P_p = 10.0$ kPa. The performance was measured in terms of permeate flux as well as RR. The results showed that as the feed velocity was increased from 0.3 m/s onward, the permeate flux increased by 70-71%. In contrast the RR reduced by 74% as shown in **Figure 4.1**. As discussed in **Section 4.1.1**, generally a high v_f range is recommended for MD operation for the purpose of reducing the boundary layer and polarization effect.

Based on the results of this study, it is emphasized that rather than a high v_f, a suitable feed flow velocity should be identified based on the permeate flux as well as RR. Another aspect that needs to be considered when identifying the suitable v_f would be the role of feed flow turbulence in reducing deposit build up and crystallization in the membrane module. A low range v_f could result in membrane surface crystallization. The relationship between feed flow rate and crystallization is examined in **Chapter 5**. Overall, an intermediate v_f range would provide the best performance output for the V-MEMD system.

4.1.3.2 Influence of feed temperature

The role of feed temperature in the V-MEMD system was investigated by varying the heating temperature, T_h from 45.0°C to 65.0°C at a fixed $v_f = 1.1$ m/s and $P_p = 10$ kPa. Increasing the feed temperature by a small variation of 44% (from 45.0°C to 65.0°C) significantly improved the permeate flux by around 200% from 3.6 LMH to 11.8 LMH as shown in **Figure 4.2**. As discussed in Section 4.1.1, it has been widely accepted in

MD studies that feed temperature is the key operating parameter that increases permeate flux. However, the feed temperature is also a very sensitive operating parameter that influences the total energy consumption of the system and the polarization effect. In this study, apart from permeate flux, the GOR value was also considered in representing the influence of the feed temperature. The results showed that the GOR improved significantly from 45.0˚C to 55.0˚C. Thereafter it remained almost constant with a slight reduction from 60°C onwards. This indicated that from 57.0˚C to 60.0˚C, the optimum V-MEMD performance was achieved. After that, however, there would be energy wastage.

4.1.3.3   Influence of permeate pressure (vacuum)

The influence of permeate pressure was analyzed by reducing the permeate pressure (increasing vacuum) from P_p =15.0 kPa to 10.0 kPa at a fixed T_h = 65.0 ˚C and v_f = 1.1 m/s. As a result, the permeate flux increased by almost 200% as shown in **Figure 4.3**. As discussed in **Section 4.1.1**, previous studies have highlighted that the presence of vacuum is one of the major operating parameters that enables a VMD system to achieve high permeate flux. Importantly, the low power requirement of the vacuum pump (0.1 kW) is an added advantage in comparison to heating temperature power requirement, which has been estimated to be approximately 2 to 4 kW at 65.0˚C (Zhao et al., 2013).

Therefore, lowering the permeate pressure (increasing the vacuum) to a further 5.0 kPa enhanced the permeate flux to 13.5 LMH for this system. Moreover, for a V-MEMD system, the presence of a high vacuum condition is vital. Zhao et al. (2013) mentioned that in a multi-effect stage design with multiple parallel membranes, low permeate pressure is necessary to create an adequate driving force. This will then make possible permeate production for all membrane stages.
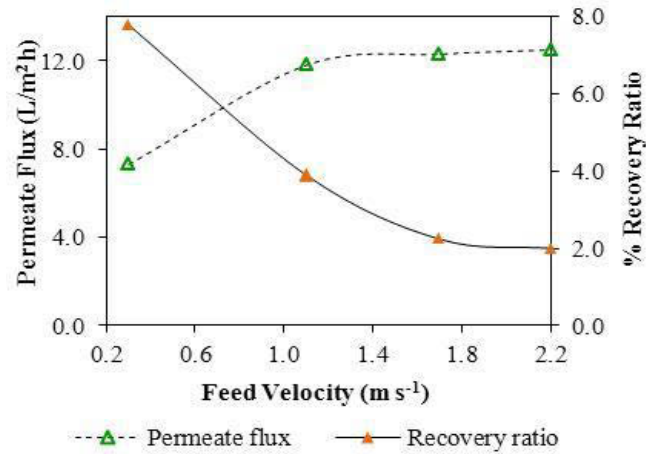
Figure 4.1 Influence of feed velocity, v_f on permeate flux and recovery ratio (T_h = 65.0 °C and P_p =10.0 kPa) (L m^{-2} h^{-1} = LMH)
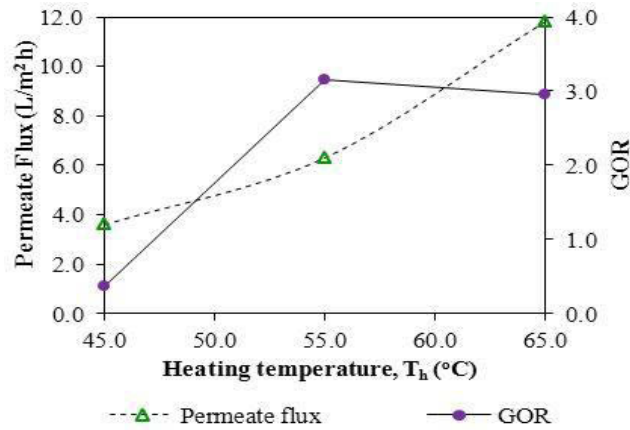
Figure 4.2 Influence of feed temperature (represented as T_h), on permeate flux and GOR (v_f= 1.1 m/s and P_p =10.0 kPa).
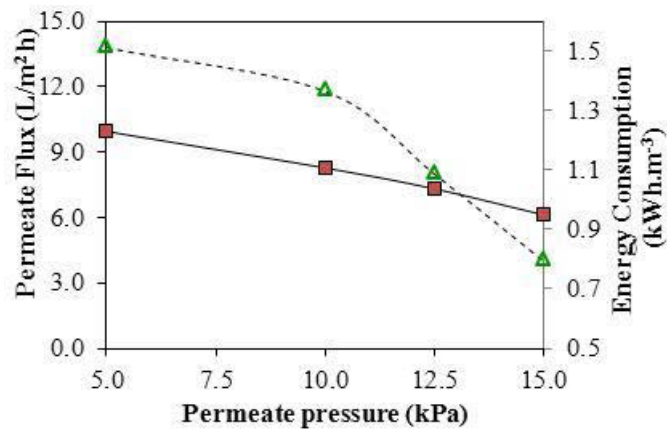
Figure 4.3 Influence of permeate pressure on permeate flux (v_f= 1.1 m/s and T_h =65.0 °C)

4.2   V-MEMD SALINITY EXPERIMENT AND MODELING

One of the highlighted advantages of MD is its ability to treat highly concentrated feed solutions because the vapour pressure driving force is only minimally affected by salinity. MD studies carried out with high salt concentrations ranging from 100 to 300 g/L reported only a 13-30% reduction of permeate flux (Martínez-Díez and Florido-Diaz, 2001; Cath et al., 2004). The VMD configuration specifically is attractive for this purpose due to the presence of a vacuum that can enhance the vapour pressure's driving force. Most VMD studies were conducted using pure water and low concentration salt solutions (Banat et al., 2003; Bandini et al., 1992). A few VMD studies were done with high saline water and they displayed positive results. For instance, Safavi and Mohamaddi (2009) confirmed that for a salt concentration of 100 g/L, an optimum net of conditions (feed temperature of 55°C; vacuum pressure of 4.0 kPa; flow rate of 30 mL/s) helped to achieve a permeate flux of 14.4 LMH. Meanwhile, Cabassud and Wirth (2003) focused on hollow fibre VMD configuration and pointed out that at high salt concentration of 300 g/L, intermediate hydrodynamic (Re of 7000) rather than a high hydrodynamic (Re of 9000) state was more appropriate to maintain a reasonable level of energy consumption. Importantly, this study highlighted that VMD coupled with solar energy could compete with RO for high saline water treatment. In another study, Mericq et al. (2010), reported permeate fluxes ranging from 7 to 17 LMH with RO brines, concentrated from 64 g/L to 300 g/L, with the experimental conditions of 6.0 kPa permeate pressure, feed temperature of 50 ºC and a Re of 4000. Importantly, this study reported that both TP and CP had a minimal effect on the permeate flux even for high salt concentrations.

While past studies have analyzed the performance of VMD with high saline water, those analyses were only based on bench-scale equipment with small membrane areas

(maximum 2 L/d water output capacity). Research on small-scale equipment may not be able to represent the performance of real conditions, especially the elevation of polarization effects. In MD operation carried out with saline feed solution, the effect of CP prevalently influences the systems performance. The CP phenomenon has been explained in detail in **Section 2.2.2.3** (**Chapter 2**). The effect of CP is an important factor for estimating the water production rate of a pilot scale MD application. Such outcomes, however, can be achieved effectively using scaled-up equipment. Hence, in this study the performance of the V-MEMD system was evaluated using a high saline feed solution.

The importance of high feed temperature in achieving high permeate flux in MD has been described in detail in **Section 4.1**. MD systems are generally operated at high feed temperature ranges. As a consequence, at higher feed temperature conditions, the effect of temperature polarization (TP) becomes critical (Martínez-Díez et al., 1999; Bahmanyar et al., 2012). The effect of the TP phenomena on MD has been described in detail in **Section 2.2.2.3** (**Chapter 2**). Compared to a traditional VMD system, a modified V-MEMD system is unique due to its integration of an internal heating system. The presence of an internal heating system made it possible to operate the system with lower feed temperatures. The effect of TP could be mitigated in the V-MEMD system due to the lower feed temperature condition**.**

In this section the strategy of experimental analysis followed by modeling was used to represent the performance of the V-MEMD system under high saline water. The effects of TP and CP were analyzed in detail.

4.2.1   EXPERIMENTAL OPERATING CONDITIONS

In this study 1 M of NaCl was used as the feed solution. The feed water solution was prepared by dissolving NaCl in deionized (DI) water, and feed water quality was measured in terms of total dissolved solids (TDS). Other sparingly dissolved salts such as $CaCO_3$ and $MgSO_4$ usually present in seawater or brackish water were not included in this feed water. The presence of sparingly dissolved salts and the related scaling development is discussed in **Chapter 5**.

Based on the optimal operating parameter ranges identified from the DI water experiment in **Section 4.1.3,** a high permeate vacuum pressure of P_p=4.5±0.5 kPa was used for this study. Meanwhile, an intermediate feed velocity, v_f of 1.1 m/s (Re of 6,100) was used as identified in **Section 4.1.3.1**. At the same time a high feed velocity, v_f of 2.2 m/s (Re of 17, 300) also served to establish the role of flow velocity in mitigating the effect of polarization.

Therefore, the experiments were categorized into two main sets based on the feed velocities (Set I: v_f =1.1 m/s and Set II: v_f =2.2 m/s). For both Set I and Set II, the feed water was concentrated from 1 M to 3 M. In Set I, the values of the three bulk feed temperature series were T_{fb} = 37.0°C, 40.5°C and 46.0°C, respectively. In Set II, the corresponding bulk feed temperature series were T_{fb} = 37.0°C, 42.5°C and 48.7°C, respectively as shown in **Table 4.1**. The T_{fb} values were retrieved from the systems control panel based on the heating temperature, T_h of 45.0°C to 65.0°C. In the V-MEMD system the bulk feed temperature, T_{fb} changed systematically when the feed flow rate was increased. The different feed flow rates and bulk feed temperatures influenced the vacuum pressure only slightly as shown in **Table 4.1**. In this system, due to a constant heat loop inlet temperature, the pressure level throughout the module was

stable and became possible to achieve a stable permeate flux. The modular design of the V-MEMD system means that less specific heat transfer and heat consumption occurs (Zhao et al., 2013).

Table 4.1 V-MEMD operating parameter setting for salinity study.

Experiment Set	Feed Velocity, v_f (m/s)	Temperature (°C)				Vacuum pressure $(P_p,$ kPa)
		Steam Raiser (inlet, T_1/T_h)	Steam Raiser (outlet, T_2)	Feed (Inlet, T_3 /T_{fb})	Feed (Brine/ Outlet, T_4)	
		45.0	39.7	37.0	32.2	3.9
I	1.1	55.0	46.6	40.5	35.5	4.4
		65.0	51.2	46.0	43.8	5.1
		45.0	39.3	37.0	31.7	4.0
II	2.2	55.0	47.5	42.5	35.6	5.0
		65.0	51.8	48.7	44.2	6.0

4.2.2 MODELING THEORY

In this section the model equations are discussed. A simple mathematical model was used to fit the experimental data. Several assumptions were adopted for the modeling procedure which is also discussed in this section. The procedure used to predict the permeate flux is presented with an algorithm.

4.2.2.1 Modeling Equations

4.2.2.1.1 Permeate flux

The fundamental permeate flux, J_w used for this study have been represented as Eq. (2.1) in **Section 2.2 (Chapter 2)**.

4.2.2.1.2 Vapour pressure

The water vapour pressure on membrane surface, $P_m(T_m, C_m)$ can be related to the feed temperature (in K) and feed solution concentration (in g/kg). This is based on Raoult's law which states that the vapour pressure of saline water is equal to the vapour pressure of water in the pure state and a**s** a function of the salinity. Raoult's law's validity is $0 < T < 200°C$ and $0 < S < 240$ g/kg (T = temperature, S = salinity, and accuracy= 0.1%). Using Raoult's law the membrane surface vapour pressure, $P_m(T_m, C_m)$ is expressed as follows (Sharqawy et al., 2010):

$$P_m\left(T_m, C_m\right) = \frac{exp\left[\frac{-5.80 \times 10^3}{T_m} + 1.39 - 4.86 \times 10^{-2} T_m + 4.18 \times 10^{-5} T_m^2 \pm 1.45 \times 10^{-8} T_m^3 + 6.55\ log(T_m)\right]}{1 + 0.57257\left(\frac{C_m}{1000 - C_m}\right)} \qquad (4.4)$$

where T_m is the membrane surface feed temperature, C_m is the solute concentration on the membrane surface in the feed side, $P_m(T_m, C_m)$ is the water vapour pressure on the membrane surface in the feed side, and P_V is the pressure in the vacuum side.

4.2.2.1.3   Membrane coefficient

If transporting species have a mean free path, λ, larger than the membrane pore size (pore radius), the mass transport mechanisms through the pores are of the Knudsen diffusion type. The average pore diameter of the membrane used in these experiments was 0.2 μm which is smaller than the mean free path of water vapour (2.8 μm at 30°C). Hence, the Knudsen flow model is employed because it represents the majority of mass transport mechanisms in the VMD process (Soni et al., 2008). In the Knudsen flow model the membrane coefficient, B, is expressed as follows (Diban et al., 2009):

$$B = \frac{MD^{kn}}{RT_m\delta} \tag{4.5}$$

with

$$D^{kn} = \frac{2\varepsilon r}{3\tau}\left(\frac{8RT_m}{\pi M}\right)^{0.5} \tag{4.6}$$

where ε is porosity; r is the pore radius; δ is the membrane thickness; τ is the pore tortuosity; M is the molecular mass of water; and R is the gas constant.

4.2.2.1.4   Heat and mass transfer

The MD process involves both mass transfer of water vapour as well as heat transfer across the membrane.

The mass transfer coefficient, k_w, can be calculated by the relationship between the dimensionless numbers (McCutcheon and Elimelech, 2006; Mengual et al., 2004).

$$k = \frac{Sh.D}{d_h} \tag{4.7}$$

with

$$Sh = 1.86 \left(Re. Sc. \frac{d_h}{L} \right)^{0.33} \qquad\qquad Re < 2100 \text{: Laminar flow} \qquad (4.8)$$

or

$$Sh = 0.023\, Re^{0.8} Sc^{0.33} \qquad\qquad Re > 4000 \text{: Turbulent flow} \qquad (4.9)$$

where Sh is Sherwood number, Re is Reynolds number, Sc is Schmidt number, D is the diffusion coefficient of solute, d_h is the hydraulic diameter and L is the length of the channel.

Heat transfer across the membrane boundary layer in an MD system is a problem for mass transfer. This is because a large amount of heat is needed to vaporize the liquid at the vapour-liquid interface. In an MD system, heat transfer occurs through latent heat transfer and conduction heat transfer (Lawson and Lloyd, 1997). The presence of a boundary layer at the membrane surface results in a lower temperature at the membrane surface, T_m, compared to the corresponding value at the feed temperature, T_f. In a V-MEMD configuration, however, the conductive heat across the membrane is negligible due to the low pressure on the permeate side of the membrane (Lawson and Lloyd, 1997). Hence, the heat flux, N through the liquid boundary layer can be represented by the following equation (Bandini et al., 1992).

$$h_w(T_f - T_m) = N.\Delta H_v \qquad\qquad\qquad (4.10)$$

where ΔH_v is the latent heat of vaporization, h_w is the heat transfer coefficient, T_f is the feed temperature, and T_m is the membrane surface feed temperature. The heat transfer coefficient is calculated using the following equation (Soni et al., 2008):

$$h_w = \frac{K_m \, Nu}{d_h} \tag{4.11}$$

with

$$Nu = 1.86 \left(Re. \, Pr. \frac{d_h}{L} \right)^{0.33} \qquad\qquad Re < 2100: \text{Laminar flow} \qquad (4.12)$$

or

$$Nu = 0.023 Re^{0.8} \, Pr^{0.33} \qquad\qquad Re > 4000: \text{Turbulent flow} \qquad (4.13)$$

where K_m is the thermal conductivity of the water, Nu, Re and Pr are the Nusselt, Reynolds and Prandtl numbers, respectively.

4.2.2.1.5 Temperature Polarization (TP) and Concentration Polarization (CP)

The salt concentration profile on the membrane surface, C_m, can be calculated according to the following equation (Khayet, 2011). This equation is based on film theory, which incorporates CP as described in **Chapter 2**.

The effect of TP was calculated in terms of T_m/T_f, which is the ratio between the feed temperature at the membrane surface (T_m) and the feed temperature (T_f) (Mericq et al., 2010). Due to the application of vacuum in this system, the boundary layer on the permeate side was not relevant and therefore not taken into consideration in the TP equation.

In this analysis, the numerical influences of the TP and CP effect were taken into account by the Newton-Raphson method using the Jacobian matrix. This is based on the Taylor expansion series for approximating the function values to obtain a better estimated value of unknown variables. The T_m and C_m values were calculated using this method by considering TP and CP. In this context, as two equations are being used

simultaneously, the Jacobian matrix was applied to obtain the roots of the Newton-Raphson method:

$$f_1 = exp\frac{B\left(\frac{exp\left[\frac{-5.80 \times 10^3}{T_m}+1.39-4.86 \times 10^{-2}T_m+ 4.18 \times 10^{-5}T_m^2 + -1.45 \times 10^{-8}T_m^3+6.55\ log(T_m)\right]}{1+0.57257\left(\frac{C_m}{1000-C_m}\right)}-P_v\right)}{k} - C_m \qquad (4.14)$$

$$f_2 = T-\frac{B\left(\frac{exp\left[\frac{-5.80 \times 10^3}{T_m}+1.39-4.86 \times 10^{-2}T_m+ 4.18 \times 10^{-5}T_m^2 + -1.45 \times 10^{-8}T_m^3+6.55\ log(T_m)\right]}{1+0.57257\left(\frac{C_m}{1000-C_m}\right)}-P_v\right)H_v}{h_w} - T_m \qquad (4.15)$$

$$J = \left[\frac{\partial f_{1,0}}{\partial x_1} \quad \frac{\partial f_{1,0}}{\partial x_2} \quad \frac{\partial f_{2,0}}{\partial x_1} \quad \frac{\partial f_{2,0}}{\partial x_2}\right] \qquad (4.16)$$

$$J = [f_1 \ f_2] \qquad (4.17)$$

Eqs. (4.14) and (4.15) were represented in matrix form by Eqs. (4.16) and Eq. (4.17). The matrix of Eq. (4.18) was used to modify Eqs. (4.14) and (4.15) to Eq. (4.19), respectively. Eq. (4.19) was then rearranged to form Eq. (4.20). The two parameters (T_m and C_m) to be obtained in the matrix were solved using the Newton-Raphson method with Jacobian matrix:

$$\{x_{i+1}\} = \{x_i\} - [J]^{-1}\{f\} \qquad (4.18)$$

$$x_{i+1} = x_i - \frac{f(x_i)}{f'(x_i)} \qquad (4.19)$$

$$f(x_{i+1}) = f(x_i)+(x_{i+1}- x_i)\,f'(x_i) \qquad (4.20)$$

4.2.2.2 Estimating Feed Temperature

In this study, for steady state conditions, the heat transferred on the membrane surface was considered equal to the amount of heat transferred inside the membrane. As an initial assumption only, the assumed value of feed temperature, T_f was taken to be the value of the inlet feed temperature/ bulk feed temperature (T_3/T_{fb}) (**Table 4.1**). Thereafter, the feed temperature, T_f was determined by continuously comparing the calculated and experimental permeate flux as discussed in the algorithm presented in **Figure 4.4**. On the other hand, the feed temperature at the membrane surface (T_m) was calculated based on heat transfer coefficient, Eq. (4.11), using the experimental permeate flux, through the modeling as described in **Figure 4.4.**

It is important to highlight that the feed temperature, T_f increases when it is heated by the steam from the steam raiser and decreases due to the generated flux from different vapour pressure between feed and permeate sides in the module. Thus, heat exchange between the steam and the steam raiser, and between the feed and the permeate side should be considered to calculate the actual feed temperature, T_f along the length of the module. However, it was assumed that the feed temperature in the module, T_f was the same along the length, because its calculation is intensely convoluted and the amount of steam heat from the steam raiser transferred to the feed water was much higher than that of heat-loss when the feed water generated flux.

4.2.2.2.1 Algorithm Procedure

The model equations to calculate water flux were solved using the procedure (algorithm) shown in **Figure 4.4**. Initially, the feed temperature, T_f was assumed to be the value of the inlet feed temperature/ bulk feed temperature (T_3/ T_{fb}). The initial feed water molarity (i) was 1 M. The mass transfer coefficient (k) was obtained using Eq. (4.7) to Eq. (4.9), and the heat transfer coefficient (h_w) was calculated using Eq. (4.11)

to Eq. (4.13). The initial T_m and C_m values were calculated using Eqs. (4.14) and (4.15). Eqs. (4.16) and (4.17) are the matrix form of Eqs. (4.14) and (4.15). This was solved using the Newton-Raphson method with the Jacobian matrix.


```
                        Start
                          ↓
              Assume feed temperature (Tf)  ←──────────────┐
                          ↓                                │
              Feed solution concentration (Cf)             │
                       i=1                                 │
                          ↓                                │
          Calculate mass transfer coefficient (k)          │
                  Eq. (4.7) to (4.9)                       │
                          ↓                                │
          Calculate heat transfer coefficient (hw)         │
                  Eq. (4.10) to (4.13)                     │
                          ↓                                │
          Calculate membrane surface feed                  │
        temperature (Tm) and concentration (Cm) by    increase i
               Newton Raphson method with                  │
                  Jacobian Matrix                          │
                Eq. (4.14) to (4.20)                       │
                          ↓                                │
          Calculate membrane VMD coefficient (B)           │
                  Eq. (4.5) to (4.6)                       │
                          ↓                                │
          Calculate membrane surface water vapour          │
              pressure, Pm (Tm, Cm)                        │
                   Eq. (4.4)                               │
                          ↓                                │
          Calculate water flux (Jw)  Eq. (2.1)             │
                          ↓ Yes                            │
                                        No                 │
                  i > 3 ─────────────────────────────────►│
                          ↓ Yes                            │
        Compare model flux and experimental flux           │
                to calculate R²                            │
                          ↓                                │
                                        No                 │
              Is R² minimum? ──────────────────────────────┘
                          ↓ Yes
                        End
```

Figure 4.4   The procedure (algorithm) used to calculate water flux

When modified to Eqs. (4.16) and (4.17), these two matrices can be used in the Newton-Raphson method. VMD coefficient (B) of the membrane is simultaneously calculated

with T_m and C_m values, using Eqs. (4.5) and (4.6). Water vapour pressure on the membrane surface was obtained from Eq. (4.4) using the calculated T_m and C_m values. Subsequently, the water flux, J_w was obtained using Eq. (2.1). This process was repeated for increased feed concentration from 1 M to 3 M. When the feed water molarity (i) of 3 M was obtained the calculation was stopped. Thereafter the model flux and the experiment flux were compared. If a minimum correlation coefficient, R^2 between the experimental flux and the model flux was not achieved, the iteration was restarted with a newly assumed T_f.

4.2.3   RESULTS AND DISCUSSION FOR THE V-MEMD SALINITY EXPERIMENT AND MODELING

The performance of the one-stage V-MEMD system (in terms of permeate flux) was studied at different feed temperatures and feed flow rates. The experimental values of the permeate flux when feed water was concentrated, with the corresponding bulk feed temperatures, T_{fb} of 37.0°C, 40.5°C and 46.0°C, at v_f of 1.1 m/s are presented in **Figure 4.5** (Set I). **Figure 4.6** (Set II) shows the permeate flux at doubled flow velocity of 2.2 m/s with the corresponding bulk feed temperatures, $T_{fb} = 37.0$°C, 42.5°C and 48.7°C. In both cases, the permeate flux increased as the feed velocity and the feed temperature increased. This trend agrees with previous MD studies (Khayet, 2011; Bandini et al., 1997).

In terms of water quality, on the feed side, the average TDS value at the initial stage (1 M NaCl of feed concentration) for all experiments was around 86.2 mS/cm. The TDS value increased to an average of 262.9 mS/cm at the end of the experiment (with a concentration factor of 3). On the permeate side, the TDS value remained quite low with an average of 0.3 mS/cm. As such, salt rejection was approximately 99.5% in all cases.

The capacity to produce high quality water irrespective of the high feed salt concentration is an advantage of the V-MEMD system.
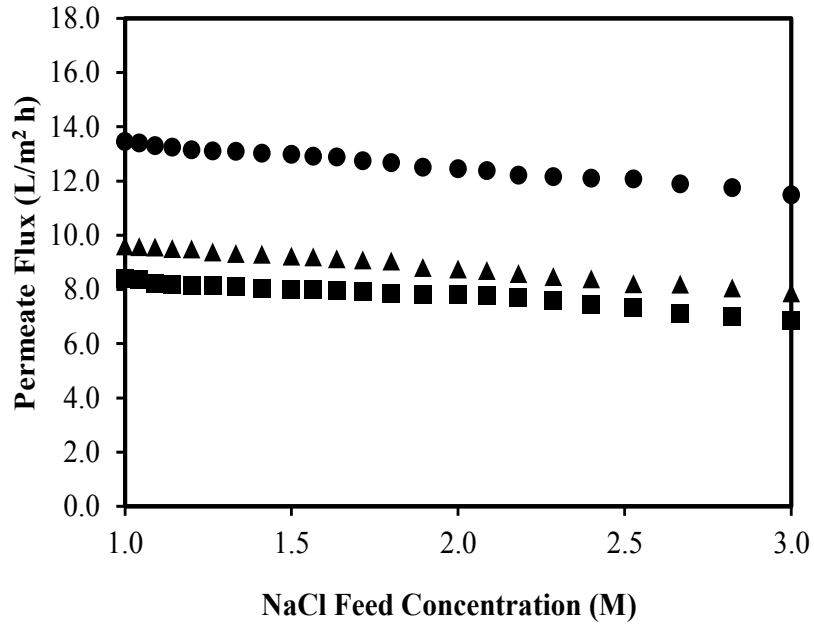
Figure 4.5 Permeate flux as a function of the feed concentration for different feed temperatures at $v_f = 1.1$ m/s (Set I) (T_{fb}: ● 46.0°C; ▲ 40.5°C; ■ 37.0°C).
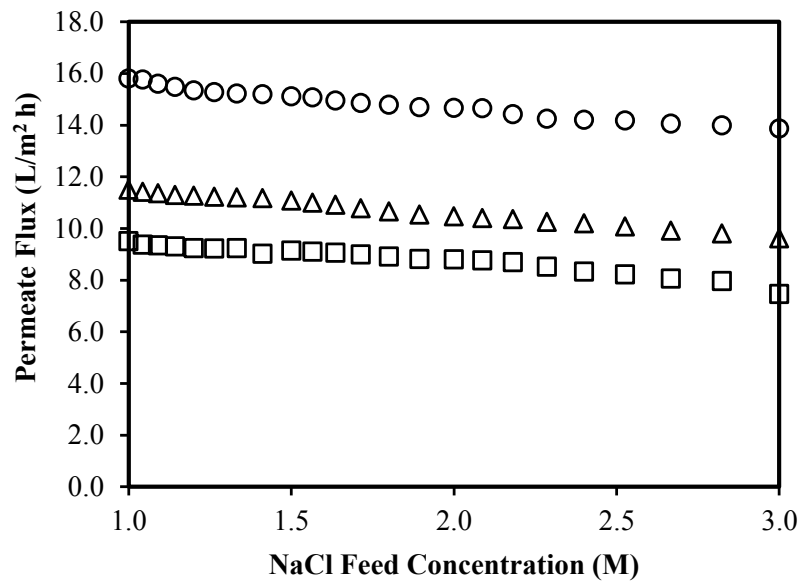
Figure 4.6 Permeate flux as a function of the feed concentration for different feed temperatures at $v_f = 2.2$ m/s (Set II) (T_{fb}: ○ 48.7°C; △ 42.5°C; □ 37.0°C).

4.2.3.1   Effect of feed water concentration

The permeate flux decreased when the feed water concentration increased. For instance, the flux obtained at the initial salt concentration of 1 M was 8.4 LMH. It declined to 6.9 LMH when NaCl was concentrated to 3 M (v_f of 1.1 m/s; T_{fb} of 37.0°C) which was only an 18% reduction. The reduction in permeate flux with feed water concentration was relatively constant under different conditions, regardless of the feed flow rate and feed temperature. The high salt concentration decreased the water vapour pressure of the feed solution. Hence, as feed salt concentration increased, the driving force for water evaporation declined, resulting in a lower permeate flux. This is represented by Eq. (4.4).

4.2.3.2   Effect of feed water temperature

At a feed concentration of 1 M of NaCl and v_f of 1.1 m/s, increasing the bulk feed temperature, T_{fb} by 9°C from 37.0°C to 46.0°C, increased the permeate flux by 64%; from 8.4 LMH to 13.5 LMH. A similar pattern was observed for all the concentrations.

4.2.3.3   Effect of feed velocity

The influence of feed flow velocity on permeate flux was investigated by increasing v_f from 1.1 m/s to 2.2 m/s. A constant flux increment of around 14-20% was observed for all bulk feed temperature values when v_f was doubled. For instance, at 1 M of feed concentration and T_{fb} of 37.0°C, the permeate flux increased from 8.4 LMH to 9.6 LMH with an increase of v_f from 1.1 m/s to 2.2 m/s. The relationship between feed flow velocity and permeate flux increment has been explained in detail in **Sections 4.1.3.1**. As established earlier, increasing v_f from 1.1 m/s to 2.2 m/s did not significantly contribute to permeate flux increment, indicating that a good mixing intensity was already achieved at the lower flow velocity used in this study. Similarly, previous studies have shown that increasing the flow velocity beyond the optimum

hydrodynamic capacity of a system will not significantly increase the permeate flux (asymptotic value) (Mericq et al., 2009).

4.2.3.4   Model simulation

The modeling data of permeate flux with different salt concentrations, feed temperature and flow rate were compared with the experimental values as shown in **Figure 4.7**. The model prediction agreed well with the experimental data, whereby $R^2 \geq 0.94$ was obtained. This indicated that the modeling data could accurately predict the expected flux.
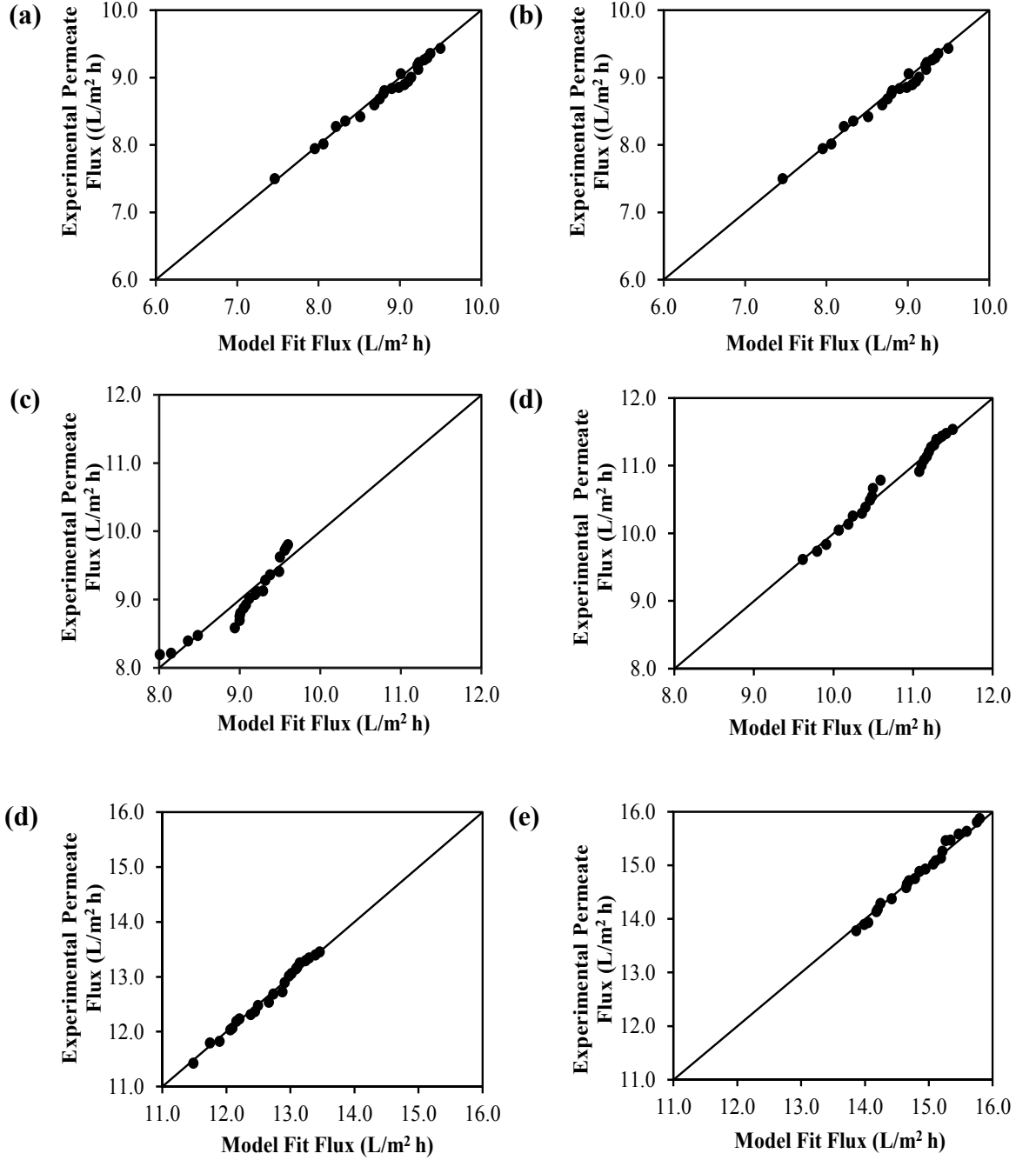
Figure 4.7 Comparison between modeling and experimental permeate flux **(a)** bulk feed temperature, T_{fb}: 37.0°C, v_f: 1.1 m/s, **(b)** bulk feed temperature, T_{fb}: 37.0°C, v_f: 2.2 m/s, **(c)** bulk feed temperature, T_{fb}: 40.5°C, v_f: 1.1 m/s, **(d)** bulk feed temperature, T_{fb}: 42.5°C, v_f: 2.2 m/s, **(e)** bulk feed temperature, T_{fb}: 46.0°C, v_f: 1.1 m/s, **(f)** bulk feed temperature, T_{fb}: 48.7°C, v_f: 2.2 m/s.

4.2.3.5 Polarization effect on V-MEMD system

To represent the effect of TP and CP, values of feed temperature and concentration close to the membrane surface (actual values) were calculated from the model equations as explained in the algorithm procedure (**Figure 4.4)**.

The effect of TP calculated in terms of T_m/T_f, is the ratio between the feed temperature at the membrane surface (T_m) and the feed temperature (T_f). Due to the application of vacuum in this system, the boundary layer on the permeate side was not relevant and therefore not included in the TP equation. A ratio value closer to 1 (higher value) indicates a lower polarization effect, while a lower value indicates a higher effect of polarization. Meanwhile, for the effect of CP, which is the ratio of C_m/C_f, a higher ratio value indicates polarization has greater effect.

Figure 4 8 (a) and **(c)** shows the TP and CP ratio as a function of feed concentration at different feed temperatures and feed flow rates (Set I and Set II), respectively. This ratio is based on the vacuum pressure values which changes with feed flow rates and feed temperatures as shown in **Table 4.1**. In view of the deviation of vacuum pressure values in the permeate side (3.9 to 5.1 kPa at v_f=1.1 m/s and 4.0 to 6.0 kPa at v_f=2.2 m/s) as given in **Table 4.1**, it was difficult to identify the influence of different operating conditions on the effect of polarization. As such, the TP and CP ratios were re-calculated based on a set (or reference) value of 4.5 kPa of vacuum pressure. This allows a comparison to be made between the TP and CP effects at a constant (or reference) pressure value. The values of TP and CP calculated based on the reference vacuum pressure value were represented as TP' and CP' (**Fig. 4.8 (b)** and **(d)**). The TP' and CP' ratio values were then used to directly identify the operating parameters that significantly influenced the polarization factor for the V-MEMD system. **Table 4.2** shows the calculated ratio of TP' and CP'. Also, the predicted permeate flux, based on

the reference vacuum pressure value was used in these calculations. The CP and TP ratio trend in **Figure 4.8 (a)** and **(c)** was the same as the TP' and CP' ratio trend illustrated in **Figure 4.8 (b)** and **(d)**.

In this study the CP ratio was in the range of 1.15 to 1.40 while that of the TP ratio was much lower, from 0.96 to 0.99 for the feed solution of 1 M of NaCl. Concentrating the feed solution from 1 M to 3 M of NaCl reduced the effect of TP further by 0.5 to 1.0%. A previous study has also shown that the effect of TP becomes insignificant at higher salinity concentrated feed solution (1.0 M to 1.7 M NaCl) (Martínez-Díez et al., 1999). This is because at higher salt concentration, vapour pressure is reduced as shown in Eq. (4.4). Because less separation is taking place, less latent heat is required and the feed temperature in the bulk side does not change significantly (Bahmanyar et al., 2012; Martínez-Díez et al., 1999).

Increasing the temperature increases the vapour pressure. The higher separation should increase the latent heat required, increasing the difference between the feed temperature and the membrane surface temperature. However, in this study, only a 2 to 4% increase in the effect of TP was observed. This was attributed to the lower range of feed temperature used and the high hydrodynamic capacity of this system. Likewise, Cath et al. (2004) investigated the performance of an enhanced DCMD configuration at a low feed temperature of 40.0°C and a high flow velocity of 2.2 m/s vacuum on the permeate side. They also observed a significantly smaller TP effect. However, several studies on the VMD system have reported that the effect of TP was dominant (Mengual et al., 2004; Martínez-Díez et al., 1999; Banat et al., 2003). These studies were carried out on simple bench scale systems with external heating. In these studies the bulk feed temperatures were set high between 55.0°C and 80.0°C. Furthermore, these experiments were conducted at a low flow velocity (0.05 m/s to 0.5 m/s).

In comparison, the advantage of the V-MEMD system was that the internal heating module enabled heat to be internally transferred to the feed water at a lower temperature range (37.0°C to 46.0°C). Consequently, heat loss could be minimal and would have led to TP having less effect. At the same time the system was set at a high hydrodynamic capacity, with a flow velocity of 1.1 m/s to 2.2 m/s. This considerably reduced the presence of polarization.

Table 4.2 Influence of different operating conditions on the ratio of TP' and CP'.

| Bulk Feed Temp., | Bulk Feed Conc., | Flow velocity, v_f (m/s) | | | |
| T_{fb} (°C) | C_b (M) | 1.1 | | 2.2 | |
		TP' Ratio	CP' Ratio	TP' Ratio	CP' ratio
	1	0.99	1.15	0.99	1.15
37.0	2	0.99	1.13	0.99	1.12
	3	0.99	1.10	0.99	1.10
	1	0.97	1.26	0.98	1.25
40.5 / 42.5	2	0.98	1.23	0.98	1.23
	3	0.98	1.20	0.98	1.20
	1	0.96	1.40	0.96	1.38
46.0/ 48.7	2	0.96	1.36	0.96	1.35
	3	0.97	1.33	0.97	1.32
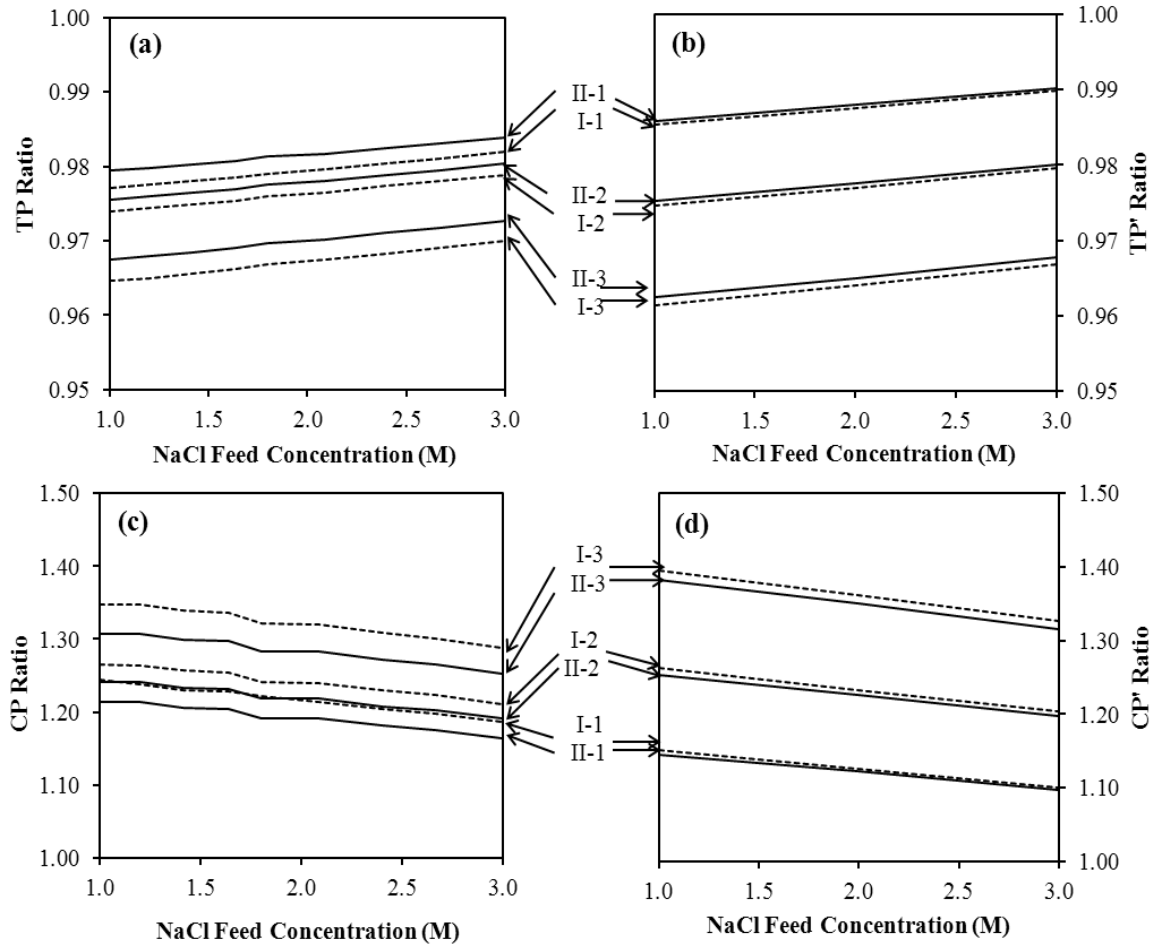
Figure 4.8 Polarization effect in the V-MEMD system **(a)** and **(c)** TP and CP ratio as a function of feed concentration with different feed temperatures and feed velocity (Set I and Set II) based on actual vacuum pressure value **(b)** and **(d)** TP' and CP' ratio as a function of feed concentration with different feed temperatures and feed velocity (Set I and Set II) based on reference value of 4.5 kPa vacuum pressure **(**----- 1.1 m/s; ——2.2 m/s; (I-1) 37.0ºC (I-2) 40.5ºC (I-3) 46.0ºC (II-1) 37.0ºC (II-2) 42.5ºC (II-3) 48.7ºC).

.

4.3 DCMD PERFORMANCE WITH SUITABLE FEED/PERMEATE VELOCITY

In DCMD studies, the importance of feed temperature in enhancing permeate flux value has been widely analysed (Srisurichan et al., 2006). Apart from feed temperature, a number of MD studies have recommended hydrodynamic conditions such as turbulent conditions and high flow velocity (normally, the highest allowable velocity in a batch-scale unit) to achieve a high permeate flux. A higher hydrodynamic turbulent condition increases the heat transfer and lowers the temperature polarization effect in MD, enabling higher permeate flux to occur (Bui et al., 2010; Banat and Simandl, 1998). In this regard, Srisurichan et al. (2006), calculated vapour transport resistance of pure water to represent the effect of flow velocities. The results showed that pure water transport resistance in the feed boundary layer decreased significantly with increasing flow velocity. Importantly, this study also pointed out that the pressure of high flow velocity would increase the risk to membrane wetting as shown by other studies (Zhang et al., 2010).

It is therefore important to optimize the flow velocities in the DCMD system design. In DCMD operation, apart from the feed flow velocity, the circulation of cooling water on the permeate side of the membrane (permeate velocity) may also play a role in the vapour transport mechanism. However, a number of MD studies have reported that permeate condition plays only a minor role in improving DCMD permeate flux (Bui et al., 2010; Banat and Simandl, 1998, Schofield et al., 1990). For instance, Banat and Simandl (1998) detected a negligible effect on the permeate flux when permeate velocity was increased. Similarly, Bui et al. (2010) reported that the permeate velocity improved the DCMD mass flux minimally and therefore, operating DCMD at a high permeate velocity may be unbeneficial.

In contrast, some MD studies have suggested that an increase in permeate velocity would be beneficial in maintaining a lower permeate temperature, contributing to higher mass transfer (Song et al., 2007). In this regard, one study lowered the permeate/cooling temperature from 20°C to 5°C instead of the feed temperature to achieve the comparable temperature gradient (Dow et al., 2010). This study is noteworthy in that it reflects the importance of permeate velocity for the DCMD system. In an attempt to improve the performance in DCMD with permeate/cooling water, two studies introduced vacuum to reduce the pressure at the DCMD unit's permeate side (Martinetti et al., 2009; Cath et al., 2004). These studies revealed that reduced permeate pressure increased the permeate flux, which was attributed to lower vapour transport resistance on the permeate side.

Hence, in this section, the relationship between optimal flow velocity (of feed and permeate) and DCMD performance was investigated. For this reason the study evaluated the performance of DCMD using a number of measurement tools to demonstrate the role of optimal feed and permeate velocity in enhancing DCMD operation.

4.3.1 EXPERIMENTAL OPERATING CONDITIONS

The DCMD baseline operating performance study was conducted with DI water. Previous DCMD studies have used different ranges of flow velocity, varying from as low as 0.05 m/s to as high as 3.0 m/s (Alkhudhiri et al., 2012). In this study, a range of feed flow velocity, v_f and permeate flow velocity, v_p (v_f & v_p = 0.5 m/s to 2.2 m/s) was used to identify the optimal range of flow velocity. The feed bulk temperature, T_{fb} was kept constant at $70\pm0.2^{\circ}$C. The feed temperature was selected from the feed temperature ranges (60 to 80°C) recommended in previous DCMD studies (Song et al., 2007; Srisurichan et al., 2006). The permeate bulk temperature, T_{pb} was kept constant at $24\pm0.2^{\circ}$C.

The performance of the DCMD system was measured in terms of permeate flux, RR and heat transfer coefficient. An empirical approach based on experimental values was adopted to calculate the heat transfer coefficient (Eqs. 4.11 to 4.13). It was assumed that brine and permeate streams enter the respective module section at a uniform temperature and the heat loss from the feed bulk to the membrane surface was minimal in the small membrane module. Hence, the membrane surface temperature, T_{fm} was taken as the average value of feed temperature inlet and feed temperature outlet (brine).

4.3.2   RESULTS AND DISCUSSION ON DCMD PERFORMANCE WITH SUITABLE FEED/PERMEATE VELOCITY

4.3.2.1   Optimal flow velocity

4.3.2.1.1   Permeate flux

Increasing the flow velocity from the range of 0.5 m/s to 1.6 m/s ($v_f = v_p$), indicated a linear increase in permeate flux with DI water, as widely reported in other DCMD studies (Alkhudhiri et al., 2012). However, at the high range flow velocity of 1.6 m/s to 2.2 m/s, the permeate flux did not increase linearly (in the experimental set-up used in this study); rather, it approaches an asymptote rate as shown in **Figure 4.9**. This could have been due to the fact that at higher velocity ranges, the mass flux is not as sensitive to increases in velocities, where the heat transfer is no longer the limiting parameter. Higher applied feed pressure could also be explained by higher membrane resistance as implied in other membrane studies (Izquierdo-Gil et al., 2008; Hoek and Elimelech, 2003; Zhang et al., 2011). Hence, it would be more appropriate to identify the optimal range of flow velocity for a lower pressure operation, rather than choosing the highest flow velocity as generally recommended in MD studies (Bui et al., 2010). To identify the optimal range of flow velocity, apart from permeate flux, other indicators such as recovery ratio, heat transfer coefficient and pumping energy were considered.

4.3.2.1.2 Recovery ratio

In membrane studies, recovery ratio is an important factor that is used to determine the design size and economic value of the membrane system. A recent publication on MD economic evaluation projected a recovery ratio of 4.4% for a single pass MD (Saffarini et al., 2012). The calculated recovery ratio values in this study (Eq. 4.1) showed a declining trend of recovery ratio when the flow velocity increased (2.4% at 0.5 m/s to 1.0% at 2.2 m/s). The same pattern was observed with the V-MEMD system.

4.3.2.1.3 Heat transfer coefficient

In MD the heat transferred is an important indicator of the system's efficiency. One of the determining factors for high heat transfer is high flow velocity/mass transfer (Schofield et al., 1990). Accordingly, in this study, a higher flow velocity resulted in a higher heat transfer coefficient (0.66×10^4 W/m^2 K at 0.5 m/s to 3.42×10^4 W/m^2 K at 2.2 m/s) on the heating side (feed side). This was calculated from Eqs. (4.11) to (4.13).

4.3.2.1.4 Pumping energy

Additionally, an important factor that needs to be taken into consideration when choosing the optimal flow velocity would be the pumping energy. As the flow velocity increased, the applied pressure increased, which is an acknowledged fluid dynamics channel flow phenomenon (Bui et al., 2010; Banat and Simandl, 1998). However, an increase in applied pressure requires a higher pumping energy. This is because, typically the pumping energy is measured as a function of flow rate and pressure in the feed and permeate side, according to Eq. (4.3). An increase in flow velocity resulted in an increased pumping energy (1.56×10^{-7} W at 0.5 m/s to 1.04×10^{-1} W at 2.2 m/s).

Based on these indicators, the optimal range of flow velocity falls between the windows of v_f & v_p = 0.8 to 1.1 m/s as shown in **Figure 4.9**. At this range the permeate flux was

between 29.8 LMH to 35.7 LMH. Although the permeate flux was lower by 20% compared to the higher flow velocity of 2.2 m/s, the recovery ratio and the pumping energy improved by 50% to 60%.
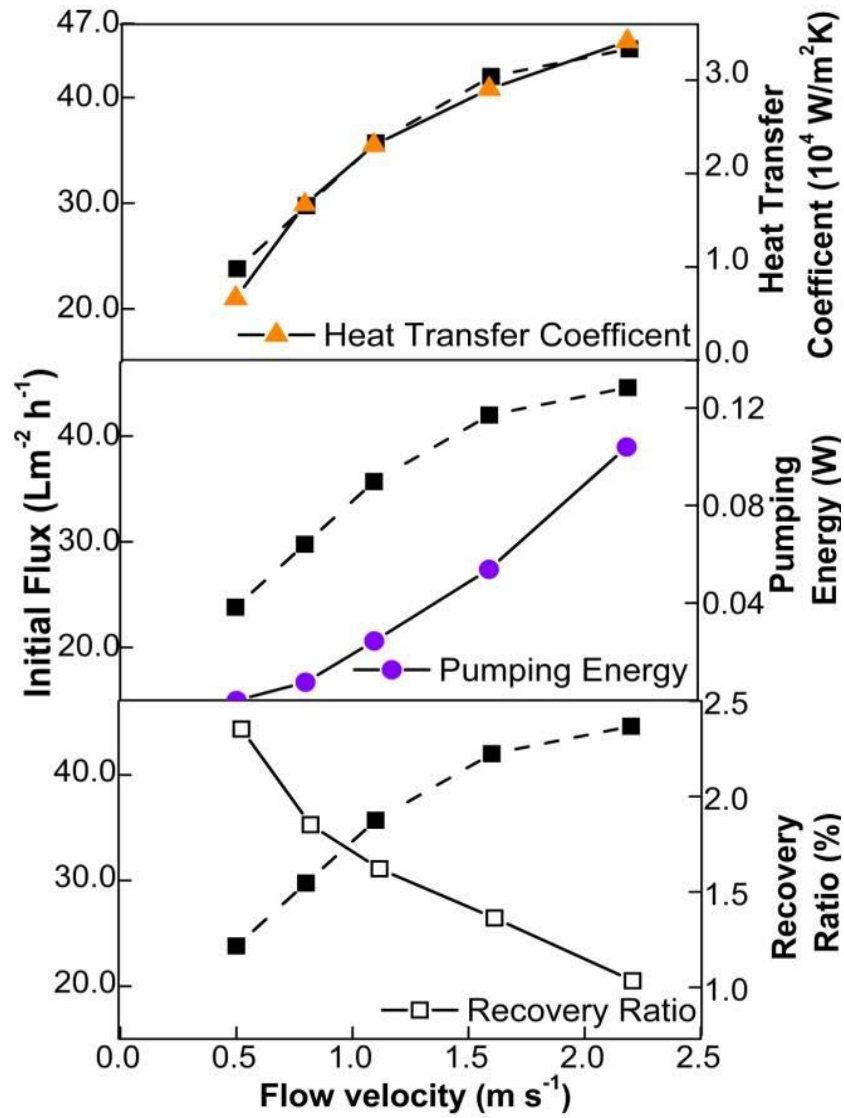
Figure 4.9 Performance output of DCMD with DI water at varied flow velocity ratio.

4.3.2.2 Optimal permeate flow velocity, v_p

Upon determining the required v_f, a suitable v_p combination was identified based on the permeate temperature gradient, the permeate to feed pressure ratio and the combination of both these cases as shown in **Table 4.3**.

Table 4.3 Influence of P'_p/P'_f and cooling temperature gradient on permeate flux based on varying v_p/v_f ($v_f = 0.8$ m/s).

v_p (m/s)	v_p/v_f	P_p/P_f	Cooling Tempt. Gradient (°C)	Flux, J (LMH)
0.5	0.6	≈ 0	5.03	34.2
0.8	1.0	0.18	4.98	29.8
1.1	1.4	0.25	4.85	35.7
1.6	2.4	0.78	4.78	22.8
2.2	2.8	1.50	4.70	18.0

4.3.2.2.1 Influence of permeate temperature gradient

An increase of v_p has been reported to be beneficial because it results in a lower permeate temperature, contributing to higher permeate flux (Song et al., 2007). Likewise in our study, at constant v_f of 0.14 m/s, increasing the v_p from 0.06 m/s to 0.26 m/s, resulted in an increase of the permeate flux by almost 30% as shown in **Figure 4.10**. The permeate temperature gradient also improved accordingly, supporting what previous studies had concluded. It is important to highlight that at these ranges of low flow velocities (0.06 m/s to 0.26 m/s), the applied pressure of the feed and permeate was negligible at around 0 kPa. However, at higher v_f of 0.8 m/s as shown in **Figure 4.11** the results of our investigation demonstrated that apart from the influence of permeate temperature gradient, the permeate to feed pressure ratio (P'_p/P'_f) and the

combination of both these factors (permeate temperature and pressure ratio) influenced the permeate flux. An equal combination of v_f & v_p of 0.8 m/s (v_p/v_f =1) led to a P'_p/P'_f ratio of 0.18, cooling temperature gradient of 4.98°C, resulting in J = 29.8 LMH.
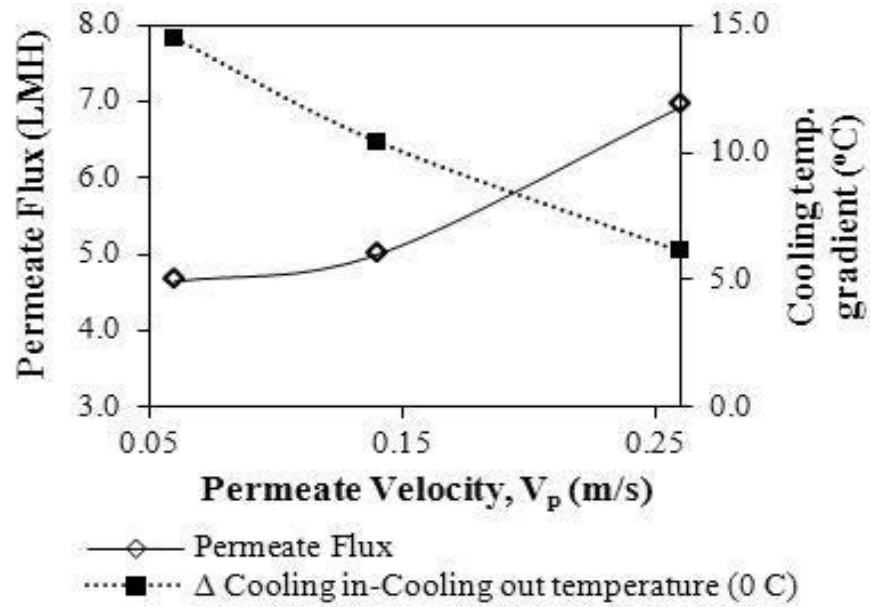
Fig. 4.10 Permeate flux as a function of varying permeate velocity at v_f= 0.14 m/s.
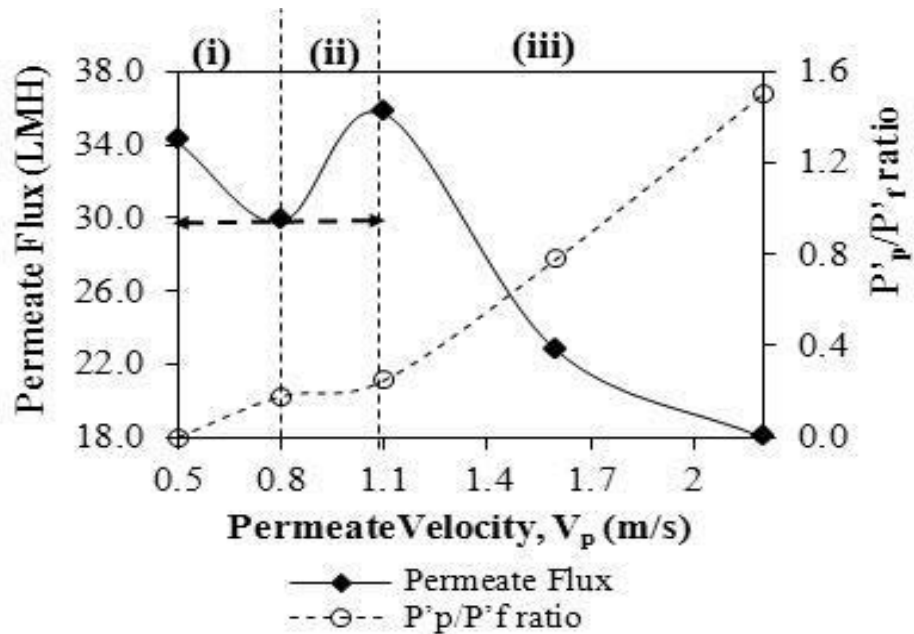
Figure 4.11 Permeate flux and P'_p/P'_f as a function of varying permeate velocity at v_f = 0.8 m/s.

4.3.2.2.2 Influence of permeate to feed pressure ratio

In one MD study, Cath et al. (2004) investigated the impact of permeate pressure on permeate flux. Their study highlighted that reducing the permeate pressure appropriately would contribute to an increase in permeate flux in DCMD as this would be similar to the presence of vacuum (i.e. lower pressure on the permeate side would lead to a higher pressure difference across the membrane). Also, air from the pores of the membrane would be reduced, resulting in less resistance to the flow of vapour across the membrane and higher permeate flux. Similarly, in our study, at a lower permeate velocity setting of $v_p/v_f = 0.6$, the effect of lower permeate on feed pressure ratio $P'_p/P'_f \approx 0$ is the dominant factor that resulted in an increase of permeate flux by 14.8% (phase (i) **Figure 4.11**) in comparison to $v_p/v_f = 1$.

4.3.2.2.3 Influence of a combination of permeate to feed pressure ratio and temperature gradient

This study also investigated the behavior of a slight increase of v_p/v_f from 1.0 to 1.4 (phase (ii) **Figure 4.11**). This led to a higher P'_p/P'_f ratio of 0.25 but a lower cooling temperature gradient of 4.85°C. This combination of conditions resulted in a permeate flux, J=35.7 LMH, with an increment of 19.8%, in comparison to $v_p/v_f = 1$. These findings demonstrated that despite a slight increase in the P'_p/P'_f ratio, the higher mass transfer from the lower cooling temperature gradient was caused by the permeate flux increment as discussed earlier (Song et al., 2007). This confirmed that a combination of P'_p/P'_f ratio as well as cooling temperature gradient was important. However, a further increase in the P'_p/P'_f ratio between 0.78 up to 1.50 led to a significant permeate flux decline despite achieving a lower cooling temperature gradient between 4.70 - 4.78°C (phase (iii) **Figure 4.11**). The increase of P'_p/P'_f could have resulted in the increase of

air pressure in the membrane pores, which in turn increased the resistance to mass transfer.

Previous DCMD studies have highlighted that air trapped in the pores of the membrane imposed molecular resistance and reduced permeate flux (Fane et al., 1987). Degasification of the pores of the membrane from the permeate side and/or reduction of pressure on the permeate side have been shown to be effective in reducing the membrane resistance (Cath et al., 2004). In view of this, finding an optimal combination of v_f and v_p based on the P'_p/P'_f ratio as well as cooling temperature gradient would be necessary to obtain a suitable permeate flux, without the need for significant pumping energy increment to increase the flow velocity. For instance, comparing the permeate flux results, at a condition of v_f & v_p =1.1 m/s, a permeate flux of 35.7 LMH was achieved as shown in **Figure 4.9**. The same permeate flux was obtained at v_f=0.8 m/s & v_p=1.1 m/s as depicted in **Table 4.4**. Based on these ranges of velocity the scaling pattern was analysed and compared as discussed in more detail in **Chapter 5**.

Table 4.4 Comparisons of DCMD performance at different combination settings of v_f & v_p.

v_f & v_p (m/s)	Initial Flux, J (LMH)	Pumping Energy $(x10^{-1}$ W)	Recovery Ratio (%)
0.8 & 0.8	29.8	0.055	1.85
0.8 & 1.1	35.7	0.062	2.21
1.1 & 1.1	35.7	0.244	1.62

4.4   SUMMARY

4.4.1   Summarizing the operating parameters influencing the performance of V-MEMD system

The results of this study established that a combination of operating factors were important in improving the performance of the V-MEMD system. Its performance was evaluated in terms of permeate flux, RR, GOR and pumping energy. Based on these results:

(1)   Lowering the permeate pressure was a positive influence on the performance of the V-MEMD system. The highest permeate flux of 13.5 LMH was achieved at 5.0 kPa with minimal additional energy consumption.

(2)   Increasing the feed temperature significantly enhanced the permeate flux, achieving a value of 11.8 LMH at 65.0°C. The GOR increased proportionally and reached a constant value from 55°C to 60°C onwards, and slightly reduced thereafter. A combination of these factors shows that a feed temperature of 57.0°C to 60.0°C, is the suitable value for this system (without incurring energy wastage).

(3)   Increasing the feed velocity increased the permeate flux, but reduced the RR. An intermediate feed velocity of 0.8 to 1.1 m/s achieved a good balance concerning the performance of both RR and permeate flux.

(4)   This study was useful to identify the suitable range of operating conditions for the V-MEMD system.

4.4.2   Summarizing V-MEMD salinity experiment and modeling

This study analyzed the performance of a modified design VMD system (V-MEMD) with highly saline water. Experiments were carried out with 1 M of NaCl feed solution that was concentrated up to 3 M at different feed flow rates (flow velocity) and feed temperatures. The results showed that the V-MEMD system employed was suitable for

producing high quality permeate (more than 99.5% rejection rate) with highly saline water. The findings are as follows:

(1) The permeate flux reduced by only 18 - 20% for all conditions when 1 M NaCl was concentrated up to 3 M NaCl. An increase in feed temperature improved the permeate flux significantly by 64%.

(2) The model prediction agreed well with the experimental data ($R^2 \geq 0.94$). This indicated that the model can effectively predict the system's performance under high salt concentration.

(3) Maintaining a reasonable permeate flux with a minimal polarization effect was important for the system's efficiency. The V-MEMD system performed well under high salt concentration, achieving a permeate flux ranging from 13.5 LMH to 15.8 LMH.

4.4.3 Summarizing DCMD operating performance with suitable feed/permeate velocity

This study demonstrated that a suitable permeate flow velocity for a feed velocity can be identified based on the permeate temperature gradient; and the permeate to feed pressure ratio. The results showed that, for DCMD, an optimum combination of feed and permeate flow velocity was able to improve the system's performance (i.e. increased recovery ratio and reduced pumping energy) while maintaining the same permeate flux. Overall the results established the importance of both feed and permeate velocity in a DCMD setting. Likewise, in a V-MEMD system, the permeate pressure wielded an important influence on how well the system performed.

In the following chapter, the influence of optimum combination of feed velocity and permeate pressure/velocity on scaling development for both the V-MEMD and DCMD system will be analysed.

CHAPTER 5

ANALYSIS OF SCALING

DEVELOPMENT IN MD

University of Technology Sydney

Faculty of Engineering & Information Technology

This chapter evaluates the development of gypsum scaling in MD. A detailed analysis of the influence of operating conditions on the scaling development was carried out. Specifically, the study focused on the role of hydrodynamic conditions and related permeate conditions. Membrane autopsy analysis was conducted to evaluate the influence of hydrodynamic conditions on the occurrence of scaling.

The first part discusses the scaling formation with different operating conditions in the V-MEMD system (**Section 5.1**). The second part looks at the scaling development analysis supported with a detailed membrane autopsy using the bench scale DCMD system (**Section 5.2**).

<Publications related to this chapter>

Naidu, G, Jeong, S., & Vigneswaran, S. (2014). Influence of feed/permeate velocity on scaling development in a direct contact membrane distillation. Separation and Purification Technology, 125, 291-300.

Naidu, G.,Jeong, S., Choi, Y., Jang, E., Hwang, T. M., & Vigneswaran, S. (2014). Application of vacuum membrane distillation for small scale drinking water production**.** Desalination, 354, 53-61.

5.1 SCALING DEVELOPMENT ANALYSIS IN MD

5.1.1 INTRODUCTION

The potential of MD as a stand-alone solar operated system has been investigated by previous studies. For instance, one modeling study established the feasibility of solar-powered MD for producing water derived from brackish water (Ding et al., 2005). Another study demonstrated the potential of hollow fiber direct contact membrane distillation (DCMD) for removing fluoride from brackish water, achieving a high permeate flux of 35.6 LMH at 80°C feed temperature. However, one study observed that membrane scaling resulted from $CaCO_3$ precipitation (Hou et al., 2010).

Since MD is not a hydraulic pressure driven process, crystal scale formation in MD has been reported to be loosely deposited on the membrane surface (Gryta, 2008b; He et al., 2008; Srisurichan et al., 2006). However, it is important to acknowledge that the characteristics of natural saline feedwater such as seawater and groundwater contain sparingly soluble salts (mainly $CaSO_4$ and $CaCO_3$). In an almost zero liquid discharge MD operation, the highly concentrated sparingly soluble salt in the feed solution would be in direct contact with the membrane. Additionally, the thermal application in MD would inverse the solubility of certain salts. Hence, it is critical to analyse the scaling development in MD operation.

In this regard, a number of bench scale MD studies investigating scaling performance, have highlighted the prevalence of $CaSO_4$ scaling in MD, compared to other types of salts such as $CaCO_3$ and Na_2SiO_3 (He et al., 2008; Srisurichan et al., 2006; Nghiem and Cath, 2011). $CaSO_4$ is inversely soluble at temperatures higher than 50°C. Hence, in the first section of this chapter, $CaSO_4$ scaling development under saline conditions is analysed in the V-MEMD system. This study evaluated the influence of different operating scenarios on the scaling development. For this to occur, a suitable operating

condition for membrane scaling reduction was identified for the V-MEMD system. In the second section, the relationship between optimal flow velocity (of feed and permeate) and $CaSO_4$ scaling development is investigated using the DCMD system.

5.1.2   MATERIALS AND METHODS

5.1.2.1   Experimental Set up

Experiments were carried out employing the MemSYS V-MEMD system as well as the bench scale DCMD system.

5.1.2.2   Feed Solution

Scaling experiments were conducted with a saline $CaSO_4$ feed solution, a mixture of $CaCl_2$ and Na_2SO_4 with NaCl (feed I). The initial total dissolved solids (TDS) of feed I was 55.6 g/L. Meanwhile, feed II comprised a mixed solution of Ca, SO_4, Mg, Na, Cl and Fe; these represented the main components of a saline groundwater at an initial TDS of 64.2 g/L as shown in **Table 5.1**.

Table 5.1 Experimental feed solutions.

	Feed solution	Purpose
Feed I	0.02 M $CaCl_2.2H_2O$ + 0.06 M Na_2SO_4 and 1.0 M NaCl	$CaSO_4$ scaling development in high saline TDS water
Feed II	0.04M $CaSO4.2H_2O$ + 1.0 M NaCl with 6.89 mM Mg and 0.09 mM Fe	Mixed combination solution representing the main components of natural saline ground water source

5.1.2.3   Scaling Experimental Operating Condition

The scaling development investigation of the V-MEMD system was executed using 20 L of saline $CaSO_4$ solution (feed I) at the following operating conditions: heating temperature, T_h= 60°C, feed velocity, v_f= 0.9 m/s and permeate vacuum, P_p=10.0 kPa (condition I). To investigate the influence of permeate pressure on scaling development

in the V-MEMD system, P_p of 12.5 kPa (condition II) and P_p of 15.0 kPa (condition III) were used. Meanwhile, to examine the influence of turbulence, v_f was varied from 0.9 m/s to 0.6 m/s (condition IV) and 0.3 m/s (condition V). The details of the experimental settings are shown in **Table 5.2**.

Table 5.2 Scaling experimental setting at a constant heating $T_h = 60^oC$.

Experimental Condition	Feed flow velocity, v_f	Permeate vacuum , kPa
I	0.9	10.0
II	0.9	12.5
III	0.9	15.0
IV	0.6	10.0
V	0.3	10.0

5.1.2.4   Scaling Measurement

For the purpose of experimentally investigating the issue of scaling, a number of measurements were used as shown below.

5.1.2.4.1   Permeate Flux

The permeate flux V-MEMD measurement has been explained in **Section 4.1.2.3.1 (Chapter 4).**

5.1.2.4.2   Saturation Ratio (SR)

The concentrations of Ca^{2+} in the feed and permeate solutions were determined using microwave plasma atomic emission spectrometer (MP-AES, Agilent 4100). The SR of $CaSO_4$ was measured based on the depletion of the dissolved Ca^{2+} over time (He et al., 2008). Hence, SR of $CaSO_4$ was defined as the ratio of dissolved $[Ca^{2+}]$ concentration in

the brine feed solution over experimental time as a function of the initial $[Ca^{2+}]$ concentration in the bulk feed solution as shown below (Lee et al., 1999):

$$SR = [Ca^{2+}]_{brine}/[Ca^{2+}]_{initial} \qquad\qquad (5.1)$$

The dissolved $[Ca^{2+}]$ concentration in the brine feed solution was measured after filtering the feed and brine solution through 0.22 μm filter for dissolve calcium $[Ca^{2+}]$. Over time, crystals are formed and since only the dissolved calcium was measured in the brine, the value of $[Ca^{2+}]$ in the brine will decrease.

5.1.2.4.3   Vapour Transport Resistance

Vapour transport resistance was used to measure the resistance in the system. In pressure operated systems, the resistance is represented by the transmembrane pressure difference of the applied pressure which is the driving force of the operation. In MD, the transport resistance is represented by the vapour pressure difference over time, which is the driving force of the operation (Srisurichan et al., 2006). The feed vapour transport resistance, VR_f and permeate vapour transport resistance, VR_p were determined as follows (Srisurichan et al., 2006):

$$VR_f = (P_{fb} - P_{fm})/J \qquad\qquad (5.2)$$

$$VR_p = (P_{pm} - P_{pb})/J \qquad\qquad (5.3)$$

where P_{fb} is the vapour pressure on the bulk feed, P_{fm} is the vapour pressure on the feed membrane surface, and P_{pb} is the vapour pressure on the bulk permeate, P_{pm} is the vapour pressure on the permeate membrane surface. The vapour pressure was determined from the experimental temperature value based on Antoine equation (Khayet, 2011).

$$P(T) = exp\left(23.1964 - \frac{3816.44}{-46.14 + T}\right) \qquad (5.4)$$

In this study, an empirical approach based on experimental values was adopted for the calculations. It was assumed that brine and permeate streams enter the respective module section at a uniform temperature and the heat loss from the feed bulk to the membrane surface was minimal in the small membrane module. Hence, the membrane surface temperature, T_{fm} was taken as the average value of feed temperature inlet and feed temperature outlet (brine).

5.1.2.4.4   Concentration Polarization (CP)

In this study, CP ratio was determined according to the film-based theory using the following equation (Khayet, 2011):

$C_{fm}/C_f = exp(J/k_w)$ $\qquad\qquad\qquad\qquad\qquad\qquad\qquad\qquad$ (5.5)

where C_{fb} and C_{fm} are the solute concentrations of bulk feed and membrane surface feed and k is the mass transfer coefficient. The mass transfer coefficient, k_w, was calculated from the dimensionless Sh number, where $Sh=(k_w \cdot D_h)$ /d; $Sh= 0.023Re^{0.8}Sc^{1/3}$ for turbulent flow.

5.1.2.4.5   Turbidity and Induction time

In the scaling investigation, the induction period (T_{ind}) is very important for indicating the development of crystals in the bulk solution. T_{ind} is defined as the time period of the formation of detectable crystals (between the creating of supersaturation and the appearance of a new solid phase) (Oh et al., 2009). Previous studies have indicated T_{ind} to be the point of rapid decrease in ion concentration (due to ion depletion) and a sharp rise in turbidity (due to precipitation) (Park et al., 2013; Shih et al., 2004). Turbidity in feed solution was measured using a portable turbidity meter (2100Q, HACH) to represent the precipitation rate of bulk crystallization (Oh et al., 2009).

The conductivity of the feed and permeate solutions was measured using a conductivity meter (HQ40d, HACH). Conductivity in the feed solution represented the increase of total ion concentration with time. The conductivity of the permeate solution was measured to determine the occurrence of membrane wetting. An increase in permeate solution conductivity during the experiment would indicate the feed solution was discharged to the permeate water through the membrane.

5.1.2.4.6   Membrane Observation

Zeiss Supra 55VP field emission scanning electron microscope (FE-SEM) operating at 15kV in conjunction with energy dispersion spectrometry (EDS) was used to examine the scaling layer deposited on the membrane. The fouled membrane coupons were dried in a desiccator and analysed without any further treatment. They were mounted on a holder using double-sided carbon tape in such a way that their cross-section was oriented perpendicular to the incoming light/electron beam.

5.1.2.4.7   Crystal Size Distribution

The crystal size of the sample was measured using a particle size analyser (Mastersizer2000, Malvern) that incorporated laser ensemble light scattering. For a uniform crystal size representation, the samples were kept in suspension by setting the mixing unit at a stirring rate of 200 rpm for 5 mins. A higher stirring rate could break the crystal formation (Erdoğdu et al., 2004). Each sample was measured three times. The instrument was set at a particle detection range of 0.02- 2000 μm, and analysis was done by using the wet dispersion method with a repeatability of +/- 0.5%. The dispersant used in the analysis was DI water. It must be acknowledged that the particle size analysing method was implemented only to show the pattern of crystal size changes at different operating conditions. The crystal size changes were represented by the crystal size distribution, CSD and volume weighted mean size, D[4, 3]. It has been

established that for crystals, the structure is characterized by a number of parameters, namely: median and the variance of the size distribution, the density and the arrangement parameter of dislocations, respectively (Ungár et al., 2001). Many studies represent the gypsum crystals by the volume weighted mean size of the crystals, D[4, 3] (Çakal et al., 2004; Seewoo et al., 2004; Kim et al., 2009). In this representation, the number of crystals is not required. It is suitable for large crystals such as gypsum compared to powder formed materials (Syvitski, 1991). The particle size analyser calculated D[4,3] as a summation of $\sum d_i^4 / \sum d_i^3$ whereby, d_i corresponds to the mean diameter of crystal spheres (Syvitski, 1991). The samples of the concentrated feed solution in the feed tank at the end of the experiment were used to represent the crystals in the final feed solution (D[4, 3]$_{\text{feed brine}}$). Following each experiment, the system was rinsed with 5 L of DI water. The brine DI water was collected to measure the crystals inside the membrane module (D[4, 3]$_{\text{module brine}}$).

5.1.3   RESULTS AND DISCUSSION FOR ANALYSIS OF SCALING DEVELOPMENT IN THE V-MEMD SYSTEM

5.1.3.1 CaSO₄ scaling development with V-MEMD (condition I)

In this study, the scaling development of the V-MEMD system was evaluated at an initial operating parameter of T_h= 60ºC, v_f=0.9 m/s, and P_v=10.0 kPa (condition I). It is the highest operating condition of the system that allows it be maintained as a stable operation.

The results showed that with experimental condition I, an initial permeate flux of 9.4 LMH was achieved as shown in **Figure 5.1**. The permeate flux showed a slight reduction of 8 to 10% due to salinity increment at the initial stage. Meanwhile, from the duration of 400 to 700 mins, 18 to 20% reduction of permeate flux was observed. The turbidity increased minimally around 8.1 to 10.3 NTU till 500 mins. Meanwhile, the increment of saturation ratio (SR) and concentration factor (CF) were similar till 500 mins. Thereafter the SR increased at a lower ratio than that of CF. The lower increment of SR suggest the gradual formation of CaSO₄, reducing the dissolved [Ca^{2+}] concentration. After 780 mins onwards, the turbidity showed significant increment up to 25.4 NTU and likewise the SR displayed a reduction in a downward trend

In pressure driven membrane processes such as NF and RO systems (which analyzed the gypsum scaling phenomenon in detail), the effect of concentration polarization (CP) is generally correlated to membrane surface scaling (Oh et al., 2009). It has been highlighted that the effect of CP is apparent when a much higher solute concentration makes contact with the membrane surface compared to the bulk concentration. This contributes to the formation of membrane surface crystallization (Lee et al., 1999; Oh et al., 2009).

Likewise, in experimental condition I of this study, the high vacuum pressure in the permeate side resulted in the rapid production of permeate. For this reason, high solute concentrate was present in the inlet membrane module, suggesting the tendency of membrane surface crystallization to be prevalent. The concentration factor (CF) was increased with time as shown in **Figure 5.1**.
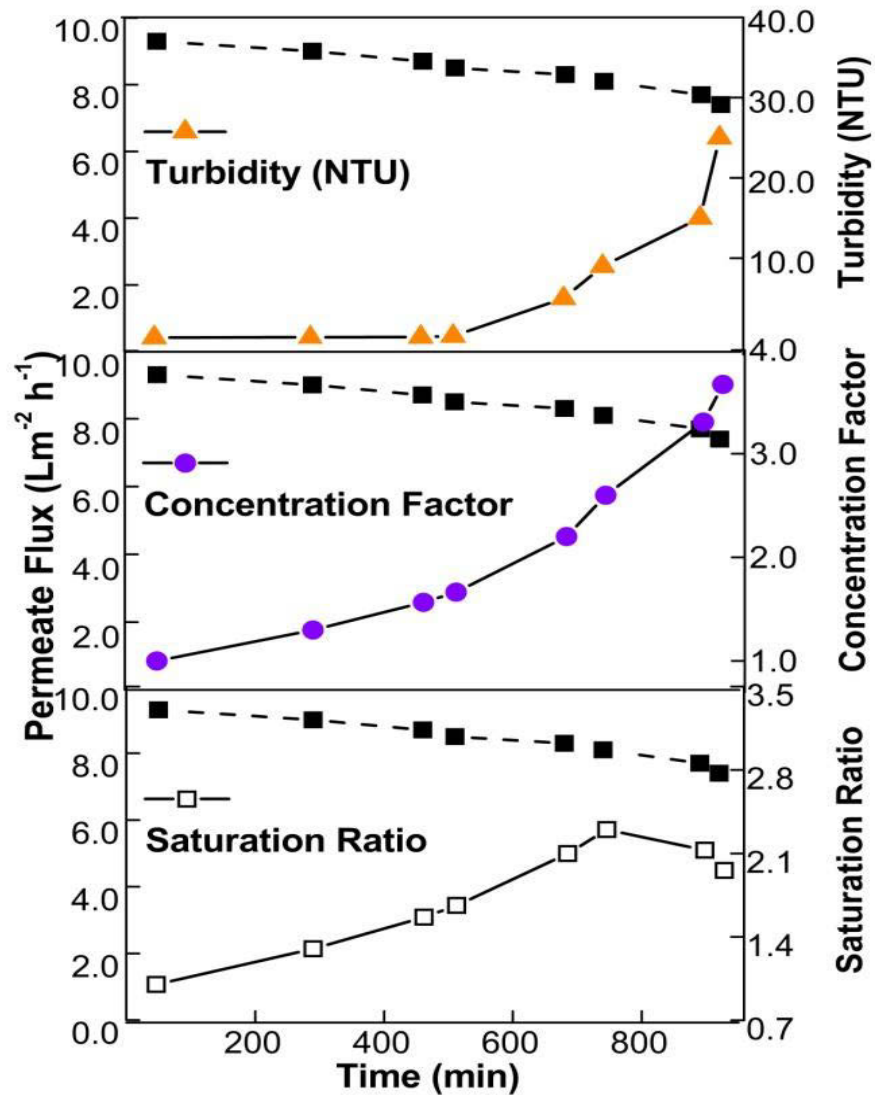
Figure 5.1 Scaling development pattern in V-MEMD condition I (T_h=60 ˚C, P_v =10.0 kPa, v_f =0.9 m/s) represented by permeate flux, turbidity, CF and SR as a function of time.

Nevertheless, in comparison to pressure driven membrane processes, the membrane surface crystal formation in V-MEMD was not severe with only an 18 to 20% permeate flux reduction. This could be attributed to the absence of hydraulic pressure, resulting in only loose deposition of crystals on the membrane surface. On the other hand, in MD operation, the presence of a thermal condition has been established to intensify crystal formation (Srisrucihan et al., 2006; Gryta, 2008b).

This phenomenon may not be prevalent in the V-MEMD system due to the low feed temperature operation. As mentioned earlier, the internal heating in the V-MEMD system enabled a low temperature operation whereby, $T_h = 60°C$, the corresponding feed temperature (retrieved from the system's control panel data) was only 47.6°C as shown in **Chapter 4**. Further, the high turbulence (Re = 5665.2) of the feed solution circulation could have contributed to channeling away the loose deposits from the membrane surface to the bulk tank. At the same time, the short residence time (21.6 s) of the concentrated solute in the membrane module minimized the formation of surface crystallization. A previous study has acknowledged that a short residence time of the concentrate solute in the membrane module would be advantageous in preventing the formation of scales in the membrane module. This is because crystal scaling requires more time prior to scale formation (Eriksson et al., 2005).

As a whole, with the saline feed solution (condition I), crystal formation appeared to adhere loosely onto the membrane. This was attributed to the lack of hydraulic pressure in MD coupled with low feed temperature, turbulent feed solution circulation and short residence time of the solute in the membrane module.

5.1.3.1.1   Flux recovery with DI water cleaning and particle size distribution analysis

At the end of this set of experiments, the V-MEMD system was rinsed with DI water to evaluate the capability of flux recovery. A volume of 5 L of DI water was used for the cleaning purpose, which represented about 20-25% of the total production volume (20.5 L of water was produced over the duration of the experiment). The results showed that with 5 L of DI water cleaning, the permeate flux was easily recovered to its initial value. This verified the observation of loose crystal adhesion on the membranes. At the same time, the first brine from the DI flushing was used to measure the crystal size inside the membrane module (brine module). This was compared to the crystal size in the final bulk feed solution (brine feed). The CSD$_{\text{brine feed}}$ displayed a wide distribution of crystal sizes between the ranges of 18.8 μm μm up to 1327.31 μm as shown in **Figure 5.2a**. Meanwhile, the CSD$_{\text{brine module}}$ was distributed between the lower ranges of 37.53 μm to 93.59 μm as shown in **Figure 5.2b**. In terms of the volume weighted mean size, the D[4, 3]$_{\text{brine feed}}$ was 455.96 μm, while the D[4, 3]$_{\text{brine module}}$ was 62.68 μm.

The results indicated that the large crystal sizes were in the final feed brine while only small crystals remained in the membrane module. The wide distribution of crystal sizes in the CSD$_{\text{brine feed}}$ could be explained in terms of crystal formation together with nucleation particles [34]. The high driving force in condition I (P$_v$=10.0 kPa) led to high production of distillate, resulting in high concentrated feed solution. The high concentrated feed solution at high temperature was channeled out from the membrane module to the feed brine tank.

The temperature and concentration difference between the brine feed solution and the bulk feed solution attributed to the initial formation of large crystals in the bulk feed tank. As mentioned earlier, the short residence time (21.6 s) could have prevented the formation of initial membrane surface nucleation. Further, as the concentrated feed solution passes through the membrane module repeatedly, nucleation occurred in the membrane module. At the lack of hydraulic pressure, the small and rapid particles formed with nucleation are channeled backed to the brine tank. As a result, a wide size distribution of crystals was detected in the $CSD_{\text{brine feed}}$. At the end of the experiment, only small amount of nucleation particle sizes that remained in the membrane module were detected by $CSD_{\text{brine module}}$.

(a)

(b)
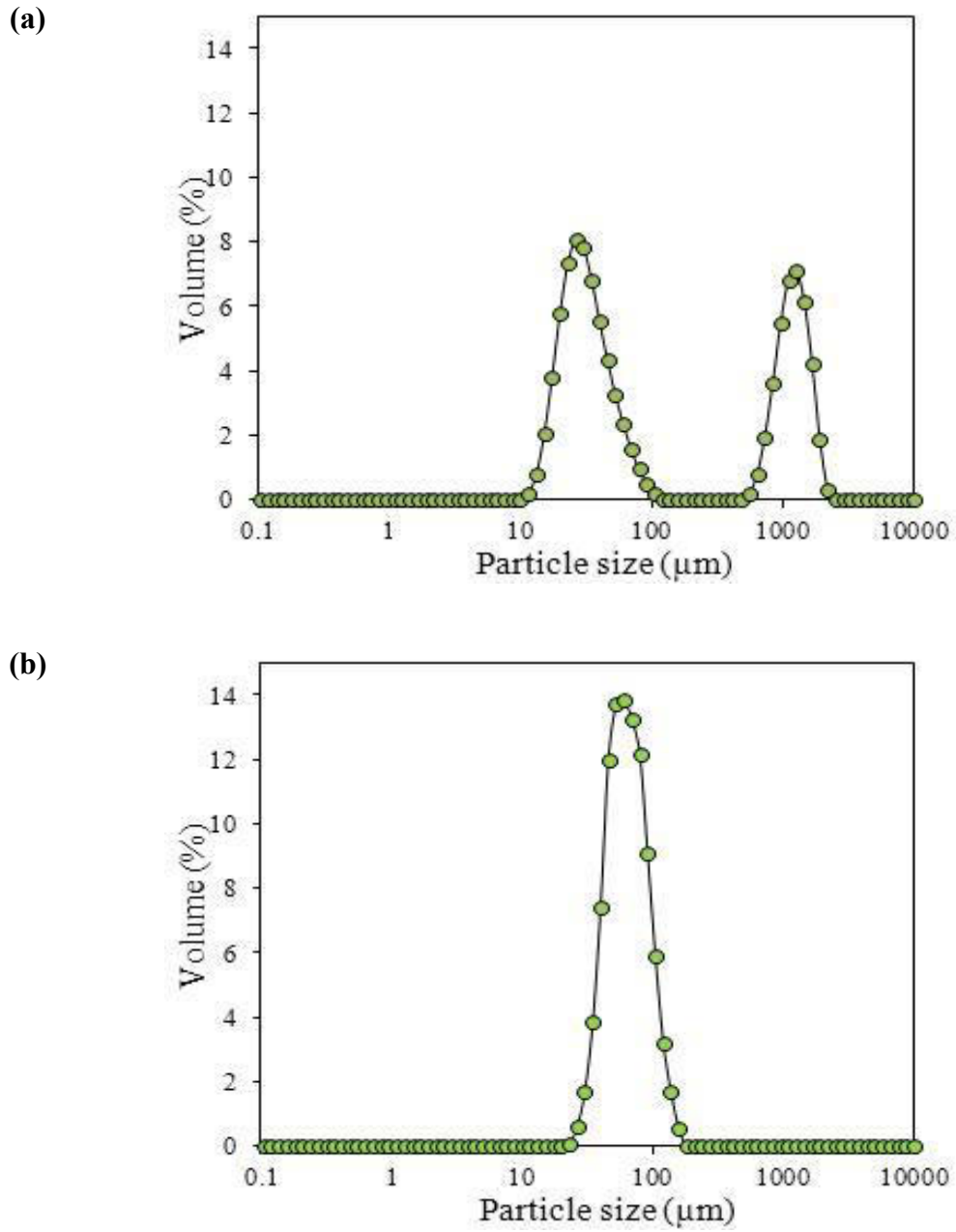
Figure 5.2 Gypsum crystal size distribution (CSD) in V-MEMD condition I **(a)** final feed solution, $CSD_{brine\ feed}$ **(b)** brine from DI water flushing, $CSD_{brine\ module}$ (*Note: average value is given from three samples*).

5.1.3.2   Influence of different operating conditions on CaSO₄ scaling

development in the V-MEMD system

To verify the influence of operation condition on the scaling pattern in the V-MEMD system, further experiments were conducted with decreased driving force (lower vacuum rate on the permeate side), and longer residence time/ lower turbulence (lower feed flow velocity).

5.1.3.2.1   Influence of driving force on scaling development in the V-MEMD

system

The influence of driving force on the scaling development in the V-MEMD system was evaluated by increasing the permeate pressure (reducing vacuum) from 10.0 kPa (condition I) to 12.5 kPa (condition II) and 15.0 kPa (condition III). The feed flow velocity as well as heating temperature was maintained at v_f= 0.9 m/s and T_h= 60ºC, respectively.

Overall, at the same residence time (21.6 s) and turbulence (Re = 5665.2), the initial permeate flux was comparatively lower at increased permeate pressure (reduced vacuum). The initial permeate flux at permeate pressure of P_p=12.5 kPa and P_p=15.0 kPa (6.7 LMH and 2.7 LMH respectively), was lower than at P_p=10.0 kPa (9.4 LMH) as shown in **Figure 5.3**. the permeate fluxes remained stable at permeate pressure of P_v= 12.5 kPa and P_v=15.0 kPa during the whole operating duration of 920 min, while a gradual 18 to 20% permeate flux decline was observed with P_v=10.0 kPa. At increased rates of permeate pressure of P_v=12.5 kPa and P_v=15.0 kPa, a sharp permeate flux decline was observed at a longer operation duration of 1000 mins and 1500 mins respectively. At the same time, at P_v=12.5 kPa and P_v=15.0 kPa, the turbidity value of the final feed solution was 15.5 NTU and 11.0 NTU, respectively as shown in **Table 5.3**
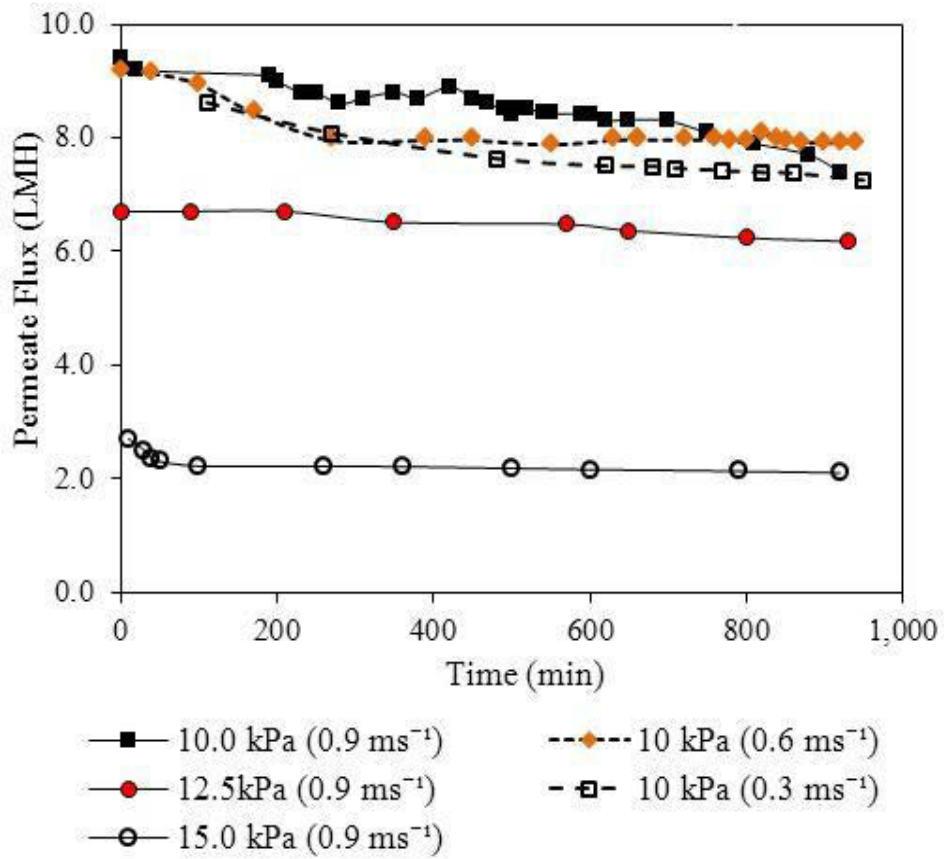
Figure 5.3 Comparing V-MEMD permeate flux pattern based on varied permeate vacuum pressure - experimental conditions I to III (P_v= 10.0 kPa to 15.0 kPa) and varied feed velocity - experimental conditions I, IV and V (v_f =0.9 m/s to v_f =0.3 m/s).

The crystal size patterns for all e three settings were also compared. The results showed that the volume weighted mean size, D[4, 3]$_{brine\ feed}$ (condition II) and D[4, 3]$_{brine\ feed}$ (condition III) was 125.23 μm and 62.71 μm respectively. In comparison, the D[4, 3]$_{brine\ feed}$ (condition I) was 455.96 μm. Meanwhile, the D[4, 3]$_{brine\ module}$ showed the reverse pattern, whereby the D[4, 3]$_{brine\ module}$ (condition III) had the highest value at 522.28 μm as shown in **Table 5.3**.

The CSD$_{brine\ feed}$ showed a shifting trend towards the higher particle size with reduced permeate pressure (high vacuum) as shown in **Figure 5.4a**, while CSD$_{brine\ module}$ showed a shifting trend towards the lower particle size with reduced permeate pressure (high

vacuum) as shown in **Figure 5.4b**. It is worth highlighting that DI water flushing was used for all three conditions, P_v=10.0 kPa, P_v=12.5 kPa and P_v=15.0 kPa. For P_v=15.0 kPa and P_v=12.5 kPa, larger crystal formations were detected in the membrane module, $CSD_{brine\ module}$ (after DI water flushing) compared to at P_v=10.0 kPa. Therefore, the influence of DI water etching on crystal sizes in the membrane module was considered to be minimal in this study. Further, the crystal size was reported in terms of volume weighted mean size that would take into account large as well as small crystals at distorted shapes.

Table 5.3 Summary of experimental results with varied permeate vacuum pressure (T_h= 60 °C, v_f =0.9 m/s).

Experiment	Condition I	Condition II	Condition III
	(P_v =10.0 kPa)	(P_v=12.5 kPa)	(P_v = 15.0 kPa)
Initial permeate flux (L MH)	9.4	6.7	2.7
Induction time (min)	550	1000	1500
Final feed turbidity (NTU)	25.2	15.5	11.0
Crystal size, D[3, 4] (µm)			
Brine feed	455.96	125.23	62.71
Brine module	62.68	108.24	522.28

The crystal size results reflected that at higher driving forces (P_v =10.0 kPa) larger crystals are formed as the feed brine solution. As explained in Section 3.1.1, it was observed that at P_v =10.0 kPa setting, the temperature and concentration difference between the brine feed solution and the bulk feed solution attributed to the initial formation of large crystals in the bulk feed tank. Further, the short residence time (21.6 s) was associated with the lack of initial membrane surface nucleation while the rapid

recirculation of the concentrated feed solution was associated with the occurrence of nucleation in the membrane module. This contributed to a mix of small and large crystal sizes in the final brine feed solution. On the other hands, at increased permeate pressure of P_v= 12.5 kPa and P = 15.0 kPa, the lower driving force resulting in lower mass transfer. As a result, at the same time duration, less distillate was produced. Therefore, the feed solution concentration did not increase as severely with the P_v=12.5 kPa and P_v =15.0 kPa setting, compared to at P_v=10.0 kPa. The feed concentration circulated back to the brine tank at similar concentration factor does not cause the formation of crystals in the feed tank. Over time, as the feed solution is re-circulated repeatedly into the membrane module, initial nucleation occurs in the membrane module followed by the formation of large crystals in the membrane module. The formation of larger crystals with low super saturation feed solutions have been studies in a number of studies (Christoffersen et al., 1982; Gryta, 2009b). Hence, large crystal were observed in the brine module at P_v=12.5 kPa and P_v=15.0 kPa setting, compared to at P_v=10.0 kPa.

(a)

(b)
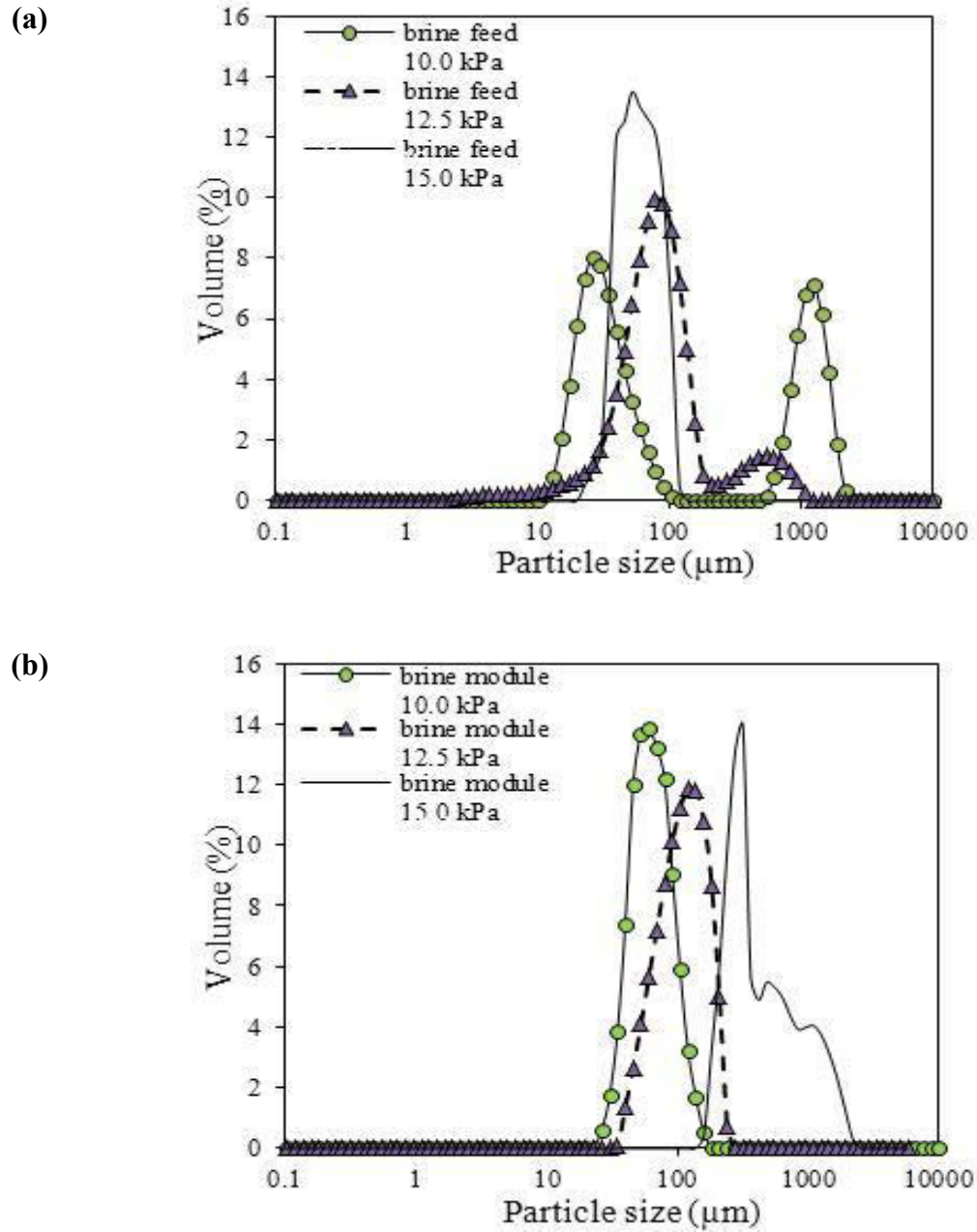
Figure 5.4 Crystal size distribution (CSD) with different permeate vacuum pressure, P_v=10.0 kPa to P_v=15.0 kPa at **(a)** final feed solution, $CSD_{brine\ feed}$ and **(b)** brine from DI water flushing, $CSD_{brine\ module}$.

5.1.3.2.2   Influence of membrane module residence time and turbulence on scaling development in the V-MEMD system

The influence of residence time on scaling development in the V-MEMD system was evaluated by decreasing the feed flow velocity from v_f =0.9 m/s (condition I) to 0.6 m/s (condition IV) and 0.3 m/s (condition V). The permeate vacuum pressure and heating temperature were maintained constantly at P_v=10.0 kPa and T_h= 60 ºC in all three conditions. Decreasing the feed flow velocity from v_f= 0.9 m/s to v_f= 0.6 m/s increased the residence time in the membrane from 21.6 s to 34.6 s, and decreased the turbulence from Re = 5665.6 to Re = 3776.8.

The experimental results showed that the reduced flow velocity resulted in a permeate flux decline by only 10 to 15%. Hence, the permeate production rate at 0.6 m/s and 0.3 m/s were comparably similar with 0.9 m/s (condition I), with the difference of residence time and turbulence in condition IV and condition V as shown in **Figure 5.3**.

The crystal size analyses were compared for all three feed velocities. The results showed a shifting pattern of higher crystal size in the $CSD_{brine\ module}$ than in the $CSD_{brine\ feed}$ as the feed flow velocity was lower from v_f= 0.9 m/s to v_f= 0.3 m/s as shown in **Figure 5.5**. The results indicated that reduced turbulence and longer residence time of feed concentrate in the membrane module were influential factors which led to higher crystal size formation in the membrane module. The volume weighted mean size, D[4, 3]$_{brine\ feed}$ (v_f= 0.6 m/s) and D[4, 3]$_{brine\ feed}$ (v_f= 0.3 m/s) were 298.51 μm and 104.54 μm, respectively. Comparatively, as discussed earlier, in the condition I (v_f= 0.9 m/s), the D[4, 3]$_{brine\ feed}$ and D[4, 3]$_{brine\ module}$ was 455.96 μm and 62.68 μm. The D[4, 3]$_{brine\ module}$ (v_f= 0.6 m/s) and D[4, 3]$_{brine\ module}$ (v_f= 0.3 m/s) were 268.62 μm and 339.03 μm, respectively, which are relatively higher than at condition I (v_f= 0.9 m/s) with the

highest turbulence. Previous studies have observed a similar phenomenon of large crystal size formation with lower feed flow velocities (Gryta, 2008a).

Although larger crystals were formed in the membrane module at both $v_f = 0.6$ ms^{-1} and $v_f = 0.3$ ms^{-1} setting compared to at $v_f = 0.9$ ms^{-1}, the permeate flux did not vary significantly. This was associated with the absence of hydraulic pressure in MD setting that did not cause a strong adhesion of the large crystals to the membrane. Therefore, the mass transfer was not affected by the crystal deposited in the duration of this experiment at these feed concentrations. Other MD studies have also observed the minimal influence of mass transfer by fouling development (He et al., 2008; . Mericq et al., 2010).

Overall, the results showed that the loose crystal deposition in the V-MEMD system was caused by the lack of hydraulic pressure, low feed temperature, high turbulence and short membrane retention time. Crystal size formation was influenced by operating conditions of permeate vacuum pressure as well as feed velocity. Scaling development in the V-MEMD system was observed to be reversible with suitable operating conditions. A further evaluation of the membrane cleaning cycle for maintaining the V-MEMD system is presented in **Chapter 7**.

(a)

(b)
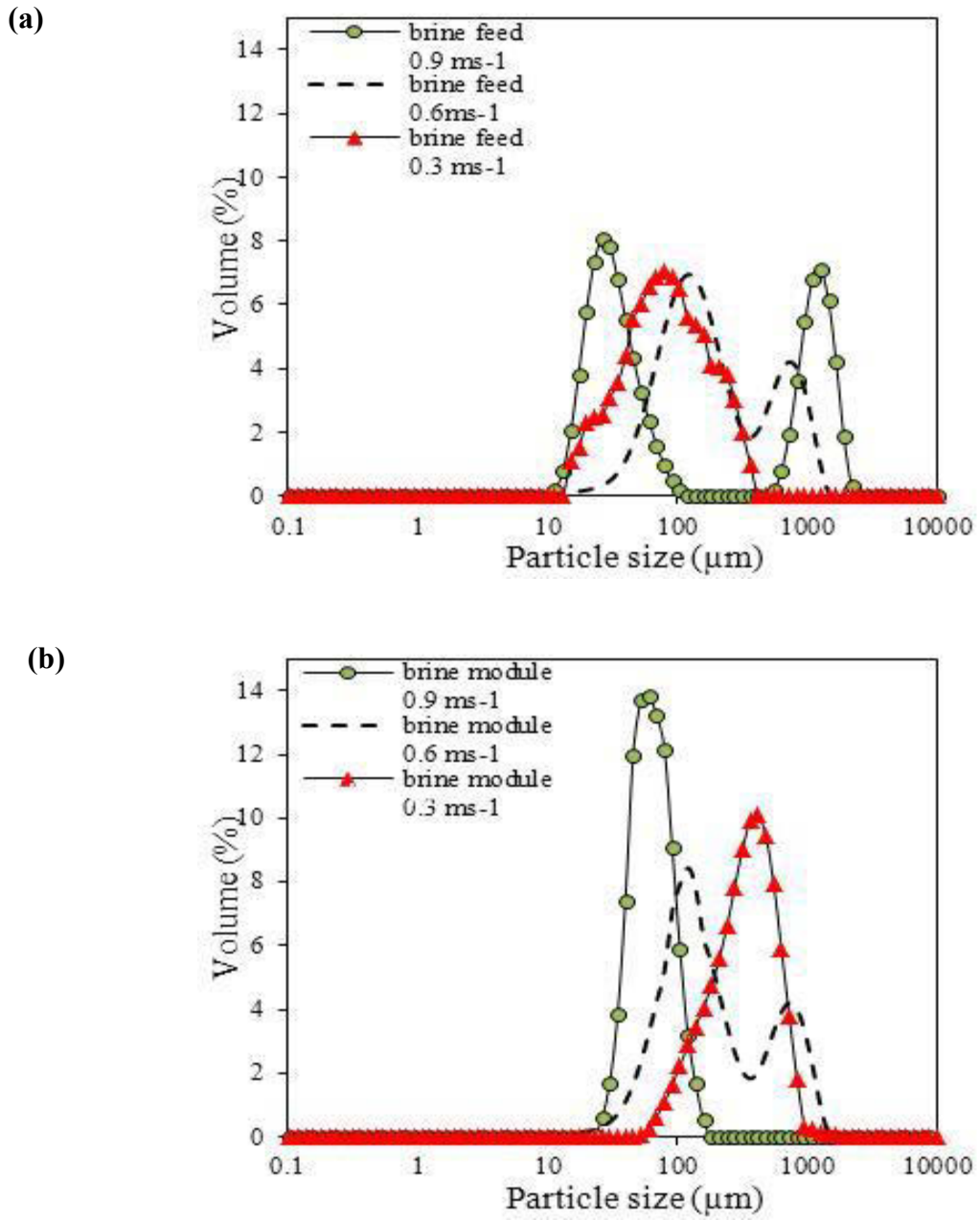
Figure 5.5 Crystal size distribution (CSD) at different feed velocities, v_f=0.9 m/s to 0.3 m/s based on (**a**) final feed solution, CSD$_{\text{brine feed}}$ and (**b**) brine from DI water flushing, CSD$_{\text{brine module}}$.

5.2   INFLUENCE OF FEED /PERMEATE VELOCITY ON SCALING DEVELOPMENT IN A DCMD SYSTEM

The V-MEMD evaluation in **Section 5.1.3.2.2** above demonstrated that hydrodynamics is an important factor in influencing scale formation. Here the crystal size formation decreased when higher feed flow velocity (turbulence) occurred.

In terms of scaling development related to hydrodynamics, several recent publications on MD have reported the significant influence of flow velocity on the scaling pattern. Gryta (2008b), for example, highlighted that the hydrodynamic conditions affects concentration polarization (CP). It was found that the hydrodynamic condition significantly influenced the size, structure and morphology of scale formation. The study indicated that a porous thin deposit was formed at high feed flow velocity (e.g. 1.2 m/s) and reduced heat transfer resistance on the membrane, while a non-porous and thick deposit was formed at low feed flow velocity (e.g. 0.35 m/s). Similarly, He et al. (2008) recommended a high flow velocity for reducing the flux decline in the presence of a significant amount of precipitate in a hollow fibre membrane setting.

In membrane separation processes, optimizing hydrodynamic conditions is a general approach to control fouling (Goosen et al., 2005). In MD, the role of flow velocities in the transport mechanism has been analysed extensively by parametric modelling studies (Khayet et al., 2007). However, the relationship between optimized flow velocities and scaling control has not been studied in detail.

Additionally, in **Section 5.1.3.2.1,** the condition of the permeate side (vacuum pressure) also demonstrated its influence on scale formation in the V-MEMD system. Likewise, in **Chapter 4**, the importance of suitable permeate velocity in enhancing the DCMD system's performance was demonstrated. However, the influence of the permeate flow

velocity in scaling development has not been analyzed. Hence, in this section, the relationship between optimal flow velocity (of feed and permeate) and scaling development was investigated. For this purpose, a bench scale DCMD system was used with $CaSO_4$ feed solution.

5.2.1   EXPERIMENTAL OPERATING CONDITIONS

For the DCMD scaling experiments, 2 L feed solution ($CaSO_4 \cdot 2H_2O$) and 2 L cooling solution (DI water) were added to the feed and permeate tanks, respectively. The feed solution was prepared by dissolving 2.0 g/L of $CaSO_4 \cdot 2H_2O$ in distilled water and filtered through a 0.45 μm filter to exclude the initial deposition of bulk suspended solids on the membrane An increasing permeate volume was recorded every 200 ml of permeate produced; 15 ml of sampling was taken from the feed tank for further analysis. Each experiment was carried out until the initial 2.0 L feed volume was reduced to a feed volume of 0.2 L, achieving a 9 to 10-fold feed volume concentration. Accordingly, the experiment's duration ranged between 3.5 and 7.0 hours based on the time required to achieve the 10-fold volume concentration.

5.2.2 **RESULTS AND DISCUSSION ON THE INFLUENCE OF FEED /PERMEATE VELOCITY ON SCALING DEVELOPMENT IN A DCMD SYSTEM**

5.2.2.1 **Influence of flow velocity on scaling development in DCMD**

For this investigation three distinct velocity ranges were selected: a high flow velocity setting (v_f & v_p = 2.2 m/s); an intermediate flow velocity setting (v_f & v_p = 1.1 m/s); and a low flow velocity setting (v_f & v_p = 0.5 m/s). A feed temperature of $70\pm0.2^{\circ}C$ was maintained. A high feed temperature range of 70°C was used in order to clearly observe the effect of scaling.

The effect of flow velocity on scaling pattern in DCMD was investigated by monitoring the permeate flux decline, turbidity, induction time, saturation ratio and concentration polarization as detailed in **Section 5.1.2.4**. For visual verification, SEM imaging of the membrane cross-section was carried out.

5.2.2.1.1 **Permeate flux trend and induction time**

It is important to highlight that for all the flow velocities investigated, the average initial conductivity value of the permeate side (5.48 ± 0.76 µS/cm) remained low at around 5.23 ± 0.41 µS/cm to 6.14 ± 0.93 µS/cm at the end of the experiment. This indicates that no wetting of the membrane occurred.

In this study, the permeate flux decline trend showed a similar pattern of having two main flux decline periods for all the flow velocity settings. Specifically, the initial permeate flux declined gradually from the initial time to the point of induction, T_{ind} (determined by the sharp increase of turbidity value). Thereafter it declined significantly by 40 - 65% (final permeate flux decline) as shown in **Figure 5.6**.

At a low flow velocity of v_f & v_p = 0.5 m/s, the initial permeate flux (23.8 LMH) declined by 25.2% till T_{ind} = 240 mins and thereafter declined significantly by 65.4%. Meanwhile, at a high flow velocity of v_f & v_p = 2.2 m/s, the initial permeate flux (44.6 LMH) declined by only 7.1% till T_{ind} = 140 mins, and thereafter declined significantly by 39.3%. The decline was observed from a VCF of 3.0 onwards. Previous DCMD studies have also reported a higher permeate flux decline trend with lower flow velocity, which is linked to the formation of porous crystals on the membrane surface (Gryta, 2008b). Likewise, this study showed that the calculated initial feed vapour transport resistance as shown in Eq. (5.2), at v_f & v_p = 0.5 m/s was 70% higher than at v_f & v_p = 2.2 m/s as shown in **Table 5.4**. At the end of the experiment, the transport resistance at the low flow velocity increased by 33.3% while at the high flow velocity, only a 10.8% increment occurred. The results suggested that the higher resistance could be associated with more surface deposit on the membrane surface at the lower flow velocity.

Table 5.4 Summary of scaling analysis at high, intermediate and low flow velocity settings.

v_f & v_p (m/s)	Re_f & Re_p	Initial Flux, J (LMH)	Flux Decline during T_{ind} (%)	Final Turbidity (NTU)	CP ratio	T_{ind} (min)	Feed Vapour Transport Resistance (Pa.m^2 h/kg)		Permeate Vapour Transport Resistance (Pa.m^2 h/kg)	
							Initial	End	Initial	End
0.5	2352	23.8	25.2	300.1	1.23	240	473.1	630.6	40.9	54.5
1.1	4950	35.7	18.6	1026.5	1.09	170	266.9	313.8	25.0	29.4
2.1	9009	44.6	7.1	1333.3	1.01	140	157.4	174.4	17.1	18.9

At the end of the experiment, the transport resistance at the low flow velocity increased by 33.3% while at the high flow velocity, only a 10.8% increment occurred. These results suggested that the higher resistance could be associated with more surface deposit on the membrane surface at the lower flow velocity.

A longer induction time trend was observed at lower flow velocity, whereby at the low flow velocity, T_{ind} = 240 mins (corresponding VFC 4.3) was considerably longer than the T_{ind} = 140 mins at the high flow velocity (VFC 3.0) as shown in **Table 5.4**. In MD, a number of studies used T_{ind} as a key parameter to control crystallization. The longer T_{ind} provides an opportunity to control and wash the membrane during the operation (He et al., 2008; Nghiem and Cath, 2011).
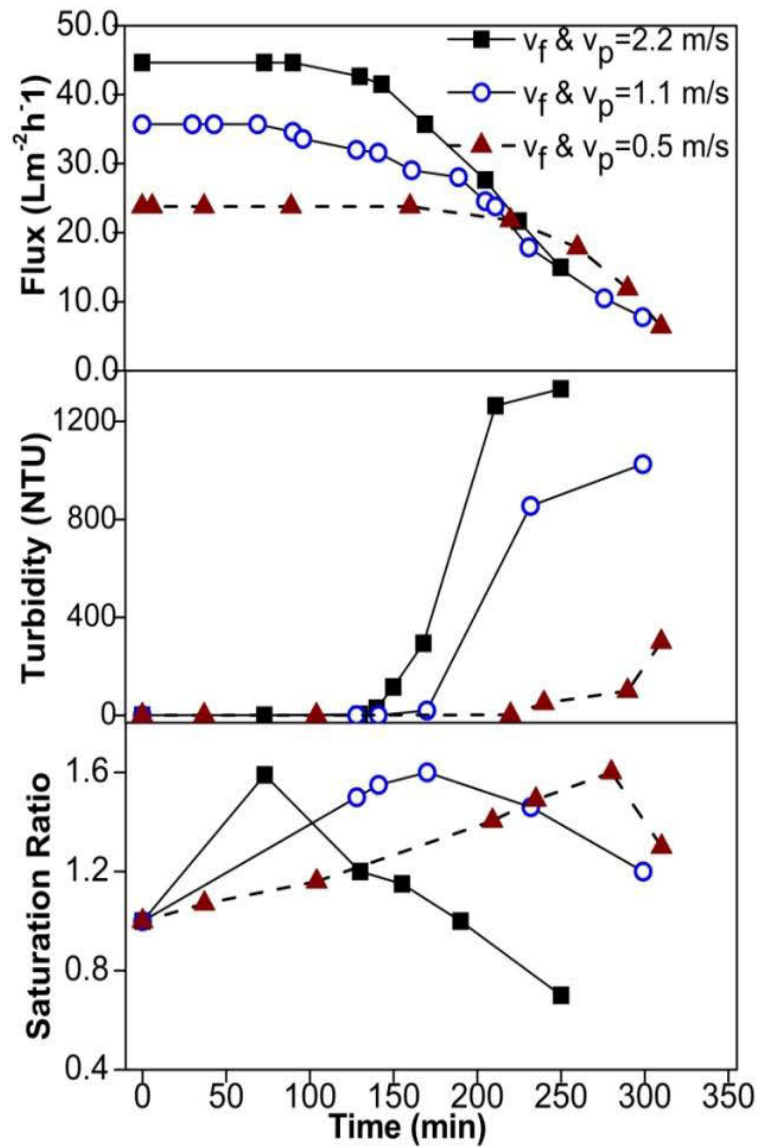
Figure 5.6 DCMD scaling pattern at high flow velocity (v_f & v_p = 2.2 m/s), intermediate flow velocity (v_f & v_p = 1.1 m/s), and low flow velocity (v_f & v_p = 0.5 m/s) (feed solution = $CaSO_4$ and F_t = 70 °C).

5.2.2.1.2 Saturation Ratio and Turbidity

The turbidity measurement was a suitable indicator to determine the crystallization pattern of the system in MD. Lee et al. (1999) used turbidity to interpret the $CaSO_4$ crystallization pattern in nanofiltration modules and associated the high turbidity of bulk solution with bulk crystallization. Similarly, Park et al. (2013) used high turbidity value

at induction time to represent the start of bulk crystallization. Comparing the turbidity results obtained in this study, at the high flow velocity of v_f&v_p =2.2 m/s, a dominant increase in feed turbidity from 28.8 to 1333.3 NTU occurred from the induction time onwards. On the other hand, at the low flow velocity of v_f&v_p = 0.5 m/s, only a small increase in feed turbidity was recorded (18.6 NTU to 300.1 NTU) from the induction time as shown in **Figure 5.6**. The high turbidity indicated that bulk crystallization occurred mainly at a high flow velocity.

The feed turbulence (Re_f = 9009) at high flow velocity will reduce the feed concentration near the membrane surface and this in turn will reduce surface crystallization. In this study, at the high flow velocity, the measured SR showed a reducing value from an initial VCF of 1.6 (73 mins) onwards as shown in **Figure 5.6**. At a low flow velocity, a longer period of high feed concentration near the membrane surface was observed, whereby the SR increased up to VCF of 3.6 (280 mins) before it dropped sharply, reflecting higher CP and dominant surface crystallization (Lee et al., 1999) Correspondingly, the CP ratio, calculated based on Eq. (5.5) showed a slightly higher value at the lower flow velocity setting as shown in **Table 5.4**.

5.2.2.1.3 Morphology of the fouling layer –SEM verification

The SEM images of the membrane cross-section further verified that the crystal deposited on the membrane surface was influenced by the flow velocity as shown in **Figure 5.7**. An SEM-EDS line analysis method of the membrane cross-section was adopted based on a previous MD scaling study (Gryta, 2008b). The SEM-EDS line analysis was carried out from point A to point B (membrane cross-section depth of 0 - 450 µm). The start of the membrane surface was at point 90-95 µm, which was determined from the virgin membrane and start of the fluoride peak, which is a compound inside the membrane structure. The SEM-EDS line analysis demonstrated

that the percentage of calcium and sulphur mass content on the membrane surface was significantly higher at the low flow velocity of $v_f \& v_p$ = 0.5 m/s. The line analysis revealed that at the low flow velocity, the element mass content was around 15-20% with a thickness of 120 to 150 μm. In comparison, at the high flow velocity of $v_f \& v_p$ =2.2 m/s, it was only 0-5%.
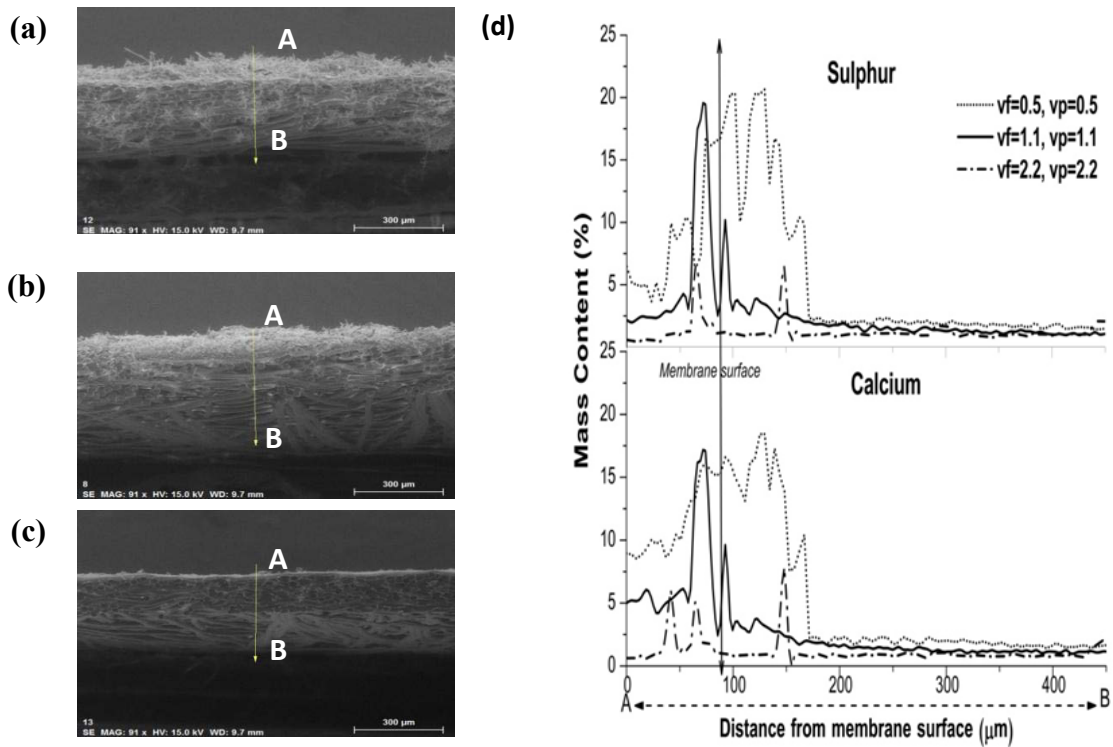
Figure 5.7 SEM – EDS images of membrane cross-section **(a)** $v_f \& v_p$ = 0.5 m/s **(b)** $v_f \& v_p$ = 1.1 m/s **(c)** $v_f \& v_p$ = 2.2 m/s **(d)** line analysis of the percentage mass of calcium and sulphur element deposit.

It is worth noting that although the percentage mass content of the membrane deposit at the high flow velocity of $v_f \& v_p$ =2.2 m/s was low, at the membrane depth of 150 μm, a small peak of element mass was detected. In comparison, for the $v_f \& v_p$ =1.1 m/s setting, a higher mass content (5 to 18%) was observed within the depth of 100 μm. From this depth onwards the mass content gradually decreased. This may suggest that

the higher applied pressure at the higher feed flow rate may have been attributed to the slight penetration of calcium and sulphur.

The SEM analysis supported the earlier suggestion that at the low velocity setting, surface crystallization was dominant while bulk crystallisation was dominant at the high velocity setting. Results of the scaling analysis showed that flow velocity influenced the scaling pattern. It can be highlighted that the increase in flow velocity led to a lower flux decline and a significantly lower membrane surface crystallization. In fact, in membrane studies such as the forward osmosis process, a high flow velocity is deemed highly desirable for membrane fouling control (Lee et al., 2010). In MD, however, a high flow velocity to mitigate fouling may increase the possible risk of membrane wetting in the long term. Apart from that the shorter induction time of the high flow velocity setting will require more frequent cleaning and the low recovery ratio may not be economically viable.

In view of this, an intermediate flow velocity appears to be more suitable for scaling control in MD. The benefit of an intermediate velocity setting is a turbulent feed flow ($Re_f = 4950$), that could minimize the development of membrane surface crystallization in comparison to the laminar feed flow of the lower velocity setting ($Re_f = 2352$). On the other hand, as shown in **Figure 4.9 (Chapter 4)**, in comparison to the high velocity setting ($v_f \& v_p = 2.2$ m/s), a lower pumping energy of 2.44×10^{-2} W is required at the intermediate velocity.

Additionally, higher induction time, higher recovery rate and lower risk of membrane wetting are noted at lower velocity ranges. As such, this study analyzed the scaling pattern development at the intermediate velocity of $v_f \& v_p = 1.1$ m/s in detail as shown in **Figure 5.8**. Three distinct phases were identified based on the permeate flux decline

pattern, with an initial stationary permeate flux phase (phase i); first observed permeate flux decline at the intermediate phase (phase ii); and significant decline in permeate flux during the final phase (phase iii).

At the initial phase (i) (between VCF 1.0 and 1.5), the initial flux was 35.7 LMH. No significant flux decline was observed and the turbidity value remained the same as the initial value (0.2 - 0.3 NTU). At the intermediate phase (ii) (between VCF 1.5 and 3.3), a flux decline of around 18.6% was observed. However, turbidity value remained similar to the initial value, suggesting an initial surface crystallization. At the final phase (iii) (between VCF 3.3 and 8.3), a drastic increase of turbidity in the feed tank (from 20.1 to 1026.5 NTU) at 170 mins was observed, which is the T_{ind}. The sharp increase in turbidity suggests that bulk crystallization was dominant in phase (iii) and crystals formed in the feed solution may have been deposited on the membrane surface. At this stage a 51.5% decline was observed in the permeate flux.
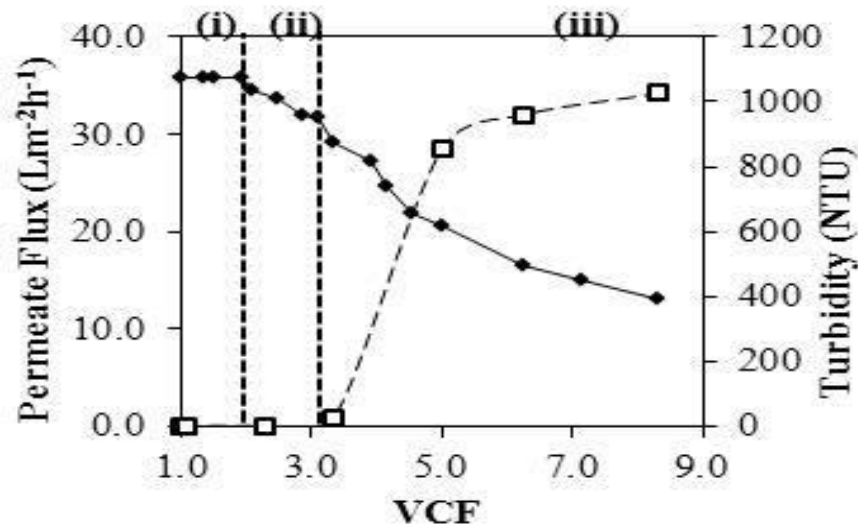
Figure 5.8 Scaling development at intermediate velocities (v_f & v_p =1.1 m/s) as a function of feed VCF in phase (i) - (iii) (permeate flux (——), feed turbidity (-----), feed solution $CaSO_4$ and F_t =70 ^{o}C). Note: Adjunct points were connected in a straight line for easy reference.

The results indicated the possibility of both surface and bulk crystallizations occurring in the DCMD unit at the intermediate setting of v_f&v_p = 1.1 m/s. However, it appears that the bulk crystallization in phase (iii) led to a more significant permeate flux decline. Based on this result, a phase membrane washing (or cleaning) with water could be recommended at VCF 3.0 (phase (iii)), prior to the permeate flux decline. This may increase the T_{ind} as suggested in another MD study that applied regular membrane flushing (Nghiem and Cath, 2011). Alternatively, in this study, an investigation to identify a matching optimal permeate flow velocity was carried out at the intermediate feed velocity setting, as a possible strategy for reducing scaling while maintaining high output in DCMD.

5.2.2.2   Influence of permeate velocity on scaling development

The intermediate velocity settings (v_f&v_p = 0.8 m/s and v_f&v_p = 1.1 m/s) were selected for a comparative analysis of the effect of v_p on DCMD output performance as shown in **Table 5.5** and scaling development as shown in **Figure 5.9**.

Table 5.5 Comparisons of DCMD performance at different v_f & v_p combination settings.

v_f & v_p (m/s)	Initial Flux, J (LMH)	T_{ind} (min)	Final Turbidity (NTU)	CP ratio	Pumping Energy ($\times 10^{-1}$ W)	Recovery Ratio (%)
0.8 & 0.8	29.8	210	574.3	1.16	0.055	1.85
0.8 & 1.1	35.7	185	874.1	1.12	0.062	2.21
1.1 & 1.1	35.7	170	1026.5	1.09	0.244	1.62

Meanwhile, for v_f&v_p= 0.8 m/s, the turbidity and T_{ind} were 574.3 NTU and 210 mins. The scaling pattern of v_f = 0.8 & v_p= 1.1 m/s was closely similar to the v_f&v_p =1.1 m/s. At v_f&v_p =1.1 m/s, the turbidity and T_{ind} was 1026.5 NTU and 170 mins.
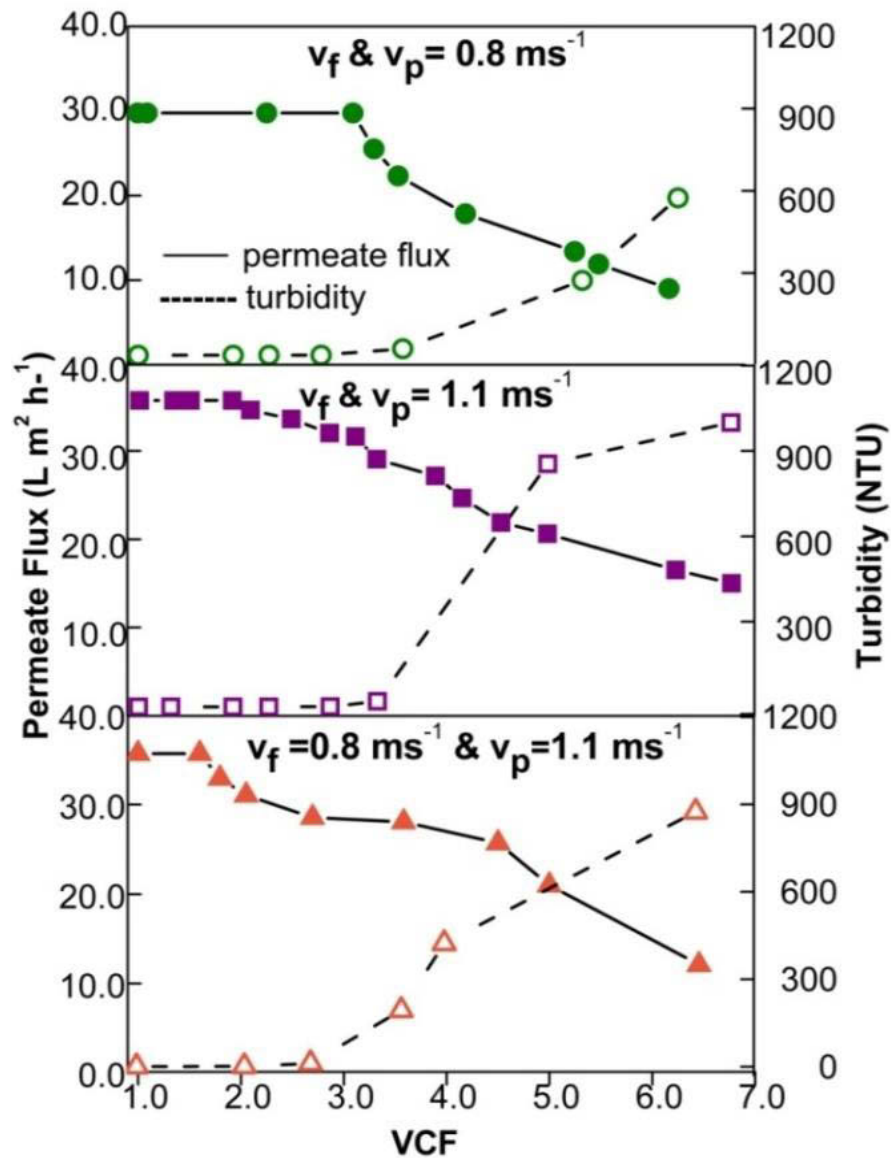
Figure 5.9 DCMD scaling pattern comparison at different combination settings of v_f & v_p (v_f & v_p = 0.8 m/s; v_f & v_p =1.1 m/s; v_f = 0.8 & v_p = 1.1 m/s) (feed solution $CaSO_4$ and F_t = 70 °C).

The SEM-EDS line analysis of the membrane cross-section supported the scaling pattern deductions as shown in **Figure 5.10**. A high mass element deposit (10 - 25%) from the top of the membrane to a depth of 190 μm was detected for the v_f & v_p= 0.8 m/s setting. This pattern was similar to the line-analysis results of v_f & v_p= 0.5 m/s, reflecting a higher surface crystallization. On the other hand, the line analysis of v_f = 0.8

& v_p= 1.1 m/s showed a peak of 20-25% of mass element content within the membrane surface depth of 60-90 μm. This gradually tapered down thereafter, reflecting the presence of element deposit similar to v_f & v_p =1.1 m/s.

The results indicated that a small change in v_p was effective in changing the scaling pattern from surface crystallization to a more dominant bulk crystallization, without the need to change v_f. At the same time, the performance at v_f = 0.8, v_p= 1.1 m/s was significantly better compared to v_f & v_p =1.1 m/s. This reflects the importance of the optimal combination of feed and permeate velocity in a DCMD setting, resulting in the system's performance being more sustainable.
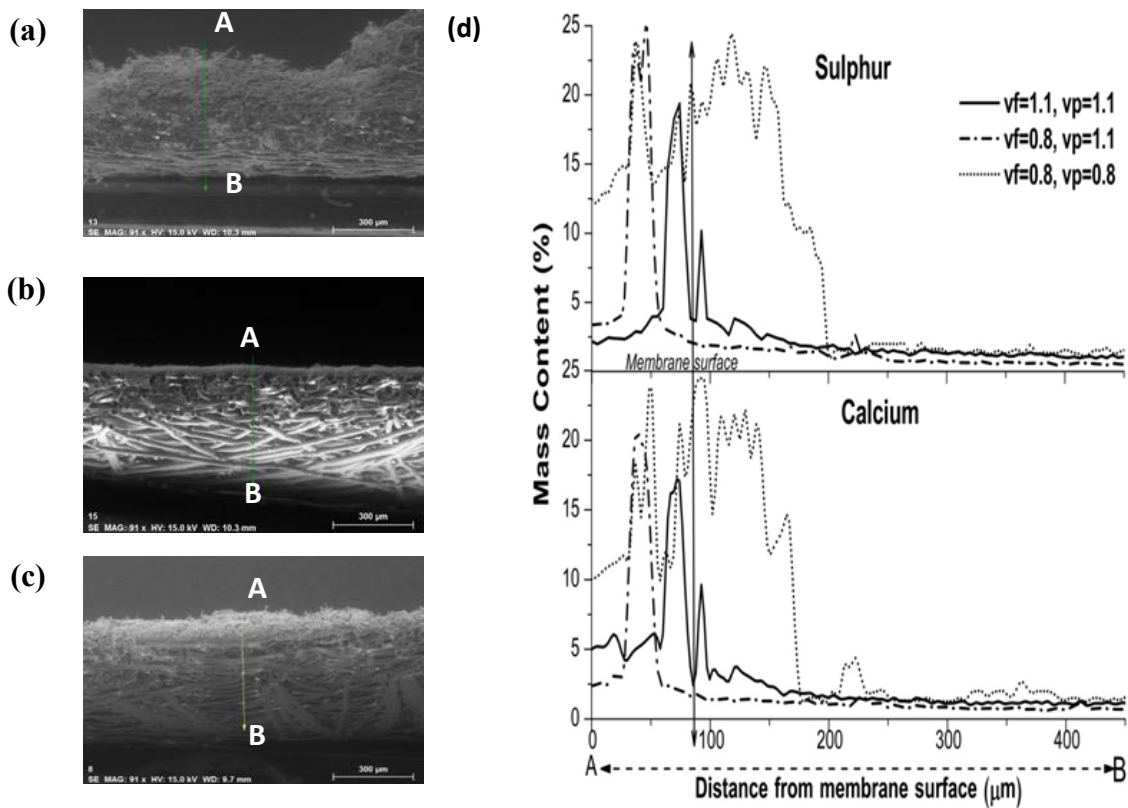
Figure 5.10 SEM –EDS images of membrane cross-section for comparison of v_p effect (a) v_f & v_p = 0.8 m/s (b) v_f = 0 .8 m/s, v_p= 1.1 m/s (c) v_f & v_p = 1.1 m/s (d) line analysis of the percentage mass of calcium and sulphur element deposit.

5.3 SUMMARY

5.3.1 Summarizing scaling development analysis of the V-MEMD system

In this study, the performance of a V-MEMD system with a high TDS feed solution of containing NaCl and $CaSO_4$ was evaluated at a setting of v_f = 0.9 m/s, T_h = 60ºC and P_p = 10.0 kPa. In terms of scaling development in the V-MEMD system, an 18-20% permeate flux decline of the initial permeate flux of 9.4 LMH was observed after a three times concentration factor for a duration of 920 mins. The permeate flux recovered to its initial value with DI water flushing, which indicated the loose deposition of $CaSO_4$ crystal formation. Therefore larger CSD was observed in the $CSD_{brine\ feed}$ (D[4,3] =455.96 µm) compared to $CSD_{brine\ module}$ (D[4,3] =62.68 µm). The loose deposition was attributed to the lack of hydraulic pressure, low feed temperature (T_f = 47.6°C), high turbulence (Re = 5665.6) and short membrane retention time (21.6 s). The CSD was influenced by permeate pressure. At higher P_p of 12.5 kPa and 15 .0 kPa, the $CSD_{brine\ module}$ increased when compared to at P_p of 10.0 kPa. Similarly, at lower v_f of 0.6 m/s and 0.3 m/s, larger crystals formed in the $CSD_{brine\ module}$. Overall, the results indicate the reversibility of scaling development in the V-MEMD system when suitable operating conditions exist. Effectiveness of the V-MEMD membrane cleaning cycle with water flushing is presented in **Chapter 7**.

5.3.2 Summarizing the influence of feed/permeate velocity on scaling development in a DCMD

The study investigated the influence of feed and permeate flow velocity on the membrane scaling formation with a batch-scale DCMD system. The results indicated that flow velocity significantly influenced scale formation (bulk or surface crystallization) in the system. The study also demonstrated that an optimized feed and

permeate flow velocity can significantly improve the performance of the DCMD system. Based on these results, it can be concluded that:

- Bulk crystallization was dominant at high flow velocity (v_f & v_p = 2.2 m/s), while membrane surface crystallization was dominant at low flow velocity (v_f & v_p = 0.5 m/s) with a longer induction time.

- The SEM-EDS line analysis detected the significantly higher calcium and sulphate element deposit on low flow velocity (v_f & v_p = 0.5 m/s), in comparison to the high flow velocity (v_f & v_p = 2.2 m/s), thus verifying the dominant membrane surface crystallization on the low flow velocity.

- Although a high flow velocity is more suitable for controlling membrane surface crystallization, the overall recovery ratio performance and induction time was considerably reduced, with increased pumping energy and risk of membrane wetting. Hence, the intermediate flow velocity of v_f & v_p = 0.8 m/s to 1.1 m/s proved to be a more suitable flow velocity range.

- An optimum combination of feed and permeate flow velocity (identified based on the permeate temperature gradient and the permeate to feed pressure ratio), would improve the system's performance (increase recovery ratio, reduce pumping energy) while maintaining the same permeate flux and membrane surface crystallization.

CHAPTER 6

ORGANIC FOULING

ANALYSIS IN DCMD

University of Technology Sydney

Faculty of Engineering & Information Technology

This chapter explores the performance of the DCMD system using synthetic model organic compounds. The aim of this study was to evaluate the organic fouling propensity in MD based on the type of organic compound present in the feed solution, the thermal condition and the physico-chemical condition of the feed solution.

The first part of this chapter evaluates the behaviour of the three main organic compounds of humic acid, alginic acid and bovine serum album (representing humic substance, polysaccharides and protein respectively) under thermal MD operation. Detailed organic characterizations of the feed and permeate solution as well as membrane foulant were carried out to identify the most influencing organic compound in MD fouling development (**Section 6.3.1**). The second part discusses the influence of physico-chemical characteristics of the feed solution on organic fouling in MD with a detailed membrane autopsy (**Section 6.3.2**).

<Publications related to this chapter>

* **Naidu, G**., Jeong, S., Kim, S., Kim, I. S., & Vigneswaran, S. (2014). Organic fouling behaviour in direct contact membrane distillation. Desalination, 347(0), 230-239.

* **Naidu, G**, Jeong, S., Vigneswaran, S. Interaction of humic on organic and biofouling in membrane distillation for seawater desalination (*submitted to Chemical Engineering Journal*).

6.1   ORGANIC FOULING ANALYSIS OF THE DCMD SYSTEM

6.1.1   INTRODUCTION

Organic fouling is a ubiquitous problem in the membrane process. In MD, organic fouling development is a critical issue that still demands considerable research attention. Moreover, operating MD at saturated feed solution levels will enhance the incidence of fouling.

It has been acknowledged that NOM is one of the primary contributors to membrane fouling (Cho et al., 1999; Jeong et al., 2013a). NOM includes a group of low molecular weight (LMW) to high molecular weight (HMW) organic compounds, generally quantified as a dissolved organic carbon (DOC). In surface water, groundwater and seawater, humic substances (HS) are the major constituents of NOM, followed by carbohydrates (including polysaccharides), protein and a variety of acidic and neutral LMW species (Jermann et al., 2007; Yuan and Zydney et al., 1999).

Membrane studies have highlighted that NOM rejection is controlled by size exclusion, electrostatic repulsion, physico-chemical feed conditions as well as the interactions between the organic foulant and the membrane. MD fouling studies have not explored these interactions in detail. This is particularly important as the hydrophobic membrane has been deemed to be more susceptible to fouling than the hydrophilic membrane (Khayet et al., 2004; Hong and Elimelech, 1997; Fan et al., 2001). It has actually been demonstrated that HS adsorb more favourably onto hydrophobic membranes (Jucker and Clark, 1994). Furthermore, the thermal heating in MD may influence HS characteristics; previous studies have observed HS disaggregation to lower molecular size HS and other organics under thermal conditions (Drastík et al., 2013; Jin et al., 2009).

However, MD studies have pointed out that fouling by HS was not severe when compared to pressure-driven membrane processes, primarily due to the vapour pressure operated application (Khayet et al., 2004; Srisurichan et al., 2005; Srisurichan et al., 2006). Instead, MD studies have indicated that feed water containing NOM compounds of proteins, amino sugars and polysaccharides showed strong tendencies to deposit on the hydrophobic membrane (Gryta et al., 2001; Gryta et al., 2008b). The application of high feed temperature (60°C and above) in MD operation intensified protein-based NOM (Gryta et al., 2001; Ortiz de Zárate et al., 1998). Previous studies have observed structural and surface charge changes in protein/BSA organics with increased temperature (Zhao et al., 2009).

In most MD fouling investigations, membrane fouling is represented by the permeate flux decline (Khayet et al., 2004; Srisurichan et al., 2005; Gryta et al., 2001). Although membrane fouling is generally interpreted by flux decline, this approach is inadequate for characterizing fouling development in MD, especially due to the effect of temperature in the operation. Characterizing the foulant on the MD membrane would provide valuable guidance to the effective application of MD operation such as membrane cleaning and deciding the necessity for a pretreatment. Recent studies have reported specific methods to represent more detailed organic foulant characteristics using Liquid Chromatography-Organic Carbon Detection (LC-OCD) (Jeong et al., 2013a; Huber et al., 2011). The effectiveness of LC-OCD in characterizing fouling material in membrane processes and identifying specific organic compounds responsible for fouling in water and wastewater treatment has been demonstrated by a number of studies (Jacquemet et al., 2005; Rosenberger et al., 2005).

Apart from the influence of the organic compound present in the feed solution, the role of the feed solution's physico-chemical condition in contributing to the complex

membrane fouling development must be explained, especially in natural water sources such as seawater (Hong and Elimelech, 1997; Seidel and Elimelech, 2002). This physico-chemical condition mainly refers to the presence of NaCl as well as the presence of inorganic scalants. For instance, in one NF membrane study it was demonstrated that NOM fouling increased significantly at higher electrolyte (NaC1) concentration and with the addition of divalent cation attributed to electrostatic charges (Hong and Elimelech, 1997).

Hence, the objective of this study was to determine the influence of organic compound present in the feed solution as well as the physiochemical conditions of the feed water in MD organic fouling development. This is based on a detailed analysis of the organic characteristics. For this purpose, a direct contact membrane distillation (DCMD) system was used with model solutions of humic acid (HA), alginic acid (AA) and bovine serum albumin (BSA). These represented the HS, polysaccharides and proteins respectively, which are the major organic components of natural water sources such a surface water, groundwater and seawater (Jermann et al., 2007). The fractions of organic compound in the feed and permeate solution as well as the membrane foulant were analysed using LC-OCD. The morphology and composition of the deposit layer formed on the membrane surface was examined using FE-SEM while contact angle was used to determine the hydrophobicity of the membrane.

6.1.2   MATERIALS AND METHODS

6.1.2.1   Synthetic organic compounds

The investigation of organic fouling was conducted utilizing model organic compounds of AA, HA and BSA to represent polysaccharides, HS, and proteins, respectively. The supplier details and molecular weight (MW) are provided in **Table 3.3 (Chapter 3)**. The organic compounds were received in powder form. Stock solutions were prepared

by dissolving 350 mg-C/L organics in DI water followed by filtration with 0.45 μm filter to exclude initial deposition of bulk suspended solids on the membrane. The initial concentration of the organic compounds (10 mg-C /L) was determined in terms of dissolved organic carbon concentration. For the mixed organic (MO) solutions, the three model organic compounds were combined at a concentration of 10 mg-C /L each.

The feed solutions were prepared without changing the natural condition of the organic compound, whereby no pH alterations were made with the addition of acid or alkaline chemicals. The initial surface charge of each feed solution was measured with zeta potential, ζ. Malvern Zetasizer 3000 was used to measure the zeta potential, with a setting of 2 min of stabilization, set at an isoelectric point of 4.2 (protein solution). The data was recorded automatically and triplicate data measurements were taken.

6.1.2.2   Fouling experimental procedure

For this study, an intermediate flow velocity of v_f & v_p of 1.1 m/s (Re = 4950) and feed and permeate temperature of $70\pm0.2^\circ$C and $24\pm0.2^\circ$C were used for this study, based on the suitable DCMD operating conditions identified in **Chapter 4**. Temperature investigation of the HA feed solution was also carried out with the DCMD unit by varying the feed temperature from $F_t =70^\circ$C to $F_t = 60^\circ$C and $F_t = 50^\circ$C as shown in **Table 6.1**

Table 6.1 Synthetic organic compound feed solution composition, representation and operating conditions.

Feed Solution	Organic Composition	Representation	F_t ($^\circ$C)
AA	AA (10 mg-C/L)	Polysaccharide	70
BSA	BSA (10 mg-C/L)	Protein	70
HA (feed I)	HA (10 mg-C/L)	HS	50, 60 and 70
MO	AA (10 mg-C/L) + BSA (10 mg-C/L) + HA (10 mg-C/L)	Mixed organics combination	70
Saline HA (feed II)	HA (10 mg-C/L) with NaCl (1 M)	Influence of physico-chemical condition	70
Inorganic HA (feed III)	HA (10 mg-C/L) with CaSO$_4$ (60 mM NaSO$_4$ + 20 mM CaCl$_2$)		70

6.1.2.2.1 LC-OCD

The detailed organic fraction of the feed solution and membrane foulant was determined as DOC concentration using LC-OCD analysis as described in **Section 3.3.1.3.1** (**Chapter 3**). After each experiment the membrane foulant was extracted by cutting the membrane into small parts and placed in a beaker with milli-Q water. Then the beaker was sonicated to extract the organic residues on the MD membrane. Sonication was carried out with an ultrasonic bath (Powersonic 420, Thermoline Scientific, 300 W) for a short time (10 mins) to prevent organic matter from denaturing.

6.1.2.2.2   Membrane observation

The morphology and composition of the deposit layer formed on the membrane was analysed using FE-SEM. The contact angle of the membrane surface was measured to determine the membrane surface's hydrophobicity range by sessile drop method using a goniometer (Theta Lite) as described in **Section 3.3.2.2** (**Chapter 3**).

6.1.2.2.3   Membrane cleaning

When the organic fouling experiment was completed, the membrane in the module was cleaned by flushing 2 L of DI water through the feed channel at the flow velocity of 1.1 m/s. The DI water was flushed until a stable water permeate flux was achieved (no further permeate flux increment), which was taken to be the restored permeate flux value. The time duration for this restoration was recorded.

6.1.2.2.4   Glassware HA heating test

HA compound at two different concentrations of 10 mg-C /L and 20 mg-C/L were tested in the glassware heating test to study the effect of heating on HS characteristics. 70 mL of HA solutions were placed in two different 150 mL conical glass flask and heated on a heating plate at 70ºC. The heating process was carried out for 40 mins, upon which the feed solution reached a stable temperature of 70ºC. Similarly, for a control test, two flasks containing 70 mL of 10 mg/L and 20 mg/L HA solution were kept at room temperature (25ºC).

6.1.3   RESULTS AND DISCUSSION

6.1.3.1   Influence of organic compounds on fouling development in MD

6.1.3.1.1   Permeate flux

In terms of permeate flux decline pattern, a similar trend was observed for all the individual organic compounds (**Figure 6.1**). The BSA compound showed a faster permeate flux declining pattern (from VCF 2.0 onwards) compared to the AA and HA (only from VCF 3.0 onwards). Higher permeate flux decline was observed with the BSA compound (64.5%), in contrast to the permeate flux decline with the HA (56.2%) and AA (44.1%) compound. A faster flux decline could be interpreted as a stronger adhesion of foulant on the membrane (Mi and Elimelech, 2008).
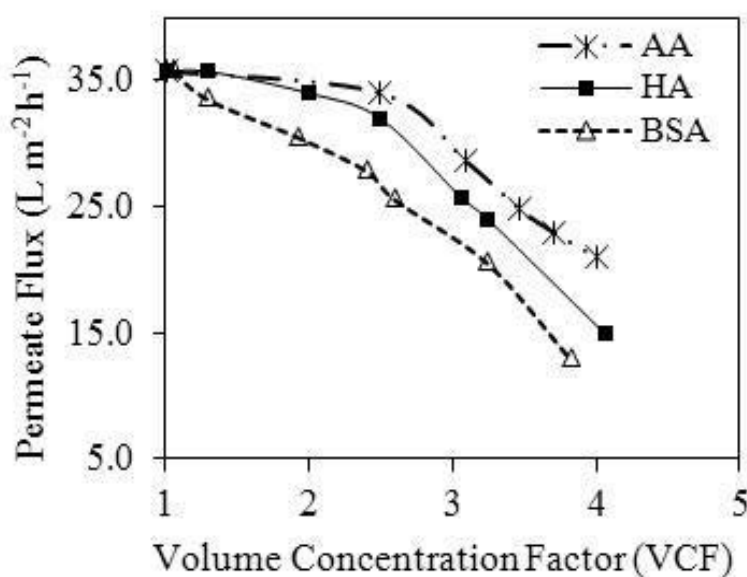
Figure 6.1 Comparison of the permeate flux pattern of the three individual organic compound feed solutions as a function of VCF.

In order to understand in detail the behavior of each individual organic compound and its intensity on the MD membrane, further investigations were carried out to study the compounds' organic characteristics (LC-OCD analysis), the membrane hydrophobicity (contact angle analysis) and membrane foulant characteristics (SEM-EDS analysis).

6.1.3.1.2 Organic compound deposition on the membrane (LC-OCD analysis)

6.1.3.1.2.1 Organic characteristics of the foulant on the membrane

LC-OCD chromatograms of the membrane foulant (extracted from the membrane at the end of the experiment) with the individual organic feed solution are presented in **Figure 6.2**. The membrane foulant of the AA feed solution was primarily composed of small peaks of LMW organics. The membrane foulant with HA feed solution also contained LMW organic compounds but with significantly larger peaks. Meanwhile with reference to the BSA feed solution, the membrane foulant contained biopolymer peaks as well as LMW organic peaks.
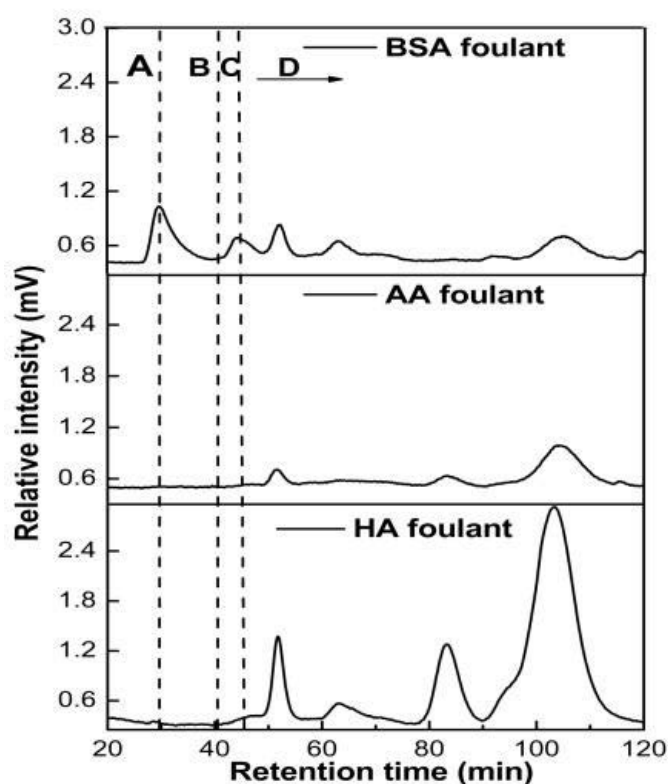
Figure 6.2 LC-OCD chromatogram of membrane foulants of the three individual organic compound feed solutions *(A: Biopolymers; B: HS; C: BB; D: LMW organics).*

6.1.3.1.2.2 Mass balance of organic compound on the membrane

For all the feed solutions, an initial 20 mg of organic compound mass was used (2 L of initial feed solution at a concentration of 10 mg C/L). At VCF 4.0, assuming no organic compound was deposited on the membrane surface and in the membrane module (organics in the feed channel), the 20 mg organic would remain in the bulk feed solution concentrate (40 mg C/L). Based on the DOC concentration at VCF 4 for the individual feed solution (**Table 6.2**), the reduced mass in the bulk feed solution concentrate was assumed to be the mass deposited on the membrane (organic mass in the feed channel was assumed to be negligible).

6.1.3.1.2.2.1   AA

The initial DOC value of the AA feed solution (VCF 1) was 10.8 C mg /L. At VCF 4, the measured DOC value of the AA feed solution was 33.3 C mg/L as shown in **Table 6.2**. Organic concentration was negligible on the permeate side. Accordingly, the AA compound mass deposited on the membrane amounted to 199.4 mg/m^2.

6.1.3.1.2.2.2   HA

At VCF 1, the measured DOC value of the HA feed solution was 9.5 mg C /L. At VCF 4, the measured DOC value of the HA feed solution was 19.2 mg C/L. Further, a 0.94 mg /L organic concentration was detected in the final permeate solution of 3.5 L. This amounted to a mass of 3.3 mg organic in the permeate side. Hence, the HA compound mass deposited on the membrane was 423.2 mg / m^2 as shown in **Table 6.2**.

6.1.3.1.2.2.3   BSA

The initial and final DOC value of the BSA feed solution was 9.6 mg C/L (VCF 1) and 13.1 mg C/L(VCF 4) as shown in Table 6.2. The organic concentration was negligible on the permeate side. Based on this, the BSA compound mass deposited on

the membrane was calculated to be 800.6 mg /m^2. Hence the highest membrane foulant

residue deposit was by the BSA compound.

Table 6.2 Detailed characteristics of the individual organic feed solutions

Feed solution	Organic content (mg/L)			pH	Zeta potential, ζ (mV)	Organic mass deposited /membrane area (mg/m^2)
	Total DOC	Hydrophobic fraction	Hydrophilic fraction			
AA						
VCF 1	10.8	1.0	9.8	5.8	−25.3±4.4	
VCF 4	33.3	8.6	24.7			199.4
HA						
VCF 1	9.5	3.9	5.6	5.0	−29.8±3.7	
VCF 4	19.2	8.4	10.8			423.2
BSA						
VCF 1	9.6	7.1	2.5	6.3	−8.9±4.9	
VCF 4	13.1	5.1	8.0			800.6

6.1.3.1.3 Organic characteristics of the individual feed solution (LC-OCD analysis)

The initial pH value of the individual feed solution was in the range of pH 5.0 to 6.3. The feed solutions were all negatively charged with BSA feed solution showing a relatively low negative zeta potential ($\zeta = -8.9 \pm 4.9$ mV), while both the AA and HA feed solutions indicated high negative zeta potential of $\zeta = -25.3 \pm 4.4$ mV and $\zeta = -29.8 \pm 3.7$ mV, respectively, as shown in **Table 6.2**.

6.1.3.1.3.1 AA

The LC-DOC chromatogram revealed that the initial AA feed solution was highly hydrophilic in nature (90.7% hydrophilic fraction and 9.3% hydrophobic fraction) as shown in **Table 6.2**. At VCF 1.0, the hydrophilic portion of the AA feed solution consisted largely of a biopolymer compound at a concentration of 8.3 mg/L (83.8%) with smaller portions of building blocks (BB) at 1.0 mg/L (10.3%) and LMW organics at 0.5 mg/L (5.9%) as shown in **Figure 6.3a**.

At VCF 4.0, the biopolymer compound increased by a ratio of 3.1 times its initial value, while the BB and LMW organics increased by a ratio of 3.8 times of their initial values, suggesting some degradation of biopolymer to BB and LMW organics. Overall, in the AA feed solution, the organic compound concentration increment was closely proportional to the VCF increase. This indicated that the bulk of the AA feed solution remained intact even at high concentrations with minimal attachment to the membrane. In line with this, the AA compound mass deposited per membrane area (199.4 mg/m^2) was the lowest compared to the BSA and HA compounds. This could be attributed to the more hydrophilic nature of the AA compound. It has been highlighted that hydrophilic compounds do not bond strongly to hydrophobic surfaces. As the MD membrane is hydrophobic in nature, the AA compound adhered minimally on the

membrane surface (Jermann et al., 2007). At the same time, the AA compound was highly negatively charged (ζ= −25.3±4.4mV), contributing to a further electrostatic repulsion with the negative surface MD membrane.

6.1.3.1.3.2 HA

The HA feed solution contained a balanced combination of both hydrophobic and hydrophilic fraction as shown in **Table 6.2**. At VCF 1.0, the hydrophilic fraction (5.6 mg/L) of the HA feed solution comprised of HS at a concentration of 4.6 mg/L with smaller portions of BB at 0.3 mg/L and LMW organics at 0.7 mg/L. At VCF 4.0, the HS increased minimally only by a ratio of 1.4 times its initial value. On the other hand, the BB and LMW organics increased significantly by a ratio of 6.2 times and 3.3 times of their initial values as shown in **Figure 6.3b**. Meanwhile with the HA feed solution, the foulant deposited on the membrane consisted only of LMW organics as shown in **Figure 6.2**. The HA concentration in the feed solution (represented as HS with the LC-OCD) did not increase proportionally with the VCF and it was also not detected on the membrane foulant. The results suggest that the HS compound was disaggregated as BB-HS and LMW-HS organics.

The HS disaggregating tendencies when temperature increased has been highlighted in the previous studies (Drastík et al., 2013; Jin et al., 2009; Palmer and Von Wandruszka, 2001). These studies used methods such as dynamic light scattering and ultrasonic velocimetry, and it was observed that HS molecular size decreased due to the disaggregation of HS by thermal agitation. On the other hand, thermal degradation structure analysis using Fourier transform infrared spectroscopy showed that the HS compound retained most of its original structure up to a high temperature of 200˚C to 400˚C (Lu et al., 2001; Giovanela et al., 2004).

Huber et al. (2011) observed that small HS compounds co-elutes with LMW organics as LMW-HS organics. This is attributed to the LC-OCD analysis principle which fractionates organic compounds based on the size exclusion method. As such the LC-OCD analysis will represent the LMW-HS organics (from thermal disaggregation) as LMW organics. This explained the significantly higher build-up of LMW organics concentration with the HA feed solution in our study.

Additionally, a glassware heating test was conducted to observe the presence of LMW-HS organics in HA compound (10 and 20 mg/L) at 25ºC and 70°C. The total DOC value of the HA-70°C compound was 11 to 20% higher than the HA-25°C compound. This is attributed to the slight increase in organic concentration with water evaporation from heating. The results showed a reduction of HS concentration by 7 to 10% with HA-70°C in comparison to HA-25°C. Meanwhile, an increase of 34 to 70% of LMW-HS organics was observed with HA-70°C as shown in **Table 6.3**. This verified the LC-OCD detection of thermally disaggregated smaller HS compounds (LMW-HS organics) as LMW organics.

Table 6.3 LC-OCD organic analysis details of the glassware test showing the effect of heating on HA compound.

Temperature condition (°C)	HA compound LC-OCD Analysis					
	Total DOC (mg/L)	Hydrophilic compound fraction (mg/L)				
		Biopolymer	HS	BB	LMW neutrals	LMW acid
25	9.39	n.q.	4.08	0.79	0.73	0.01
	16.53	n.q.	6.44	2.18	1.45	0.02
70	10.43	n.q.	3.79	1.22	0.98	0.01
	20.10	n.q.	6.36	2.48	2.29	0.01

Investigating the temperature of the HA feed solution was done using the DCMD unit by varying the feed temperature from $F_t = 70°C$ to $F_t = 60°C$ and $F_t = 50°C$. Using the same initial HA feed solution (VCF 1), the results were compared at VCF 3. At VCF 3, the total DOC values were nearly similar for all three feed temperatures studied. It was in the range of 15.2 mg/L to 15.6 mg/L thus enabling a relative comparison to be made as shown in **Table 6.4**. At VCF 3, the HS concentration was the highest at $F_t = 50°C$, while the BB-HS and LMW-HS organics were the lowest. In contrast, the highest BB-HS and LMW-HS organics emerged at $F_t = 70°C$, with a lower concentration of the HS. The results showed that temperature in MD operation effectively caused higher disaggregation of HS to BB-HS and LMW-HS organics.

Table 6.4 LC-OCD organic characteristics of HA compound at different feed temperatures ($F_t = 50$ºC, $F_t = 60$ºC and $F_t = 70$ºC) with DCMD operation.

HA feed solution	Total DOC (mg/L)	Hydrophilic compound fraction (mg/L)				
		Biopolymer	HS	BB	LMW neutrals	LMW acid
Initial HA(VCF1)	9.54	n.q	4.43	0.28	0.57	0.30
HA-50°C (VCF 2)	15.23	n.q	5.32	0.64	1.38	0.21
HA-60ºC (VCF2)	15.33	n.q	5.06	0.65	1.44	0.33
HA-70°C (VCF 2)	15.58	n.q	4.84	0.71	1.54	0.26

6.1.3.1.3.3 BSA

The initial BSA feed solution (VCF 1) was hydrophobic in nature (74.0%) as shown in **Table 6.2**. At VCF 1, the BSA feed solution mainly consisted of the biopolymer compound at a concentration of 1.3 mg/L (52.7%) followed by similar portions of BB and LMW organics (0.5 mg/L concentration each (23.5%)) as shown in **Figure 6.3c**.

From VCF 2 onwards, the BSA chromatogram revealed that the concentration of the biopolymer compound in the feed solution reduced gradually and at VCF 4, the biopolymer concentration was only 0.8 times its initial value. In line with this, the presence of a biopolymer peak was also observed in the membrane foulant. The results suggest that the biopolymer's adhesion to the membrane surface could be attributed to the lower concentration of biopolymer in the feed solution from VCF 2 onwards. Also, the highest membrane foulant mass occurred in the BSA feed solution (800.6 mg/m^2), which is comparable to the deposits by the HA and AA feed solutions as shown in **Table 6.2**. This could be associated with the higher adsorption of the hydrophobic biopolymer on the hydrophobic membrane surface as suggested by other membrane

fouling studies (Marshall et al., 1993; Li et al., 2007). Furthermore the low negative zeta potential of the BSA compound ($\zeta=-8.9\pm4.9mV$) accounted for less electric repulsion with the negative membrane surface. In fact, it has been highlighted that under thermal conditions, the negative surface charge of the BSA compound would further decline, thus increasing the adsorption onto a negatively charged surface (Zhao et al., 2009).

MD fouling studies have also analysed the fouling of protein/BSA on hydrophobic membrane, acknowledging the high intensity of protein foulant deposited on the hydrophobic membranes under thermal conditions (Gryta et al., 2001; Gryta, 2008b). From VCF 2 onwards, the hydrophobic fraction of the BSA feed solution decreased, while the hydrophilic fraction increased. At VCF 4, the hydrophobic fraction reduced to 38.9% of the total DOC while the hydrophilic fraction increased to 61.1% of the total DOC. This suggests that the BSA foulant adhesion was highly likely to be at the initial hydrophobic stage of the feed solution and less adhesion occurred as the hydrophobic fraction reduced.

In the BSA feed solution from VCF 2 to VCF 4 onwards, the remaining biopolymer degraded under the thermal MD operating conditions to BB and LMW organics. The BB and LMW organics increased by 7.1-fold and 5.9-fold of their initial concentration values, respectively. At VCF 4, the LMW organics concentration reduced slightly. In line with this, LMW organics were detected on the BSA membrane foulant. The combination of early biopolymer adhesion followed by LMW organics adhering to the biopolymer layer of the membrane, was most likely attributed to the faster permeate flux decline with the BSA compound compared to the other organic compounds.

(a) (b) (c)
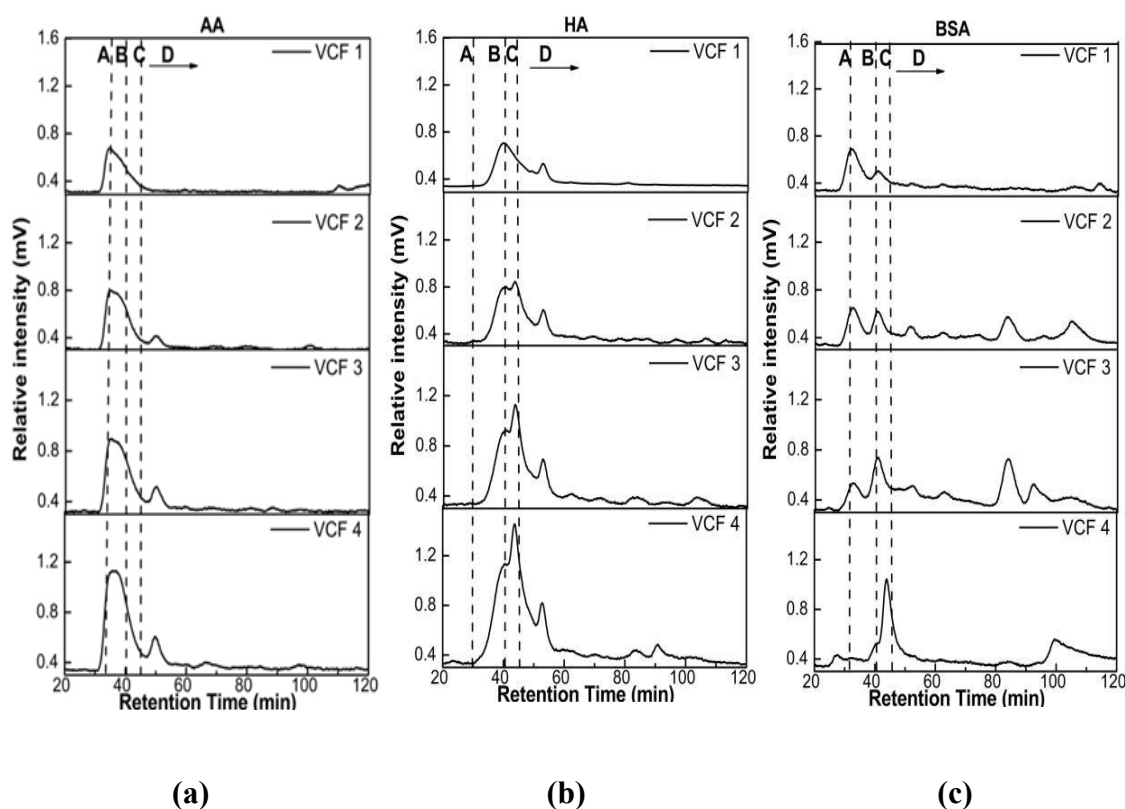
Figure 6.3 LC-OCD chromatogram of the three organic feed solutions **(a)** AA **(b)** HA and **(c)** BSA *(A: Biopolymers; B: HS; C: BB; D: LMW organics).*

6.1.3.1.4 Organic characteristics of the individual permeate solution (LC-OCD analysis)

The permeate DOC details for the individual organic compounds (AA, HA and BSA) are shown in **Table 6.5**. At VCF 4, the permeate DOC of the HA feed solution revealed the highest concentration at 0.94 mg/L, mainly comprising LMW organics. The permeate DOC for both the AA and BSA feed solutions was less than 0.3 mg/L at VCF 4. Both these DOC values were similar to the MQ baseline value.

Table 6.5 LC-OCD organic characteristics details of the permeate solution at VCF 4.0.

Permeate	Total DOC	Hydrophilic compound fraction (mg/L)				
(VCF 4)	(mg/L)	Biopolymer	HS	BB	LMW neutrals	LMW acid
MQ	0.15	n.q	0.01	0.10	0.02	n.q
AA	0.21	0.01	0.01	0.03	0.10	0.01
BSA	0.27	n.q.	0.02	0.08	0.12	0.02
HA	0.94	n.q.	0.01	0.10	0.58	0.10

6.1.3.1.5   Membrane hydrophobicity (contact angle analysis)

6.1.3.1.5.1 AA

In terms of the impact of the foulant on the membrane hydrophobicity (contact angle), AA compound only impacted the membrane hydrophobicity minimally, reducing it from 139.9±1.2° to130.6±4.7°. Upon cleaning using DI water, the hydrophobicity of the membrane was restored to its original state. This suggests that the AA compound does not display major fouling tendencies under MD operating conditions.

6.1.3.1.5.2 HA

With the HA compound, the hydrophobicity of the membrane reduced significantly to 93.5±6.2°. Further, the hydrophobicity of the HA fouled membrane was only able to be restored up to 98.3±4.1° upon DI water cleaning. This implies that the HA compound: firstly, has a strong capacity to adhere to the hydrophobic MD membrane; and secondly, cannot be restored by DI water cleaning only.

6.1.3.1.5.3 BSA

The hydrophobicity of the BSA fouled membrane reduced to the lowest value of 84.2±4.7° in comparison to the other organic compounds. This implied that the protein residues deposited on the membrane surface had the ability to reduce the hydrophobicity significantly. However, upon DI water cleaning, the hydrophobicity of the BSA fouled

membrane could be restored to 104.3±3.8°. Better recovery of membrane hydrophobicity was obtained using the BSA fouled membrane compared to the HA fouled membrane.

6.1.3.1.6 Membrane characterization (SEM-EDS Analysis)

To further verify the fouling pattern of the three organic compounds, an analysis of SEM-EDS was carried out to quantify the organic contents across membrane surfaces as well as penetration through the membrane pores (line depth analysis) (Gryta, 2008b). The carbon (C) and oxygen (O) element peaks were used to represent the organic fouling deposit. This approach was adopted based on other membrane studies that analysed organic fouling through the carbon and oxygen element peak (Tran et al., 2007; Chon et al., 2012). For the line depth analysis, the C and O elements of the virgin membrane were used as a baseline. The elements on the fouled membrane were offset from the virgin baseline value. The O element peak had only a small increment on BSA and therefore was omitted from the subsequent analysis. The SEM-EDS line analysis was carried out from point A to point C (membrane cross-section depth of 0-300 µm) as shown in **Figure 6.5b**. The start of the membrane surface was at point B (90-95 µm), which was determined from the start of the fluoride peak in the virgin membrane, which is a compound residing inside the membrane's structure.

6.1.3.1.6.1 AA

The SEM-EDS (membrane surface) results detected only small traces of C element peak (19.26 CPS/keV) on the membrane surface in comparison to the virgin membrane (18.74 CPS/keV) as shown in **Figure 6.4a & 6.4c**. At the same time, the SEM-EDS (membrane cross-section line depth analysis) showed minimal traces of organic residues (C element) through the pores of the AA fouled membrane as shown in **Figure 6.5a & 6.5c**. Overall, the membrane with the AA compound exhibited a constant pattern of

minimal element detection for all conditions studied. This supports our earlier finding that only minimal fouling impact was observed when using the hydrophilic AA organic compounds.

6.1.3.1.6.2 HA

The HA fouled membrane displayed only a slightly higher C element peak at 19.43 CPS/keV in comparison to the virgin membrane (18.74 CPS/keV) with SEM-EDS (membrane surface) analysis (**Figure 6.4a & 6.4b**). However, SEM-EDS (membrane cross-section line depth analysis) demonstrated that a significant C element penetrated through the membrane pores from 90 μm to 280 μm (**Figure 6.5a & 6.5d**). The membrane foulant chromatogram as well as the permeate solution chromatogram of the HA compound displayed similar patterns of dominant peaks of LMW-HS organics. At the same time, the SEM–EDS (cross-section) results displayed the penetration of organics through the membrane pores. These results suggest that the LMW-HS organics from the thermal disaggregation of the HS adsorbed to the membrane surface and penetrated through the pores of the membrane.

6.1.3.1.6.3 BSA

The SEM-EDS (membrane surface) on the BSA fouled membrane displayed significant C element peak at an intensity of 30.21 CPS/keV in comparison to the virgin membrane (18.74 CPS/keV) (**Figure 6.4a & 6.4d**). This was the highest C element content on the membrane surface compared to the other two foulants. The SEM-EDS (cross-section line depth analysis) results also showed that for the BSA foulant, the C element was only detected on the top layer of the membrane surface (in the range of 40 μm to 90 μm) (**Figure 6.5a & 6.5e**). From a depth of 90 μm to 300 μm, only traces of organic residues were detected in the pores. The results suggest that the HMW biopolymer (BSA) showed initial deposition across the membrane surface and formed a cake/gel

layer, resulting in faster flux decline. However, the HMW compound did not show significant penetration into the MD membrane pores. Although at the later stage the BSA compound degraded to BB and LMW organics, the LMW organics most likely did not penetrate through the membrane due to the gel-like foulant layer formation on the membrane surface by the biopolymer compounds.
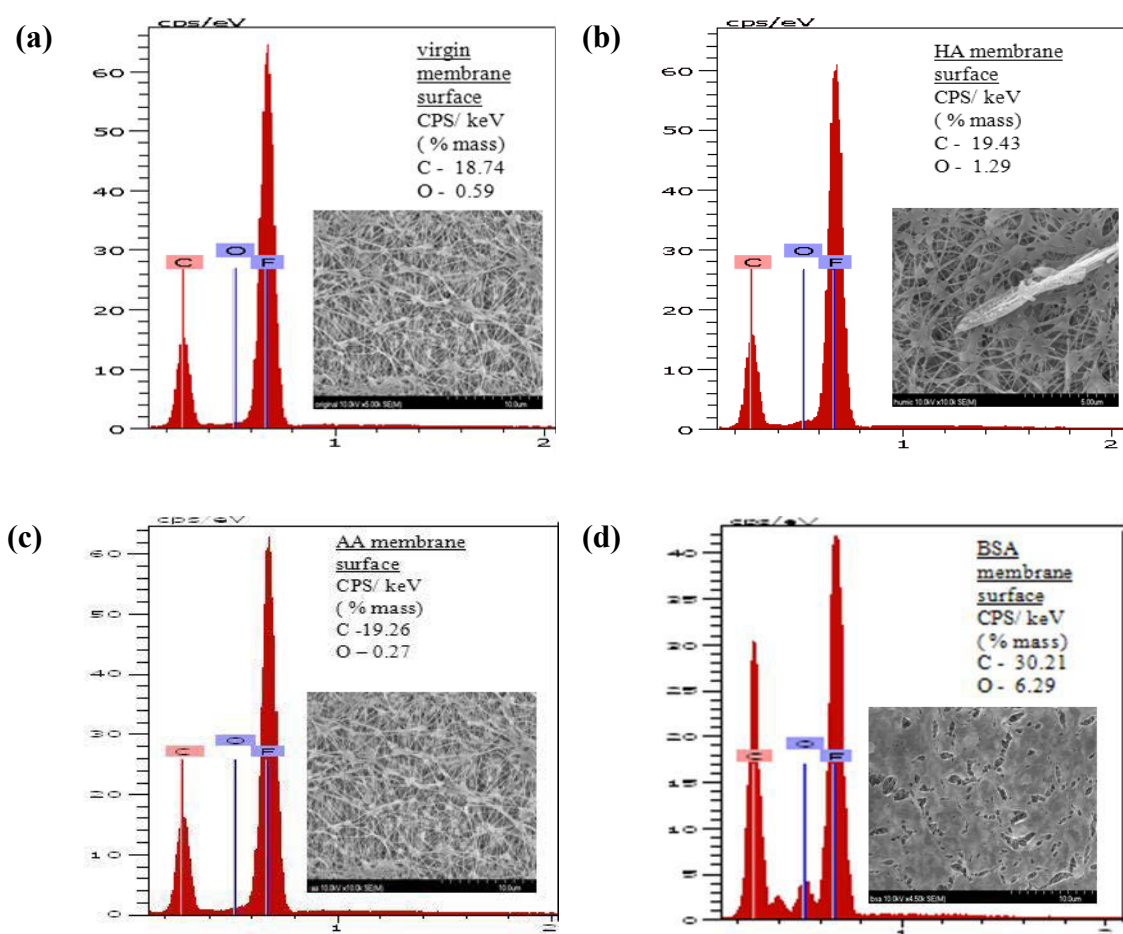
Figure 6.4 SEM-EDS membrane surface analysis of **(a)** virgin **(b)** HA **(c)** AA and **(d)** BSA.
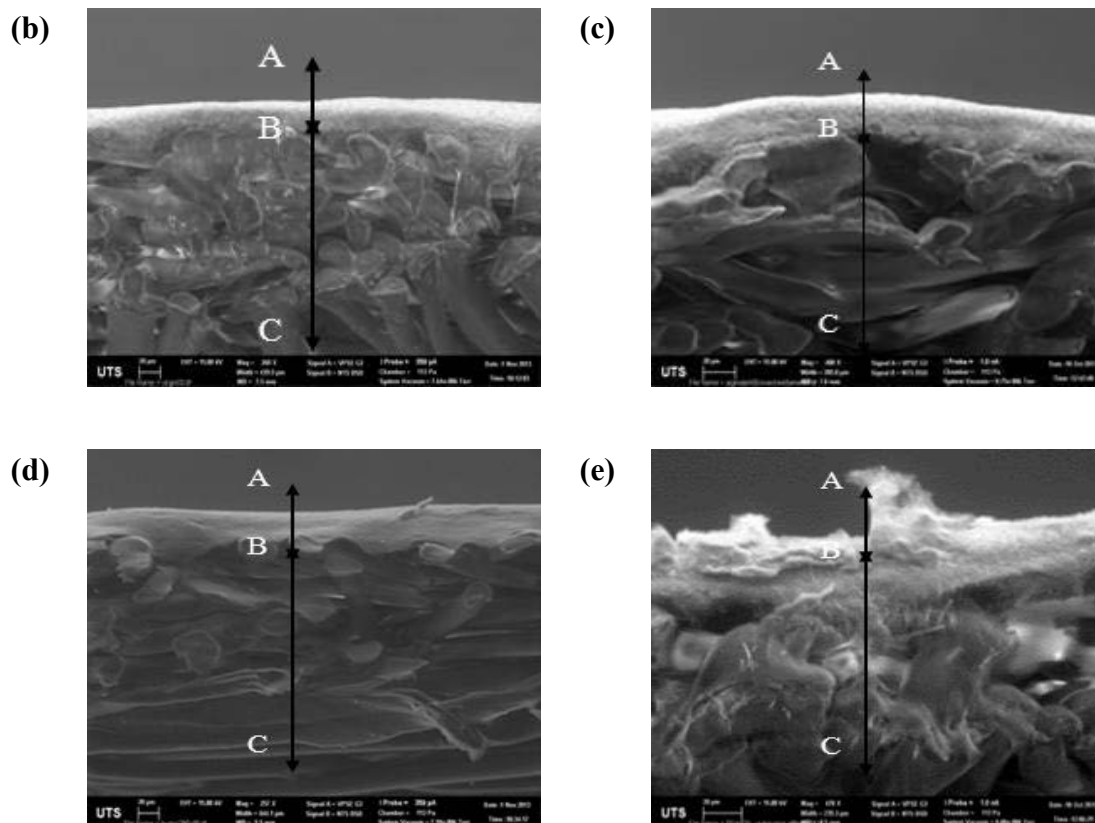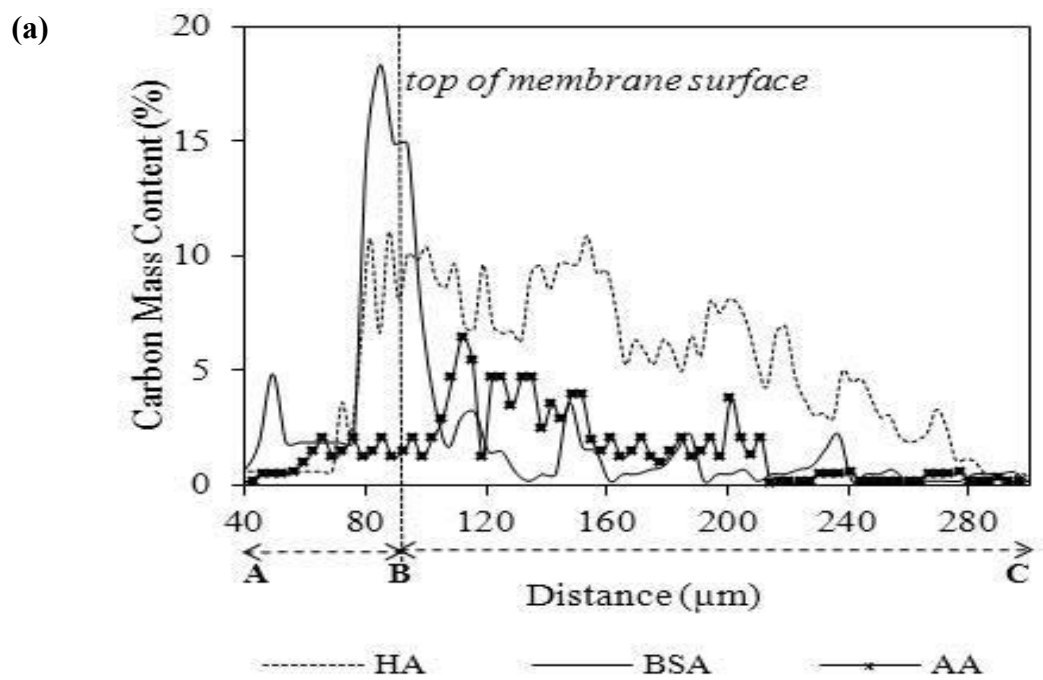
Figure 6.5 SEM-EDS membrane cross-section line analysis **(a)** carbon element mass as a function of membrane depth on HA, BSA and AA fouled membrane and SEM images of **(b)** virgin membrane **(c)** AA **(d)** HA and **(e)** BSA.

In summary, both the HA and BSA compounds resulted in significant fouling in MD. The HA compund showed a higher tendency to penetrate into the pores of the membrane and hence potentially causing membrane wetting. On the other hand, BSA compounds predominantly got adsorbed onto the membrane surface.

The reversibility of fouling by the HA and BSA compounds was also studied by cleaning the membrane with DI water as explained in **Section 6.1.2.2.3**. Upon cleaning, a 97-98% flux recovery was obtained for both HA and BSA foulants. A slightly faster restoration period (20 mins) was observed with the BSA fouled membrane in comparison with that of HA (34 mins). The results indicated that with the MD operating conditions and organic concentration levels being studied, fouling was reversible; with a faster restoration capacity with BSA fouled membrane. In fact, in previous MD studies, protein (BSA) deposits have been acknowledged to be intense but mitigation was made possible by adopting a straight forward measure of pre-boiling the protein solution at 90-95°C for a short duration (30 mins) in a pressure vessel (Gryta et al., 2001; Gryta et al., 2008b).

In view of the different fouling patterns of the individual organic compounds on the hydrophobic membrane, a study was carried out with a feed solution containing a mixture of all three organic compounds. This is especially relevant as most natural water sources would have a combination of organic compounds (Jermann et al., 2007).

6.1.3.1.7 Fouling pattern of mixed organic (MO) compounds on hydrophobic membrane

The MO feed solution contained a mixture of the three model organic compounds (HA, BSA and AA) at a concentration of 10 mg/L each. From the LC-OCD analysis, the organic compound concentration in the initial MO feed solution (VCF 1.0) was largely

hydrophilic (18.5 mg/L) in nature, with a relatively small hydrophobic fraction (8.1 mg/L). The hydrophilic fraction consisted largely of biopolymer (13.7 to 13.8 mg/L) with smaller portions of HS (1.9 to 2.0 mg/L) as well as 2.0 to 2.1 mg/L of lower MW organics (BB and LMW organics) as shown in **Figure 6.6**. The presence of high concentrations of the biopolymer compound in the initial feed solution could be explained by the combination of the two high MW organics - BSA and AA. During the MD operation, a steady permeate flux pattern was observed with MO solution till VCF 3.5. Thereafter the permeate flux gradually declined by 65% till it reached VCF 5.0 as shown in **Figure 6.7a**. In comparison, the permeate flux pattern of the individual organic compounds showed an initial permeate flux decline from VCF 2.0 onwards and thereafter sharply declined by 46 - 55%. The MO feed solution permeate flux pattern suggests that the individual organic compounds' behaviour could differ in a mixed feed solution condition. Recent organic foulant studies UF membrane process, focusing on MO solutions, have indicated that in a combined organics solution, the NOM interplay (foulant and foulant interaction) influences individual foulant behavior (Jermann et al., 2007; Myat et al., 2014).

In our study, although a high concentration of biopolymer compound was present in the initial MO feed solution (VCF 1), the concentration only increased by 1.4 times its initial concentration by VCF 4. Meanwhile, the initial HS concentration in the MO feed solution increased as the VCF increased and was 3.4 times its initial value at VCF 4. In terms of the lower MW organics, at VCF 4, the BB compounds increased significantly by 6.5 times its initial concentration while the LMW organics increased by only 1.1 times its initial concentration. Regarding the MO membrane foulant, the LC-OCD chromatogram displayed the presence of high peaks of LMW organics as shown in **Figure 6.7b**.

The results of the MO feed organic characterization suggest that the BSA compound may have interacted with HA compound. This interaction altered the structure of the HS as established by the molecular dynamic simulation study (Myat et al., 2014). This could have resulted in minimal increase of the biopolymer compound concentration, while the HS concentration increased gradually with VCF. In comparison, in the individual HA feed solution, the HS increased by only 1.5 times at VCF 4 with a prevalent pattern of HS disaggregating to LMW-HS organics. The study by Myat et al. (2014) provided evidence for interactions occurring between the individual HA and BSA organic compounds through molecular dynamic simulations. It was explained that the individual organic characteristics were altered by the interaction of aliphatic and aromatic moieties of the HS with hydrophobic regions of the protein surface as well as by hydrogen bonding.

The MO membrane foulant also predominantly highlighted the presence of LMW organic peaks. The organics in the form of LMW organics dominantly attached themselves to the hydrophobic membrane. This means that a feed solution comprising of LMW organics or organic compounds (for instance HS) that disaggregates to LMW-HS organics, would tend to cause more severe membrane fouling under MD operation. In the case of individual HA feed solution, the disaggregation of HS to LMW-HS was significant, resulting in permeate flux decline from VCF 2.0 onwards. In MO feed solution, although the initial organic feed concentration was higher due to a combination of the three organics, the foulants' interaction resulted in less disaggregation of HS until the feed volume was reduced (VCF 3.0 onwards). As such the permeate flux was stable for a longer time before a sharp decline was observed due to LMW organics adhering on the membrane.
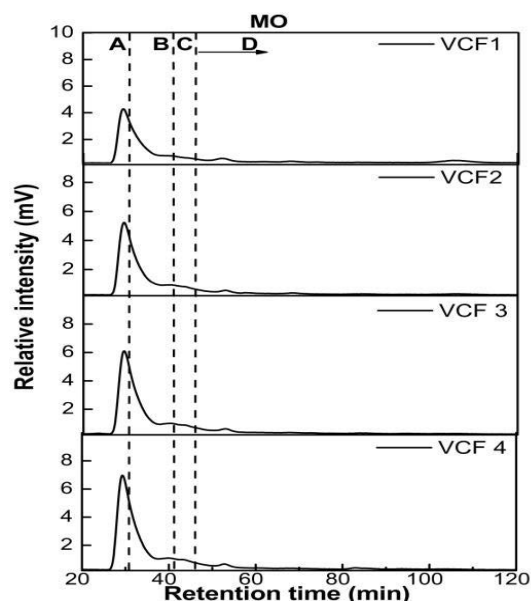
Figure 6.6 LC-OCD chromatograms of the MO feed solution *(A: Biopolymers; B: HS; C: BB; D: LMW organics).*
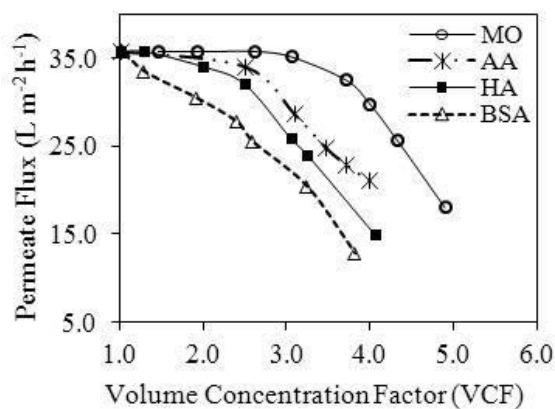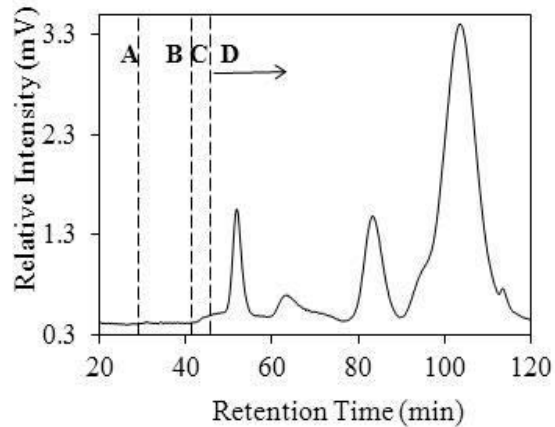
| (a) | (b) |

Figure 6.7 Comparison of fouling pattern with MO solution **(a)** permeate flux decline as a function of VCF **(b)** LC-OCD chromatogram of MO foulant *(A: Biopolymers; B: HS; C: BB; D: LMW organics).*

6.1.3.2   Influence of feed solution's physico-chemical conditions on organic fouling development in MD

In **Section 6.13.1** of this chapter, the evaluation of organic fouling was conducted with individual model organic compounds. The findings detected the severity of HA fouling under MD thermal operation. Moreover, it has been acknowledged that HS is one of the prevalent organic compounds present in natural water sources such as seawater (Jermann et al., 2007; Yuan and Zydney, 1999; Jucker and Clark, 1994). Hence, in this section, the evaluation of feed solution physico-chemical condition is carried out with synthetic HA feed solution. For this purpose, results for the individual HA compound analysis (feed I) were compared to the saline HA feed (feed II) and inorganic divalent HA feed solution (feed III) as shown in **Table 6.1**.

6.1.3.2.1   Influence of the presence of NaCl

For the HA feed solution (feed I), at the initial stages of VCF 1.0 to 2.0, the permeate flux declined by 5.8%. Thereafter, the permeate flux declined by 50.4% up to VCF 4.0 as shown in **Figure 6.1**. Meanwhile, the organic mass deposited on the membrane with HA feed I was 423.2 mg-organic mass /m^2 as displayed in **Table 6.2**

Comparatively, HA in the presence of 1 M of NaCl (HA feed II), resulted in a permeate flux decline of 65.6% at VCF 4.0 as shown in **Figure 6.8a**. This suggested that the presence of NaCl (salt) influenced the permeate flux pattern of organic fouling. Further, a thick brown layer of foulant was found covering the membrane's surface at the end of the experiment with HA feed II. This indicated the influence of the physico-chemical condition of the feed solution on MD organic fouling, apart from the presence of the organic compound.

(a)

(d)

(b)

(e)

(c)

(f)
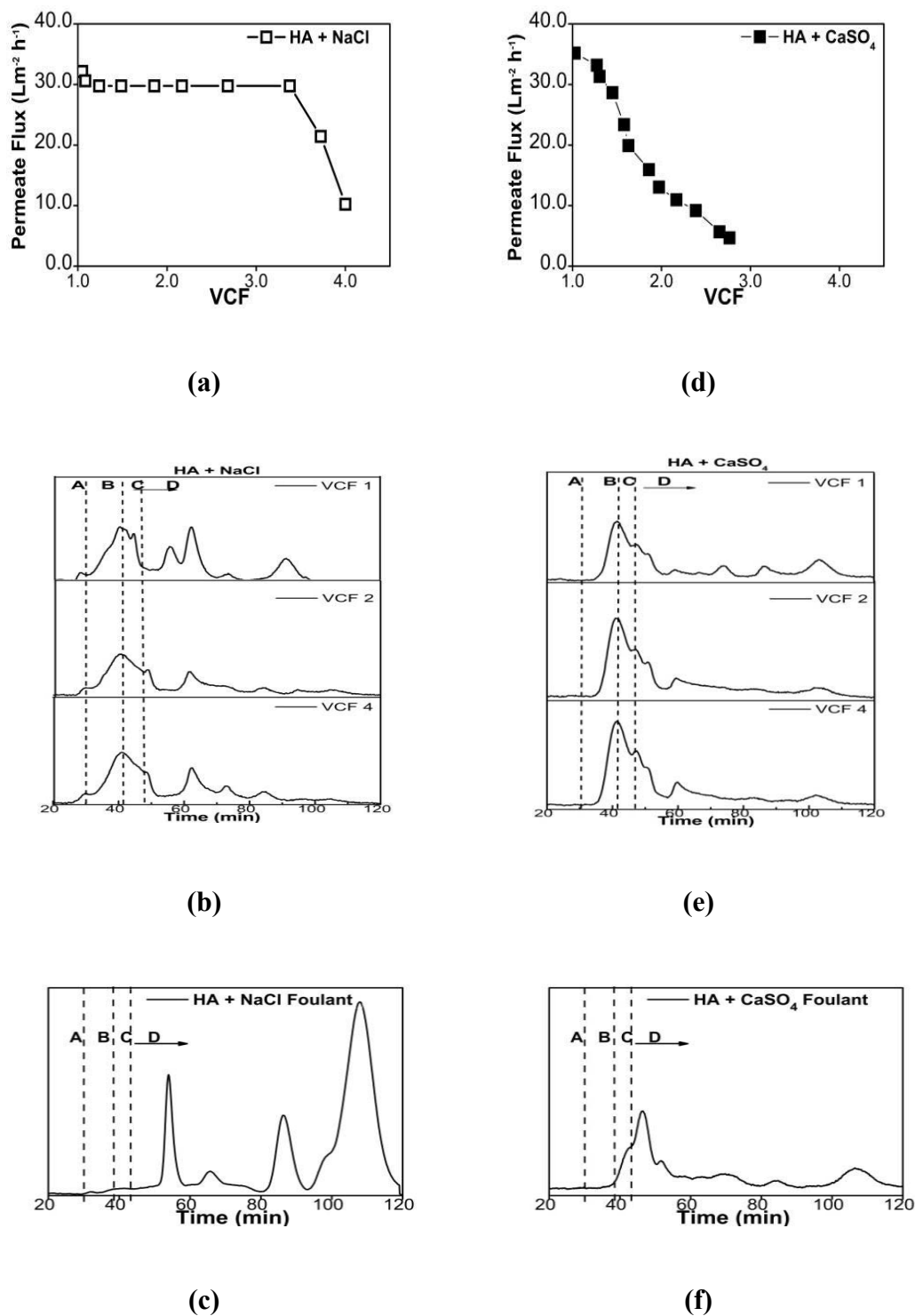
Figure 6.8 Physico-chemical influence of fouling pattern of HA compound based on permeate flux decline, LC-OCD chromatograms of feed solution and membrane foulant **(a-c)** feed II (saline HA) **(d - f)** feed III (inorganic scalant HA compound ($CaSO_4$)) *(A: Biopolymers; B: HS; C: BB; D: LMW organics).*

The LC-OCD chromatogram of the initial feed solution demonstrated that the presence of NaCl resulted in a more significant disaggregation of the HS to the LMW-HS organics as shown in **Figure 6.8b**. At VCF 1.0, the initial feed II included the HS at a concentration of 2.1 mg/L with higher contents of LMW organics of 2.7 mg/L. In comparison, the initial feed I contained about half the portion of LMW organics at only 0.74 mg/L. Recent studies have analyzed the formation of HS using nuclear magnetic resonance spectroscopy and size exclusion chromatography (Piccolo, 2001; Baalousha et al., 2006). These studies concluded that the high molecular weight HS is a result of small HS molecules aggregating, and they interact with each other through hydrophobic bonding (Van der Walls) and hydrogen bonding. These studies observed the disruption of the weak hydrogen and hydrophobic bonding in the presence of salts. Similar to the HS thermal disaggregation, small HS organics were formed in the presence of salt (NaCl).

Meanwhile, the membrane foulant with HA feed II displayed in **Figure 6.8c** showed 112% higher concentration of LMW organics than the membrane foulant with HA feed I as shown in **Figure 6.2**. Based on the initial DOC concentration of HA feed II at VCF 1.0 (9.84 mg/L), and the final DOC concentration of HA feed II at VCF 4.0 (12.69 mg/L), an organic mass reduction of 11.68 mg was estimated. Further, a 2.1 mg mass was measured on the permeate side. As a result, an organic mass of 694.4 mg-organic mass/m^2 was deposited on the membrane with HA feed II. In comparison, in HA feed I, relatively lower organic mass of 423.2 mg-organic mass/m^2 was deposited on the membrane. This investigation found that HA in the presence of NaCl contributed to more foulant being deposited on the membrane in MD. This is because HA becomes coiled and spherical in shape due to the electrostatic shielding between the negative charges of carboxyl function groups of HA molecules by the Na^{2+} ions. This

consequently decreases the electrostatic repulsion between the membrane surface and saline HA, resulting in more foulant deposition (Srisurichan et al., 2005; Hong and Elimelech, 1997). As a result, higher permeate flux decline occurred with HA feed II. Similarly, a study on DCMD with saline feed solution showed that the organic compound (protein) deposition increased in the presence of salt (Gryta et al., 2001).

6.1.3.2.2 Influence of the presence of inorganic scalant, $CaSO_4$

For this investigation, $CaSO_4$ was used as the inorganic scalant, representing one of the main scalants in natural water sources such as seawater (Gryta et al., 2008b). The presence of $CaSO_4$ (inorganic scalant) in HA feed solution (HA feed III) resulted in significant permeate flux decline from the initial stages onwards (from VCF 1.0 to 2.0 – 76.7% permeate flux decline) as seen in **Figure 6.8d**. Similarly, in a previous DCMD study, only a minimal flux decline was observed with 30 mg/L HA compound at F_t of 70°C. On the other hand, a higher permeate flux decline of 43-45% was observed with the addition of Ca^{2+} (3.78 mM $CaCl_2$) (Srisurichan et al., 2005). Another study associated the combination of divalent ion in HA solution with the reduction of electrostatic repulsion, complexation and bridging effects resulting in a coagulated mixture (Jermann et al., 2007). In line with this, at the end of our experiment a thick layer of deposit was observed on the membrane. It should be stated that in actual natural water sources such as seawater, unlike HA feed III, the presence of divalent ion and HA organics in smaller concentrations may not result in the formation of a thick layer of deposit (Srisurichan et al., 2005).

In terms of feed solution organics, the LC-OCD chromatogram showed that in the presence of $CaSO_4$ (HA feed III), the HS peak increased by 2.1 times its initial value from VCF 1.0 to 4.0 as shown in **Figure 6.8e**. This HS concentration increment was much higher compared to HA feed I (1.3 times) as shown in **Figure 6.3** and feed II (1.6

times) as shown in **Figure 6.8b**. On the other hand, the disaggregation of HS compound to LMW-HS organics portion was much lower in feed III (only 1.9 times increase from VCF 1.0 to 4.0) compared to HA feed I and HA feed II. This could be attributed to the presence of the divalent Ca^{2+} and its role as a binding agent of the carboxyl functional groups. The Ca^{2+} interacted with the increased concentrated HS, forming a thick cake deposit on the membrane as established in previous MD study (Curcio et al., 2010).

The LC-OCD chromatogram of the fouled membrane with HA feed III showed a pattern of HS (20 to 25% of foulant) together with LMW organics (75 to 80% of foulant) as depicted in **Figure 6.8f**. In comparison, the membrane foulant chromatogram of HA feed I and HA feed II did not detect the presence of the HS. This could be attributed to the lower disaggregation of this compound in HA feed III. It can be suggested that the presence of Ca^{2+} binds the HS, reducing the disaggregation of HS to LMW-HS organics. However, this causes a thick formation of foulant deposit to occur, resulting in significant permeate flux decline. The summary of the fouling patterns of feed I to feed III is shown in **Table 6.6**.

Table 6.6 HA organics fouling pattern under MD operation with different physico-chemical conditions (HA feed I to feed III).

HA solution	Flux decline %	Foulant residue mass (mg/m^2)	Feed solution hydrophilic compound fraction (mg/L)	
			HS	LMW organics
HA feed I	56.2	423.2	4.61	0.74
HA feed II	65.6	694.4	2.06	2.72
HA feed III	76.7	508.3	2.27	2.01

6.1.4   SUMMARY

6.1.4.1   Summarizing the influence of organic compounds on fouling development in MD

In this study, the behaviour of organic fouling was studied using three model organic compound feed solutions (HA, BSA and AA) and combining these into a DCMD system. The results led to the following conclusions:

(1) BSA and HA compounds showed significant membrane fouling while minimal fouling was observed with the AA compound (199.4 mg/m^2 organic mass per membrane area). This was attributed to its hydrophilic nature and electrostatic repulsion.

(2) The BSA compound in the feed solution predominantly formed a deposit on the membrane surface, at an early stage (VCF 2 onwards) due to its hydrophobic bonding with the membrane. The remaining BSA compound in the feed solution thermally degraded to BB and LMW organics. 800.6 mg/m^2 organic mass was deposited on the BSA membrane surface compared to the 423.2 mg/m^2 deposit on the HA membrane surface.

(3) The HA compound in the feed solution showed thermal disaggregation tendencies, forming LMW-HS organics with increased feed temperature (50°C to 70°C). The penetration of organics through the membrane with HA feed solution was observed with SEM-EDS line depth analysis. This was attributed to the LMW-HS organics.

(4) In a MO solution foulant to foulant interaction was observed, resulting in a steady increase of HS and BB compound concentration as the VCF of the feed solution increased. At the later stage (VCF 3) onwards, the formation of BB and LMW organics led to the adhesion of LMW organics on the membrane, resulting in sharp flux decline (from VCF 3.5).

6.1.4.2   Summarizing the influence of feed solution physico-chemical conditions on fouling development in MD

Making an evaluation with the synthetic HA compound confirmed the effect of salinity (NaCl) and inorganic scalant ($CaSO_4$) on organic fouling development in MD. This outcome suggests that permeate flux decline was not only due to the presence of an organic compound. Rather, the physico-chemical condition of the feed solution strongly influences the intensity of the permeate flux decline. Under saline conditions (HA feed II) the permeate flux declined by 65.5% compared to the synthetic HA feed solution (feed 1), which showed a 56.2% permeate flux decline. The presence of inorganic scalant (HA feed III) led to a significant 76.7% permeate flux decline due to the binding of HA with Ca^{2+}, forming a cake layer.

Similarly, the behavior of the organic compounds (i.e. HS) in contributing to membrane fouling development was influenced by the physico-chemical condition of the feed solution. For instance, in saline feed solution (feed II), the disaggregation of the HS to LMW-HS organics intensified during MD operation. This resulted in 694.4 mg/m^2 organic mass deposit on the membrane and the penetration of LMW-HS organics throughout the membrane. In comparison, the synthetic HA feed solution (feed 1) resulted in less organic mass deposit on the membrane foulant (423.2 mg/m^2). Finally, the presence of inorganic scalant ($CaSO_4$) bound the HS, reducing its disaggregation to LMW-HS organics. This resulted in two things: firstly, the HS compound being present on the fouled membrane; and secondly, the formation of a thick foulant deposit.

CHAPTER 7

MD PERFORMANCE WITH PRETREATMENT AND MEMBRANE CLEANING
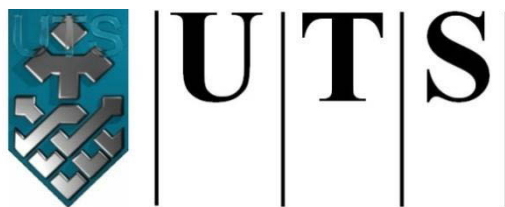
University of Technology Sydney

Faculty of Engineering & Information Technology

This chapter focuses on sustainable MD operation using pretreatment and appropriate cleaning methods to reduce membrane fouling in MD. The chapter is divided into two main sections. The first section highlights the importance of sustainable pretreatment to achieve efficient MD operation. The performance of a deep-bed biofilter and membrane adsorption bioreactor as pretreatment was analysed. The main purpose of these pretreatment strategies is to mitigate organic and biofouling development. The second section discusses improving the performance of MD with a suitable pretreatment and appropriate membrane cleaning method. Membrane cleaning focuses on removing inorganic scalants while the pretreatment concentrates on controlling organic fouling development.

\<Publications related to this chapter\>

Naidu, G., Jeong, S., Vigneswaran, S., & Rice, S. A. (2013). Microbial activity in biofilter used as a pretreatment for seawater desalination. Desalination, 309, 254-260

Jeong, S., **Naidu, G**., & Vigneswaran, S. (2013). Submerged membrane adsorption bioreactor as a pretreatment in seawater desalination for biofouling control. Bioresource technology, 141, 57-64.

Naidu, G., Jeong, S., Vigneswaran, S. Interaction of humic on organic and biofouling in membrane distillation for seawater desalination (article submitted to Chemical Engineering Journal).

7.1   SUSTAINABLE PRETREATMENT PROCESSES

7.1.1   INTRODUCTION

The performance efficiency of membrane processes strongly relies on the quality of raw feed water. In other words, feed water of a consistently high quality is important for the long-term efficient operation of membrane process when treating water and waste water. Poor quality feed water will shorten the membrane's operational time and consequently increase maintenance costs. For this reason, generally in membrane-based processes, a pretreatment of raw feed water strategy is implemented (Sutzkover-Gutman and Hasson, 2010). The main purpose of pretreatment is to remove undesirable compounds from the raw feed solution, which otherwise could adversely affect the membrane's operation.

Using a membrane-based pretreatment strategy, namely NF, UF and micro-filtration (MF) processes, has garnered much research attention in recent times. MF and UF are attractive membrane pretreatments because they produce continuous good quality water (consistently reduced turbidity and particles), with minimal chemical usage and at low operating pressure. However, these membrane pretreatments are not particularly suitable for organic and biofouling mitigation due to severe membrane fouling and pore plugging (Wilf and Schierach, 2001; Brehant et al., 2002). For instance, although UF can remove a significant part of the large molecular weight (MW) organics such as biopolymers, it cannot remove small MW organic compounds (Tansakul et al., 2011). In natural water sources the proportion of low molecular weight organic compounds is high and they are mainly responsible for biofouling (Penru et al., 2011; Tansakul et al., 2011).

Previous studies that examined the performance of UF membrane pretreatment have reached similar results in terms of the efficient removal of organic matter (Halle et al.,

2009; Mijatović et al., 2004). Halle et al. (2009) investigated the organic removal performance of surface water with low pressure UF membranes and biofilter (dual media - sand and anthracite). DOC analysis with LC-OCD revealed that the UF membrane achieved 86% removal of the biopolymer fraction. However the removal of humic substances was only 7% (Halle et al., 2009). In another study the UF membrane proved to be ineffective in removing the LMW organic matter in lake water (Mijatović et al., 2004). In fact only or less than 22% removal efficiency of LMW organic matter was achieved.

Meanwhile, pretreatment technologies such as deep-bed biofiltration, are simple pretreatments utilizing adsorption and biodegradation for effective minimization of organic and biofouling. These pretreatments are especially sustainable and cost effective enough to support the production of drinking water in small communities (Halle et al., 2009). The physico-chemical adsorption by the media in the filters can remove dissolved organic matter, thereby reducing membrane fouling. Common media materials include sand, anthracite and activated carbon. In this context carbon activated media materials such as granular activate carbon (GAC) and powder activated carbon (PAC) have the capacity to hold more biomass, forming thick layers of microorganisms due to their porous nature and large surface area (Halle et al., 2009).

Recently, more innovative pretreatment methods such as the membrane adsorption bioreactor system have proved their effectiveness in increasing the organic pollutant removal capacity. These hybrid bioreactor systems are efficient due to the combined effect of adsorption (with PAC) coupled with biological treatment and consistent solids removal. In this system, the PAC adsorption and biodegradation with cake layer formation within the integrated membrane system is likely to enhance the system's performance (Oh et al., 2006; Ye et al., 2010).

In the first section of this chapter, the performance efficiency of a deep-bed GAC biofilter with seawater as well as an innovative hybrid membrane-adsorption pretreatment system was evaluated. This is known as submerged membrane adsorption bioreactor (SMABR). The operational performances of these two pretreatment options are discussed in terms of organic removal and biofouling reduction with seawater.

In the next section **(Section 7.2)** MD performance is evaluated with pretreatment as well as membrane cleaning cycles.

7.1.2   MATERIALS AND METHODS

7.1.2.1 Materials

7.1.2.1.1 Seawater

In this study, seawater was collected from Chowder Bay, Sydney, Australia. Since the SMABR and deep-bed biofilter experiments were conducted in different seasons, the seawater characteristics varied slightly. Throughout the experimental investigation of the GAC biofilter, the average turbidity, pH, DOC of the seawater was 0.68 ± 0.13 NTU, 7.4, and 1.85 ± 0.42 mg/L, respectively. During the SMABR study the average turbidity, pH and DOC of the seawater was 0.75 ± 0.15 NTU, 8.1, and 2.15 ± 0.85 mg/L, respectively.

7.1.2.1.2 Filter medium

7.1.2.1.2.1 Granular Activated Carbon (GAC)

The deep-bed filter was packed with granular activated carbon (GAC) medium. The nominal size of GAC used in this study was 0.41 mm having a bulk density of 280 to 320 kg/m^3 and surface area of 1000 ± 50 m^2/g.

7.1.2.1.2.2 Powder Activated Carbon (PAC)

PAC (MDW3545CB powder, coal-based) was used as an adsorbent for the submerged membrane adsorption bioreactor (SMABR) system. The mean diameter and the nominal size of PAC were 19.7μm and 75.0μm, respectively.

7.1.2.1.3 Microfilter (MF) membrane

In the SMABR system, a hollow fibre microfiltration (MF) membrane was used. The hollow fibre MF (Cleanfil®-S, Polysulfone, Polyethersulfone, PVDF of 0.1 μm, Kolon membrane) was vertically submerged directly into a reactor. The U-type membrane length was 47.0 to 48.5 cm with an outer diameter of 2.0 mm and an inner fibre diameter of 0.8 mm. The effective membrane surface area was 0.044 m^2.

7.1.2.2 Experimental Methods

7.1.2.2.1 Pretreatment evaluation

7.1.2.2.1.1 Deep-bed biofilter

The experimental set-up is shown in **Figure 7.1**. A transparent acrylic filter column with an internal diameter of 20 mm was operated in a down-flow mode. The column was packed with GAC as the preferred medium and operated with a filtration velocity of 5.0 m/h. This filtration velocity was selected based on the standard filtration velocity values used in deep-bed water filters (Droste, 1997; Sutherland, 2011). In order to maintain stable biological activity in the biofilter, the low range velocity was selected. Based on the filtration velocity, the corresponding empty bed contact time (EBCT) of the GAC biofilter was 7.8 min. GAC media was packed to a depth of 65 cm from the bottom. Sampling ports were placed at 60 cm, 30 cm and 10 cm for GAC collection for organic foulant (biofilm) analysis. The filtration was carried out for a period of 20 days.
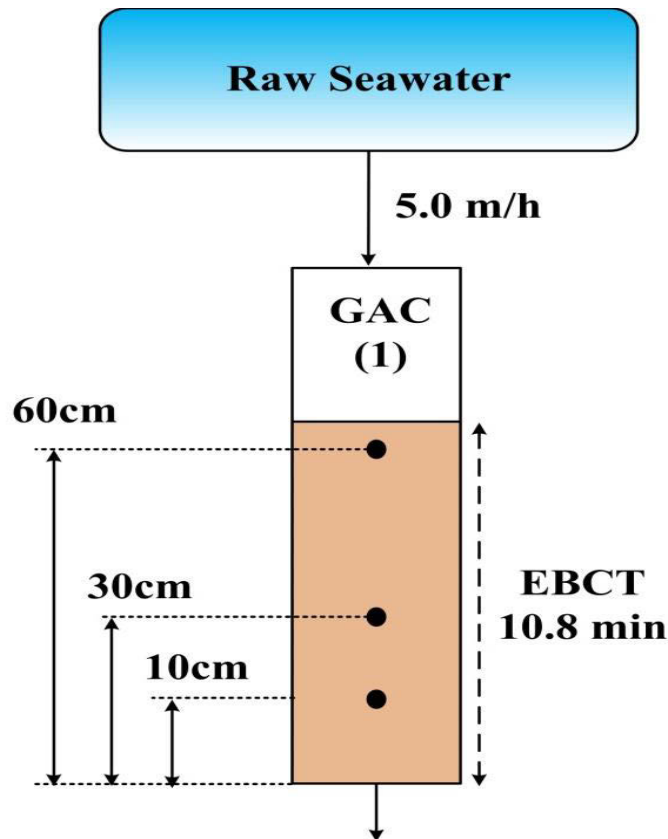
Figure 7.1 Experimental set-up of GAC deep-bed biofilter.

7.1.2.2.1.2 Submerged membrane adsorption bioreactor (SMABR)

The experimental set-up is shown in **Figure 7.2**. Here, 1.5% of PAC was replaced on a daily basis which corresponds to a PAC residence time of 66 d. The operational period was 50d. Initially, 3.0 g of PAC was dosed to 2.0 L volume reactor (i.e. 1.5 g/L). Air was supplied to the bottom of the reactor using an external aerator. This helped to suspend the PAC and biomass in the reactor, so that the PAC was completely mixed in with the seawater and reduced the particle deposition on the MF membrane. The aeration rate was 1.36 m^3/m^2h (a pre-determined rate), but it was increased to 2.72 m^3/m^2h to help the biomass with PAC in suspension after 14 d. In the long-term operation, the aeration was increased only to suspend the PAC when biomass concentration also increased. Permeate was pumped out using a peristaltic pump at a

constant flux of 20 LMH. Correspondingly, HRT of the SMABR unit was 2.27 hours.

The unit was backwashed once every two days for 5 min at 40 LMH.
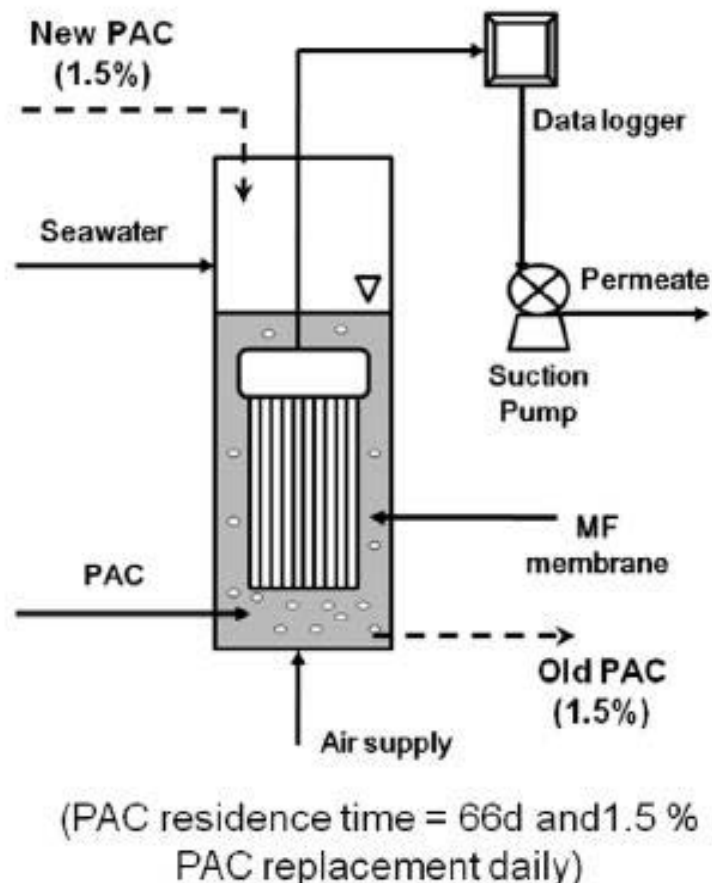
Figure 7.2 Experimental set-up of the SMABR system.

7.1.2.2.2 MD performance evaluation

Experiments were carried out with the bench scale DCMD system and the MemSYS V-MEMD system.

7.1.2.2.2.1 MD pretreatment

Evaluating the performance of MD with pretreatment was done using the DCMD system. Here, seawater (SW) and SMABR pretreated SW as feed solution at feed temperature of 70°C were employed.

7.1.2.2.2.2 MD cleaning cycle

MD operation with the membrane cleaning cycle was carried with the V-MEMD system. A high TDS saline feed solution (initial TDS of 64.2 g/L) consisting of a mixed solution of Ca, SO_4, Mg, Na, Cl and Fe was used for this purpose to represent the main components of a saline groundwater. Membrane cleaning was carried out with DI water as well as 0.1 M HCl to establish the reversibility of scale formation in the V-MEMD system. The DI water was channeled into the membrane module through the feed channel at the end of the experiment. The same experimental conditions were used for the experiment and cleaning. The volume of DI water used for cleaning was recorded. The effectiveness of the DI water flushing strategy was verified through a mass balance analysis of brine components. Similarly, the brine used after HCl acid cleaning was collected for mass balance analysis.

7.1.2.3 Experimental Analysis

7.1.2.3.1 Solids assessment

Particulate fouling potential of seawater and effluent through biofilters was measured in terms of turbidity and modified fouling index with UF membrane (UF-MFI). The UF-MFI test was used to indicate the effectiveness of the pretreatment method in reducing the membrane's fouling potential. In the UF-MFI test, UF membrane of NTR 7410 (Nitto Denko Corp., Japan) was used. The methodology was explained in more detail in **Section 3.3.1.3.1 (Chapter 3)**.

7.1.2.3.2 Organics assessment

In this study, LC-OCD analysis was used to characterize the DOC present in the seawater and effluents.

7.1.2.3.3 Microbial/biological assessment

7.1.2.3.3.1 Adenosine tri-phosphate (ATP) and total cell count

ATP is a biomolecular compound used in living cells. It plays a critical role in cell energy metabolism and also serves in a number of cell signaling processes. Therefore, ATP is an indicative parameter that estimates the active biomass. In this study, BacTiter-Glo Microbial Assay kit was used for ATP measurement of seawater (influent), biofilter effluent and biofilm on filter media. A 96-well luminometer (Wallac 1420 VICTOR2™ multilabel, multitask plate reader (PerkinElmer Inc., US)) was used to measure luminescence produced from ATP reaction at room temperature. The procedure that was employed followed the manufacturer's guidelines.

7.1.2.3.3.2 Assimilable organic carbon (AOC)

AOC is a parameter used to assess the regrowth potential of bacteria in various water sources. In this study a rapid marine AOC method was used to measure the AOC concentration of the seawater and biofilter effluents. This method was explained in more detail in **Section 3.3.1.4.1 (Chapter 3)**.

7.1.2.3.4   MD performance evaluation

7.1.2.3.4.1 MD pretreatment

The performances of MD with SW and SMABR pretreated SW were studied. The SW and pretreated SW organic characteristics were analyzed with LC-OCD while the membrane autopsy was carried out utilizing FE-SEM analysis. Contact angle measurement served to present the membrane hydrophobicity after SW operation.

7.1.2.3.4.2 MD membrane cleaning cycle

The effectiveness of the membrane cleaning cycle was evaluated with an ion mass balance. The ion mass concentration in feed solution and concentrate (brine) was determined using ion chromatography (IC3000, Dionex and inductively coupled plasma

optical emission spectrometry (ICP-OES, Perkin Elmer OPTIMA 7300)) analysis. Both systems were equipped with auto samplers and conductivity cell detectors. A mobile phase of potassium hydroxide was used for the IC analyser.

7.1.3   RESULTS AND DISCUSSION OF PRETREATMENT EVALUATION

7.1.3.1   Solids removal

The performances of the deep-bed biofilter and SMABR were evaluated in terms of the removal of solids by turbidity and UF-MFI rate. Turbidity usually expresses the particulate fouling while UF-MFI is indicative of organic fouling in addition to colloidal fouling.

7.1.3.1.1   Deep-bed biofilter

The average turbidity value of raw seawater was 0.68±0.13 NTU during the filtration period of 20 d. An efficiency rate of more than 60% in removing turbidity was achieved using the GAC biofilter (0.22±0.06 NTU) at 5.0 m/h. On the other hand, the head-loss of the biofilter was 13.0 cm after 5 d of operation, but the head-loss was recovered by backwashing.

The UF-MFI value of raw seawater was 9,101±1,948 s/L^2 during the experiment. The UF-MFI value decreased to 35% with GAC biofilter treatment when it reached the intermediate stage (10 to 15 d). Thereafter it remained relatively stable at 6,000±1,200 s/L^2 throughout the filtration period.

7.1.3.1.2   SMABR

After SMABR the turbidity in the effluent decreased from the turbidity of raw seawater (SW) of 0.75±0.12 NTU to 0.29±0.08 NTU. The turbidity rate remained relatively stable. A similar trend was observed in the UF-MFI value, whereby the value of raw

seawater (SW) of $11{,}826\pm1{,}523$ s/L^2 was reduced to a UF-MFI value of $4{,}395\pm881$ s/L^2 after SMABR. These results indicated that both the deep-bed biofilter and SMABR system were able to produce feed water with low particulate and organic fouling potential.

7.1.3.2   Organics removal

The organics removal capacity of both pretreatment systems were assessed in terms of DOC concentration and detailed organic compound characterization. These features are discussed in more detail below.

7.1.3.2.1   Deep-bed biofilter

The DOC concentration of raw seawater was 1.85 ± 0.42 mg/L, comprising hydrophilic fraction (70 - 80%) and hydrophobic fraction (20 - 30%). The hydrophilic fraction of the raw seawater was composed of biopolymer (0.038 ± 0.017 mg/L), HS (0.350 ± 0.150 mg/L) and LMW organics (0.730 ± 0.150 mg/L).

The GAC biofilter was able to reduce 70% of DOC concentration to 0.75 ± 0.13mg/L in the intermediate stage (10-15 d) of the biofilter run. The organic concentration in the biofilter remained stable from this stage onwards. The LC-OCD chromatogram representing the seawater DOC characteristics as well as the GAC biofilter effluent's organic removal trend at different stages is shown in **Figure 7.3**.

A significant reduction (60 - 70%) in biopolymer was achieved at the intermediate stage (10 - 15 d). while a 48% removal efficiency was observed with HS (0.18 ± 0.021 mg/L). The HS reduction was gradual throughout the stages. The results showed that the characteristics of GAC media (large surface area and high porosity) enabled a good adsorption; hence a gradual removal of HS was achieved with GAC biofilter. This was documented by previous studies (LeChevallier et al., 1992; Wang et al., 1995). On the

other hand, up to the intermediate stage, the GAC biofilter effluent showed an increase in LMW organics. This signified that biodegradation began at the initial stage of operation. However, upon reaching the mature stage (15 - 20 d), the LMW organics concentration of the GAC effluent declined by 41%. These results indicated that the 41% reduction in LMW organics dominated the biodegradation phase and they were utilized by microbes on media. Previous research supports this trend (Arnosti et al., 1998). It is suggested that the GAC medium has attractive forces that retain more microbes on its surface (LeChevallier et al., 1992). This may have resulted in higher assimilation of LMW compounds in the GAC filter. The relationship between microbial growth and organic removal in the GAC biofilter is discussed in **Section 7.1.3.3**.
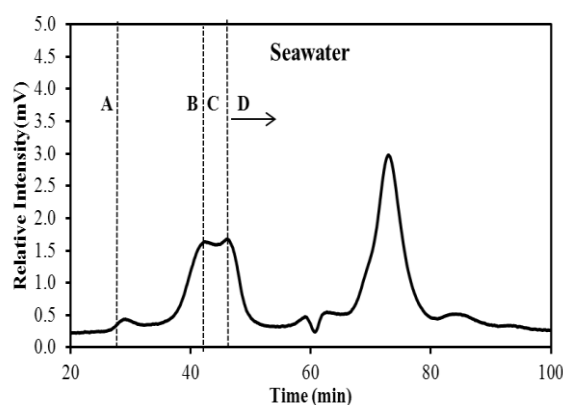
(a)
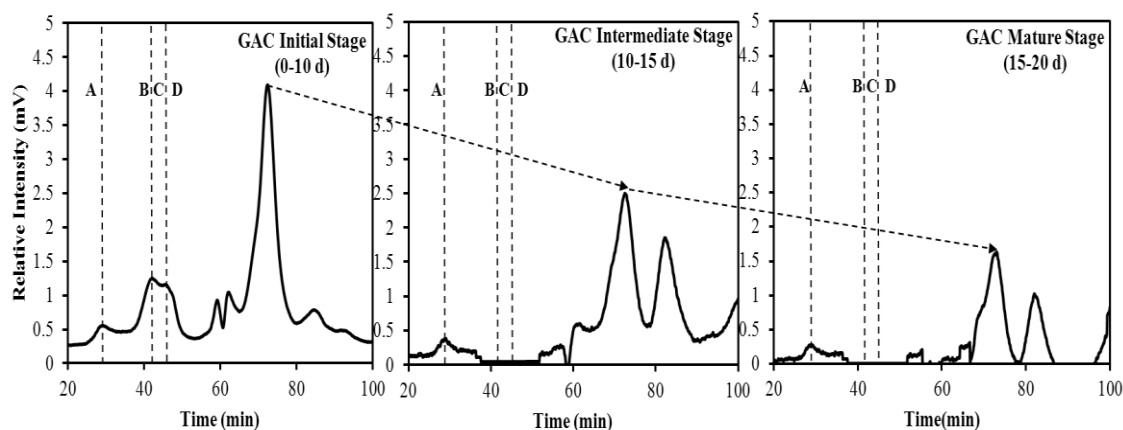
(b)

Figure 7.3 LC-OCD chromatogram representing the characteristics of the organic compounds present in the seawater **(b)** LC-OCD chromatograms of GAC biofilter effluent highlighting the reduction of LMW organics at different stages *(A: Biopolymers; B: HS; C: BB; D: LMW organics).*

7.1.3.2.2 SMABR

Initially on the first day (1 d) the system depicted a superior DOC removal efficiency of 73% with high hydrophilic DOC fraction removal of 94-97% (biopolymers), 71-76% (HS), 63-69% (BB), and 55-61% (LMW neutrals). After 6 d of operation, DOC removal efficiency began falling to 51-56% (total DOC), and after 13 d, it deteriorated to 39%. This increase is due to the presence of LMW organics (neutrals and acids) in SMABR effluents. After 6 d of operation, the concentration of LMW acids in the effluent increased from 0.01 mg/L to 0.14 mg/L. This signifies that microbes began acting in the reactors, resulting in the generation of lower molecular organics from the decomposition of high molecular organics such as biopolymers and HS absorbed onto PAC. A long-term outcome that is shown in **Table 7.1** indicated most biopolymers and HS (87±9% and 61±22%) were removed by SMABR. After 13 d of operation, the total DOC removal was stabilized at 60-64% and of this, up to 86% of LMW organics was removed on day 47.

The organic removal results highlight that a more superior DOC removal was achieved with SMABR compared to GAC biofilter. Specifically, higher removal of LMW organics (86%) with the SMABR compared to GAC biofilter (41%).

Table 7.1 Organic fraction of seawater (SW) and SMABR effluent for duration of 47 days (Unit: mg/L).

Days	Sample	DOC	Bio-polymers	HS	BB	LMW Neutrals	LMW Acids
1	SW	2.28	0.33	0.75	0.16	0.89	0.02
	SMABR	0.62	0.01	0.18	0.05	0.35	0.01
6	SW	2.35	0.25	0.81	0.14	0.84	0.01
	SMABR	1.01	0.02	0.30	0.08	0.47	0.14
13	SW	2.65	0.42	0.84	0.20	0.87	0.02
	SMABR	1.63	0.08	0.33	0.03	1.10	0.08
21	SW	2.39	0.23	0.81	0.19	0.80	0.02
	SMABR	0.86	0.02	0.15	0.16	0.28	0.16
47	SW	2.45	0.25	0.94	0.21	0.85	0.01
	SMABR	0.98	0.06	0.70	0.01	0.12	0.00

7.1.3.3   The role of bioactivity in deep-bed biofilter and SMABR

7.1.3.3.1 Deep-bed biofilter

Based on the organic results obtained, the experimental period was defined into three main stages: (i) initial stage (0 - 5 d) where there was a fluctuating trend (increase and decrease) due to the stabilization period; (ii) intermediate stage (10 - 15 d) where there was a distinct change trend (significant increment/ decrease) of the measured parameter from the initial stage; and (iii) mature stage (15 - 20 d), where measured parameters showed a stable value. As shown in **Figure 7.4**, the DOC removal trend when using the

GAC biofilter correlated to the total cell number in the top layer of the GAC media. The number of cells on the top layer of the GAC media increased significantly to 1.0×10^8 CFU/g media upon the mature stage (15-20 d) (from 2.0×10^6 CFU/g of media in the initial stage). This corresponded to the improved DOC removal efficiency. On reaching a steady state at the mature stage (15-20 d), higher quality effluent (0.51±0.12 mg/L of DOC) was produced by the GAC biofilter. This outcome agreed with the findings of previous studies (Velten et al., 2011; Tian et al., 2009). At the initial stage of the biofiltration process, organic carbon removal occurred through adsorption on medium. Over time a rapid increment in biomass concentration was observed. The increase in colonized bacteria on the medium led to an increase in the removal of dissolved organics, mainly through biological degradation.

Similarly, at the initial stage (0 - 5 d), only a low value of biomass concentration (0.9 ±0.5 μg ATP/g media) was detected at the top layer of the biofilter. At the intermediate stage (5 − 10 d), the active biomass measured at the top layer of the GAC biofilter increased significantly to 21.0±9.3 μg ATP/g medium, and at the mature stage (15 - 20 d) it reached 51.0±11.8 μg ATP/g. At the same time, it was observed that the number of attached biomass decreased as filter media depth reduced, whereby the high accumulation of active biomass was on the top layer (top 10 cm) of the media while low biomass concentration was present on the bottom layer (bottom 10 cm). This indicated that the removal of DOC occurred at the top layer of the biofilter dominantly as shown in **Figure 7.5**. This outcome suggested that: firstly, the GAC media could contain a large amount of biomass; and secondly, there was much biomass activity within the medium. This could be because microorganisms formed a thicker layer on porous medium material of the GAC compared to less porous mediums such as sand and

anthracite (Wang et al., 1995). Therefore, a high level of active biomass accumulation on the GAC media may have contributed to the high organics removal.
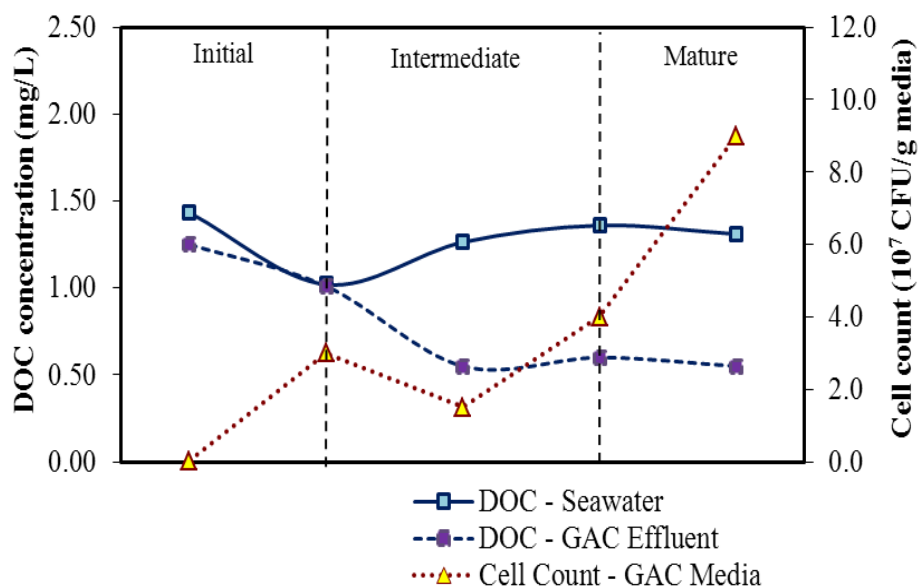
Figure 7.4 Relationship between bacterial growth and DOC removal on the GAC biofilter at different stages.
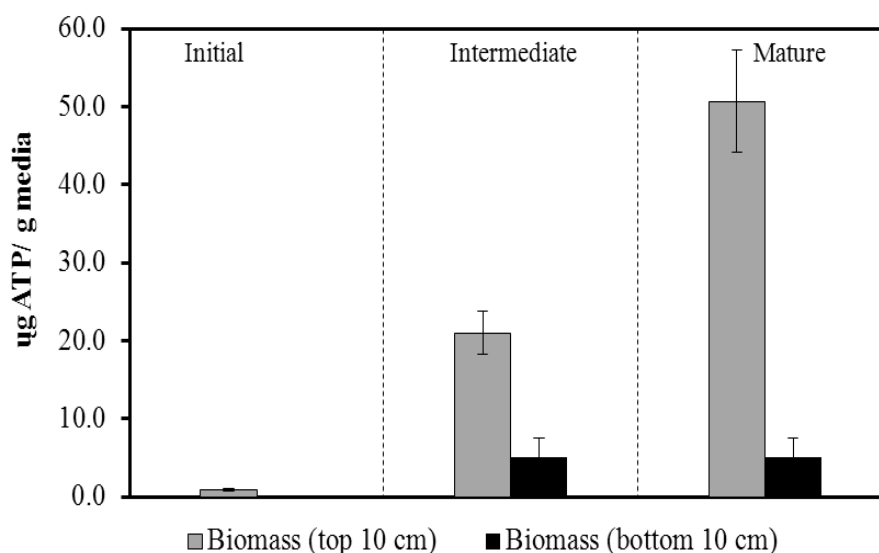
Figure 7.5 ATP concentration at different depths of media of the GAC biofilter at different stages.

7.1.3.3.2 SMABR

Similarly, bioactivity in SMABR was measured in terms of cell number counts (CFU; colony forming unit) and ATP (as live biomass concentration). Cell number counts were performed for mixed liquor of SMABR. Here the mixed liquor is the content in the reactor (liquid and biomass). The bioreactor showed a stable and gradual increase in biomass (from $4.0\pm1.0 \times 10^3$ to $12.0\pm1.0 \times 10^3$ CFU/mL). During the SMABR's operation, ATP increased gradually from 1.17 to 6.30 pg of ATP/L. This biological activity had the same trend as organic removal.

The dominance of adsorption over biological activity is roughly controlled by the retention time of activated carbon (or the age of the activated carbon) within the reactor. In the SMABR one can expect that both adsorption and biodegradation play a role in the overall process. When the operation commences, adsorption was dominant and this effective organic adsorption by the PAC helps in the growth of microorganisms. They rapidly dominate and led to more effective removal of organic matter through biodegradation.

7.1.3.4 Biofouling potential reduction

The AOC measurement was used to indicate the biological growth potential of the water (or biofouling potential) and serves as a suitable parameter for predicting fouling potential. Thus, a high value of AOC concentration in the feed solution is directly linked to rapid biofilm formation and loss of performance in membrane processes (Hambsch and Werner, 1996; Chien et al., 2007).

7.1.3.4.1 Deep-bed biofilter

Figure 7.6 presents the AOC concentration in seawater and effluent of the GAC biofilter. The AOC concentration of seawater was 24.5±2.1 µg-C glucose equivalents/L.

The AOC concentration of effluent through the GAC biofilter was around 18.0±1.4 µg-C glucose/L at the initial stage (0 – 5 d). This high AOC concentration at the initial stage could be attributed to the high MW compounds changing to LMW compounds during the biodegradation process. Upon reaching the mature stage of the operation (15 - 20 d), this value decreased to 9.6±0.2 µg-C glucose equivalents/L, corresponding to AOC reduction of 60.8%. This could be attributed to a specific microbial community that developed on the medium and assimilated the LMW compounds in the GAC biofilter. The AOC removal pattern was similar to the reduction trend involving LMW organic compounds.
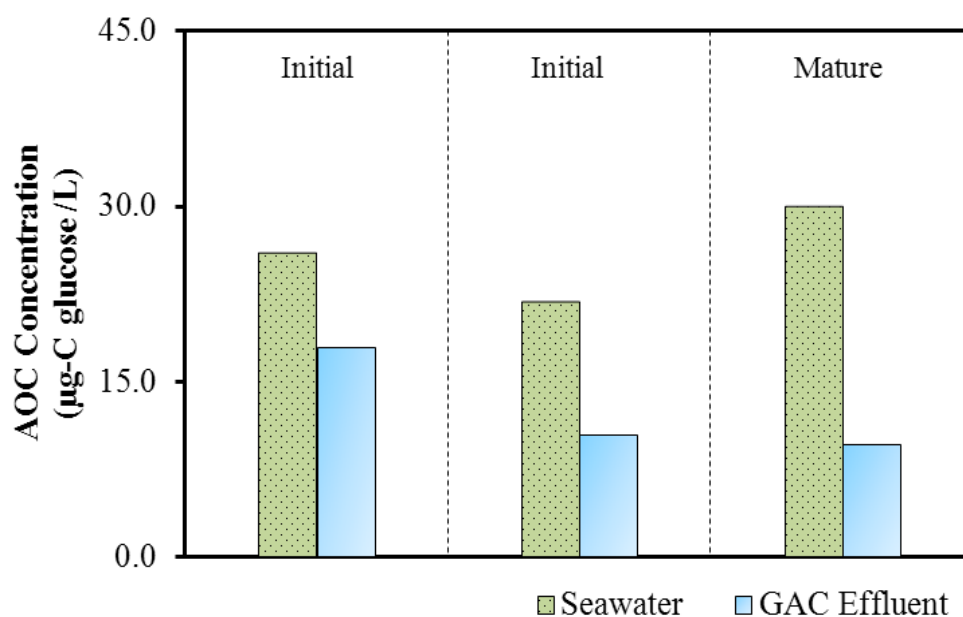
Figure 7.6 AOC concentration of seawater and GAC biofilter effluent at different stages.

7.1.3.4.2   SMABR

The difference in AOC concentration of raw SW (feed water) and SMABR effluent during the operation is presented in **Figure 7.7**. The AOC concentration of raw SW was 20.8±4.0 µg-C glucose equivalents/L. On average the AOC removal by SMABR (66 d)

was significant. The effluent AOC concentration was 6.0±2.9 µg-C glucose equivalents /L which corresponds to 71.0% (as a mean value with less than 5% of standard deviation) of AOC removal. During most of the operation period, AOC in SMABR effluent was less than 10 µg-C glucose equivalents /L as shown in **Figure 7.7**. It has been reported that AOC levels of <10µg/L can limit the growth/regrowth of some heterotrophic plate counts and coliform bacteria (Van der Kooij, 2000). Therefore SMABR can reduce the incidence of biofouling by removing AOC compounds.

Both these pretreatment options resulted in large amounts of AOC being removed from SW. Comparatively, one previous study carried out with NF observed a poor ability to remove AOC concentration (Escobar and Randall, 2001).
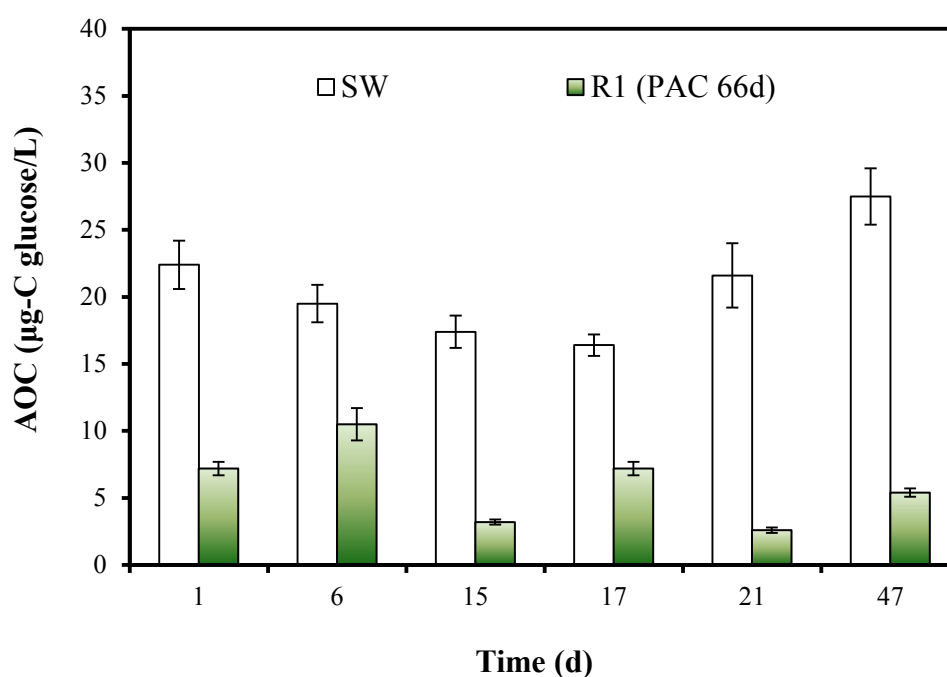
Figure 7.7 Changes in AOC concentrations of SW and effluents.

Generally the results revealed that both the deep-bed biofilter and SMABR - as chemical-free and energy efficient pretreatments - were effective in reducing the organic contents in the feed and they controlled biofouling. The combination of adsorption coupled with biodegradation was essential in achieving these reduction rates,

making these pretreatment types more attractive compared to membrane-based pretreatments. The performance efficiency of both these pretreatments was similar; however, the hybrid SMABR removed LMW organics and controlled biofouling better.

7.2 MD PERFORMANCE EVALUATION

7.2.1 MD PERFORMANCE WITH PRETREATMENT

The usage of pretreatment in MD system for drinking water production has not been explored in great detail. This is primarily due to the relatively smaller fouling and scaling intensity in the absence of hydraulic pressure under MD operation compared to pressure driven membrane processes. Scale formation in MD as shown in **Chapter 5** was loosely deposited on the membrane. Studies have shown that scale formation could be minimized by periodically flushing the MD system (Nghiem and Cath, 2011). Other studies have also used chemical cleaning as an option to remove the scale layer on the membrane (Gryta, 2009a). However, in the case of organic fouling, cleaning may not re-establish productivity, specifically the wetting phenomenon, which could be due to LMW-HS organics and LMW organics as described in **Chapter 6**. In MD the occurrence of membrane wetting is one of the major reasons for the reduction in process efficiency.

A few MD studies have acknowledged the improved efficiency of MD performance through the use of membrane-based pretreatments, namely the NF, UF and MF processes (Hsu et al., 2002; Karakulski et al., 2002; Karakulski and Gryta, 2005). These studies concluded that the membrane pretreatment produced continuous good quality water (consistently reduced turbidity and particles). Nevertheless, due consideration must be given to the additional treatment costs incurred with such pretreatments, because they are expensive compared to conventional pretreatment strategies. In

addition membrane pretreatment does not specifically address the issue of organic fouling development as discussed earlier.

It was shown in **section 7.1** (**Chapter 7**) that simple pretreatment utilizing adsorption and biodegradation strategies was highly effective in minimizing organic fouling and biofouling. These pretreatments are especially sustainable and cost effective to support the production of drinking water in small communities. Hence, the following section evaluates organic fouling development in DCMD operation using raw SW and SMABR pretreated SW.

7.2.1.1 RESULTS AND DISCUSSION FOR MD PERFORMANCE WITH PRETREATMENT

7.2.1.1.1 MD performance with SW

The DCMD operated with SW showed a 7-10% permeate flux decline at the initial stage (from VCF 1.0 to 1.4). This is attributed to salinity as observed in other MD studies (Al-Obaidani et al., 2008). From VCF 1.4 to 2.6 the permeate flux remained relatively stable. Thereafter the permeate flux gradually declined and a significant permeate flux decline of 31.9% was observed by VCF 3.6 as shown in **Figure 7.8a**. Initially the permeate DOC concentration was stable but from VCF 3.0 onwards, permeate DOC concentration indicated a gradual increasing pattern as the feed DOC concentration increased. This suggests that the permeation of DOC occurred through the membrane.

The LC-OCD analysis of the SW feed solution organic characteristics is shown in **Figure 7.8b**. The humic substance (HS) concentration revealed an increasing trend. From VCF 1.0 to 2.0, the concentration of the initial HS (0.49 mg/L) in the feed solution increased by twice its initial value. At VCF 4.0, the HS increased by 3.5 times

its initial concentration value, suggesting a reduction of the HS concentration by 0.25 mg/L. Meanwhile from VCF 1.0 to 2.0, the LMW organics increased by 2.7 times from 1.32 mg/L to 3.53 mg/L. However, from VCF 2.0 onwards the LMW organics showed a decreasing trend. At the same time, the permeate flux from VCF 2.6 onwards also indicated a declining trend. These results suggest that the LMW organics could have been deposited on the membrane from VCF 2.0 onwards, thus contributing to the permeate flux decline.

(a)

(b)

(c)

(d)
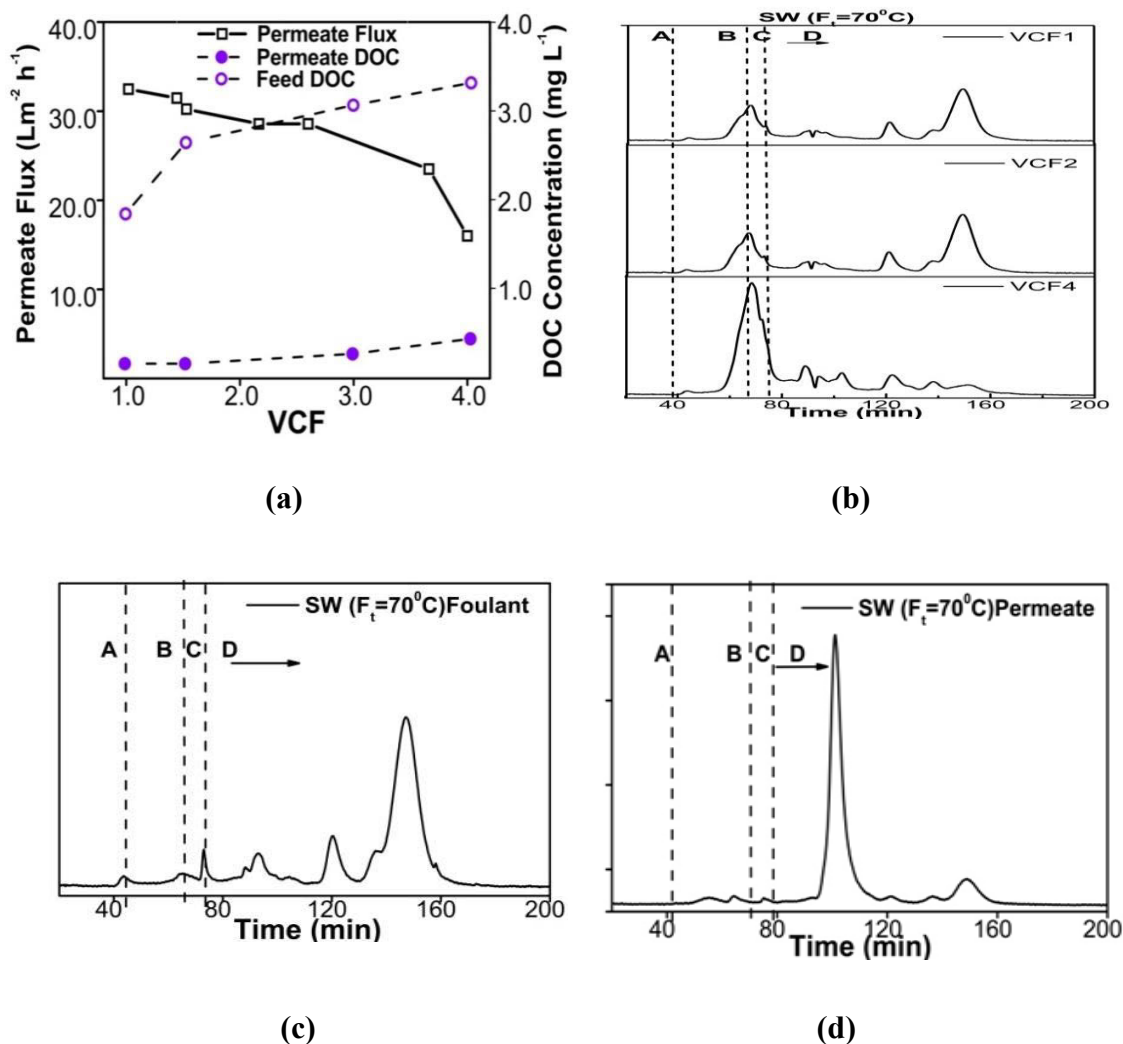
Figure 7.8 DCMD fouling pattern with SW **(a)** permeate flux pattern **(b)** LC-OCD chromatogram changes of SW feed solution from VCF 1.0 to VCF 4.0 **(c)** LC-OCD

chromatogram of membrane foulant at VCF 4.0 **(d)** LC-OCD chromatogram of permeate at VCF 4.0 *(A: Biopolymers; B: HS; C: BB; D: LMW organics).*

At the end of the experiment (VCF 4.0), a visible brown layer was displayed on the membrane. LC-OCD chromatogram showed that the foulant deposited on the MD membrane with SW consisted of LMW organics as shown in **Figure 7.8c**. Furthermore, the LC-OCD chromatogram of the MD permeate solution with SW at VCF 4.0 displayed predominantly the presence of LMW organics, indicating the penetration of LWM organics into the pores of the hydrophobic membrane as shown in **Figure 7.8d**. These results demonstrated that the LMW organics were not only deposited on the membrane but also had penetrated through the pores of the membrane**.** Meanwhile, the average hydrophobicity of the membrane after DI water cleaning was 113.1±7.2° (19% reduction from the virgin membrane hydrophobicity of 139.9±1.2°), indicating the reduction of hydrophobicity in the membrane. At the same time the AOC concentration in the SW was 105.7±3.9 μg-C glucose equivalents/L. This increased to 143.3±11.3 μg-C glucose equivalents/L at the end of the experiment (VCF = 4.0). Meanwhile, an AOC concentration of 384.7±8.4 μg-C glucose equivalents/m^2 was detected on the membrane. The presence of AOC concentration in both the SW feed solution and membrane foulant provided evidence of biofouling potential when SW was treated with DCMD. The results were compared to the performance of the MD system with pretreated SW, which is explained in the next section.

7.2.1.1.2   MD performance with pretreated SW

In terms of permeate flux comparison of SW and pretreated SW, a longer stabilization period was achieved with the latter, prior to flux decline occurring at VCF 3.6 to 3.7 as shown in **Figure 7.9**. At VCF 4.0, the permeate DOC concentration was 72% lower with the pretreated SW in comparison to the raw SW as shown in **Table 7.2**
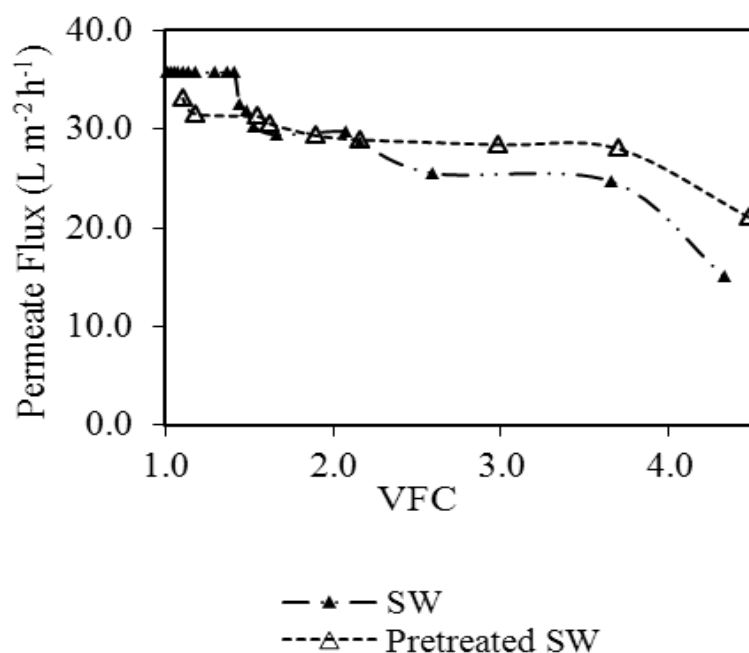
Figure 7.9 Comparison of permeate flux pattern in raw and pretreated SW-70ºC operation.

The initial DOC concentration of the pretreated SW was 0.89 mg/L compared to the DOC concentration of the raw SW at 1.85 mg/L. Essentially the pretreated SW had 20% less HS and 65% less LMW organics as summarized in **Table 7.2**. The LC-OCD chromatogram of the pretreated SW feed solution (VCF 1.0 to VCF 4.0) compared to that for the SW feed solution (VCF 1.0 to VCF 4.0) is shown in **Figure 7.10 a&b**. It should be noted that the feed solution was heated at 70˚C during the MD experiment (although the samples were at room temperature during the LC-OCD measurement). The results revealed a pattern of increase in LMW organics from VCF 1.0 to VCF 4.0. A distinct feature of the raw SW feed solution was the reduction of LMW organics from VCF 2.0 onwards as depicted in **Figure 7.10b**. In comparison, the pretreated SW feed solution showed a continuous increment in LMW organic peak from an initial VCF 1.0 to VCF 4.0. This suggests that the LMW organics may not have adhered excessively onto the membrane with the pretreatment. In line with this, the LC-OCD chromatogram

indicated that the LWM organics deposited on the MD membrane with pretreated SW were much smaller when compared to the raw SW as shown in **Figure 7.11** and **Figure 7.12**. A further membrane SEM-EDS analysis was carried out to verify this finding.

(a) (b)
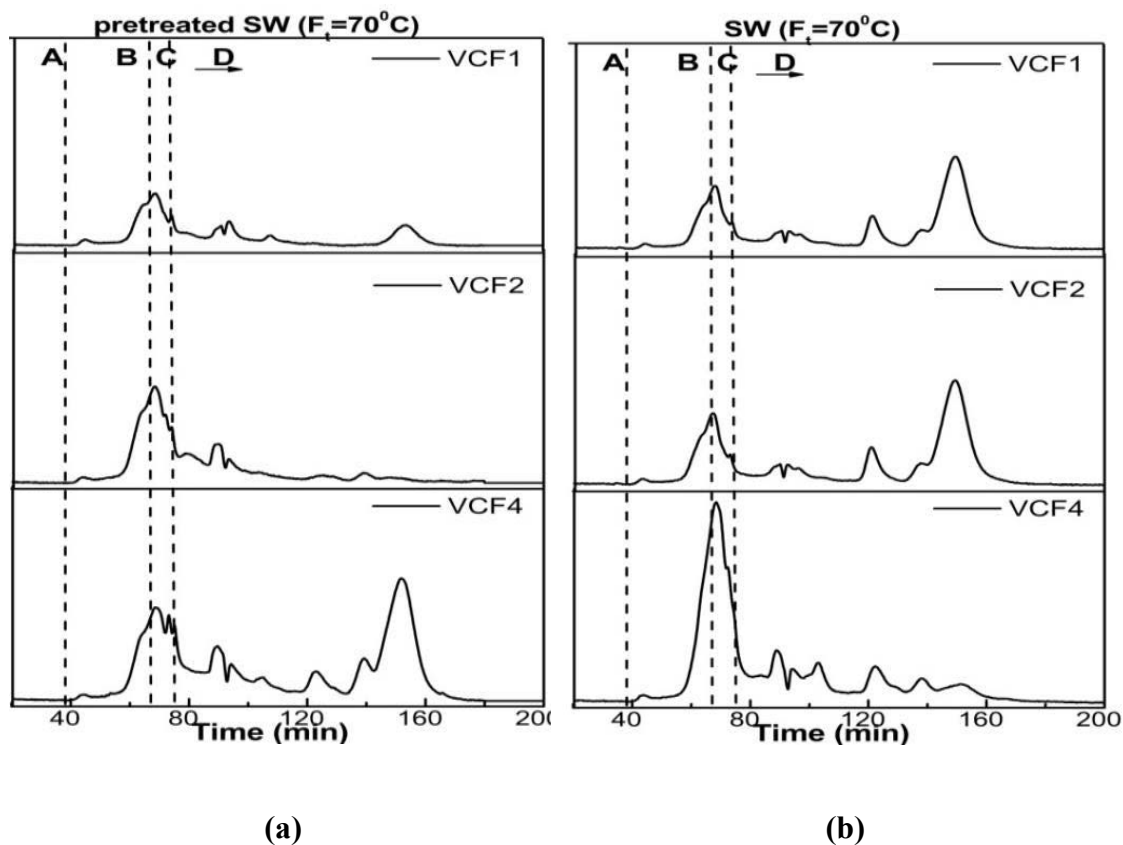
Figure 7.10 Feed solution chromatogram analysis of **(a)** pretreated SW-70ºC operation **(b)** raw SW-70ºC operation *(A: Biopolymers; B: HS; C: BB; D: LMW organics).*
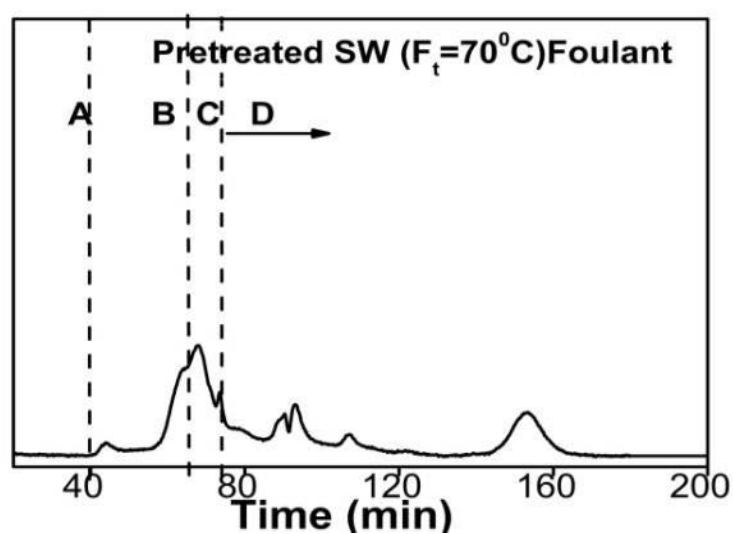
Figure 7.11 Membrane foulant chromatogram analysis of pretreated SW-70ºC operation *(A: Biopolymers; B: HS; C: BB; D: LMW organics)*.
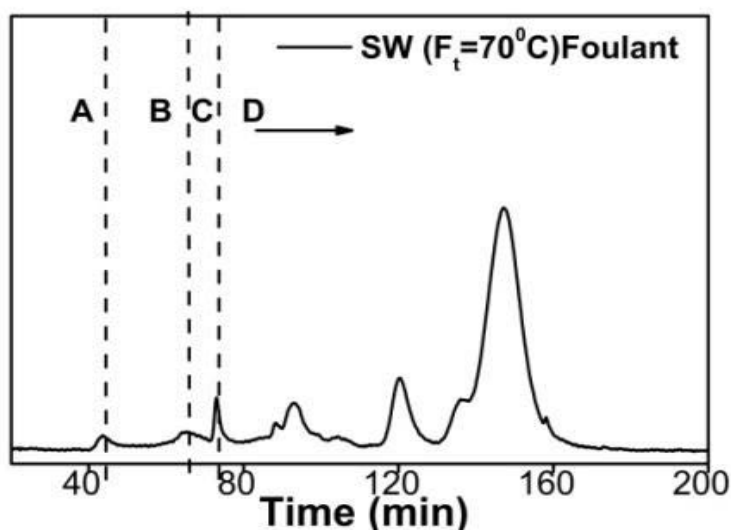
Figure 7.12 Membrane foulant chromatogram analysis of SW-70ºC operation *(A: Biopolymers; B: HS; C: BB; D: LMW organics)*.

Table 7.2 The DOC characteristics of feed and permeate of the raw SW and pretreated SW.

Solution Type	Total DOC (mg/L)	Hydrophilic compound fraction (mg/L)		
		Biopolymer	HS	LMW organics
Feed (VCF 1.0)				
Raw seawater	1.85	0.04	0.49	1.31
Pretreated SW	0.89	0.03	0.39	0.46
Permeate (VCF 4.0)				
Raw seawater	0.51	0.01	0.01	0.50
Pretreated SW	0.18	>0.01	n.q	0.18
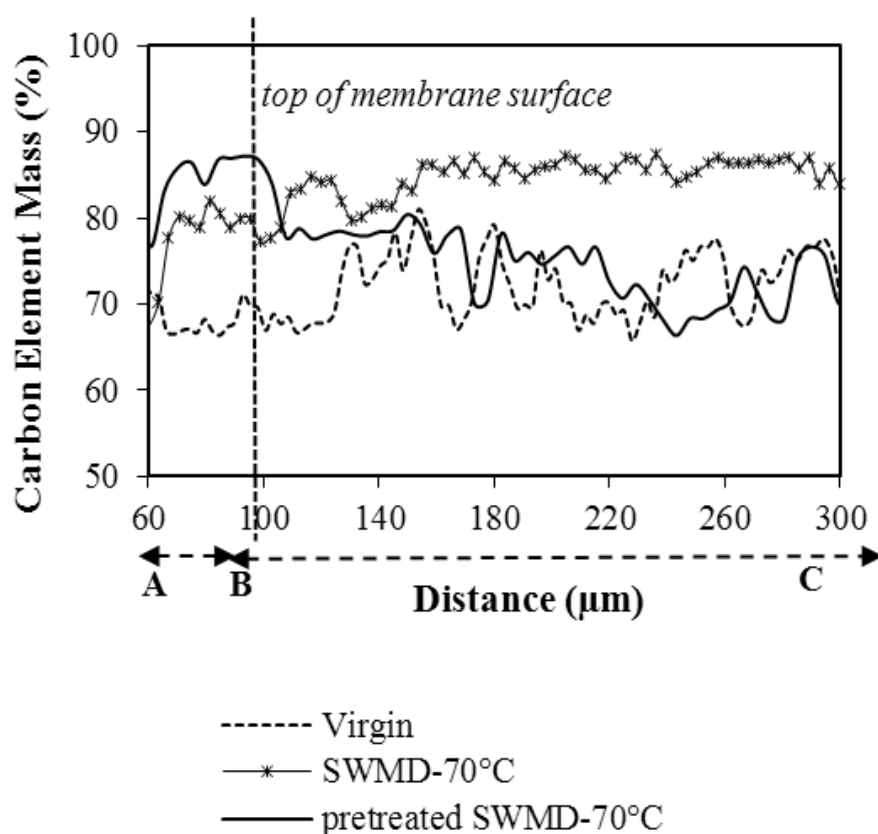
Figure 7.11 SEM-EDS membrane cross-section line analysis of virgin, SW and pretreated SW membrane.

A comparison of the membrane (virgin, raw SW and pretreated SW) was carried out employing SEM-EDS line depth analysis as shown in **Figure 7.11**. The analysis of the pretreated SW showed a pattern of C deposit on the membrane surface with minimal pore penetration. This result supports the contention that organic pretreatment is a suitable fouling mitigation strategy for DCMD. Meanwhile, when the membrane was physically cleaned with DI water, the contact angle of the pretreated SW membrane was restored to a value $137.1 \pm 1.1°$, in other words close to its original value of $140.2 \pm 1.8°$. Overall, pretreated SW with reduced organic contents was a positive measure that reduced the occurrence of membrane fouling in DCMD.

7.2.2   MD PERFORMANCE WITH CLEANING CYCLE

This section evaluates the effectiveness of membrane flushing/cleaning method in mitigating scaling and enhancing the MD performance. The scaling evaluation in **Section 5.3.2** (**Chapter 5**) confirmed that the experimental scenario of $T_f = 60 °C$, $P_p = 12.5$ kPa, $v_f = 0.9$ m/s achieved a reasonable permeate flux with high turbulence and short residence time in the membrane module. On this basis the cleaning evaluation was carried out with the same experimental scenario for 740 mins (prior to the induction time, as identified in the scaling evaluation). At the end of the experiment a cleaning cycle was undertaken to monitor the cleaning efficiency and establish an effective maintenance regime for on-site V-MEMD systems.

7.2.2.1 RESULTS AND DISCUSSION OF MD PERFORMANCE WITH CLEANING CYCLE

7.2.2.1.1 Permeate flux and permeate quality

The V-MEMD system achieved an initial permeate flux of 9.4 LMH and the performance remained stable for a period of 740 min. The feed solution was concentrated up to three times its initial TDS value with a slight decline of 12 to 15% permeate flux as shown in **Figure 7.12**.
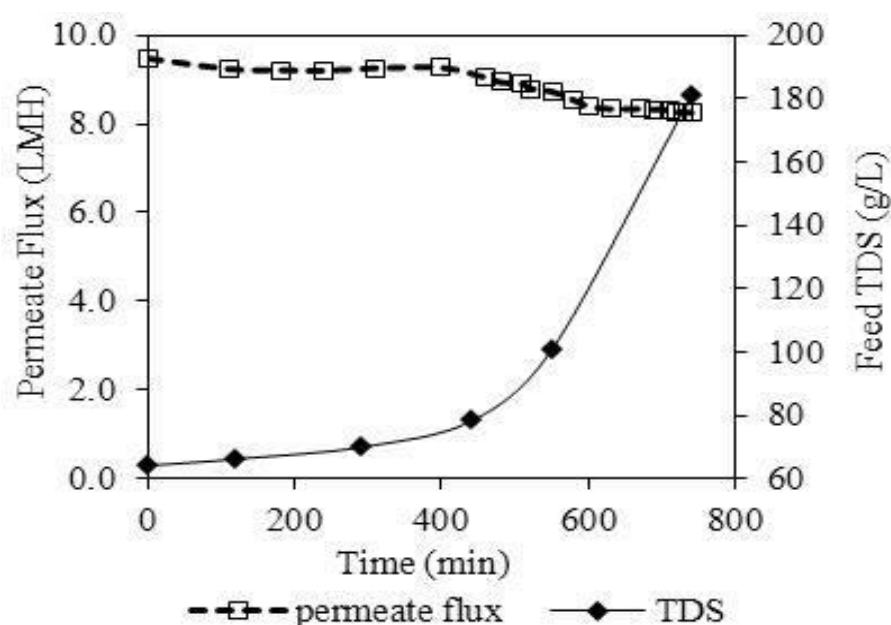
Figure 7.12 The V-MEMD performance over time with high TDS saline feed solution.

A superior permeate quality was maintained throughout the experiment with approximately 99% of all ions being rejected. A mass balance of the main components in the feed solution was carried out based on the feed concentration factor (CF) as shown in **Table 7.3.** This indicated the percentage mass of components remaining in the feed solution at the end of the experiment (CF 3.3). The results showed that 60 to 70% of Na, Cl and Mg remained in the feed solution while only 33% of Ca and 9% of Fe

remained in the feed solution. The reduced mass was assumed to have been deposited in the system.

Table 7.3 Mass balance of the components in feed II from the initial feed solution concentration factor (CF 1.0) to the final feed solution concentration factor (CF 3.3).

Component	Component mass in feed solution (g)				Mass remaining in the feed solution (%)
	CF 1.0	CF 1.5	CF 2.0	CF 3.3	
Ca	15.74	12.69	11.64	5.23	33.2
SO$_4$	130.85	108.59	97.81	72.99	55.8
Mg	3.29	3.06	3.04	1.95	59.3
Na	463.21	366.34	317.88	319.77	69.1
Cl	627.38	491.66	446.15	389.08	62.0
Iron (Fe)	0.10	0.06	0.03	<0.01	8.8

7.2.2.1.2   Cleaning cycle and maintenance

7.2.2.1.2.1 DI water flushing

When the experiment was completed the system was cleaned with DI water (through flushing the feed channel). The effectiveness of the DI water cleaning cycle was evaluated based on the capacity to recover the remaining mass of the feed component in the system. A total of 13 L of DI water was used for cleaning without recirculation. Samples of the brine (DI water flushing waste) were collected at volume intervals of 2L, 5L, 8L and 13 L. This determined the suitable volume of DI water required to restore the system's performance. The results showed that when flushing with 2L of DI water most of the remaining feed components were flushed out from the membrane module as

shown in **Table 7.4**. Following this procedure no further significant feed solution component remains were recovered with the subsequent DI water flushing. This indicates that more than 90% of Mg, Na, Cl residues was recovered when using only 2L DI water cleaning. Ca and SO_4 recovery was slightly less at 73% and 90%, respectively. Meanwhile the recovery of Fe was the lowest at 61%.

Table 7.4 Recovery of components in feed II with DI water flushing.

Component	Component mass in DI feed solution (g)		Total mass recovered
	2L DI water	5L DI water	(DI flushing + final feed) (%)
Ca	6.35	<0.01	73.57
SO_4	45.18	<0.01	90.31
Mg	1.32	<0.01	99.39
Na	138.77	<0.01	98.99
Cl	201.37	<0.01	94.11
Iron (Fe)	0.05	<0.01	60.78

7.2.2.1.2.2 Chemical cleaning

Chemical cleaning was done using HCl acid after the DI water flushing to determine whether the V-MEMD system required chemical cleaning. The results show that the remaining Ca, SO_4, Cl was recovered through chemical cleaning. An additional 0.8 g mass of Cl was observed, which was most likely from the HCl acid itself (used for cleaning). The results suggest that 2 L of DI water flushing was sufficient to rinse the system effectively. More frequent cleaning cycles between the operations may also remove more Ca and SO_4 components from the module.

Only the removal of Fe proved to be a challenge in the V-MEMD system. Hence chemical cleaning was mostly relevant for the complete removal of Fe. However, in view of the amount of Fe remaining in the system, a simple pretreatment for its removal such as oxidation (through aeration or passing through a granular media filter) and separation of ferric oxide precipitation (through a sand filter) would be suitable control measures rather than chemical cleaning. Therefore, for the V-MEMD system, frequent DI water flushing coupled with a simple pretreatment would be sufficient to maintain the residue deposition to a minimum level. Minimal chemical cleaning is recommended for the V-MEMD chemical brine and it minimizes the risk of chemicals coming into contact with the V-MEMD module materials.

7.3   SUMMARY

7.3.1   Summarizing pretreatment performance

The performances of the deep-bed biofilter and SMABR were evaluated in terms of three issues: solids removal, organics removal and biofouling reduction. The results show that both chemical-free and energy efficient pretreatments were effective in reducing the organic contents in the feed and they controlled biofouling. Combining adsorption with biodegradation was essential in achieving these reduction rates, making these pretreatment types more attractive compared to membrane-based pretreatments. The performance efficiency of both these pretreatment strategies was similar, but nevertheless the hybrid SMABR was better at removing LMW organics and controlling biofouling. At the same time, the integrated membrane enabled SMABR to offer a more robust performance and last longer. On the other hand the deep-bed biofilter requires a precise backwashing procedure to maintain low head-loss while ensuring the biomass remains intact in the media filters. Maintaining this balance is therefore a challenge. Based on these results the SMABR was chosen as the preferred pretreatment option for the MD system.

7.3.2   Summarizing MD performance evaluation

7.3.2.1   MD performance with pretreatment

The results attest to the fact that a suitable pretreatment strategy will improve the efficiency of MD operation. It is important to choose a sustainable and cost effective pretreatment that does not incur high additional costs. With regard to organic fouling, the main challenge in MD was the presence of LMW-HS organics and LMW organics. The SMABR pretreated seawater with low concentration of LMW organics enabled to reduce MD flux decline as well as permeation of LMW-HS organics.

7.3.2.2   MD performance with membrane cleaning

For inorganic scaling (gypsum) deposited in the membrane module, a straightforward membrane flushing with DI water was effective in cleaning the system. In MD, the crystals were only loosely deposited on the membrane surface due to the lack of hydraulic pressure; the crystals were easily removed through DI water flushing. The effectiveness of membrane cleaning with DI water flushing was established by using a detailed mass balance of the brine solution components. The results revealed that most of the feed ion components (i.e. Mg, Na and Cl ions) were able to be flushed out with 2 L of DI water, meaning that frequent DI water flushing maintained the V-MEMD system. The use of a simple pretreatment may be considered for Fe reduction.

CHAPTER 8

CONCLUSIONS AND RECOMMENDATIONS

University of Technology Sydney

Faculty of Engineering & Information Technology

8. 1 CONCLUSIONS

Membrane distillation (MD) is a promising alternative technology for small-scale drinking water production in inland remote areas. Existing technologies such as reverse osmosis (RO) and thermal distillation, face implementation challenges in these areas, primarily poor performance caused by high salinity, the required additional brine treatment, high energy usage as large footprint. Consequently these communities still lack proper drinking water supplies. Ultimately, the feasibility of MD depends on whether it can demonstrate its advantages over already established technologies.

Features and performance of Vacuum Multi-Effect Membrane Distillation (V-MEMD)

This study evaluated the performance of the V-MEMD system, a modified version of the VMD design. Essentially, the V-MEMD system is integrated with an internal heating and cooling mechanism. This allows the system to be operated at a low feed temperature of 45ºC to 55ºC while producing a reasonable permeate flux. Operating at a lower feed temperature was beneficial to reduce the effect of TP and minimize heat loss. Accordingly, the TP ratio of the V-MEMD remained in the low range of 0.96 to 0.99. The low thermal requirement makes the V-MEMD a suitable candidate for integration with alternative energy such as solar energy. Furthermore the system indicated only a slight reduction in permeate flux (10-15%) even under conditions of high salinity, up to 3M of NaCl as presented in **Chapter 4**. Added to this, the presence of a vacuum makes it possible to build a compact modular unit.

Feasibility of V-MEMD application for small scale drinking water production compared to existing RO technology

In **Chapter 4** of this study the optimal operating environment of the V-MEMD system was evaluated. Permeate pressure and heating temperature were recognized as the most influential operating parameters on the permeate flux. The highest water flux of 13.5 LMH was obtained by a combined setting of highest permeate vacuum pressure, P_p=5.0 kPa and highest heating temperature, T_h=65ºC. As mentioned in **Chapter 4**, to achieve the best performance efficiency, apart from permeate flux, what must be considered are the gain output ratio, recovery ratio and permeate vacuum stability. In this context a combination of T_h=60 ºC, v_f =0.9 m/s and P_p= 10.0 kPa achieved an optimum gain output ratio and recovery ratio with a stable permeate flux of 9.4 LMH.

In these optimal operating conditions the single stage V-MEMD system (with a membrane area of 0.16 m^2) obtained a production rate of 1.5 L/h with a high TDS feed solution of 64.2 g/L, as described in **Chapter 5**. The system maintained a stable permeate flux, achieving a rejection rate of 99%. Using these results, the production rate of a scaled-up V-MEMD system with a membrane area of 3.0 m^2 was estimated to be around 28.1 L/h. Hence, a large-scale V-MEMD system is able to achieve a recovery ratio of approximately 70% even with a high TDS feed solution, as shown in **Figure 8.1a**.

Based on the available studies, a small-scale RO system with similar capacity would be able to perform only at a recovery ratio of 34% with a 98% rejection rate (Banat et al., 2012; Schäfer et al., 2004). This is based on an operating pressure of 4.5 to 5.0 bar, feed flow rate of 99 L/h and at low TDS feed solution (less than 2 g/L) as shown in **Figure 8.1b**. With increased TDS feed solution, for instance at 5 g/L, at the same operating

pressure of 4.5 bar, the recovery ratio of the small-scale RO system was reported to be less than 15% (Schäfer et al., 2004). Increasing the operating pressure from 5.0 bar to 7.0 bar would increase the specific energy consumption, in that the small-scale RO at an average of 5 kWh/m^3 is estimated to increase up to 26 kWh/m^3. At the same time, the rejection rate of the RO system will decline when the operating pressure increases (Richards and Schäfer, 2003).

(a)

V-MEMD System
(684 L/day)

Feed flow rate
(40 L/h)

Feed solution
(44.2 to 60 g/L
TDS)

Brine
Concentrate
11.9 L/h

Recovery ratio =
70.3%

Permeate
rate
(28.1 L/h)

(b)

RO System
(816 L/day)

Feed flow rate
(99 L/h)

Feed solution
(2.0 g/L TDS)

Brine
Concentrate
65 L/h

Recovery ratio =
34%

Permeate rate
(34 L/h)
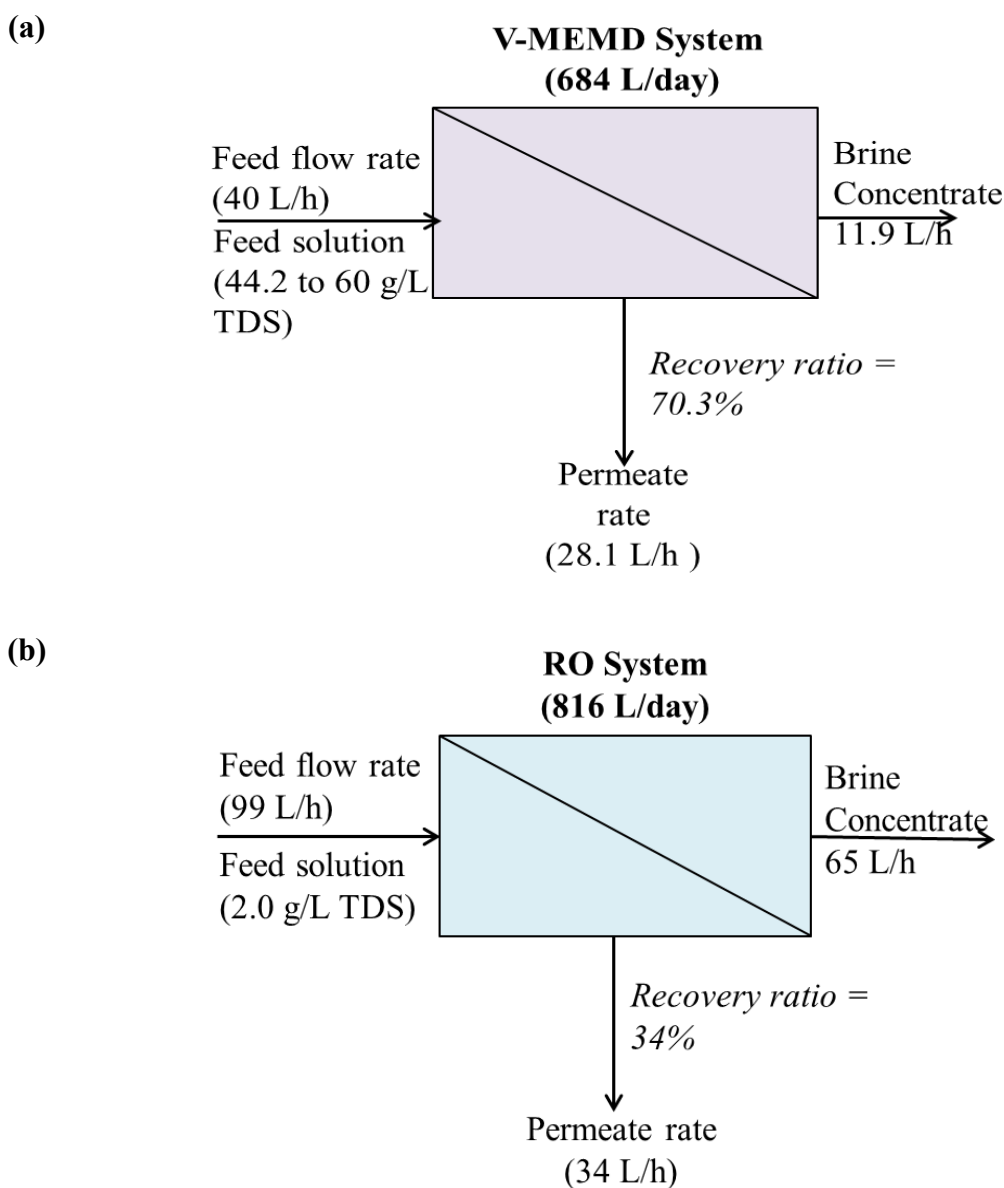
Figure 8.1 Comparison of the production rate of **(a)** V-MEMD system and **(b)** small-scale RO system (data of small-scale RO system adopted from Banat et al., 2012).

The high recovery ratio of the V-MEMD system is especially beneficial for minimizing the management of brine water in inland areas. Indeed the simple maintenance of the system with DI water cleaning cycles makes MD an attractive option as a small-scale drinking water production system. The capacity of the V-MEMD system can be easily increased in a compact modular design due to the internal heating unit and vacuum application as noted in **Chapter 4**.

The superiority of the V-MEMD system over existing RO technology for the production of small-scale drinking water supplies, originating from highly saline source water, has been established in this study.

Scaling and organic fouling development in MD system

Aside from the performance feasibility establishing the suitability of MD system for small-scale drinking water production, the detailed evaluation of scaling and organic fouling development in MD operation is essential. Membrane fouling has emerged as one of the main challenges facing the RO system as a hydraulic pressured membrane process. In comparison, the lack of hydraulic pressure in MD is an advantage for loose fouling deposition. However, the presence of thermal conditions in MD contributes to a complex scaling development. The correlation of scaling development with MD thermal operations has been investigated in a number of studies. Hence, this study's investigation focused on the role of hydrodynamic parameters (flow velocity) on scaling development and membrane cleaning.

The findings of this study acknowledge the influential role of both feed and permeate velocity on $CaSO_4$ scaling development in a direct contact MD (DCMD) configuration. The SEM-EDS line analysis of the scaling evaluation showed that significantly higher calcium and sulphate elements were deposited on the membrane at low flow velocity (v_f

&v_p of 0.5 m/s), compared to the high flow velocity (v_f&v_p of 2.2 m/s). This action verified the important role played by high flow velocity (turbulence) in controlling membrane surface crystallization. Nevertheless, at high flow velocity, the overall recovery ratio performance will decrease and the risk of membrane wetting wil increase. For instance, in the DCMD evaluation, at feed and permeate velocity, v_f&v_p of 2.2 m/s, the recovery ratio and pumping energy was 1.0% and 1.04 x 10^{-1} W, respectively. In contrast at v_f&v_p of 0.5 m/s, the recovery ratio and pumping energy was 2.4% and 1.56 x 10^{-7} W, respectively. Hence, the findings of this study confirmed that the intermediate flow velocity of v_f&v_p 1.1 m/s was a more suitable flow velocity range for maintaining a good performance output while controlling membrane surface scaling. Another important finding of the DCMD scaling evaluation was the role played by permeate velocity. For instance at a combination of v_f of 0.8 m/s and v_p of 1.1 m/s, the same permeate flux was achieved as v_f&v_p 1.1 m/s. However, compared to v_f&v_p 1.1 m/s, the system's performance was improved in terms of higher recovery ratio, less pumping energy and reduced membrane surface crystallization with the combined v_f of 0.8 m/s and v_p of 1.1 m/s. A suitable feed and permeate velocity can be identified based on the permeate temperature gradient and the permeate to feed pressure ratio.

With reference to the V-MEMD system, even with high TDS saline $CaSO_4$ solution, the initial permeate flux of 9.4 LMH declined by only 18 to 20% with loosely deposited crystals. This loose deposition was attributed to the lack of hydraulic pressure, low feed temperature (T_f = 47.6 °C), high turbulence at v_f = 0.9 m/s (Re = 5665.6) and short membrane retention time (21.6 s). The scaling was reversible with DI water flushing. Further, in the V-MEMD system, the role of feed flow velocity in influencing the crystal size was also observed. Here the crystal size was measured in terms of volume weighted mean size, D[4,3] and the crystal size in the membrane module was measured

from the brine solution collected from the module after DI water flushing. The findings indicated that $D[4,3]_{brine\ module}$, increased from 62.8 μm at v_f of 0.9 m/s to 339.1 μm at v_f of 0.3 m/s.

As for organic fouling development, this study provided a detailed understanding of the characteristics concerning individual organic compounds under thermal MD operation using LC-OCD analysis. The study observed that polysaccharides represented by the alginic acid (AA) compound exhibited minimal fouling tendencies (199.4 mg/m^2 organic mass per membrane area) due to its hydrophilic nature and and negative electrostatic repulsion. Yet, in hydraulic membrane processes such as RO, the AA compound exhibited a severe fouling tendency due to the compressible and deformable nature of AA when it was subjected to pressure.

In the MD process both the humic acid (HA) and bovine serum albumin (BSA) compound showed dominant fouling tendencies. The BSA compound, representing protein, was sensitive to temperature and degraded to smaller molecular weight organics and LMW organics. Due to the hydrophobic nature of the BSA compound, it bonded with the hydrophobic MD membrane, forming a dominant deposit on the membrane surface (800.6 mg/m^2 organic mass per membrane area). On the other hand, the HA compound (representing humic substances, HS) had relatively lower deposits on the membrane surface (423.2 mg/m^2 deposit on the membrane surface). However, the LC-OCD analysis showed the thermal disaggregation of HS, forming LMW-HS organics while the membrane autopsy observed the penetration of the LMW-HS organics through the membrane pores, causing partial wetting. The physico-chemical state of the feed solution also impacted on the organic compound's behavior. The addition of salinity (NaCl) contributed to greater HS disaggregation to LMW-HS organics.

Meanwhile, in the presence of inorganic scalant, the Ca^{2+} ion acts as a binding agent, whereby a cake layer was formed on the membrane.

In natural seawater, which is a mixture of organic components where the HA compound predominates, a similar formation of LMW-HS organics and LMW organics under MD thermal conditions was observed to have penetrated through the membrane. This evaluation furthermore established that irreversible fouling with seawater occurred after two operational cycles. The assimilable organic carbon (AOC) concentration detected on the MD membrane foulant with SW highlighted the biofouling challenge of MD with SW.

Practical MD application for small-scale drinking water production

An important factor concerning the practical application of MD to small-scale drinking water production is maintaining the system. The scaling evaluation carried out in this study indicated the loose deposition of crystals in the V-MEMD system and its reversibility with DI water flushing. In line with this, a further evaluation using feed solution ion mass balance established that DI water flushing helped to maintain the system. With only 2L of DI water, most ions in the feed solution, namely the Mg, Na and Cl ions, could be removed. Frequent DI water flushing or a simple precipitation is recommended to control higher retention ions such as Fe and Ca. This established the suitability of operating the V-MEMD system using only DI water flushing (frequent but small amounts of DI water).

On the other hand, organic fouling occurred due to the formation of LMW-HS organics and LMW organics, as a result of thermal disaggregation of the HS compound, penetrating to the pores of the membrane. In this study, the need for a pretreatment to reduce the HS and LMW organics compound in the raw feed solution was evaluated.

The performance of two chemical-free pretreatments, a deep-bed biofilter and a submerged membrane adsorption bioreactor hybrid system (SMABR), was evaluated. Both systems exhibited superior abilities in reducing HS and LMW organics through adsorption and biodegradation. The instrumental role of bioactivity in both these pretreatment systems was reflected by the AOC measurement and active microbial, adenosine tri-phosphate (ATP). The low contents of HS and LMW organics in the pre-treated seawater feed solution resulted in minimal adhesion of LMW-HS and LMW organics onto the membrane. Thus a stable permeate flux was achieved for a longer period of time and with no membrane wetting. The results confirmed the suitability of SMABR and deep-bed biofilters as chemical-free pretreatments to reduce organic fouling in MD.

8.2 RECOMMENDATIONS

The findings in this study validated the potential of MD for obtaining high quality drinking water production with a suitable pretreatment strategy. The recommended set-up of the V-MEMD system for an inland drinking water application is shown in **Figure 8.2**.
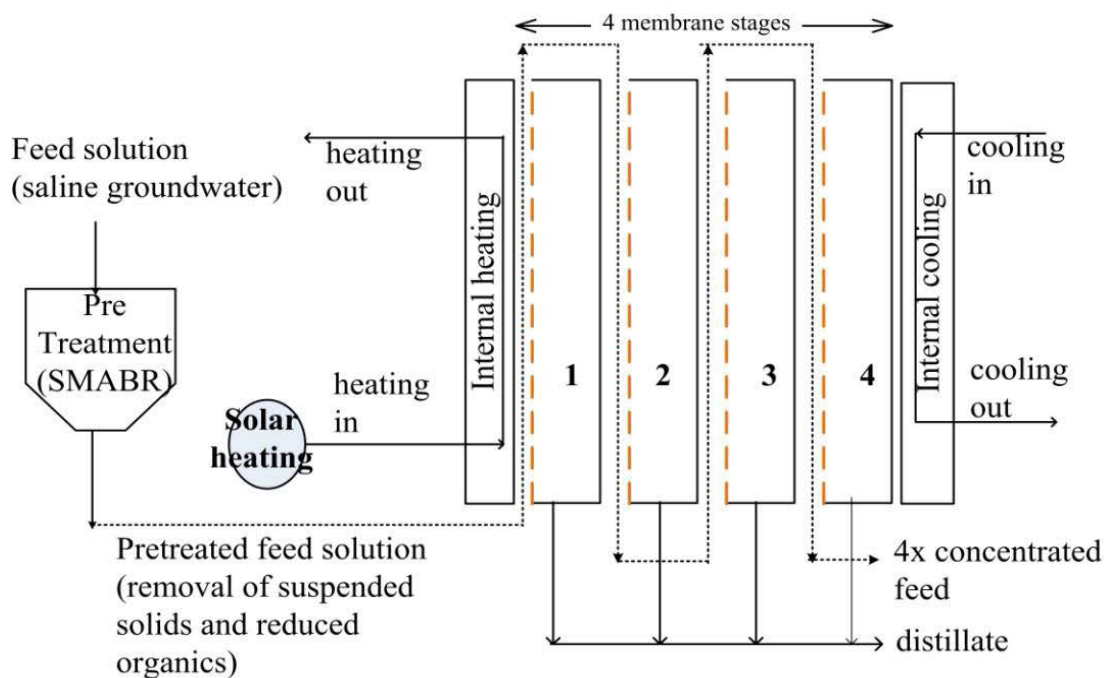
Figure 8.2 Schematic diagram of MD design concept for drinking water production in inland area.

In this recommended design a four-stage membrane in a modular setting should be employed to achieve a compact scaled-up system while maintaining a sustainable footprint. Further, coupling the system with solar heating will help achieve an energy efficient system.

The gaps in this dissertation are highlighted in detail as show below. These gaps are highlighted as a recommendation for future MD research studies.

Economic assessment

A detail economic analysis should be carried out to quantitatively document the advantages of the MD system over existing technologies for small-scale drinking water production. Capital costing's of MD have been estimated by several studies, with the conclusion that MD will have a higher initial cost compared to current technologies. An over-arching economic analysis including the operation and maintenance costs must be

done to assess the economic benefits of this system. Factors such as membrane lifespan, simple pretreatment requirements and straightforward membrane cleaning and minimal brine management are critical to establishing competitive water production costs.

Solar energy integrated MD system

It should be stated that the specific energy needs of the small-scale RO at 26 kWh/m^3 are still considerably less compared to MD at around 100 kWh/m^3 (Koschikowski et al., 2009). However, coupling MD with solar energy will overcome this problem as shown in **Figure 8.2**. Nevertheless the capital costs and performance stability and efficiency of solar integration must be examined more closely.

V-MEMD design modification

Although the V-MEMD design constitutes an innovation to conventional MD designs, a number of MD design modifications can improve the system's performance. For instance, the internal heating and cooling mechanisms allowed the system to operate at low feed temperature and minimize the effects of polarization. However, in a compact modular design system with internal heating, maintaining a stable cooling temperature in a hot remote inland area is a challenge. Using a heat exchanger must be evaluated. Deposits from concentrated feed solution easily clog the feed channel, disrupting the operation of the system. The small and narrow feed channel sizes in the MD design will reduce heat losses. However, more detailed design evaluation to overcome this feed channel clogging will enhance future MD designs.

Organic fouling development

This study established profound findings on the correlation of HA compound thermal disaggregation and membrane pore penetration by small molecular organics. It is recommended to evaluate this phenomenon with other type of membrane geometries.

Currently extensive research is being carried out on MD membrane modification and new MD membrane development such as hollow fibre, ceramic membrane and nanofibres. These membranes incorporate advantageous features such as high hydrophobicity, reduced wetting environment, pore size and thickness modification and nano-particle electro-spun fibres. Evaluating the extent of the HA organic compound fouling these new membrane types will enable researchers to obtain new perspectives on organic fouling development in MD operations. Further, a guideline for MD fouling mitigation for industrial application must be tabulated.

Biofouling development

The findings in this study have indicated the biofouling potential of MD operation with SW based on the AOC concentration of the membrane foulant and feed solution. More detailed physico-chemical analyses are required on the occurrence of biofouling in MD. Although previous studies have indicated that biofouling MD operation was minimal due to the thermal application, this topic needs to be reconsidered in long-term MD operations at high feed concentration and low feed temperatures.

REFERENCES

Al-Amoudi, A., & Lovitt, R. W. (2007). Fouling strategies and the cleaning system of NF membranes and factors affecting cleaning efficiency. Journal of Membrane Science, 303(1), 4-28.

Alkhudhiri, A., Darwish, N., & Hilal, N. (2012). Membrane distillation: A comprehensive review. Desalination, 287(0), 2-18.

Alklaibi, A., & Lior, N. (2005). Membrane-distillation desalination: Status and potential. Desalination, 171(2), 111-131.

Al-Obaidani, S., Curcio, E., Macedonio, F., Di Profio, G., Al-Hinai, H., & Drioli, E. (2008). Potential of membrane distillation in seawater desalination: Thermal efficiency, sensitivity study and cost estimation. Journal of Membrane Science, 323(1), 85-98.

Amy, G. (2008). Fundamental understanding of organic matter fouling of membranes. Desalination, 231(1), 44-51.

Andersson, S., Kjellander, N., & Rodesjö, B. (1985). Design and field tests of a new membrane distillation desalination process. Desalination, 56 (0), 345-354.

Arnosti, C., Jørgensen, B., Sagemann, J., & Thamdrup, B. (1998). Temperature dependence of microbial degradation of organic matter in marine sediments: Polysaccharide hydrolysis, oxygen consumption, and sulfate reduction. Marine Ecology-Progress Series, 165, 59-70.

Australia Bureau of Meteorology, Commonwealth of Australia (2014) http://www.bom.gov.au

Baalousha, M., Motelica-Heino, M., & Coustumer, P. L. (2006). Conformation and size of humic substances: Effects of major cation concentration and type, pH, salinity, and residence time. Colloids and Surfaces A: Physicochemical and Engineering Aspects, 272(1), 48-55.

Bahmanyar, A., Asghari, M., & Khoobi, N. (2012). Numerical simulation and theoretical study on simultaneously effects of operating parameters in direct

contact membrane distillation. Chemical Engineering and Processing: Process Intensification, 61(0), 42-50.

Bailie, R. S., & Wayte, K. J. (2006). Housing and health in indigenous communities: Key issues for housing and health improvement in remote aboriginal and torres strait islander communities. Australian Journal of Rural Health, 14(5), 178-183.

Baker, J., & Dudley, L. (1998). Biofouling in membrane systems—a review. Desalination, 118(1), 81-89.

Banat, F. A., & Simandl, J. (1994). Theoretical and experimental study in membrane distillation. Desalination, 95(1), 39-52.

Banat, F. A., & Simandl, J. (1998). Desalination by membrane distillation: A parametric study.

Banat, F., & Jwaied, N. (2010). Autonomous membrane distillation pilot plant unit driven by solar energy: Experiences and lessons learned. International Journal of Sustainable Water and Environmental Systems, 1, 21-24.

Banat, F., Al-Rub, F. A., & Bani-Melhem, K. (2003). Desalination by vacuum membrane distillation: Sensitivity analysis. Separation and Purification Technology, 33(1), 75-87.

Banat, F., Qiblawey, H., & Al-Nasser, Q. (2012). Design and operation of small-scale photovoltaic-driven reverse osmosis (PV-RO) desalination plant for water supply in rural areas. Computational Water, Energy, and Environmental Engineering, 1, 31.

Bandini, S., & Sarti, G. C. (1999). Heat and mass transport resistances in vacuum membrane distillation per drop. American Institute Of Chemical Engineers Journal , 45(7), 1422-1433.

Bandini, S., Gostoli, C., & Sarti, G. (1992). Separation efficiency in vacuum membrane distillation. Journal of Membrane Science, 73(2), 217-229.

Bandini, S., Saavedra, A., & Sarti, G. C. (1997). Vacuum membrane distillation: Experiments and modeling. American Institute Of Chemical Engineers Journal, 43(2), 398-408.

Brehant, A., Bonnelye, V., & Perez, M. (2002). Comparison of MF/UF pretreatment with conventional filtration prior to RO membranes for surface seawater desalination. Desalination, 144(1), 353-360.

Bui, V. A., Vu, L. T. T., & Nguyen, M. H. (2010). Simulation and optimisation of direct contact membrane distillation for energy efficiency. Desalination, 259(1–3), 29-37.

Burgoyne, A., & Vahdati, M. (2000). Direct contact membrane distillation. Separation Science and Technology, 35(8), 1257-1284.

Cabassud, C., & Wirth, D. (2003). Membrane distillation for water desalination: How to chose an appropriate membrane? Desalination, 157(1), 307-314.

Çakal, G., Erdoğdu, A., Eroğlu, İ., & Özkar, S (2004). Comparison of the partide sizes of gypsum crystals obtained in the production of boric acid by batch and continuous flow systems. U. Uluslararası Bor Sempozyumu, Eskişehir

Calabro, V., Jiao, B. L., & Drioli, E. (1994). Theoretical and experimental study on membrane distillation in the concentration of orange juice. Industrial and Engineering Chemistry Research, 33(7), 1803-1808.

Cao, X., Ma, J., Shi, X., & Ren, Z. (2006). Effect of TiO_2 nanoparticle size on the performance of PVDF membrane. Applied Surface Science, 253(4), 2003-2010.

Cath, T. Y., Adams, V. D., & Childress, A. E. (2004). Experimental study of desalination using direct contact membrane distillation: A new approach to flux enhancement. Journal of Membrane Science, 228(1), 5-16.

Charcosset, C. (2009). A review of membrane processes and renewable energies for desalination. Desalination, 245(1), 214-231.

Chien, C., Kao, C., Dong, C., Chen, T., & Chen, J. (2007). Effectiveness of AOC removal by advanced water treatment systems: A case study. Desalination, 202(1), 318-325.

Childress, A. E., & Elimelech, M. (1996). Effect of solution chemistry on the surface charge of polymeric reverse osmosis and nanofiltration membranes. Journal of Membrane Science, 119(2), 253-268.

Cho, J., Amy, G., & Pellegrino, J. (1999). Membrane filtration of natural organic matter: Initial comparison of rejection and flux decline characteristics with ultrafiltration and nanofiltration membranes. Water Research, 33(11), 2517-2526.

Chon, K., Kim, S. J., Moon, J., & Cho, J. (2012). Combined coagulation-disk filtration process as a pretreatment of ultrafiltration and reverse osmosis membrane for wastewater reclamation: An autopsy study of a pilot plant. Water Research, 46(6), 1803-1816.

Christoffersen, M., Christoffersen, J., Weijnen, M., & Van Rosmalen, G. (1982). Crystal growth of calcium sulphate dihydrate at low supersaturation. Journal of Crystal Growth, 58(3), 585-595.

Chua, K., Hawlader, M., & Malek, A. (2003). Pretreatment of seawater: Results of pilot trials in singapore. Desalination, 159(3), 225-243.

Criscuoli, A., Carnevale, M. C., & Drioli, E. (2008). Evaluation of energy requirements in membrane distillation. Chemical Engineering and Processing: Process Intensification, 47(7), 1098-1105.

Curcio, E., Criscuoli, A., & Drioli, E. (2001). Membrane crystallizers. Industrial and Engineering Chemistry Research, 40(12), 2679-2684.

Curcio, E., Ji, X., Di Profio, G., Sulaiman, A. O., Fontananova, E., & Drioli, E. (2010). Membrane distillation operated at high seawater concentration factors: Role of the membrane on $CaCO_3$ scaling in presence of humic acid.Journal of Membrane Science, 346(2), 263-269.

Diban, N., Voinea, O. C., Urtiaga, A., & Ortiz, I. (2009). Vacuum membrane distillation of the main pear aroma compound: Experimental study and mass transfer modeling. Journal of Membrane Science, 326(1), 64-75.

Ding, Z., Liu, L., El-Bourawi, M. S., & Ma, R. (2005). Analysis of a solar-powered membrane distillation system. Desalination, 172(1), 27-40.

Dow, N., Duke, M., Zhang, J., O'Rielly, T., Li, J., Gray, S., Ostarcevic, E., Atherton, P. (2010). Demonstration of solar driven membrane distillation in remote

victoria. Australian Water Association (AWA) Ozwater Conference and Exhibition, Brisbane, Australia, 8-10.

Drastík, M., Novák, F., & Kučerík, J. (2013). Origin of heat-induced structural changes in dissolved organic matter. Chemosphere, 90(2), 789-795.

Drioli, E., & Wu, Y. (1985). Membrane distillation: An experimental study. Desalination, 53(1), 339-346.

Drioli, E., Curcio, E., Criscuoli, A., & Profio, G. D. (2004). Integrated system for recovery of CaCO$_3$, NaCl and MgSO$_4$·7H$_2$O from nanofiltration retentate. Journal of Membrane Science, 239(1), 27-38.

Drioli, E., Wu, Y., & Calabro, V. (1987). Membrane distillataion in the treatment of aqueous solutions. Journal of Membrane Science, 33(3), 277-284.

Droste, R. L. (1997). Theory and Practice of Water and Wastewater Treatment, New York etc: Wiley, 622-629.

El-Bourawi, M., Ding, Z., Ma, R., & Khayet, M. (2006). A framework for better understanding membrane distillation separation process. Journal of Membrane Science, 285(1), 4-29.

Elimelech, M., & Phillip, W. A. (2011). The future of seawater desalination: Energy, technology, and the environment. Science (New York, N.Y.), 333(6043), 712-717.

Erdoğdu A., Çakal G.Ö., Özkar S., Eroğlu İ.(2004). The effect of Stirring Rate on Dissolution of Colemanite and Particle Size of Gypsum Crystals during the Boric Acid Production in a Batch Reactor. U. Uluslararası Bor Sempozyumu, Eskişehir 23-25.

Eriksson, P., Kyburz, M., & Pergande, W. (2005). NF membrane characteristics and evaluation for sea water processing applications. Desalination, 184(1), 281-294.

Escobar, I. C., & Randall, A. A. (2001). Assimilable organic carbon (AOC) and biodegradable dissolved organic carbon (BDOC):: Complementary measurements. Water Research, 35(18), 4444-4454.

Fan, L., Harris, J. L., Roddick, F. A., & Booker, N. A. (2001). Influence of the characteristics of natural organic matter on the fouling of microfiltration membranes. Water Research, 35(18), 4455-4463.

Fane, A., Schofield, R., & Fell, C. (1987). The efficient use of energy in membrane distillation. Desalination, 64, 231-243.

Findley, M. (1967). Vaporization through porous membranes. Industrial & Engineering Chemistry Process Design and Development, 6(2), 226-230.

Franken, A. C. M., Nolten, J. A. M., Mulder, M. H. V., Bargeman, D., & Smolders, C. A. (1987). Wetting criteria for the applicability of membrane distillation. Journal of Membrane Science, 33(3), 315-328.

Gabsi, S., & Chehbouni, A. (2013). Solar vacuum membrane distillation for seawater desalination. Renewable and Sustainable Energy Conference (IRSEC), 2013 International, 182-185.

Gao, W., Liang, H., Ma, J., Han, M., Chen, Z., Han, Z., Li, G. (2011). Membrane fouling control in ultrafiltration technology for drinking water production: A review. Desalination, 272(1), 1-8.

Garcıa-Payo, M., Izquierdo-Gil, M., & Fernández-Pineda, C. (2000). Wetting study of hydrophobic membranes via liquid entry pressure measurements with aqueous alcohol solutions. Journal of colloid and interface science, 230(2), 420-431.

Gethard, K., Sae-Khow, O., & Mitra, S. (2012). Carbon nanotube enhanced membrane distillation for simultaneous generation of pure water and concentrating pharmaceutical waste. Separation and Purification Technology, 90, 239-245.

Gilron, J., Ladizansky, Y., & Korin, E. (2013). Silica fouling in direct contact membrane distillation. Industrial & Engineering Chemistry Research, 52(31), 10521-10529.

Giovanela, M., Parlanti, E., Soriano-Sierra, E., Soldi, M., & Sierra, M. (2004). Elemental compositions, FT-IR spectra and thermal behavior of sedimentary fulvic and humic acids from aquatic and terrestrial environments. Geochem. J. 38(3), 255-264.

Goosen, M., Sablani, S., Al-Hinai, H., Al-Obeidani, S., Al-Belushi, R., & Jackson, D. (2005). Fouling of reverse osmosis and ultrafiltration membranes: A critical review. Separation Science and Technology, 39(10), 2261-2297.

Gore, D.W. (1982). Gore-Tex membrane distillation, in: Proceedings of the 10th Annual Convention of the Water Supply Improvement Assoc, Hononulu, USA.

Greenlee, L. F., Lawler, D. F., Freeman, B. D., Marrot, B., & Moulin, P. (2009). Reverse osmosis desalination: Water sources, technology, and today's challenges. Water Research, 43(9), 2317-2348.

Gryta, M. (2000). Concentration of saline wastewater from the production of heparin. Desalination, 129(1), 35-44.

Gryta, M. (2002). The assessment of microorganism growth in the membrane distillation system. Desalination, 142(1), 79-88.

Gryta, M. (2007). Effect of iron oxides scaling on the MD process performance. Desalination, 216(1), 88-102.

Gryta, M. (2008a). Alkaline scaling in the membrane distillation process. Desalination, 228(1), 128-134.

Gryta, M. (2008b). Fouling in direct contact membrane distillation process. Journal of Membrane Science, 325(1), 383-394.

Gryta, M. (2009a). Calcium sulphate scaling in membrane distillation process. Chemical Papers, 63(2), 146-151.

Gryta, M. (2009b). Scaling diminution by heterogeneous crystallization in a filtration element integrated with membrane distillation module. Polish Journal of Chemical Technology, 11(2), 60-65.

Gryta, M., & Barancewicz, M. (2010). Influence of morphology of PVDF capillary membranes on the performance of direct contact membrane distillation. Journal of Membrane Science, 358(1), 158-167.

Gryta, M., Tomaszewska, M., & Karakulski, K. (2006). Wastewater treatment by membrane distillation. Desalination, 198(1), 67-73.

Gryta, M., Tomaszewska, M., Grzechulska, J., & Morawski, A. W. (2001). Membrane distillation of NaCl solution containing natural organic matter. Journal of Membrane Science, 181(2), 279-287.

Guillén-Burrieza, E., Zaragoza, G., Miralles-Cuevas, S., & Blanco, J. (2012). Experimental evaluation of two pilot-scale membrane distillation modules used for solar desalination. Journal of Membrane Science, 409–410(0), 264-275.

Halle, C., Huck, P. M., Peldszus, S., Haberkamp, J., & Jekel, M. (2009). Assessing the performance of biological filtration as pretreatment to low pressure membranes for drinking water. Environmental Science and Technology, 43(10), 3878-3884.

Hambsch, B., & Werner, P. (1996). The removal of regrowth enhancing organic matter by slow sand filtration. Advances in Slow Sand and Alternative Biological Filtration, , 21-28.

He, F., Gilron, J., Lee, H., Song, L., & Sirkar, K. K. (2008). Potential for scaling by sparingly soluble salts in crossflow DCMD. Journal of Membrane Science, 311(1–2), 68-80.

He, F., Sirkar, K. K., & Gilron, J. (2009). Studies on scaling of membranes in desalination by direct contact membrane distillation: $CaCO_3$ and mixed $CaCO_3$/$CaSO_4$ systems. Chemical Engineering Science, 64(8), 1844-1859.

He, K., Hwang, H. J., Woo, M. W., & Moon, I. S. (2011). Production of drinking water from saline water by direct contact membrane distillation (DCMD). Journal of Industrial and Engineering Chemistry, 17(1), 41-48.

Hendren, Z., Brant, J., & Wiesner, M. (2009). Surface modification of nanostructured ceramic membranes for direct contact membrane distillation. Journal of Membrane Science, 331(1), 1-10.

Herczeg, A., Dogramaci, S., & Leaney, F. (2001). Origin of dissolved salts in a large, semi-arid groundwater system: Murray basin, australia. Marine and Freshwater Research, 52(1), 41-52.

Hoek, E. M., & Elimelech, M. (2003). Cake-enhanced concentration polarization: A new fouling mechanism for salt-rejecting membranes. Environmental Science and Technology, 37(24), 5581-5588.

Hogan, P., Fane, A., & Morrison, G. (1991). Desalination by solar heated membrane distillation. Desalination, 81(1), 81-90.

Hong, S., & Elimelech, M. (1997). Chemical and physical aspects of natural organic matter (NOM) fouling of nanofiltration membranes. Journal of Membrane Science, 132(2), 159-181.

Hou, D., Wang, J., Zhao, C., Wang, B., Luan, Z., & Sun, X. (2010). Fluoride removal from brackish groundwater by direct contact membrane distillation. Journal of Environmental Sciences, 22(12), 1860-1867.

Hsu, S., Cheng, K., & Chiou, J. (2002). Seawater desalination by direct contact membrane distillation. Desalination, 143(3), 279-287.

Huber, S. A., & Frimmel, F. H. (1994). Direct gel chromatographic characterization and quantification of marine dissolved organic carbon using high-sensitivity DOC detection. Environmental Science and Technology, 28(6), 1194-1197.

Huber, S. A., Balz, A., Abert, M., & Pronk, W. (2011). Characterisation of aquatic humic and non-humic matter with size-exclusion chromatography – organic carbon detection – organic nitrogen detection (LC-OCD-OND). Water Research,45(2), 879-885.

Imdakm, A., & Matsuura, T. (2004). A monte carlo simulation model for membrane distillation processes: Direct contact (MD). Journal of Membrane Science, 237(1), 51-59.

Izquierdo-Gil, M. A., Fernández-Pineda, C., & Lorenz, M. (2008). Flow rate influence on direct contact membrane distillation experiments: Different empirical correlations for nusselt number. Journal of Membrane Science, 321(2), 356-363.

Jacquemet, V., Gaval, G., Rosenberger, S., Lesjean, B., & Schrotter, J. (2005). Towards a better characterisation and understanding of membrane fouling in water treatment. Desalination, 178(1), 13-20.

Jeong, S., Kim, S., Hee Kim, L., Seop Shin, M., Vigneswaran, S., Vinh Nguyen, T., Kim, I. (2013a). Foulant analysis of a reverse osmosis membrane used pretreated seawater. Journal of Membrane Science, 428, 434-444.

Jeong, S., Naidu, G., Vigneswaran, S., Ma, C. H., & Rice, S. A. (2013b). A rapid bioluminescence-based test of assimilable organic carbon for seawater. Desalination, 317, 160-165.

Jermann, D., Pronk, W., Meylan, S., & Boller, M. (2007). Interplay of different NOM fouling mechanisms during ultrafiltration for drinking water production. Water Research, 41(8), 1713-1722.

Ji, X., Curcio, E., Al Obaidani, S., Di Profio, G., Fontananova, E., & Drioli, E. (2010). Membrane distillation-crystallization of seawater reverse osmosis brines. Separation and Purification Technology, 71(1), 76-82.

Jiao, B., Cassano, A., & Drioli, E. (2004). Recent advances on membrane processes for the concentration of fruit juices: A review. Journal of Food Engineering, 63(3), 303-324.

Jin, X., Jawor, A., Kim, S., & Hoek, E. (2009). Effects of feed water temperature on separation performance and organic fouling of brackish water RO membranes. Desalination, 239(1), 346-359.

Jucker, C., & Clark, M. (1994). Adsorption of aquatic humic substances on hydrophobic ultrafiltration membranes. Journal of Membrane Science, 97, 37-52.

Karakulski, K., & Gryta, M. (2005). Water demineralisation by NF/MD integrated processes. Desalination, 177(1), 109-119.

Karakulski, K., & Gryta, M. (2005). Water demineralisation by NF/MD integrated processes. Desalination, 177(1), 109-119.

Karakulski, K., Gryta, M., & Morawski, A. (2002). Membrane processes used for potable water quality improvement. Desalination, 145(1), 315-319.

Karakulski, K., Gryta, M., & Morawski, A. (2002). Membrane processes used for potable water quality improvement. Desalination, 145(1), 315-319.

Khayet, M. (2011). Membranes and theoretical modeling of membrane distillation: A review. Advances in Colloid and Interface Science, 164(1-2), 56-88.

Khayet, M., & Mengual, J. (2004). Effect of salt concentration during the treatment of humic acid solutions by membrane distillation. Desalination, 168, 373-381.

Khayet, M., Cojocaru, C., & García-Payo, C. (2007). Application of response surface methodology and experimental design in direct contact membrane distillation. Industrial and Engineering Chemistry Research, 46(17), 5673-5685.

Khayet, M., Velázquez, A., & Mengual, J. (2004). Direct contact membrane distillation of humic acid solutions. Journal of Membrane Science, 240(1), 123-128.

Khayet, M., Velázquez, A., & Mengual, J. I. (2004). Direct contact membrane distillation of humic acid solutions. Journal of Membrane Science, 240(1–2), 123-128.

Kim, J., Kim, J., Kim, H., & Koo, K. (2009). Characterization of liquid inclusion of RDX crystals with a cooling crystallization. Crystal Growth and Design, 9(6), 2700-2706.

Kimura, S., Nakao, S., & Shimatani, S. (1987). Transport phenomena in membrane distillation. Journal of Membrane Science, 33(3), 285-298.

Koschikowski, J., Wieghaus, M., & Rommel, M. (2003). Solar thermal-driven desalination plants based on membrane distillation. Desalination, 156(1), 295-304.

Koschikowski, J., Wieghaus, M., Rommel, M., Ortin, V. S., Suarez, B. P., & Betancort Rodríguez, J. R. (2009). Experimental investigations on solar driven stand-alone membrane distillation systems for remote areas. Desalination, 248(1), 125-131.

Krivorot, M., Kushmaro, A., Oren, Y., & Gilron, J. (2011). Factors affecting biofilm formation and biofouling in membrane distillation of seawater. Journal of Membrane Science, 376(1), 15-24.

Krivorot, M., Kushmaro, A., Oren, Y., & Gilron, J. (2011). Factors affecting biofilm formation and biofouling in membrane distillation of seawater. Journal of Membrane Science, 376(1), 15-24.

Laganà, F., Barbieri, G., & Drioli, E. (2000). Direct contact membrane distillation: Modelling and concentration experiments. Journal of Membrane Science, 166(1), 1-11.

Lawson, K. W., & Lloyd, D. R. (1996). Membrane distillation. I. module design and performance evaluation using vacuum membrane distillation. Journal of Membrane Science, 120(1), 111-121.

Lawson, K. W., & Lloyd, D. R. (1996). Membrane distillation. I. module design and performance evaluation using vacuum membrane distillation. Journal of Membrane Science, 120(1), 111-121.

Lawson, K. W., & Lloyd, D. R. (1997). Membrane distillation. Journal of Membrane Science, 124(1), 1-25.

Lawson, K. W., & Lloyd, D. R. (1997). Membrane distillation. Journal of Membrane Science, 124(1), 1-25.

LeChevallier, M. W., Becker, W. C., Schorr, P., & Lee, R. G. (1992). Evaluating the performance of biologically active rapid filters. Journal (American Water Works Association), 136-146.

Lee, K. P., Arnot, T. C., & Mattia, D. (2011). A review of reverse osmosis membrane materials for desalination—development to date and future potential. Journal of Membrane Science, 370(1), 1-22.

Lee, S., & Elimelech, M. (2006). Relating organic fouling of reverse osmosis membranes to intermolecular adhesion forces. Environmental Science and Technology, 40(3), 980-987.

Lee, S., Boo, C., Elimelech, M., & Hong, S. (2010). Comparison of fouling behavior in forward osmosis (FO) and reverse osmosis (RO). Journal of Membrane Science, 365(1), 34-39.

Lee, S., Kim, J., & Lee, C. (1999). Analysis of $CaSO_4$ scale formation mechanism in various nanofiltration modules. Journal of Membrane Science, 163(1), 63-74.

Li, B., & Sirkar, K. K. (2004). Novel membrane and device for direct contact membrane distillation-based desalination process. Industrial and Engineering Chemistry Research, 43(17), 5300-5309.

Li, B., & Sirkar, K. K. (2005). Novel membrane and device for vacuum membrane distillation-based desalination process. Journal of Membrane Science, 257(1), 60-75.

Li, N. N., Fane, A. G., Ho, W. W., & Matsuura, T. (2011). Advanced Membrane Technology and Applications John Wiley & Sons.

Li, Q., Xu, Z., & Pinnau, I. (2007). Fouling of reverse osmosis membranes by biopolymers in wastewater secondary effluent: Role of membrane surface properties and initial permeate flux. Journal of Membrane Science, 290(1–2), 173-181.

Liao, Y., Wang, R., Tian, M., Qiu, C., & Fane, A. G. (2013). Fabrication of polyvinylidene fluoride (PVDF) nanofiber membranes by electro-spinning for direct contact membrane distillation. Journal of Membrane Science, 425, 30-39.

Lu, X., Hanna, J., & Johnson, W. (2001). Evidence of chemical pathways of humification: A study of aquatic humic substances heated at various temperatures. Chemical Geology, 177(3), 249-264.

Macedonio, F., Curcio, E., & Drioli, E. (2007). Integrated membrane systems for seawater desalination: Energetic and exergetic analysis, economic evaluation, experimental study. Desalination, 203(1), 260-276.

Malaeb, L., & Ayoub, G. M. (2011). Reverse osmosis technology for water treatment: State of the art review. Desalination, 267(1), 1-8.

Marshall, A. D., Munro, P. A., & Trägårdh, G. (1993). The effect of protein fouling in microfiltration and ultrafiltration on permeate flux, protein retention and selectivity: A literature review. Desalination, 91(1), 65-108.

Martinetti, C. R., Childress, A. E., & Cath, T. Y. (2009). High recovery of concentrated RO brines using forward osmosis and membrane distillation. Journal of Membrane Science, 331(1–2), 31-39.

Martínez-Díez, L., & Florido-Diaz, F. (2001). Desalination of brines by membrane distillation. Desalination, 137(1), 267-273.

Martínez-Díez, L., & Vázquez-Gonzàlez, M. (1996). Temperature polarization in mass transport through hydrophobic porous membranes. American Institute Of Chemical Engineers Journal, 42(7), 1844-1852.

Martínez-Díez, L., Florido-Diaz, F., & Vazquez-Gonzalez, M. (1999). Study of evaporation efficiency in membrane distillation. Desalination, 126(1), 193-198.

McCutcheon, J. R., & Elimelech, M. (2006). Influence of concentrative and dilutive internal concentration polarization on flux behavior in forward osmosis. Journal of Membrane Science, 284(1), 237-247.

Mengual, J., Khayet, M., & Godino, M. (2004). Heat and mass transfer in vacuum membrane distillation. International Journal of Heat and Mass Transfer, 47(4), 865-875.

Mericq, J., Laborie, S., & Cabassud, C. (2009). Vacuum membrane distillation for an integrated seawater desalination process. Desalination and Water Treatment, 9(1-3), 287-296.

Mericq, J., Laborie, S., & Cabassud, C. (2010). Vacuum membrane distillation of seawater reverse osmosis brines. Water Research, 44(18), 5260-5273.

Mi, B., & Elimelech, M. (2008). Chemical and physical aspects of organic fouling of forward osmosis membranes. Journal of Membrane Science, 320(1–2), 292-302.

Mijatović, I., Matošić, M., Hajduk Černeha, B., & Bratulić, D. (2004). Removal of natural organic matter by ultrafiltration and nanofiltration for drinking water production. Desalination, 169(3), 223-230.

Morton, S. R., Stafford Smith, D. M., Friedel, M. H., Griffin, G. F., & Pickup, G. (1995). The stewardship of arid australia: Ecology and landscape management. Journal of Environmental Management, 43(3), 195-217.

Myat, D. T., Stewart, M. B., Mergen, M., Zhao, O., Orbell, J. D., & Gray, S. (2014). Experimental and computational investigations of the interactions between

model organic compounds and subsequent membrane fouling. Water Research,48(0), 108-118.

Nghiem, L. D., & Cath, T. (2011). A scaling mitigation approach during direct contact membrane distillation. Separation and Purification Technology, 80(2), 315-322.

Nghiem, L. D., Hildinger, F., Hai, F. I., & Cath, T. (2011). Treatment of saline aqueous solutions using direct contact membrane distillation. Desalination and Water Treatment, 32(1-3), 234-241.

Oh, H., Choung, Y., Lee, S., Choi, J., Hwang, T., & Kim, J. H. (2009). Scale formation in reverse osmosis desalination: Model development. Desalination, 238(1–3), 333-346.

Oh, H., Yu, M., Takizawa, S., & Ohgaki, S. (2006). Evaluation of PAC behavior and fouling formation in an integrated PAC–UF membrane for surface water treatment. Desalination, 192(1), 54-62.

Ortiz de Zárate, J. M., Rincón, C., & Mengual, J. (1998). Concentration of bovine serum albumin aqueous solutions by membrane distillation. Separation Science and Technology, 33(3), 283-296.

Ortiz-Zárate, J. M., García López, F., & Mengual, J. (1991). Non-isothermal water transport through membranes. Journal of Membrane Science, 56(2), 181-194.

Park, Y., Lee, C., Kim, S., Oh, H., Lee, S., & Choi, J. (2013). Effect of temperature difference on performance of membrane crystallization-based membrane distillation system. Desalination and Water Treatment, 51(7-9), 1362-1365.

Partridge, E. P., & White, A. H. (1929). The solubility of calcium sulfate from 0 to 200. Journal of the American Chemical Society, 51(2), 360-370.

Penru, Y., F. X. Simon, A. R. Guastalli, S. Esplugas, J. Llorrens, S. Baig. (2011). Characterization of natural organic matter from Mediterranean coastal seawater. In Fourth IWA Specialty Conference on Natural Organic Matter: From Source to Tap and Beyond.

Pérez-González, A., Urtiaga, A., Ibáñez, R., & Ortiz, I. (2012). State of the art and review on the treatment technologies of water reverse osmosis concentrates. Water Research, 46(2), 267-283.

Phattaranawik, J., Fane, A. G., Pasquier, A., & Bing, W. (2008). A novel membrane bioreactor based on membrane distillation. Desalination, 223(1), 386-395.

Phattaranawik, J., Jiraratananon, R., & Fane, A. (2003). Heat transport and membrane distillation coefficients in direct contact membrane distillation. Journal of Membrane Science, 212(1), 177-193.

Piccolo, A. (2001). The supramolecular structure of humic substances. Soil Science, 166(11), 810-832.

Potts, D., Ahlert, R., & Wang, S. (1981). A critical review of fouling of reverse osmosis membranes. Desalination, 36(3), 235-264.

Prihasto, N., Liu, Q., & Kim, S. (2009). Pre-treatment strategies for seawater desalination by reverse osmosis system. Desalination, 249(1), 308-316.

Qtaishat, M. R., & Banat, F. (2013). Desalination by solar powered membrane distillation systems. Desalination, 308 (0), 186-197.

Richards, B. S., & Schäfer, A. I. (2003). Photovoltaic-powered desalination system for remote australian communities. Renewable Energy, 28(13), 2013-2022.

Rosenberger, S., Evenblij, H., Te Poele, S., Wintgens, T., & Laabs, C. (2005). The importance of liquid phase analyses to understand fouling in membrane assisted activated sludge processes—six case studies of different european research groups. Journal of Membrane Science, 263(1), 113-126

Safavi, M., & Mohammadi, T. (2009). High-salinity water desalination using VMD. Chemical Engineering Journal, 149(1), 191-195.

Saffarini, R. B., Summers, E. K., Arafat, H. A., & Lienhard V, J. H. (2012). Technical evaluation of stand-alone solar powered membrane distillation systems. Desalination, 286(0), 332-341.

Schäfer, A., Remy, C., & Richards, B. (2004). Performance of a small solar-powered hybrid membrane system for remote communities under varying feedwater salinities. Water Science and Technology: Water Supply, 4(5-6), 233-243.

Schippers, J., & Verdouw, J. (1980). The modified fouling index, a method of determining the fouling characteristics of water. Desalination, 32, 137-148.

Schofield, R., Fane, A., & Fell, C. (1987). Heat and mass transfer in membrane distillation. Journal of Membrane Science, 33(3), 299-313.

Schofield, R., Fane, A., Fell, C., & Macoun, R. (1990). Factors affecting flux in membrane distillation. Desalination, 77(0), 279-294.

Seewoo, S., Van Hille, R., & Lewis, A. (2004). Aspects of gypsum precipitation in scaling waters. Hydrometallurgy, 75(1), 135-146.

Seidel, A., & Elimelech, M. (2002). Coupling between chemical and physical interactions in natural organic matter (NOM) fouling of nanofiltration membranes: Implications for fouling control. Journal of Membrane Science, 203(1), 245-255.

Sharqawy, M. H., John H. Lienhard V, & Zubair, S. M. (2010). Thermophysical properties of seawater: A review of existing correlations and data. Desalination and Water Treatment, 16(1-3), 354-380.

Shih, W., Albrecht, K., Glater, J., & Cohen, Y. (2004). A dual-probe approach for evaluation of gypsum crystallization in response to antiscalant treatment. Desalination, 169(3), 213-221.

Shirazi, M. M. A., Kargari, A., & Shirazi, M. J. A. (2012). Direct contact membrane distillation for seawater desalination. Desalination and Water Treatment, 49(1-3), 368-375.

Shirazi, S., Lin, C., & Chen, D. (2010). Inorganic fouling of pressure-driven membrane processes—a critical review. Desalination, 250(1), 236-248.

Song, L., Li, B., Sirkar, K. K., & Gilron, J. L. (2007). Direct contact membrane distillation-based desalination: Novel membranes, devices, larger-scale studies, and a model. Industrial and Engineering Chemistry Research, 46(8), 2307-2323.

Song, L., Ma, Z., Liao, X., Kosaraju, P. B., Irish, J. R., & Sirkar, K. K. (2008). Pilot plant studies of novel membranes and devices for direct contact membrane distillation-based desalination. Journal of Membrane Science, 323(2), 257-270.

Soni, V., Abildskov, J., Jonsson, G., & Gani, R. (2008). Modeling and analysis of vacuum membrane distillation for the recovery of volatile aroma compounds from black currant juice. Journal of Membrane Science, 320(1–2), 442-455.

Srisurichan, S., Jiraratananon, R., & Fane, A. G. (2005). Humic acid fouling in the membrane distillation process. Desalination, 174(1), 63-72.

Srisurichan, S., Jiraratananon, R., & Fane, A. G. (2006). Mass transfer mechanisms and transport resistances in direct contact membrane distillation process. Journal of Membrane Science, 277(1–2), 186-194.

Sutherland, K. S. (2011). Filters and filtration handbook. Elsevier., 205–209.

Sutzkover-Gutman, I., & Hasson, D. (2010). Feed water pretreatment for desalination plants. Desalination, 264(3), 289-296.

Syvitski, J.P.M. (1991). Principles, methods and application of particle size analysis. Cambridge University Press, Cambridge.

Tang, C. Y., Kwon, Y., & Leckie, J. O. (2007). Fouling of reverse osmosis and nanofiltration membranes by humic acid—effects of solution composition and hydrodynamic conditions. Journal of Membrane Science, 290(1), 86-94.

Tansakul, C., Laborie, S., & Cabassud, C. (2011). Adsorption combined with ultrafiltration to remove organic matter from seawater. Water Research, 45(19), 6362-6370.

Tay, J., Low, S., & Jeyaseelan, S. (1996). Vacuum desalination for water purification using waste heat. Desalination, 106(1), 131-135.

Teng, C., Hawlader, M., & Malek, A. (2003). An experiment with different pretreatment methods. Desalination, 156(1), 51-58.

Tian, J., Chen, Z., Liang, H., Li, X., Wang, Z., & Li, G. (2009). Comparison of biological activated carbon (BAC) and membrane bioreactor (MBR) for

pollutants removal in drinking water treatment. Water Science and Technology, 60 (6), 1515–1523.

Tran, T., Bolto, B., Gray, S., Hoang, M., & Ostarcevic, E. (2007). An autopsy study of a fouled reverse osmosis membrane element used in a brackish water treatment plant. Water Research, 41(17), 3915-3923.

Tun, C. M., Fane, A. G., Matheickal, J. T., & Sheikholeslami, R. (2005). Membrane distillation crystallization of concentrated salts—flux and crystal formation. Journal of Membrane Science, 257(1), 144-155.

Ungár, T., Gubicza, J., Ribárik, G., & Borbély, A. (2001). Crystallite size distribution and dislocation structure determined by diffraction profile analysis: Principles and practical application to cubic and hexagonal crystals. Journal of Applied Crystallography, 34(3), 298-310.

UN-Water (2012). The United Nations World Water Development Report 4: Managing Water under Uncertainty and Risk. Paris, UNESCO.

Van der Kooij, D. (2000). Biological stability: A multidimensional quality aspect of treated water. Water, air, and soil pollution, 123(1-4), 25-34.

Vedavyasan, C. (2007). Pretreatment trends—an overview. Desalination, 203(1), 296-299.

Velten, S., Boller, M., Köster, O., Helbing, J., Weilenmann, H., & Hammes, F. (2011). Development of biomass in a drinking water granular active carbon (GAC) filter. Water Research, 45(19), 6347-6354.

Vrouwenvelder, J., & Van der Kooij, D. (2001). Diagnosis, prediction and prevention of biofouling of NF and RO membranes. Desalination, 139(1), 65-71.

Walton, J., Lu, H., Tumer, C., Solis, S., & Hein, H. (2004). Solar and waste heat desalination by membrane distillation, Desalination and Water Purification Research and Development Program Report No. 81.

Wang, J. Z., Summers, R. S., & Miltner, R. J. (1995). Biofiltration performance: Part 1, relationship to biomass. Journal of American Water Works Association, 87(12), 55-63.

Wilf, M., & Schierach, M. K. (2001). Improved performance and cost reduction of RO seawater systems using UF pretreatment. Desalination, 135(1), 61-68.

Wirth, D., & Cabassud, C. (2002). Water desalination using membrane distillation: Comparison between inside/out and outside/in permeation. Desalination, 147(1), 139-145.

Xu, Y., Zhu, B., & Xu, Y. (2006). Pilot test of vacuum membrane distillation for seawater desalination on a ship. Desalination, 189(1), 165-169.

Ye, Y., Sim, L. N., Herulah, B., Chen, V., & Fane, A. (2010). Effects of operating conditions on submerged hollow fibre membrane systems used as pre-treatment for seawater reverse osmosis. Journal of Membrane Science, 365(1), 78-88.

Yuan, W., & Zydney, A. L. (1999). Humic acid fouling during microfiltration. Journal of Membrane Science, 157(1), 1-12.

Zhang, J., Dow, N., Duke, M., Ostarcevic, E., Li, J., & Gray, S. (2010). Identification of material and physical features of membrane distillation membranes for high performance desalination. Journal of Membrane Science, 349(1–2), 295-303.

Zhang, J., Li, J., & Gray, S. (2011). Effect of applied pressure on performance of PTFE membrane in DCMD. Journal of Membrane Science, 369(1), 514-525.

Zhao, K., Heinzl, W., Wenzel, M., Büttner, S., Bollen, F., Lange, G., Heinzl, S., Sarda, N. (2013). Experimental study of the memsys vacuum-multi-effect-membrane-distillation (V-MEMD) module. Desalination, 323(0), 150-160.

Zhao, Y., Li, F., Carvajal, M. T., & Harris, M. T. (2009). Interactions between bovine serum albumin and alginate: An evaluation of alginate as protein carrier. Journal of Colloid and Iinterface Science, 332(2), 345-353.

Zuo, G., Wang, R., Field, R., & Fane, A. G. (2011). Energy efficiency evaluation and economic analyses of direct contact membrane distillation system using aspen plus. Desalination, 283(0), 237-244.